DCT 252

System Capacity of Vintage Reinforced Concrete Moment Frame Culverts with No Overlay

By

Timothy Porter
Thomas Schumacher

August, 2015

Delaware Center for Transportation
University of Delaware
355 DuPont Hall
Newark, Delaware 19716
(302) 831-1446

The Delaware Center for Transportation is a university-wide multi-disciplinary research unit reporting to the Chair of the Department of Civil and Environmental Engineering, and is co-sponsored by the University of Delaware and the Delaware Department of Transportation.

DCT Staff

The research reported in this document was prepared through participation in an Agreement sponsored by the State of Delaware's Department of Transportation and the Federal Highway Administration. The views and conclusions contained in this document are those of the author(s) and should not be interpreted as presenting the official policies or position, either expressed or implied, of the State of Delaware's Department of Transportation or the U.S. Federal Government unless so designated by other authorized documents.

Delaware Center for Transportation
University of Delaware
Newark, DE 19716
(302) 831-1446

DelDOT Final Report

SYSTEM CAPACITY OF VINTAGE REINFORCED CONCRETE MOMENT FRAME CULVERTS WITH NO OVERLAY

Timothy Porter, Graduate Research Assistant
and
Thomas Schumacher, PhD, PE, Assistant Professor (PI)

August 31, 2015
University of Delaware

TABLE OF CONTENTS

LIST OF FIGURES

LIST OF TABLES

LIST OF EQUATIONS

EXECUTIVE SUMMARY

The Delaware Department of Transportation (DelDOT) currently has around 300 reinforced concrete moment frame culverts with spans ranging from 6 to 20 ft (1829 and 6096 mm) in its inventory. A problem that DelDOT's bridge engineers have is that these culverts often do not pass current LRFR load rating procedures and as a result many of them have to be posted to prohibit larger trucks from passing. However, none of these structures have shown significant wear or deterioration or experienced failure. Hence it has been suggested that the problem may be associated with over-conservative modeling assumptions or the load rating software that is used. Additionally, The Manual for Bridge Evaluation (MBE) (2011) has provisions for box culverts, incl. an illustrated example. However, these structures have soil overlay, which leads to significant earth forces. As such, these provisions do not apply for the culverts discussed in this research. This research project therefore answers the following questions:

- What is the flexural capacity of the upper moment frame corner?
- What is the cracking moment and how does cracking evolve?
- What is the overall system capacity?
- What analysis methodology should be used for load ratings?

In order to answer the four questions, experimental and analytical research work was performed and an evaluation methodology is proposed suitable for reinforced concrete moment frame culverts with the following properties:

- Span length (clear span) between 6 and 20 ft (1.83 and 6.10 m)
- Negative flexural reinforcement (corner) detail consisting of either (a) diagonal rebar with end-hook (see **Figure 2**) or (b) combination of alternating straight (horizontal) and diagonal rebar with end-hook (see **Figure 4**)
- Reinforcing steel consisting of deformed rebars having a distinct yield plateau
- No soil or asphalt overlay, i.e. traffic loads applied directly on top of slab
- Loading patch consistent with AASHTO tire, i.e. l x b = 10 in x 20 in (254 mm x 508 mm)

A total of five full-scale culvert specimens were constructed and tested in the University of Delaware Structures Laboratory and are presented in **Table 2**. Target vintage material properties were achieved by scaling the rebar area by a factor of approximately 40 ksi/60 ksi = 0.667 and by monitoring the development of concrete strength and performing the tests before 4000 psi (27.6 MPa) was reached (see **Table 2**). The width and loading configuration of the five specimens varied as follows:

Table 1. Overview of Tested Laboratory Culvert Specimens.

Spec.	Clear span length, ft (m)	Specimen width, ft (m)	Deck depth, in (mm)	Loading Configuration
1	10.0 (3.05)	2.0 (0.610)	12 (305)	One tire patch (= AASHTO single-axle loading) centered about mid-span
2	10.0 (3.05)	2.0 (0.610)	12 (305)	Two tire patches (= AASTHO tandem-axle loading), centered about mid-span
3	10.0 (3.05)	2.0 (0.610)	12 (305)	Two tire patches (= AASTHO tandem-axle loading), one patch d_v away from the left support
4	10.0 (3.05)	11.3 (3.45)	12 (305)	Sequence 1: One tire patch (= AASHTO single-axle loading) centered about mid-span Sequence 2: Two tire patches (= AASTHO tandem-axle loading), centered about mid-span Sequence 3: One tire patch (= AASHTO single-axle loading) centered about mid-span
5	16.0 (4.88)	2.0 (0.610)	18 (457)	One tire patch (= AASHTO single-axle loading) centered about mid-span

Detailed rebar strain and displacement data at critical locations were collected for each specimen during testing. The loading protocol consisted of loading the specimen to a specific load level and holding the load until the displacements and strains did not change anymore. Subsequently, the specimen was unloaded to a small value before it was reloaded to a higher load. This was repeated until the specimens failed. The evolution of concrete cracks was monitored and mapped during each load holding.

The ultimate failure modes for Specimens 1, 2, 3, and 5 was shear-compression failure near loading locations, which occurred after excessive deflections were present, and after yield moments had been exceeded. In all cases, the regions with the maximum positive and negative bending moments were able to develop plastic hinges, i.e. yield moments were reached to form a plastic mechanism. This was true even for the first three specimens where one large crack formed due to the unique corner reinforcing detail. Specimen 4 failed in two-way (or punching) shear rather than flexural-mode due to the effective transverse load distribution. Also, the angle of the failure crack was found to be approximately 30 °, compared to the common assumption used by ACI of 45 °, for all five specimens.

The experimental data was analyzed and evaluated with available design methodologies based on ACI 318-14, Eurocode 2, and AASHTO LRFD. The most accurate prediction was achieved by considering the actual failure mode and here it occurred. For all Specimens, the most accurate prediction was achieved when a mechanism was assumed using the maximum (or probable) moment. For Specimen 4, the actual failure mode, however, was two-way shear (or punching). One-way shear was above the code-predicted values at the supports, which has been confirmed by other researchers.

Based on the findings of this research, for load rating purposes of reinforced concrete moment frame culverts with no overlay, two main strength checks should be evaluated: (1) flexural system capacity assuming plastic mechanisms and (2) two-way (or punching) shear under the tire patches. Depending on the location and axle configuration, one or the other will likely control. In addition, although this was not observed in any of the experiments, it is recommended that one-way shear be evaluated (1) at the face of the support and (2) 2*d* away from the face of the support. An Excel spreadsheet following the LRFR load rating procedure is currently under development and will be made available to DelDOT.

1 Introduction and Background

Currently, the Delaware Department of Transportation (DelDOT) is having difficulty with load rating culverts throughout the State that were built prior to the 1950's. The culverts that the State is having the most difficulties with are so-called reinforced concrete moment frame culverts, also known as three sided culverts, which have live load applied directly to the top or on to a small bituminous asphalt layer. The largest problems DelDOT is encountering when trying to load rate these structures, are how these culverts behave in-service and what assumptions should be made to estimate the system capacity due to the unique rebar designs, which will be described in more detail in Chapter 2, and to determine what proper load distribution for the live load should be utilized. These problems often lead to the culverts having to be load-posted, even though during inspections of the culverts there are no signs of deterioration found other than typical hairline cracks. Over the past 20 years, research has been completed on the behavior, performance, and analysis for three-sided culverts.

Research completed by Frederick and Tarhini (2000) on three-sided concrete culverts with clear spans between 14 and 36 ft (4.27 and 10.9 m). The goal of the research was to determine the best way to design and analyze three-sided culverts. Culverts were analyzed using 3-D finite element analysis (FEA) and two dimensional plane frame analysis. The results were verified by completing scale modeled testing. Frederick and Tarhini showed that culverts are accurately analyzed using plane frame analysis using a specified strip width. 3-D FEA provides moments and shear forces in the transverse direction but these forces are minimal and typical minimum shrinkage crack reinforcement will adequately withstand the moment and shear forces.

Similarly, in 2008, 108 boxed culverts were analyzed using the FEA program SAP 2000 (Awwad, Mabsout et al. 2008). The culverts had spans that were 12, 18, and 24 ft (3.66, 5.49, and 7.32 m) with varying levels of soil cover and location of the AASHTO tire patch (20 x 10 in (508 x 254 mm)) (AASHTO 2012). The location of the AASHTO tire patch was either edge span or midspan. The results showed that at soil cover less than 3 ft (0.914 m) and a center tire patch, plane frame analysis overestimates the maximum positive and negative moments while for soil cover less than 3 ft (0.914 m) and edge tire patch loading, plane frame analysis underestimates the maximum moments. Along with this result, it was proven that the maximum positive moment occurs at midspan and the maximum negative moment occurs at the interface between the wall and slab (= face of the support).

Full-scale precast box culverts were monotonically loaded to determine the shear capacity of the culverts at different clear spans. Four 4 ft x 4 ft x 4 ft (1.22 m x 122 m x 122 m) box culverts (Garg, Abolmaali et al. 2007) and six 8 ft x 4 ft x 4 ft (2.44 m x 1.22 m x 1.22 m) concrete culverts (Abolmaali and Garg 2008) with varying placements of the AASHTO tire patch were loaded to determine if shear capacity was the controlling factor in the design of culverts. From the experimental results, it was concluded that "flexural cracks governed the behavior at and beyond the factored loads." Although all specimens ultimately failed in shear, shear cracks did not appear on average until almost double the AASHTO factored load had been reached. These cracks ultimately lead to a flexure/shear/bond failure. Another observation noted by the research was that noticeable corner rotation occurred, allowing for more moment capacity in the top slab, which in turn caused the flexural cracks to form first. This observation helped explain the failure type that occurred at the late developing shear cracks. The previous experiments were then compared to results from the FEA program ABAQUS (Garg and Abolmaali 2009). The finite element models were developed using the properties and loading of the actual full-scale experiments. The results from the FEA verified the findings from the full-scale experiments. The first visible cracks were flexural cracks that appeared on the underside of the top slab. Similarly, shear cracks did not form until about two times the AASHTO factored load was reached, proving that flexural capacity is controlling until just before failure.

Recently, a study on the effective width of concrete slab bridges was completed in the state of Delaware (Jones and Shenton 2012). The study looked at six slab bridges with varying dimensions and clear spans. The bridges were gauged and then loaded trucks were driven across. The data was analyzed and an effective width formulation was developed and compared to effective widths from AASHTO LRFD (AASHTO 2012) (4.6.2.3-1) as well as AASHTO Standard Specifications for Highway Bridges (3.24.3.2). It was concluded that both the LRFD and Standard Specifications equations for effective width were over-conservative and a new equation for calculating the effective slab width, E (in) was proposed using the data gathered from the field as follows:

$$E = 10 + 5.8\sqrt{L_1 W_1} \text{ in (in), for single lane loading} \qquad \textbf{Equation 1}$$

where L_1 is span length (ft) and W_1 = minimum of the edge to edge width of the bridge or 30 ft. This equation accounts for multiple-presence and has been adapted by the Delaware DOT.

The research that has been completed gives a good understanding of the general behavior of reinforced concrete culverts even though full-scale testing was completed on box culverts. The results from the full-scale testing showed that hinges developed in the corner of the top slab when loaded, allowing for an increase in moment capacity and that the negative and positive moments occur at the corner of the top slab and center span, respectively. Frederick and Tarhini (2000) verified that two-dimensional analysis can be used when calculating the capacity of moment frame culverts. Finally, Jones and Shenton

(2012) showed that AASHTO LRFD and AASHTO Bridge Specifications gave a conservative effective width and provided a new equation.

The findings from these studies provide some guidance on how to calculate the capacity of moment frame culverts. However, further full-scale experiments were deemed necessary to verify that these findings could be applied to DelDOT's reinforced concrete moment frame culverts with their unique rebar designs.

2 Test Specimens

As mentioned previously, the main problem that exists for the Delaware Department of Transportation, when attempting to load rate their vintage reinforced concrete moment frame culverts, is what assumptions should be made to estimate the system capacity. The typical flexural reinforcement detail for the positive moment region is a straight rebar that runs the entire span and is anchored via end hooks into both the legs. The flexural reinforcement detail for the negative moment region, which is located in the corners, however, is considered unique due to its sloped reinforcement rebar with an end hook. **Figure 1** shows the unique rebar detail for a typical 10 ft (3.05 m) clear span culvert. These culverts were built starting in the 1950s and used, according to DelDOT, deformed Grade 40 (276 MPa) steel reinforcing bars. The culverts with this unique rebar design have a clear span between 8 and 16 ft (2.44 and 4.88 m). Some culverts with clear spans of more than 16 ft (4.88 m) have a slightly modified rebar corner detail, which was also tested in this research.

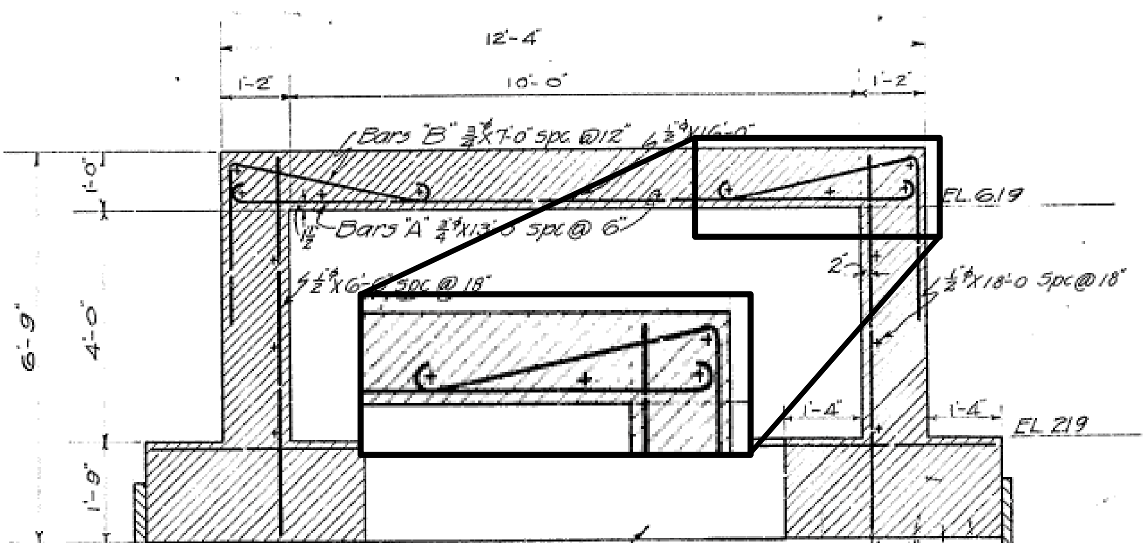

Figure 1. Sample culvert with unique corner rebar detail (Insert).

In order to determine the behavior and ultimate system capacity of these particular culverts, five full-scale laboratory specimens were constructed and tested in the laboratory. Four of the specimens had a width of 24 in (610 mm) and the fifth specimen had a width of 11 ft – 4 in (3.45 m). The 24 in (610 mm) width was chosen because the capacity for the load ratings is usually based on a constant strip width.

The in-service moment frame culverts have soil pressure acting on the legs. Since the specimens were tested in the lab, it was not feasible to have compacted soil placed along the sides of the specimen. To represent this horizontal confinement, each of the five specimens had a minimum of two horizontal #8 (ø 25 mm) tension ties located at the typical inflection point of the legs (see **Figure 2**). These bars were evenly spaced through the width of the legs. The legs were cast on two 24 in x 12 in x 1 in (610 mm x 305 mm x 25 mm) plates with a 2 in (51 mm) roller in between for the 24 in (610 mm) width specimens and four 24 in x 12 in x 1 in (610 mm x 305 mm x 25 mm) plate (two on each leg) with a 2 in (51 mm) roller in between for Specimen 4. One leg was free to horizontally move and rotate, similar to a roller support, and the second leg had the roller welded to the bottom plate to allow for only rotation. For all specimens, a concrete cover of 1.5 in (38 mm) was maintained using plastic spacers.

2.1 Specimen 1 through 4

After reviewing the different culvert design plans, it was determined to use a 10 ft (3.05 m) clear span specimen with a 24 in (610 mm) width for the first three test specimens. These specimens were identical in geometry and rebar configuration but loaded differently as described in Sections 4.2.1 to 4.2.3. The fourth specimen tested had a 10 ft (3.05 m) clear span and a width of 11 ft – 4 in (3.45 m). The larger width was based on the research completed by Jones and Shenton (2012) to determine the effective width of a concrete slab bridge. The loading is discussed in Section 4.3. An elevation view of Specimens 1 through 4 is shown in **Figure 2**. The typical 24 in (610 mm) cross section view of Specimens 1 through 3 at the leg-lab interface is shown in **Figure 3**. The edge-to-edge distance is 11 ft – 4 in (3.45 m) and the clear span is 10 ft (3.05 m). The depth of the slab is 12 in (305 mm).

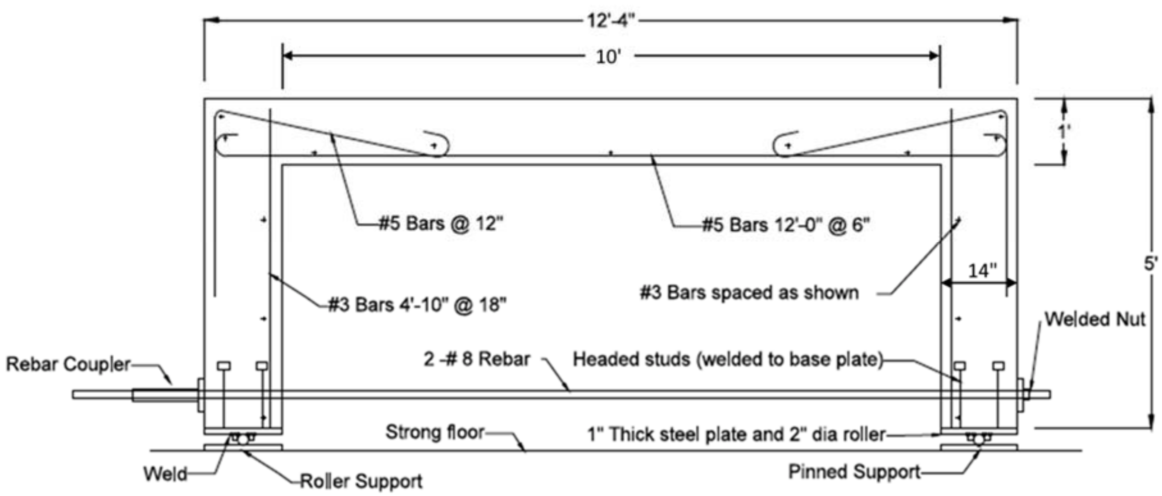

Figure 2. Elevation view of Specimens 1 through 4.

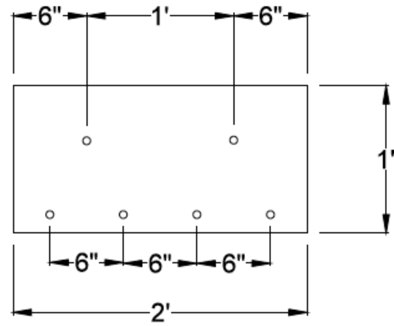

Figure 3. Typical cross section at the leg-slab interface of Specimens 1 to 3.

The unique corner bar is a #5 (ø 16 mm) rebar and the long rebar, that spans from leg to leg, is also a #5 (ø 16 mm) rebar. The vertical reinforcement in the legs and the longitudinal reinforcement are #4 (ø 13 mm) bars. The first three specimens were cast in a single pour with the specimen lying on its side. Specimen 4 was cast in place but in two segments. The first segment consisted of pouring both legs. After the legs cured, the slab was constructed and then cast. The pour of each specimen will be discussed in further detail in the results chapter.

2.2 Specimen 5

The fifth experimental specimen was a 16 ft (4.88 m) clear span culvert with a 24 in (610 mm) width, similar to that of the Specimens 1 through 3. Specimen 5 was tested to confirm observations that were found in the first three specimens and to verify the analytical approach to estimate the capacity of the overall system. The 'L' corner rebar reinforcement and the unique long rebar reinforcement are #6 (ø 19 mm) rebars. The longitudinal rebar reinforcement and the vertical rebar reinforcement are #4 (ø 13 mm) rebars. The 'L' reinforcement was spaced at 12 in (305 mm) and the unique reinforcement was spaced at 12 in (305 mm) alternating, to create an actual spacing of 6 in (152 mm) as shown in **Figure 4** and **Figure 5**.

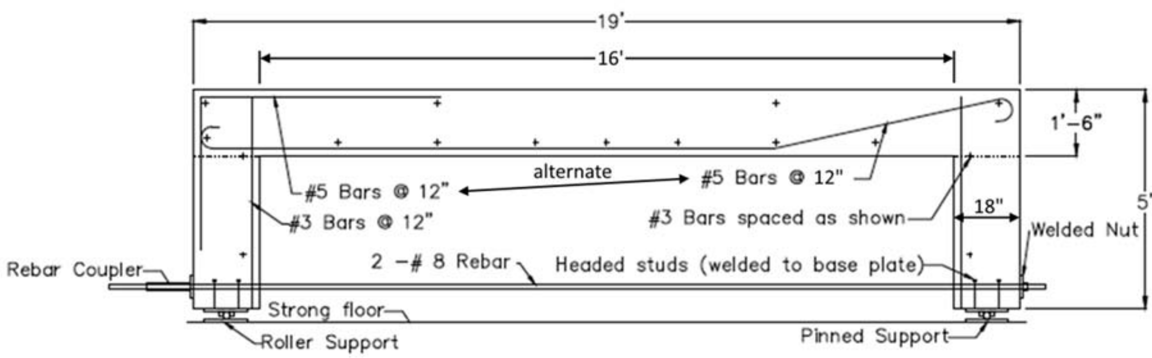

Figure 4. Elevation view of Specimen 5.

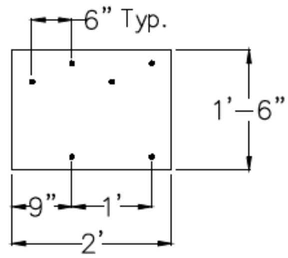

Figure 5. Cross section at leg slab interface of Specimen 5.

2.3 Material Properties

The five specimens were constructed to resemble the in-service culverts. These culverts were built prior to the 1950's. Therefore, the reinforcing bars that were used during the construction of the culverts were Grade 40 (yield strength = 40 ksi (276 MPa)) with deformations, as confirmed by DelDOT. Currently, 40 ksi (276 MPa) steel is rarely produced and many steel distributers do not have 40 ksi (276 MPa) steel in stock. Therefore, a 60 ksi (414 MPa) strength rebar was used. To account for this difference, the overall area of the rebar was scaled by a factor of 40 ksi/60 ksi = 0.667. The strength of the rebar was verified by completing a tension test that followed ASTM Standard E8 (ASTM 2011). Tension coupons were made of the used rebars from each section of the specimen (i.e. positive moment region, negative moment region, and vertical rebar) and loaded to failure. These were tested in a calibrated 200 kip (890 kN) Tinius Olson universal testing machine to determine the actual stress-strain curves used for the analysis of the specimens. Results for average yield stress, f_y and maximum stress, f_{su} are reported in **Table 2**. Detailed stress-strain curves can be found in Appendix B.

The current strength of the concrete in the in-service culverts is unknown. Therefore, the strength was assumed to be 3000 psi (20.7 MPa). Three 6 in x 12 in (152 mm x 305 mm) concrete cylinders were cast and tested in accordance with ASTM C39 (ASTM 2005) on test day. The five test specimens had concrete strengths between 3366 and 3790 psi (23.2 and 26.1 MPa) and the specimens were tested no earlier than 20 days after they were poured (**Table 2**). Detailed strength vs. time curves can be found in Appendix A.

Table 2. Average material properties for all laboratory test specimens.

Specimen	*f'_c* psi (MPa)	*$f_{y,long}$* ksi (MPa)	*$f_{y,corner}$* ksi (MPa)	*$f_{su,long}$* ksi (MPa)	*$f_{su,corner}$* ksi (MPa)
1	3790 (26.1)	65.8 (454)	73.6 (508)	98.8 (681)	120 (827)
2	3788 (26.1)	65.9 (454)	73.6 (508)	108 (745)	120 (827)
3	3339 (23.2)	65.9 (454)	73.6 (508)	108 (745)	120 (827)
4	3469 (23.9)*	62.2 (429)	64.3 (443)	100 (689)	102 (703)
5	3366 (23.2)	63.2 (436)	63.2 (436)	106 (731)	106 (731)
*f'_c is being reported only for slab pour					

3 Experimental Setup

3.1 Experimental Setup and Loading

The specimens were tested using one or two MTS Test Star LLM Actuators. Each actuator used was calibrated and had a load capacity of 150 kip (667 kN). The specimens were tested using a steel load frame, which is anchored into a concrete strong floor. Tension ties consisting of 2 (Specimens 1, 2, 3, and 5) and 4 (Specimen 4) #8 (ø 25 mm) rebars represented the horizontal restraint due to the soil. Each specimen had a predetermined loading scenario. A typical setup is shown in **Figure 6**. The 24 in (610 mm) width specimens (Specimen 1, 2, 3, and 5) were loaded in load-controlled mode at 5 kip (22.2 kN) increments. After the actuator reached its determined applied load, the load was held until the displacement read outs were stable, i.e. creep had settled. During this time, the specimens were visually inspected for cracks and visible cracks were marked and labeled. The specimen was then unloaded to 0.5 kip (2.22 kN). Afterwards the specimen was reloaded to the next 5 kip (22.2 kN) increment. This loading scenario continued until failure was determined to be impending (see **Figure 10**). The specimens were then loaded in displacement-controlled mode allowing for better control. Specimen 4 had a loading scenario similar to that of the 24 in (610 mm) width specimens. Instead of loading the specimens in 5 kip (22.2 kN) increments, the specimen was loaded in 10 kip (44.5 kN) increments due to the expected higher failure load. Cracks were measured and marked at each load increment.

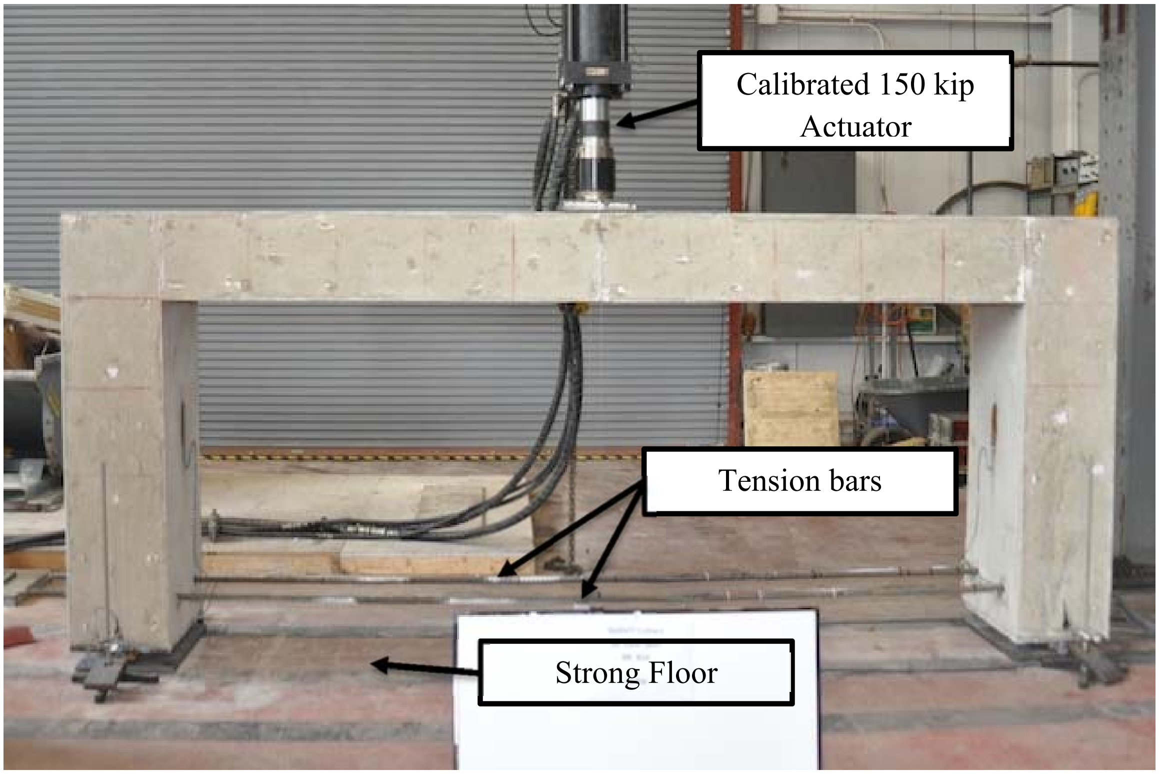

Figure 6. Experimental setup shown for Specimen 1.

3.2 Strain Gauges

While testing the specimens, the stresses were measured at different locations throughout the specimens using Vishay Precision Group ¼ in. (6.4 mm) long strain gauges. The specimens were instrumented with these gauges placed in various locations in the specimen prior to the specimen being cast. To install the strain gauges, the rebar deformations (or ribs) were grinded down to the net diameter, the area was then cleaned, and a strain gauge was placed on the rebar using AE-10 adhesive (**Figure 7**, left). After the adhesive had been cured, a three-wire cable was attached to the wire and then covered with M-Coat J (**Figure 7**, right).

Figure 7. Strain gauge installation.

The gauges were ¼ in (6.4 mm) long linear gauges with a resistance of 350 Ω. Specimens 1 through 4 had the same rebar arrangement (**Figure 8**). However, due to Specimen 4's larger width, more bars were gauged (also see **Figure 34**). Specimens 1 through 3 had 18 strain gauges attached to the rebars and embedded in the concrete, two strain gauges placed on the tension bars, and two gauges were placed on the concrete surface prior to testing. Specimen 4 had 36 gauges placed on the rebar and embedded in the concrete, four strain gauges on the tension bars, and two gauges placed on the surface of the concrete legs. 18 of the 36 gauges in Specimen 4 were placed in the same location as Specimen 1 so that direct comparisons were possible.

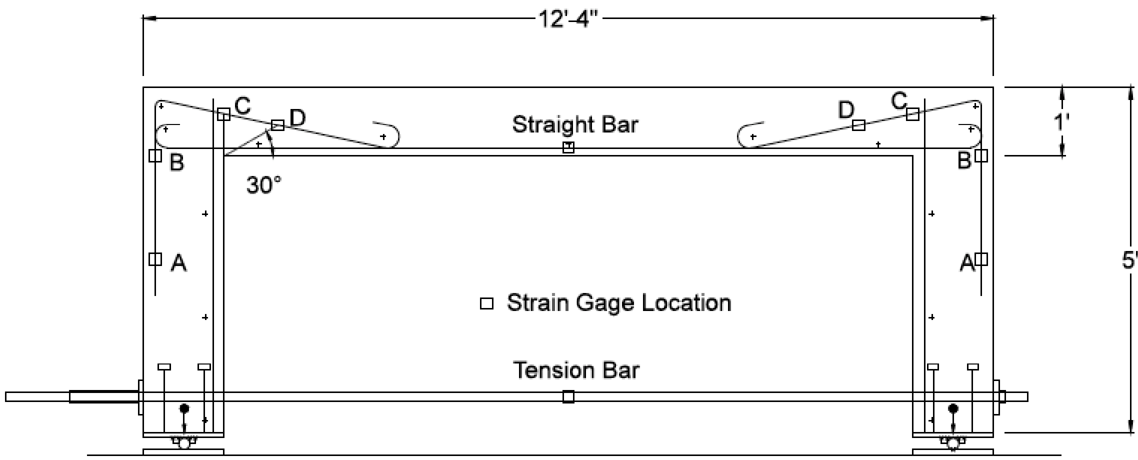

Figure 8. Strain gauge locations for Specimens 1 through 4.

Specimen 5 had a different strain gauge arrangement due to its different rebar design (**Figure 9**). There were 14 strain gauges placed on the rebar that was embedded in the concrete, two gauges placed in the center of the tension bar, and two concrete gauges installed on the surface of the legs. Similar to the gauges in proximity to the corners in Specimens 1 through 4, strain gauges were placed at the interface between the slab and the legs. Another gauge was placed at a 30 ° angle from the bottom of the slab, assuming that a failure crack would likely have the same angle.

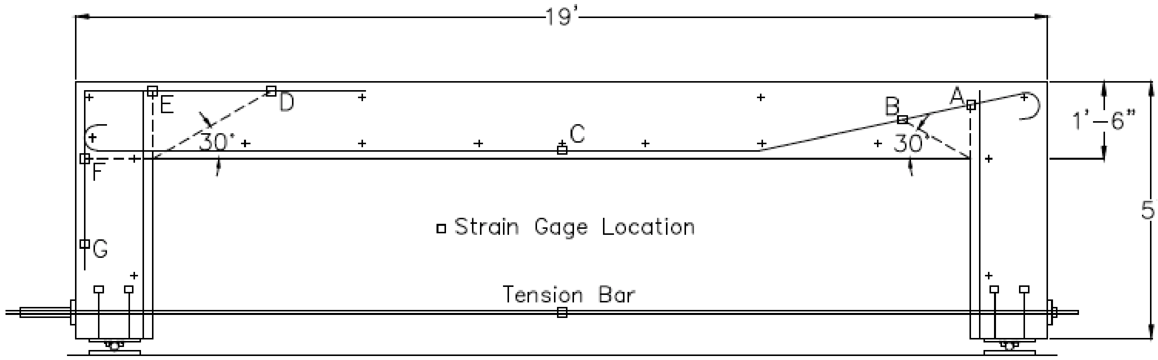

Figure 9. Strain gauge locations for Specimen 5.

The specimens also had concrete gauges placed on the outside of the legs, placed at mid-height. These gauges were 2 in (51 mm) linear strain gauges with a resistance of 350 Ω. The installation process for the concrete gauges was similar to the steel strain gauge installation. The gauge area was prepared and cleaned and M-Bond 200 Adhesive was used to place the 2 in (51 mm) gauge. Strain measurements for all strain gauges were taken at 10 Hz throughout the loading scenario.

3.3 Displacement Sensors

Along with recording strain readings at different locations throughout the specimen, mid-span and support displacements were recorded over the duration of the loading scenario. The displacements were measured using 2 in (51 mm) and 5 in (127 mm) string potentiometers (or string pots). The specimens with a 24 in (610 mm) width (Specimen 1, 2, 3, and 5) used two Unimeasure model PA-5-DS-L3M 5 in (127 mm) string pots, attached at mid-height on the concrete slab. To measure the displacement of Specimen 4, which has a 11 ft – 4 in (3.45 m) width, two 5 in (127 mm) string pots and 9 Unimeasure LX-PA-2 2 in (51 mm) string pots were used. All string pots were attached on the bottom of the concrete slab at 12 in (305 mm) intervals. The 5 in (127 mm) string pots were placed at the same location, with respect to the load plate, as the 24 in (610 mm) specimens. This allowed for a comparison between Specimens 1, 2, and 4. The support displacements were recorded for both supports on each side of the specimen. This allowed for the correction of any effects on the mid-span displacement caused by support settlements.

3.4 Data Acquisition System

Measurements for all load readouts, strain gauges, and string pots were recorded at 10 Hz using a Micro-Measurements System 5000 throughout the loading scenario.

4 Construction and Experimental Results

4.1 Loading Protocol

The loading protocol consisted of loading each specimen to a specific load, holding that load until there was no significant observable change in strains and displacement, followed by unloading to a nominal value of 0.5 kip (2.22 kN). This was repeated until failure of the specimen was reached. The tests were conducted in load-controlled mode using a MTS servo-hydraulic system. Specimens 1 through 3 were loaded in 5 kip (22.2 kN) increments. Specimen 4 was loaded in 10 kip (44.4 kN) increments, due to its larger expected load. Finally, Specimen 5 was loaded in 5 kip (22.2 kN) increments similar to Specimen 1 through 3. **Figure 10** shows the typical loading protocol normalized to 1 for failure load and time of failure.

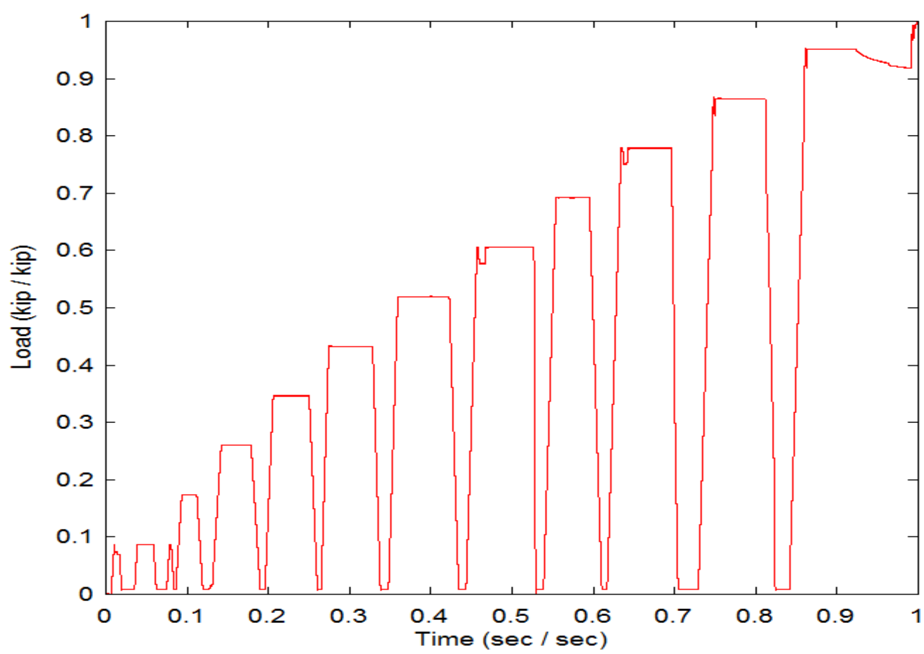

Figure 10. Typical loading protocol (normalized).

4.2 Specimens 1 through 3

Specimens 1 through 3 were constructed using the same forms. The reinforcement bars were gauged, then the formwork was built using 2 x 4's (51 mm x 102 mm) and 0.5 in (13 mm) plywood with the open area of the formwork being the side of the specimen. The formwork was measured and dimensions were verified to match the drawings for the specimens. The specimens were cast in one pour. After the specimen was poured, moist burlap and a thick plastic tarp were placed on the open side of the form for a minimum of 10 days to minimize early shrinkage cracks. The cast specimen remained in the forms until the average of the 6 in x 12 in (152 mm x 305 mm) cylinders reached 1500 psi (10.3 MPa).

Once the specimen reached 2000 psi (13.8 MPa), the specimen was lifted and positioned in the loading frame to be tested. **Figure 11** is a photo of Specimen 1 formwork.

Figure 11. Typical formwork prior to casting (Specimen 1 shown).

4.2.1 Specimen 1

Specimen 1 was loaded with a single AASHTO-type tire patch (20 in x 10 in (508 mm x 254 mm)) load plate centered at mid-span of the 10 ft (3.05 m) clear span, representing the case where there is no asphalt overlay. The specimen was loaded at 5 kip (22.2 kN) increments as mentioned previously. **Figure 12** shows the location of the load plate.

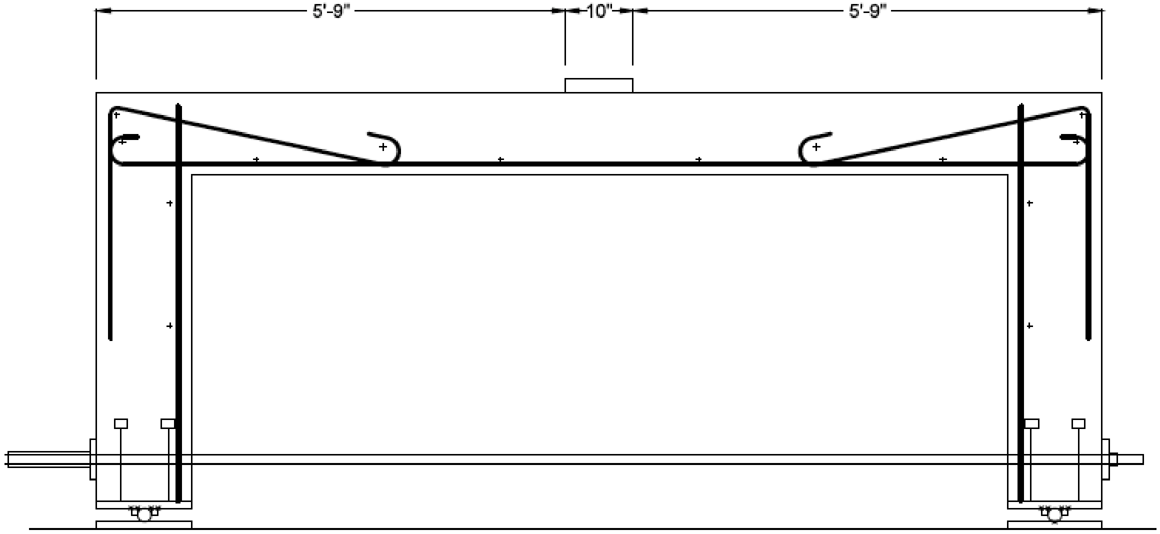

Figure 12. Specimen 1 load plate location (AASHTO single-axle patch centered about mid-span).

4.2.1.1 Behavior

Specimen 1 did not show any cracking until a load of 20 kip (89.0 kN) was reached. The first visible cracks were vertical flexural cracks at three locations along the mid-span in the positive moment region. The next visible cracking occurred at 25 kip (111 kN) in the top left corner, the negative moment region, of the specimen. This crack was a vertical flexural crack. In addition, at this loading, two more flexural cracks in the positive moment region developed and two of the previous flexural cracks continued to propagate. At a 30 kip (133 kN) loading, the top right corner cracked, a second flexural crack developed in the top left corner and merged with the crack that developed at 25 kip (111 kN). The flexural crack to the right, in the positive moment region, started to propagate in a diagonal direction towards the loading plate. The remaining flexural cracks continued to grow. At this loading, there were five flexural cracks and one inclined crack in the positive moment region and two flexural cracks in the negative moment, one in each corner. The flexural cracks continued to propagate during the rest of the loading scenario. At a 35 kip (156 kN) loading and a 45 kip (200 kN) loading, cracks developed where the slab and the legs intersect on the outside of the left and right leg respectively. **Figure 13** shows the observed cracking for Specimen 1.

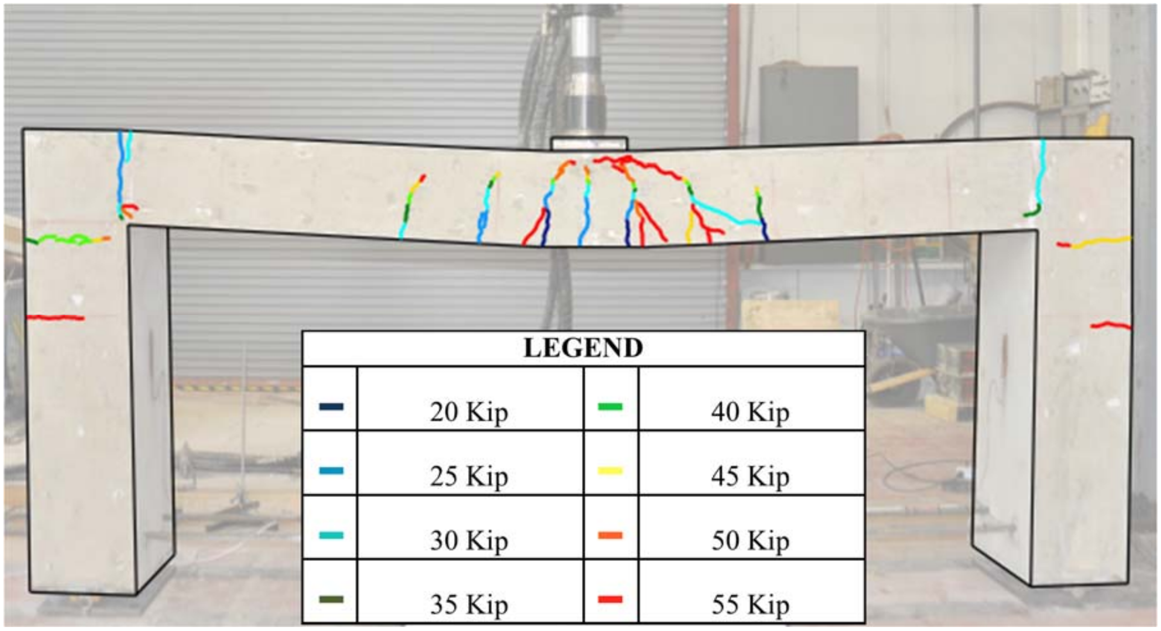

Figure 13. Specimen 1 crack map during 55 kip (245 kN) load holding.

Along with crack mapping at every load increment, crack width measurements were taken at various cracks throughout the specimen. **Figure 14** shows a graph of the crack widths vs. the normalized load and within the graph is a drawing of where the cracks were located. Three of the vertical cracks in the positive moment region and two of the vertical cracks in the negative moment region had their crack widths measured and graphed. As **Figure 15** shows, after the applied load reached 45 kip (200 kN), the strain at mid-span dramatically increased, and the five measured cracks have a large increase in width. The crack widths on both top corners, in the negative moment region, were measured to be 0.28 in (7.1 mm) at 55 kip (245 kN) applied load. The largest crack width in the positive moment region was measured to be 0.16 in (4.0 mm). This crack was located below the centerline of the load plate. Crack E has two locations that were measured – the side of the specimen and the top of the specimen. Just before failure, when the applied load was 55 kip (245 kN), the crack width on the side of crack E was 0.28 in (7.1 mm). This crack width was a large increase from the previously measured crack from the 0.01 in (0.25 mm) width at 30 kip (133 kN).

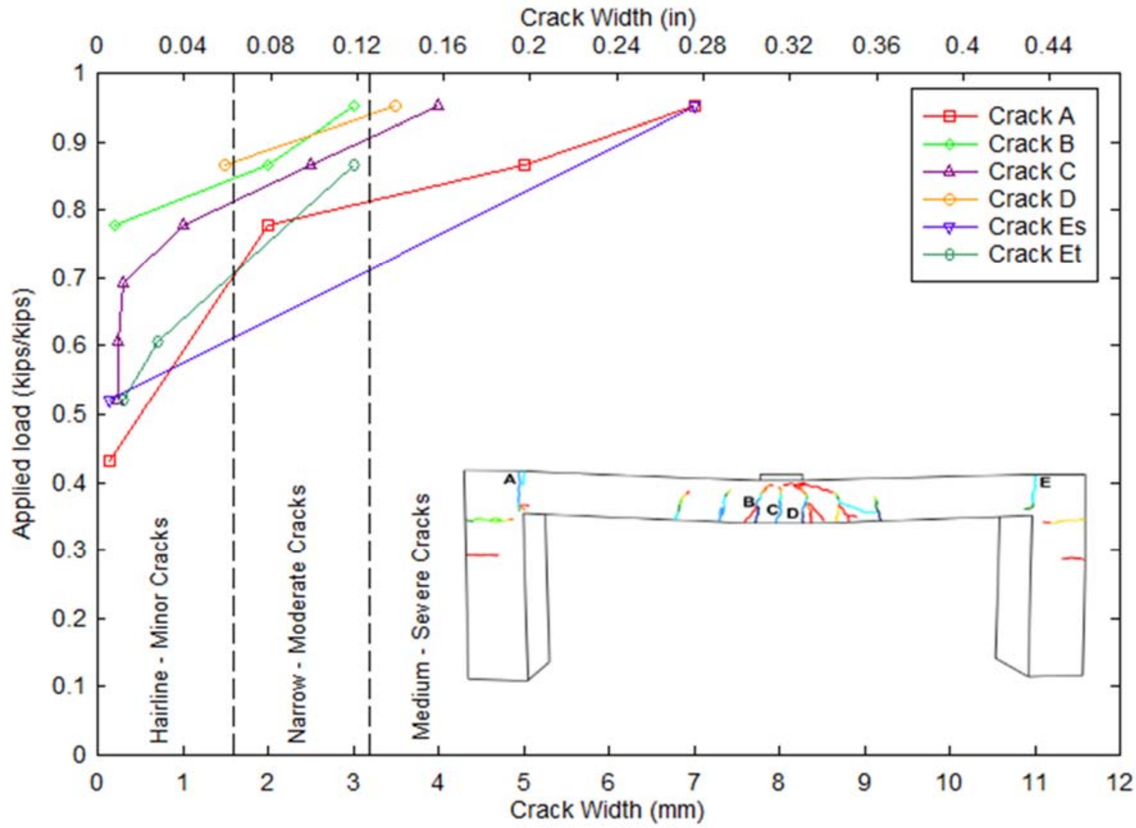

Figure 14. Specimen 1 crack widths. The vertical dashed lines represent crack width limits according to the AASHTO Guide Manual for Element Inspection (AASHTO 2011).

The strain gauge placed on the lower leg (Location A) experienced little to no strain. It was not until an applied load of 55 kip (245 kN) that the rebar in the location had a recorded strain above 75 με. The strain gauge placed on the unique hook bar at the same height as the bottom of the slab (Location B) did not see significant strain until 35 kip (156 kN) for the left leg and 45 kip (200 kN) on the right leg. The gauge placed on a 30 ° angle from the bottom of the slab (Location D) exhibited little strain until just before failure when the strain surpassed theoretical yield. The strain gauges placed at the corners and the strain gauge located at mid-span experienced the highest strains.

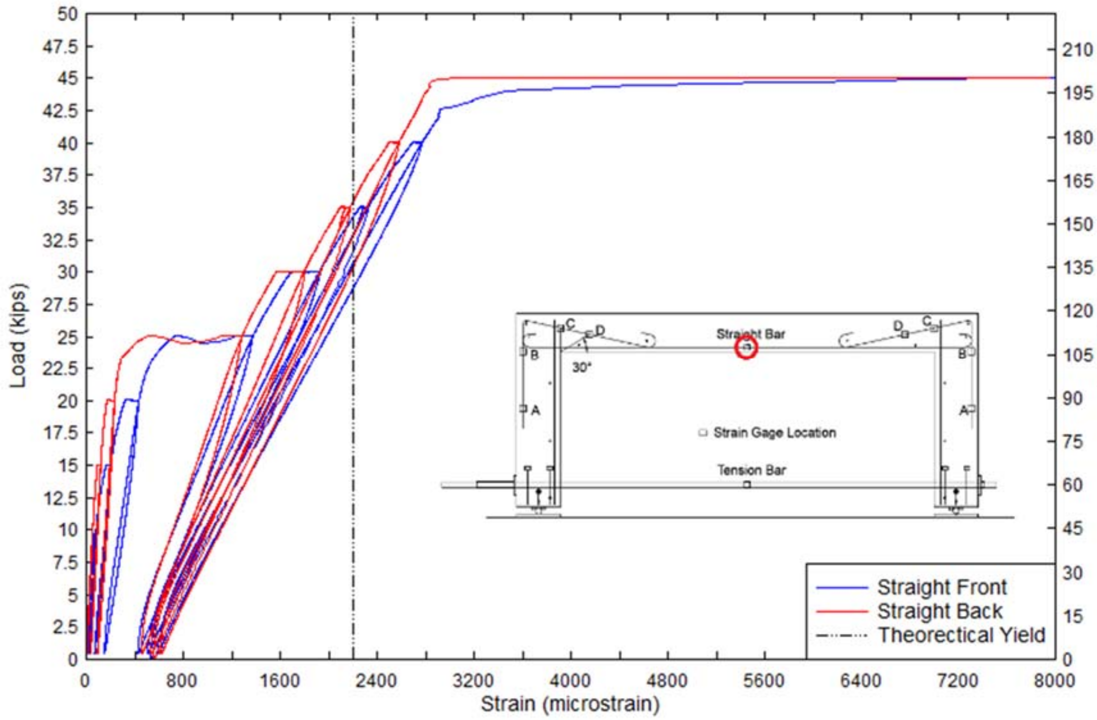

Figure 15. Specimen 1 rebar strain mid-span (Location straight bar). The dashed vertical line corresponds to theoretical yield of the rebar.

The cracking that was observed matches up with the results recorded from the strain gauges on the rebar. The first cracking in the center of the clear span, as seen in the crack map, occurred at 25 kip (111 kN). At this same load, on the load vs. strain graph of the center gauge (**Figure 15**), there is a noticeable increase in strain. At every new crack or propagation of an already visible crack, in the center of the span, there is a noticeable increase in strain. The graph of the strain gauge in the top corners of the specimen mirrors the cracking that was observed. The load vs strain graphs for strain gauges at mid-span and at the top corner (Location C) are shown in **Figure 15** and **Figure 16**, respectively. Load vs. strain graphs for locations A, B, and D are shown in Appendix C.

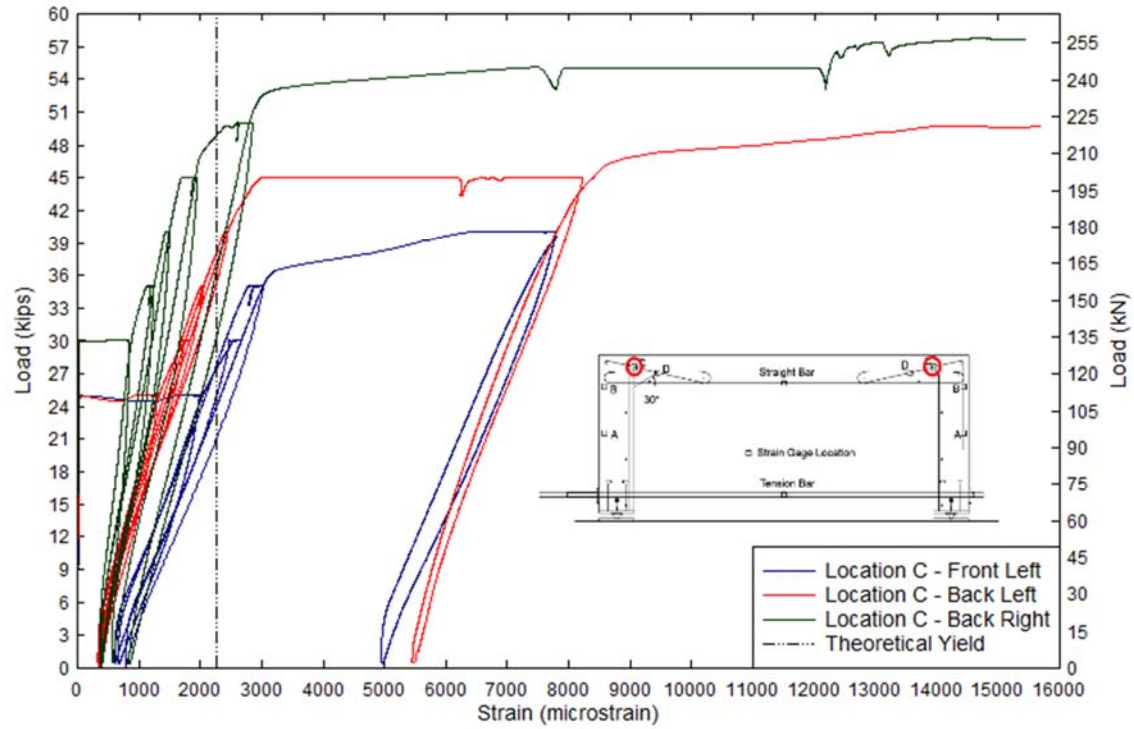

Figure 16. Specimen 1 rebar strain diagonal bars (Location C). The dashed vertical line corresponds to theoretical yield of the rebar.

Displacement measurements were taken on each side of mid-span using string potentiometers and are shown in **Figure 17**. Along with these measurements, four linear potentiometers were placed on each side of the supports to determine the displacement at these locations. The mid-span displacements were averaged. The average of the support displacements, although it was negligible, was then subtracted out. The results were then graphed, load vs. displacement. The results from the displacement graph matched up closely with the results from the mid-span strain gauge. The first noticeable change in displacement occurred at a loading of 25 kip (111 kN). The displacement, after it had been loaded to the specified increment, left a residual displacement. The largest residual displacement occurred during the 50 kip (222 kN) load increment. The displacement increased from 0.41 in (10.4 mm) when the loading reached 50 kip (222 kN) and 0.84 in (21 mm) when the specimen was unloaded. Prior to the 45 kip (200 kN) loading increment, there was minimal residual displacement. After the applied 45 kip (200 kN) was unloaded to 0.5 kip (2.22 kN), there was a residual displacement of 0.15 in (3.8 mm). The largest residual displacement occurred after the 50 kip (222 kN) load increment. During the 55 kip (245 kN) loading, the string potentiometers were removed to protect them after the specimen failed.

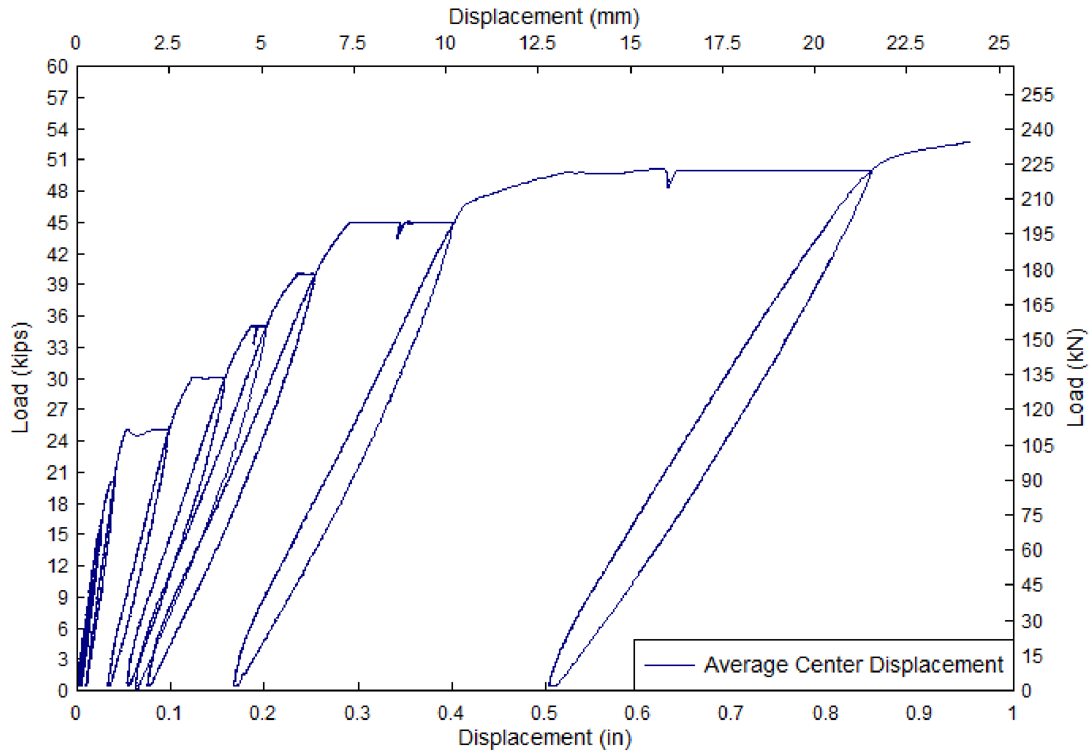

Figure 17. Specimen 1 mid-span displacement.

4.2.1.2 Failure

The failure load for Specimen 1 was 57.8 kip (257 kN). The failure-type was flexural-shear failure. Prior to specimen failure, the mid-span rebar and the top corner rebar yielded, i.e. developed plastic moment hinges in these locations. After the rebars had yielded, the specimen at mid-span was able to have a larger increase in deflection. Extensive deformation at the mid-span location led to the specimen ultimately failing in shear. The beginning of the shear crack first started at 30 kip (133 kN). The ACI 318-14 code assumes that shear cracks develop at an angle of 45 °. Specimen 1, however, had an average failure crack angle of 30 °, as illustrated in **Figure 18**, originating from the edge of the loading plate.

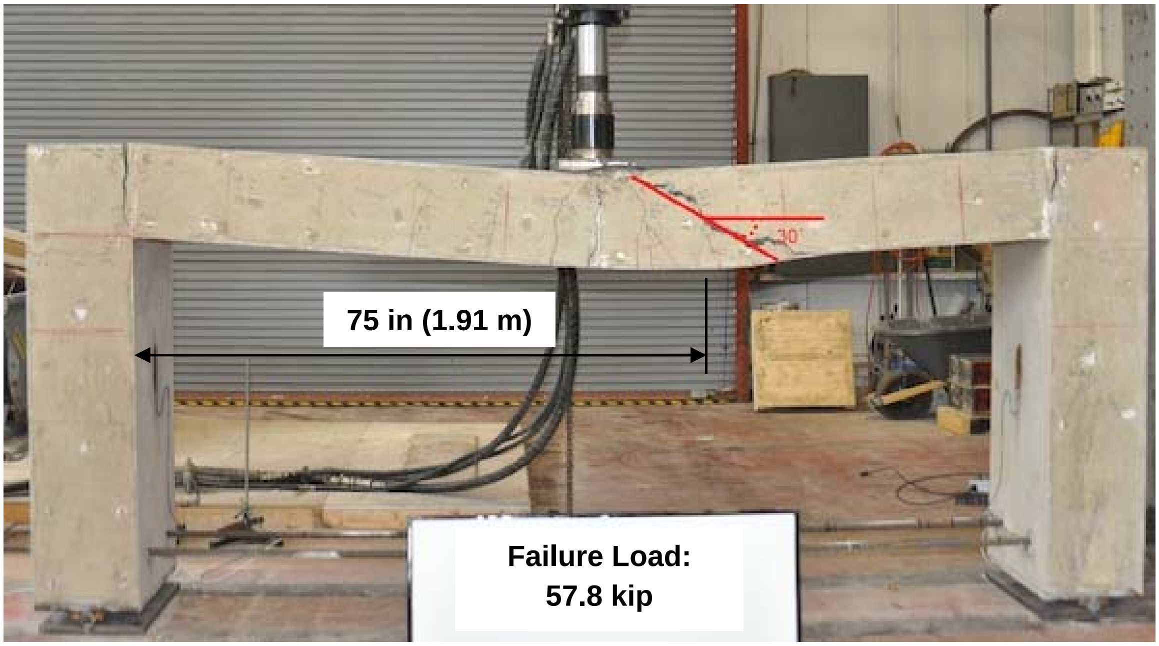

Figure 18. Specimen 1 after failure.

4.2.2 Specimen 2

Specimen 2 was loaded with two (2) AASHTO-type tire patch (20 in x 10 in (508 mm x 254 mm)) load plates with the plate centerlines spaced 4 ft (1.22 m) apart, which represents the tandem axle spacing (AASHTO 2012). The plates were centered about mid-span. The specimen was loaded in 5 kip (22.2 kN) increments and then unloaded to 0.5 kip (2.2 kN). When the failure load was approached, the loading was changed from the predetermined 5 kip (22.2 kN) increment loading to displacement-controlled loading to failure. Displacement-controlled loading allowed for increased control and capture of post-peak behavior. **Figure 19** shows the location of the load plates.

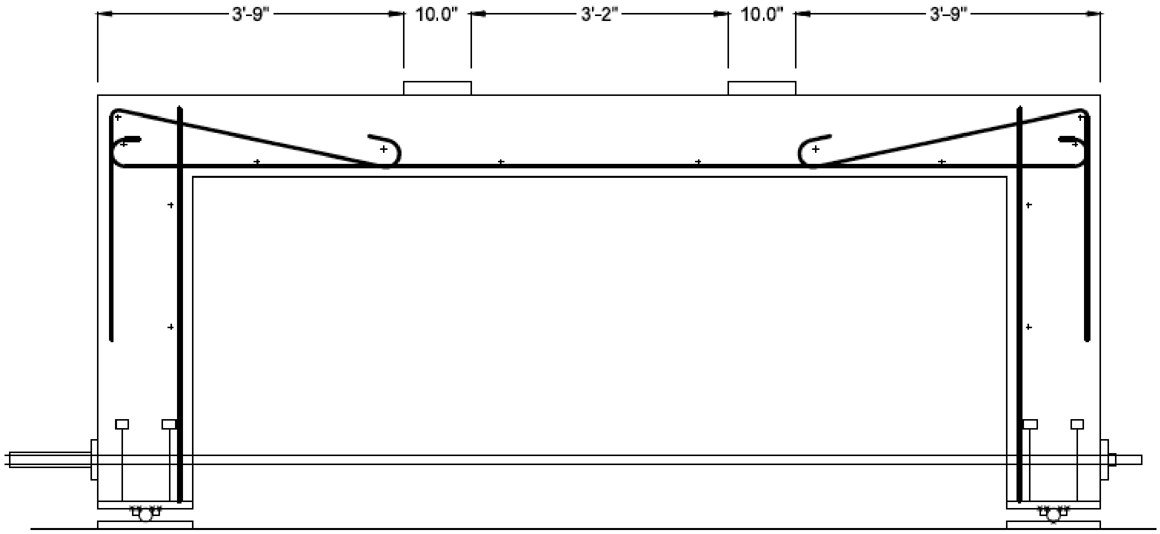

Figure 19. Specimen 2 load plate locations (AASTHO tandem-axle patches centered about mid-span).

4.2.2.1 Behavior

Specimen 2 did not show any cracking until a total load of 2 x 17.5 kip = 35 kip (2 x 77.8 kN = 156 kN) was reached. At this load, the top left corner showed a vertical flexural crack and five vertical flexural cracks developed between the two load plates. At 40 kip (178 kN), the right corner cracked and three new flexural cracks developed between the load plates in the positive moment region. The cracks that developed at the 35 kip (156 kN) applied load all continued to propagate. At 2 x 22.5 kip = 45 kip (2 x 100 kN = 200 kN) applied load, a crack developed on the outside of each leg at the height of the bottom of the slab. At 2 x 37.5 kip = 75 kip (2 x 167 kN = 334 kN) applied load, the outermost flexural cracks in the positive moment region began to crack on the diagonal. At that point, the approximately vertical cracks began to propagate at an angle. **Figure 20** shows the crack map during an applied total load of 2 x 45 kip = 90 kip (2 x 200 kN = 400 kN).

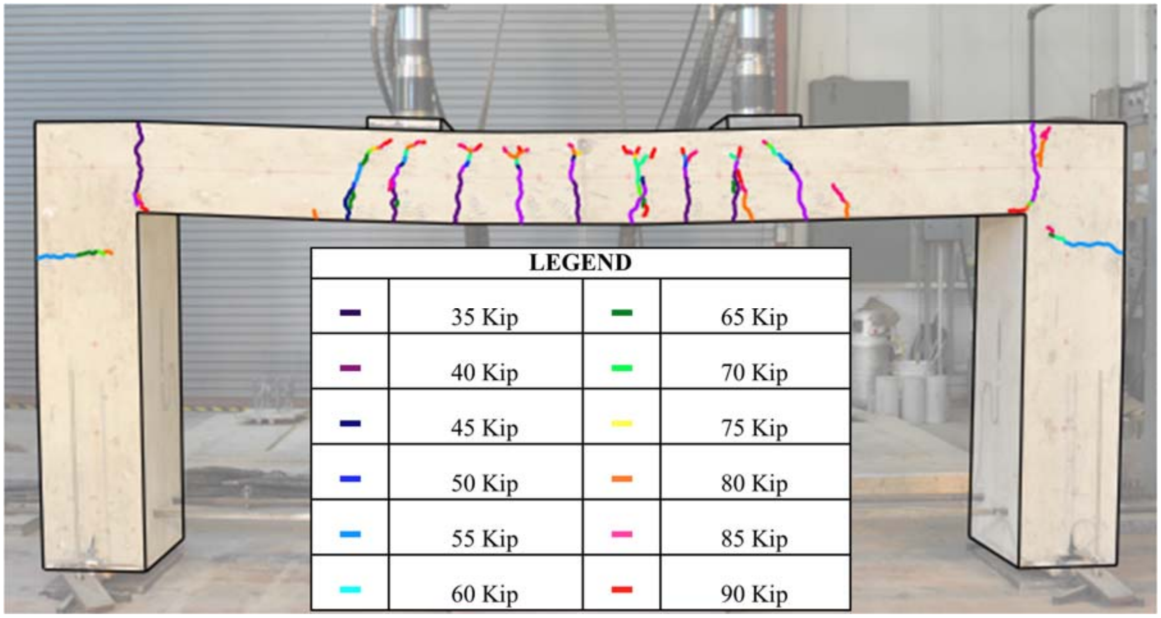

Figure 20. Specimen 2 crack map (total applied load = 90 kip (400 kN)).

Along with crack mapping at every load increment, crack width measurements were taken at various cracks throughout the specimen. **Figure 21** shows a graph of the crack widths vs. the normalized load and within the graph is a drawing indicating which cracks were measured. Overall, 13 cracks were measured and graphed. 9 cracks were located in the positive moment region and the other four were located in the negative moment region. Between total applied loads of 85 kip (378 kN) and 90 kip (400 kN), the two top corner cracks experienced a large increase in width. Both cracks increased from 0.22 in (5.6 mm) to 0.40 in (10.2 mm). These cracks were the largest cracks measured on Specimen 2. The cracks on the legs measured 0.02 in (0.5 mm) and 0.03 in (0.8 mm) for the left and right side, respectively. The flexural cracks in the positive moment region, at an applied load of 90 kip (400 kN), ranged from 0.04 in (1.0 mm) to 0.12 in (3.0 mm). The widest crack was located at the mid-span and the narrowest cracks were located on the outside edges of the load plates.

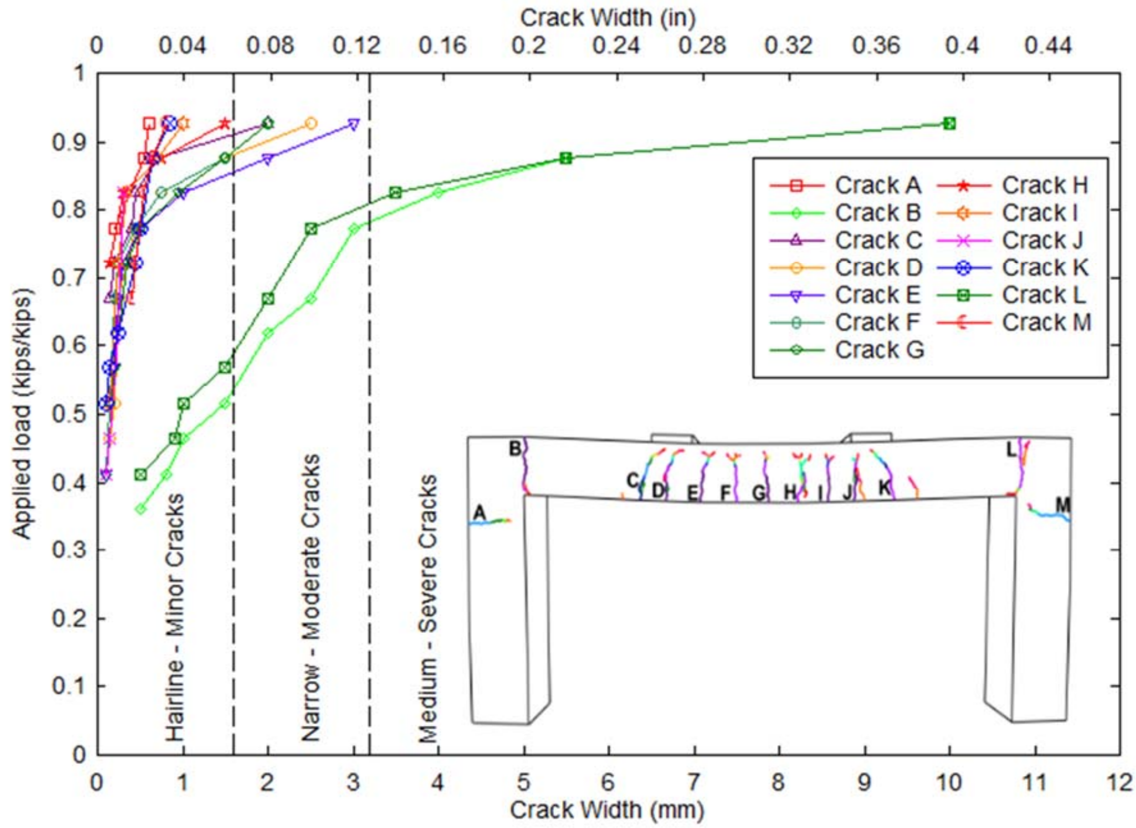

Figure 21. Specimen 2 crack widths. The vertical dashed lines represent crack width limits according to the AASHTO Guide Manual for Element Inspection (AASHTO 2011).

The strain gauge placed on the lower leg experienced little to no strain, similar to Specimen 1. At the failure load, the strain gauge placed on the bottom of the unique hook bars only had a strain between 225 με to 450 με. The strain gauge placed on the unique hook bar at the same height as the bottom of the slab (Location B), did not see significant strain until 50 kip (222 kN) for the right leg and 60 kip (267 kN) on the right leg. The gauge placed on a 30 ° angle from the bottom of the slab (Location D) exhibited little strain throughout the entire testing. The strain never surpassed theoretical yield, 2346 με. The strain gauges placed at the corners (**Figure 23**) and the strain gauge located at mid-span (**Figure 22**) experienced the most strain.

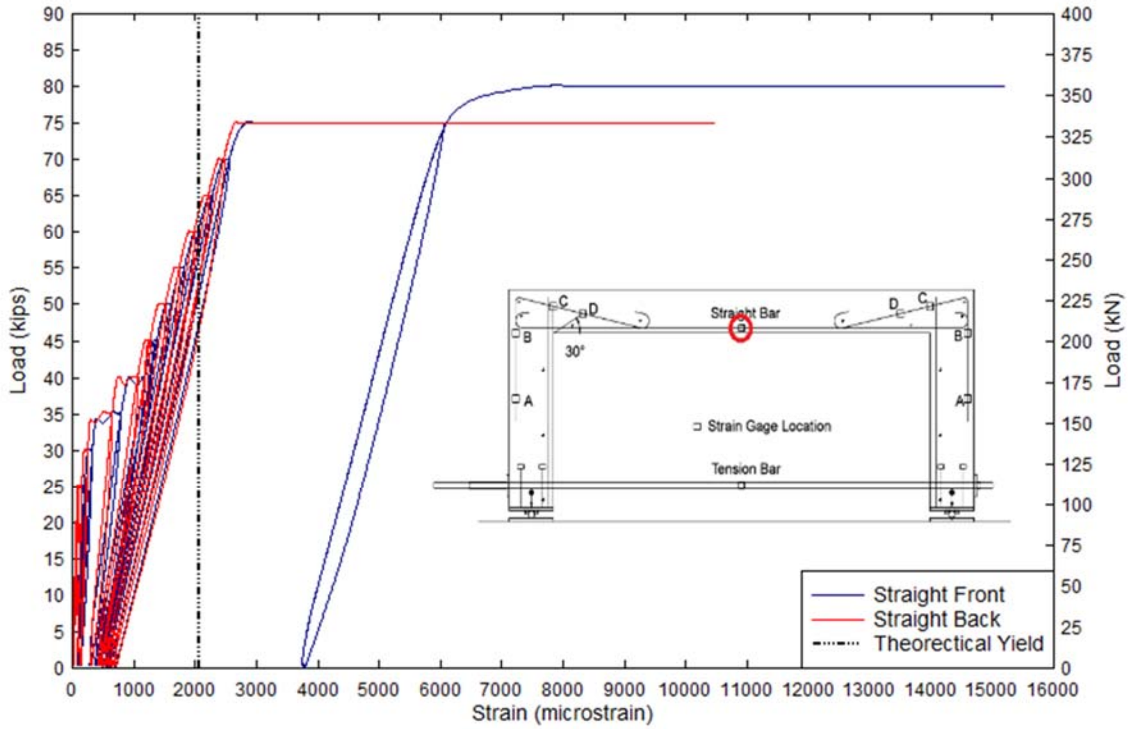

Figure 22. Specimen 2 rebar strain mid-span (Location straight bar). The dashed vertical line corresponds to theoretical yield of the rebar.

The cracking that was observed matches up with the results recorded from the strain gauges in the top corner and the mid-span on the rebar. The first cracking in the center of the clear span, as seen in the crack map, occurred at 35 kip (156 kN). However, the first noticeable change in the stress strain graph occurs at 25 kip (111 kN). At the first crack, there is another noticeable change in the stress strain graph. At every new crack or propagation of an already visible crack, in the center of the span, there is a noticeable increase in strain. The graph of the strain gauge in the top corners of the specimen mirrors the cracking that was observed. The first noticeable change in strain occurs on the left corner strain gauges at an applied load of 35 kip (156 kN), which is when the first crack appeared. The top right corner first cracked at an applied load of 40 kip (178 kN) as well as the first significant change in strain. The large strain values in the top corners correspond with the large crack widths measured. The load vs strain graphs for strain gauges at mid-span and at the top corner (Location C) are shown in **Figure 22** and **Figure 23** respectively. Load vs. strain graphs for locations A, B, and D are shown in Appendix C.

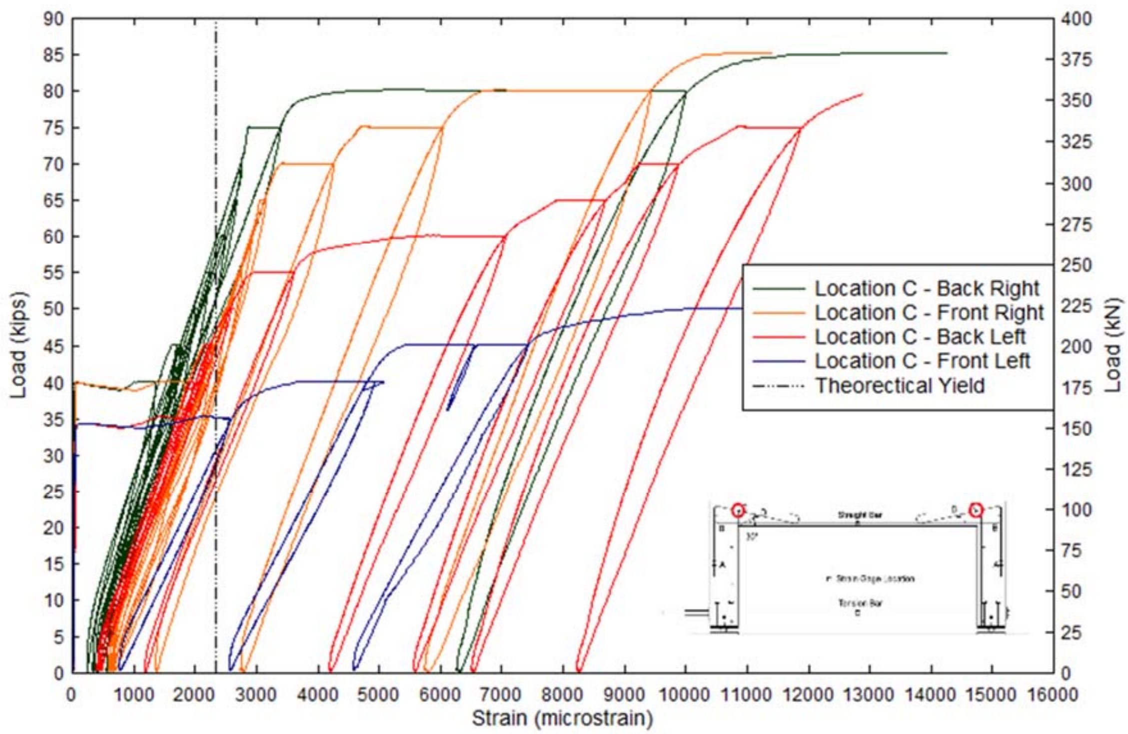

Figure 23. Specimen 2 rebar strain diagonal bars (Location C). The dashed vertical line corresponds to theoretical yield of the rebar.

The displacement results were graphed, load vs. displacement, as done with Specimen 1 in **Figure 24**. The results matched up closely with the results from the mid-span cracks and crack widths gauge. As the displacements began to increase, cracks began to become more noticeable. The first noticeable change in displacement occurred at a loading of 35 kip (156 kN), which corresponds to the first crack developing at mid-span. At a total load of 35 kip (156 kN), the displacement at each incremental applied load produced residuals. The largest residual displacement occurred during the 95 kip (423 kN) load increment. The displacement increased from 1.4 in (35.6 mm) to 2.9 in (73.7 mm) when the specimen was unloaded. Prior to the 80 kip (356 kN) loading increment, there was minimal (less than 0.1 in (2.5 mm)) residual displacement. After the 95 kip (423 kN) loading, the string potentiometers were removed to protect them after the specimen failed.

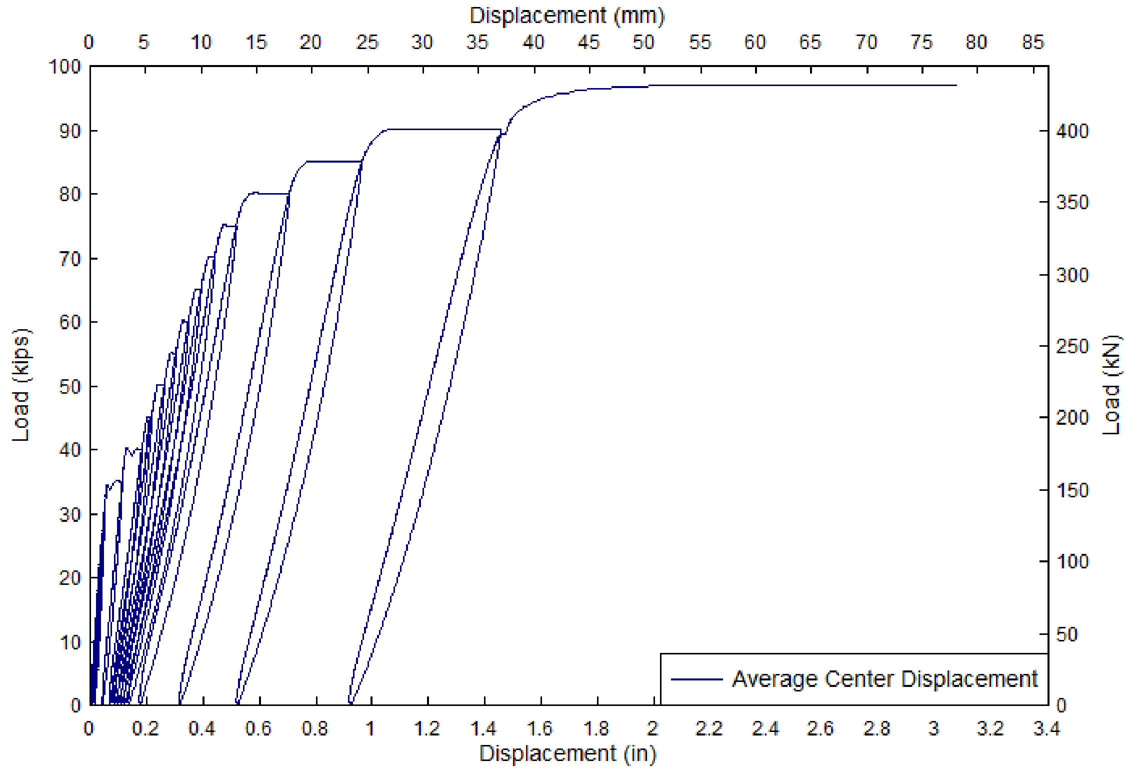

Figure 24. Specimen 2 mid-span displacement.

4.2.2.2 Failure

The failure load for Specimen 2 was 2 x 48.5 kip = 97.0 kip (2 x 216 kN = 431 kN). The failure-type was flexural-shear failure as shown in **Figure 25**. Prior to specimen failure, the mid-span rebar and the top corner rebar yielded. After the rebars yielded, mid-span deflection continued to increase. The deflection then led to the specimen to ultimately have a shear-type failure. Similar to Specimen 1, the failure crack angle for Specimen 2 was approximately 30 °. The crack started at the middle of the left load plate. The shear crack was within mid-span, just on the edge the unique hooked corner bar.

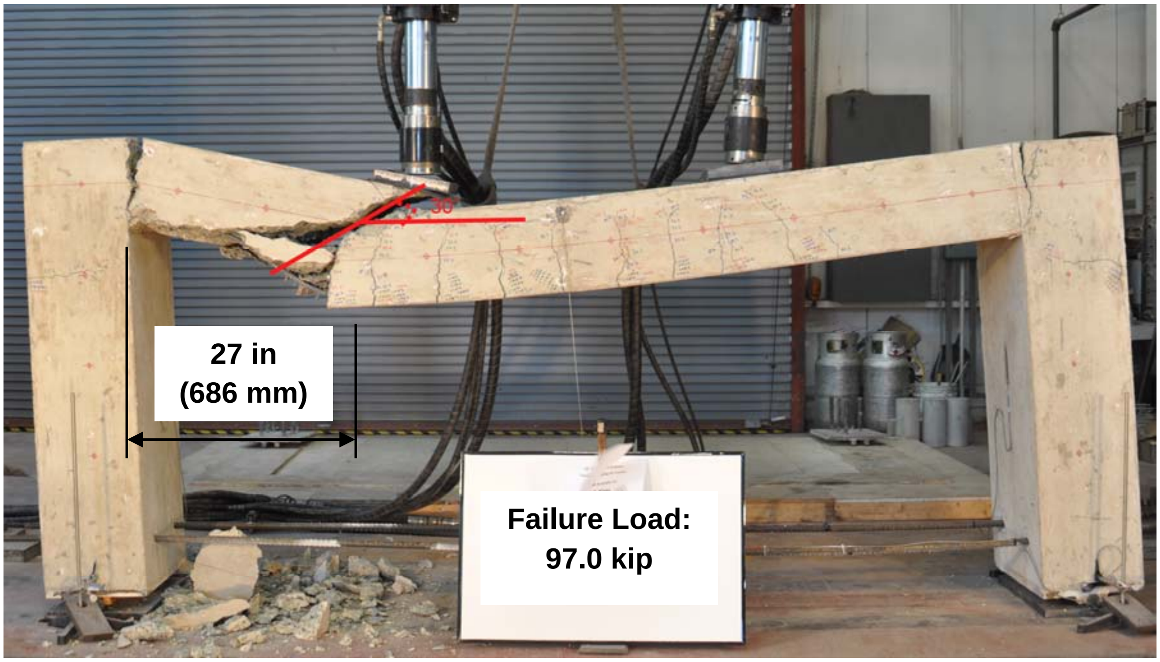

Figure 25. Specimen 2 after failure.

4.2.3 Specimen 3

Specimen 3 was the last 24 in (610 mm) wide specimen with 10 ft (3.05 m) clear span that was tested. The two load plates were again placed according to AASHTO tandem axle spacing ((i.e. 4 ft (1.22 m) spacing)) as illustrated in **Figure 26**. During this testing, the left most loading plate was placed so that the outside of the plate was the effective depth, *d* = 10.2 in (259 mm) away from the inside face of the leg. The plates were placed *d* away from the face of the leg because the largest shear force is expected to be caused in this configuration. The loading scenario was the same for Specimen 3, as it was for Specimens 1 and 2. The specimen was loaded in 5 kip (22.2 kN) increments and after each applied load the specimen was unloaded to 0.5 kip (2.22 kN).

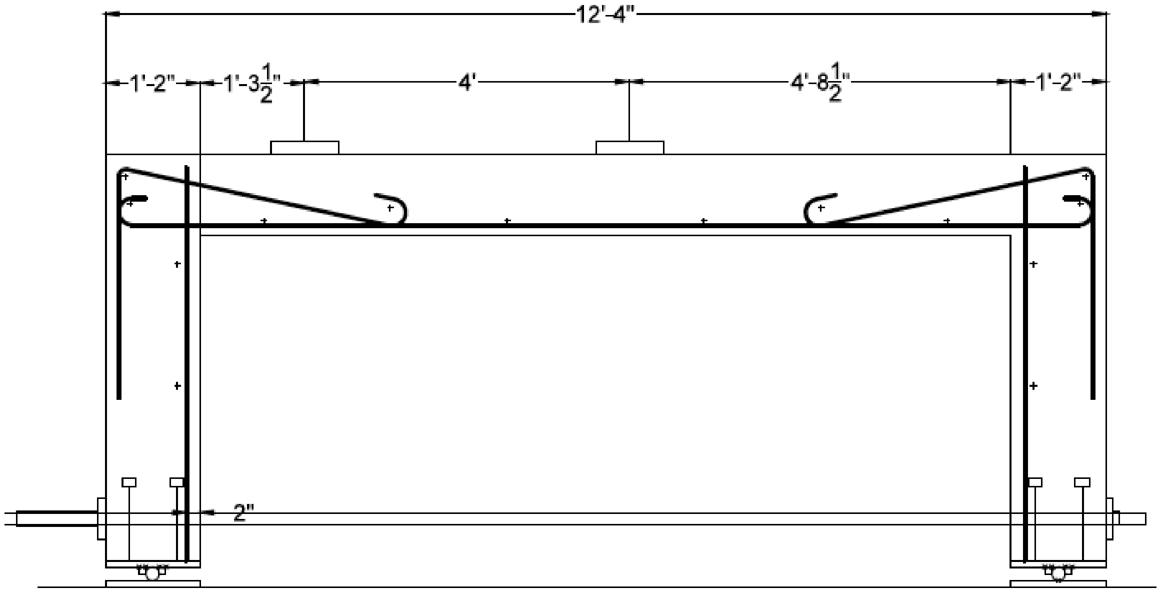

Figure 26. Specimen 3 load plate locations (AASTHO tandem-axle patches with one patch *d* away from the edge of the left support).

4.2.3.1 Behavior

Specimen 3 did not begin to crack until a total load of 30 kip (133 kN) was reached. **Figure 27** shows a detailed crack map. Four cracks developed in the positive moment span. Two cracks developed on each side of mid-span. Another crack developed on the right side of the specimen, opposite of the location where the load was applied. This observation was contrary to the expected location of the first crack. It was predicted that the top left corner would be the first location to crack since, according to ACI 318-14, the largest shear force is located effective depth, *d*, away from the face of the support. Two more cracks developed to the left of mid-span in the positive moment region at 35 kip (156 kN). At 45 kip (200 kN), a crack on the right leg developed, in line with the bottom of the slab. Between 35 kip (156 kN) and 60 kip (267 kN), the cracks around mid-span continued to propagate. At 60 kip (267 kN), the left corner developed a crack and the left leg developed a crack in line with the bottom the slab. At 65 kip (289 kN), two (2) cracks to the right of mid-span began to develop into shear cracks. Up until 75 kip (334 kN), all cracks in the positive moment region were centered about the load plate placed close to mid-span. At 75 kip (334 kN), two flexural cracks developed below the left load plate and a third flexural crack developed at 80 kip (356 kN) applied loading.

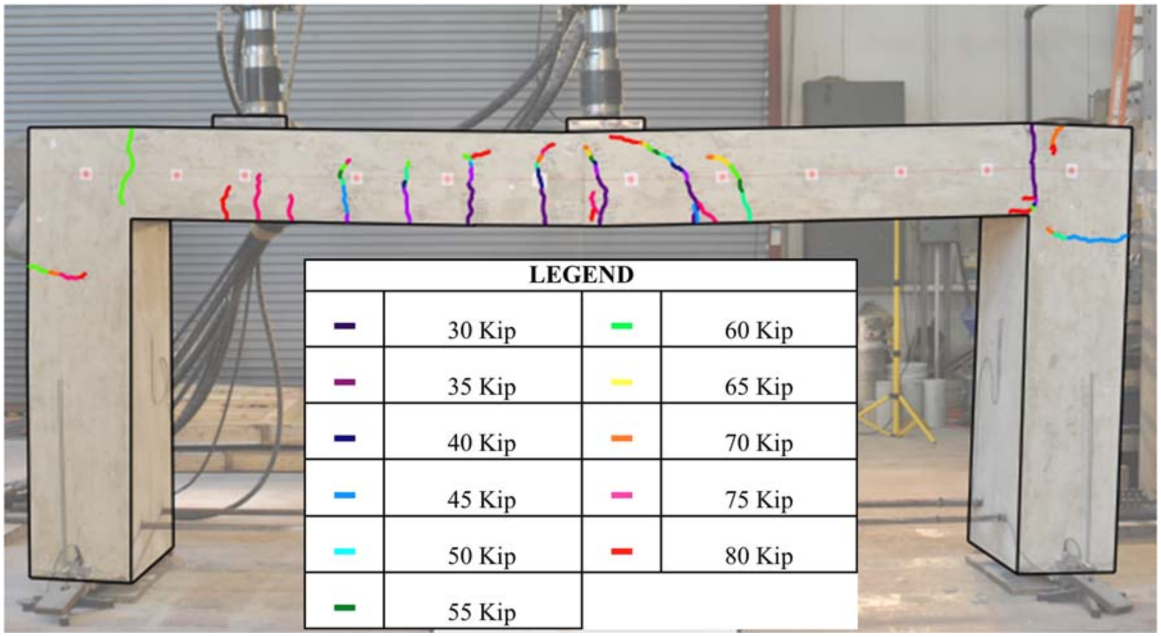

Figure 27. Specimen 3 crack map during an applied load of 80 kip (356 kN).

Similar to Specimens 1 and 2, along with crack mapping at each load increment, crack width measurements were taken at crack locations. **Figure 28** shows a graph of the crack widths vs. the normalized load and within the graph is a drawing of which cracks were measured. The largest crack widths were located in the top left corner, crack H. Between 30 kip (133 kN) and 65 kip (289 kN), the crack widths increased linearly from 0.01 in (.35 mm) to 0.10 in (2.75 mm). The largest width increase occurred between 65 kip (289 kN) and 80 kip (256 kN). Between these two applied loads, the crack width increased from 0.01 in (0.3 mm) to 0.28 in (7.1 mm). Crack F, located below the centerline of the right load plate reached a maximum width of 0.12 in (3.0 mm) prior to failure and crack E, located at the left edge of the right load plate, reached a maximum width of 0.08 in (2.0 mm). The other six (6), including the failure crack, G measured cracks reached a maximum of 0.04 in (1.0 mm).

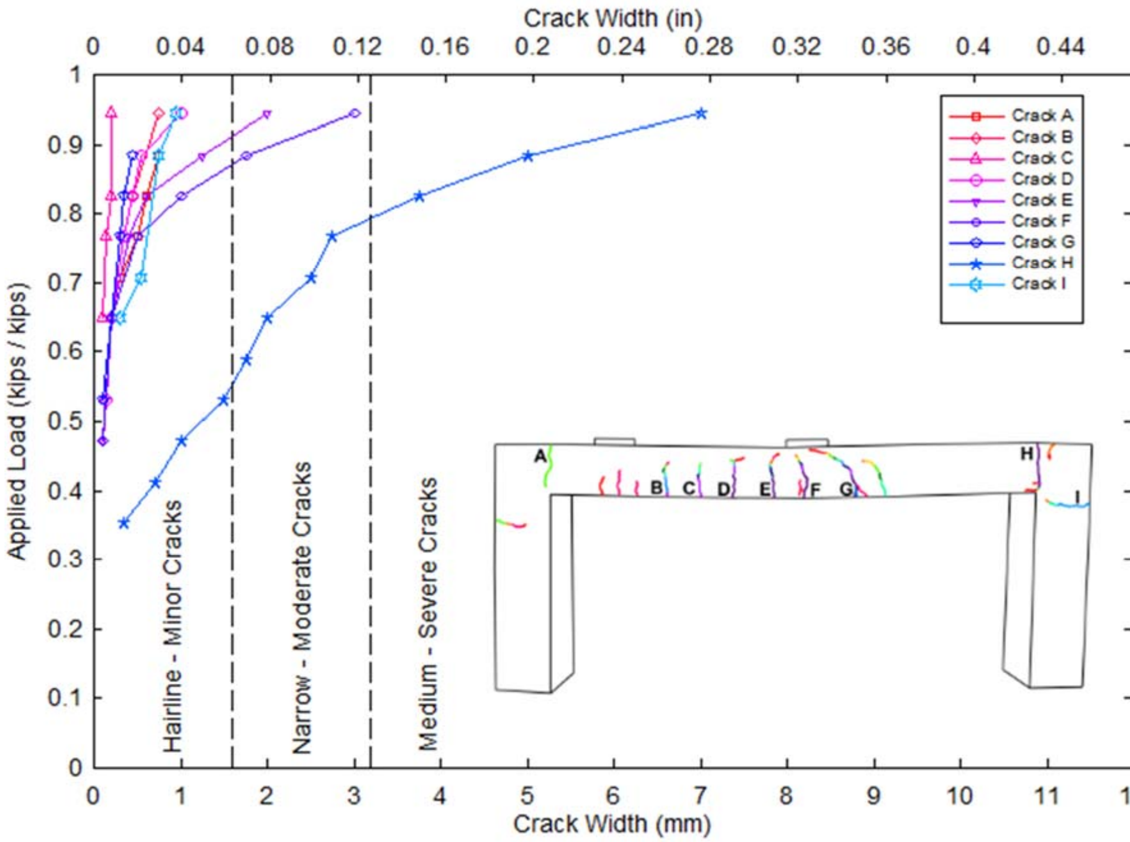

Figure 28. Specimen 3 crack widths. The vertical dashed lines represent crack width limits according to the AASHTO Guide Manual for Element Inspection (AASHTO 2011).

The strain gauge placed on the lower leg experienced little to no strain, similar to the first two specimens. At the failure load, the strain gauge placed on the bottom of the hooked bars only had a strain between 250 με on the left leg to 1000 με on the right leg. The strain gauges placed in the left leg on the hook bar at the same height as the bottom of the slab, did not see any significant strain. The maximum strain was recorded to be approximately 350 με. The strain gauge placed in the right leg however began to experience strain after the 45 kip (200 kN) loading and at 60 kip (267 kN), when a crack developed, there was significant change in strain. At failure, the strain was approximately 2950 με, which is beyond theoretical yield. The gauge placed below the left loading patch on a 30 ° angle from the bottom of the slab exhibited little strain throughout the entire testing. The strain reached a maximum of 100 με. Once again, the right side (away from the loading) experienced strain around 1800 με. The strain began to rapidly increase after the 30 kip (133 kN) loading, which corresponds with the first crack.

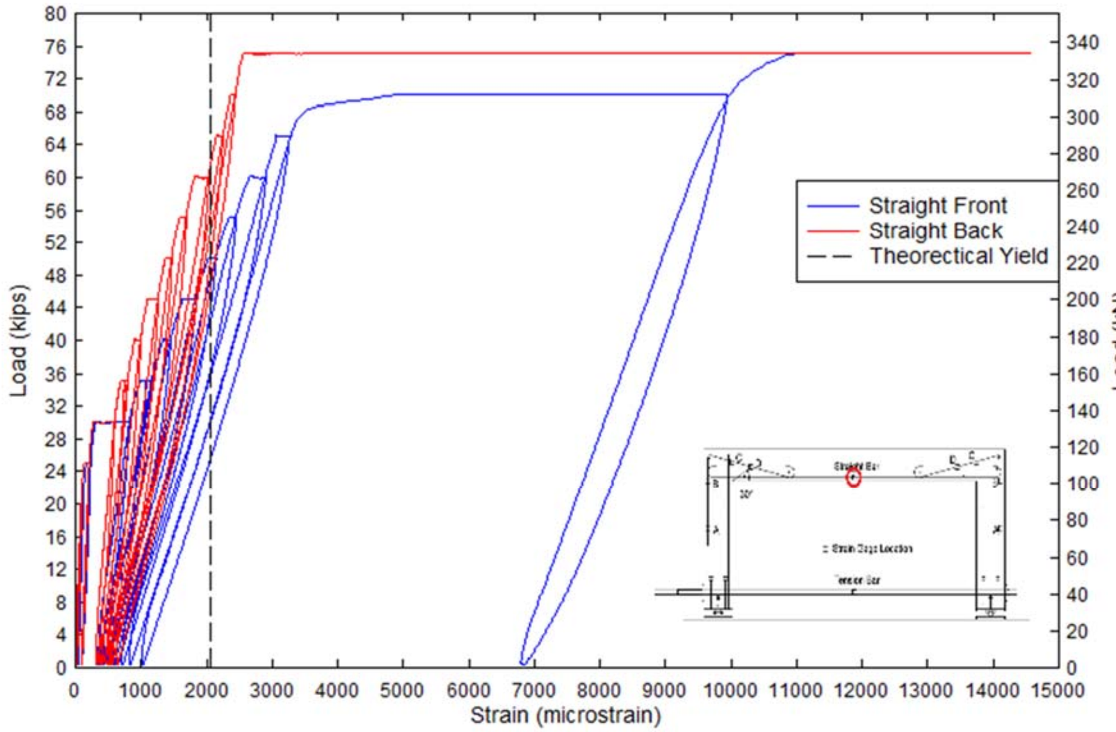

Figure 29. Specimen 3 rebar strain mid-span (Location straight bar). The dashed vertical line corresponds to theoretical yield of the rebar.

The strain gauges placed at the corners and the strain gauge located at mid-span experienced the most strain (**Figure 29**). The cracking that was observed matches up with the results recorded from the strain gauges in the top corner and the mid-span on the rebar. The first cracking in the center of the clear span, as seen in the crack map, occurred at 30 kip (133 kN), which coincided with the two flexural cracks that developed on each side of the loading plate closest to mid-span. At every new crack or propagation of an already visible crack, in the center of the span, there was a noticeable increase in strain. The graph of the strain gauge in the top corners of the specimen mirrors the cracking that was observed (**Figure 30**). The first noticeable change in strain occurred on the right corner strain gauge at an applied load of 30 kip (133 kN), which is when the first crack appeared. The top left corner first cracked at an applied load of 60 kip (267 kN) as well as the first significant change in strain. The large strain values in the top right corner correspond with the large crack widths shown in Figure 4-18. The load vs strain graphs for strain gauges at mid-span and at the top corner (Location C) are shown in **Figure 29** and **Figure 30**, respectively. Load vs. strain graphs for locations A, B, and D are shown in Appendix C.

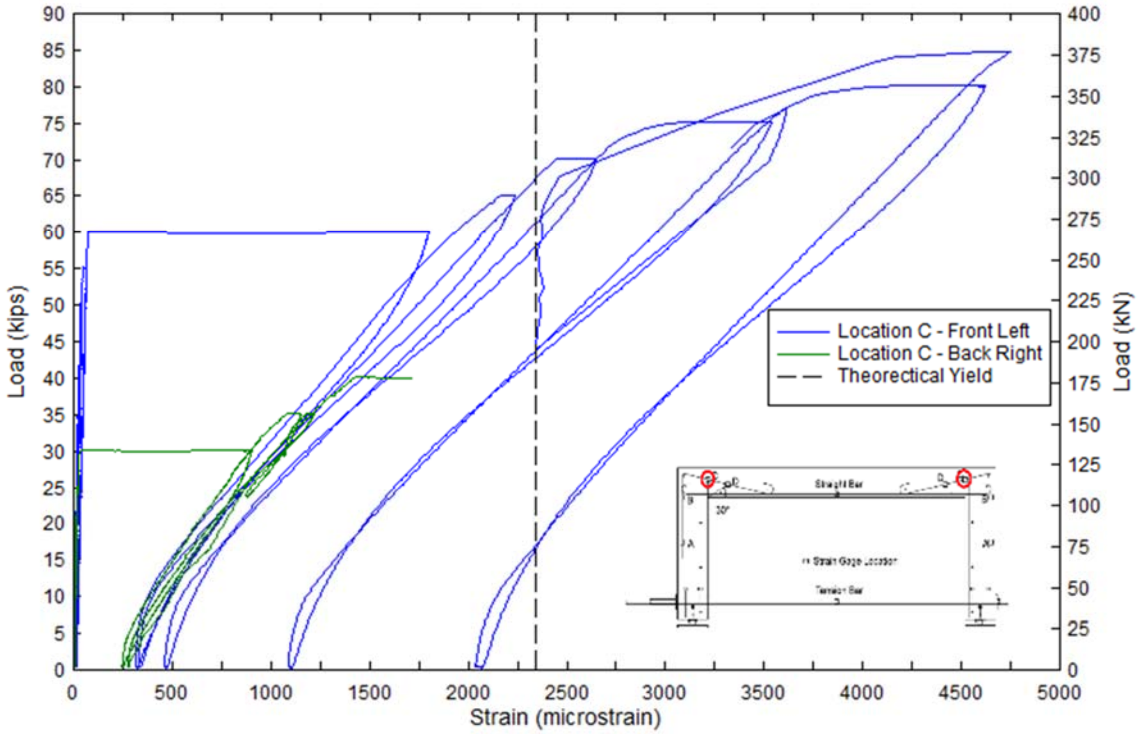

Figure 30. Specimen 3 rebar strain diagonal bars (Location C). The dashed vertical line corresponds to theoretical yield of the rebar.

The displacement results were graphed, load vs. displacement, as done with Specimen 1 and Specimen 2 (**Figure 31**). The results matched up closely with the results from the mid-span cracks and crack widths gauge. The first noticeable change in displacement occurred at a loading of 30 kip (133 kN), which corresponds to the first crack developing at mid-span. After the applied 30 kip (133 kN), the displacement at each incremental applied load resulted in residual displacements. Prior to the 70 kip (311 kN) loading increment, there was minimal (less than 0.2 in (5.1 mm)) residual displacement. The largest residual occurred during the 85 kip (378 kN) load increment. The displacement increased from 1.0 in (25.4 mm) to 1.7 in (43.2 mm) when the specimen was unloaded. After the 85 kip (378 kN) loading, the string pots were removed to protect them after the specimen failed.

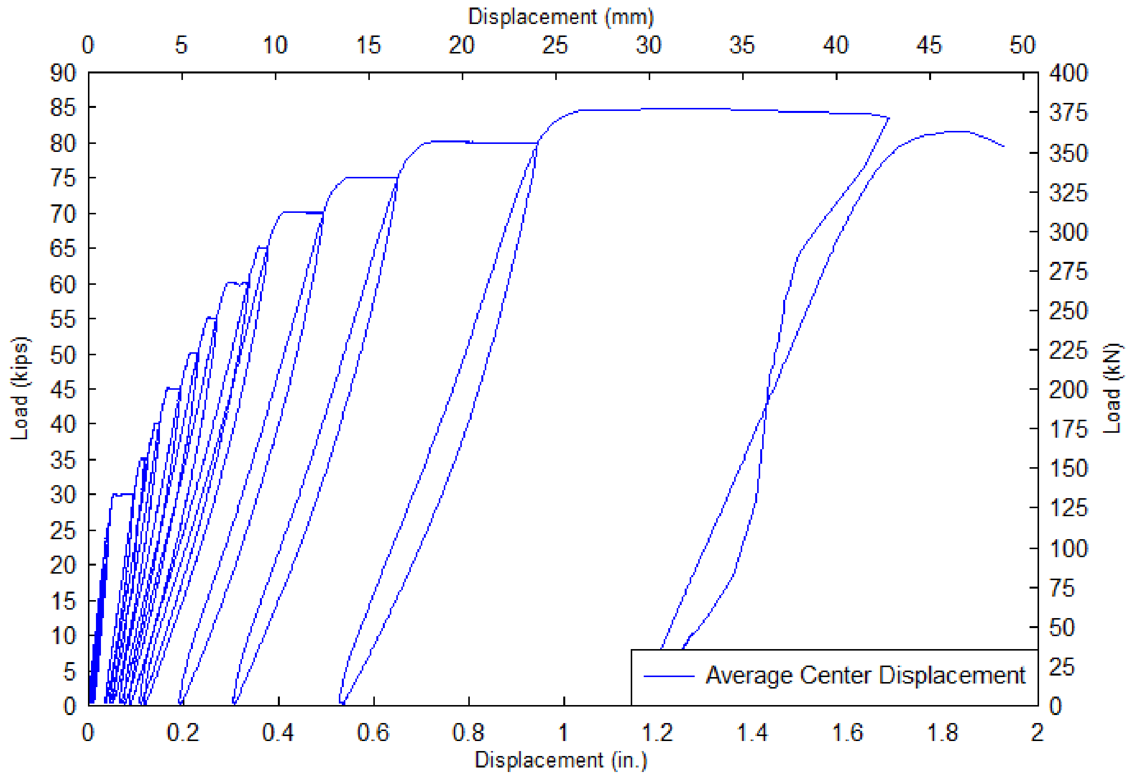

Figure 31. Specimen 3 mid-span displacement.

4.2.3.2 Failure

The failure load for Specimen 3 was 2 x 42.5 kip = 85 kip (2 x 189 kN = 378 kN). The failure method was a flexural-shear failure, similar to the first two specimens (**Figure 32**). The failure mirrored the failure for Specimen 1. The failure crack occurred on the edge of the mid-span loading plate closest to the roller support. Prior to specimen failure, the mid-span rebar and the top corner rebar yielded. After the rebar yielded, the specimen at mid-span was able to have a larger increase in deflection. The deflection then led to the specimen to ultimately have a shear failure. Similar to Specimens 1 and 2, the failure crack for Specimen 3 was approximately 30 °. The crack started at the right edge of the right load plate. The shear crack once again was within mid-span, between the hooked bars. An explanation for the high shear strength in the left corner is the proximity of the concentrated load to the support, which has been found by other researchers (Sherwood 2008). Essentially, the portion between the support and the left load patch is a disturbed region that does not follow beam theory. As such, a strut-and-tie approach would be more appropriate to model this region. Alternatively, the shear strength factor, β, which ACI 318-14 assumes to be equal to 2 for their simple method, may be increased. A more detailed discussion of this observation can be found in Section 5.1.3.

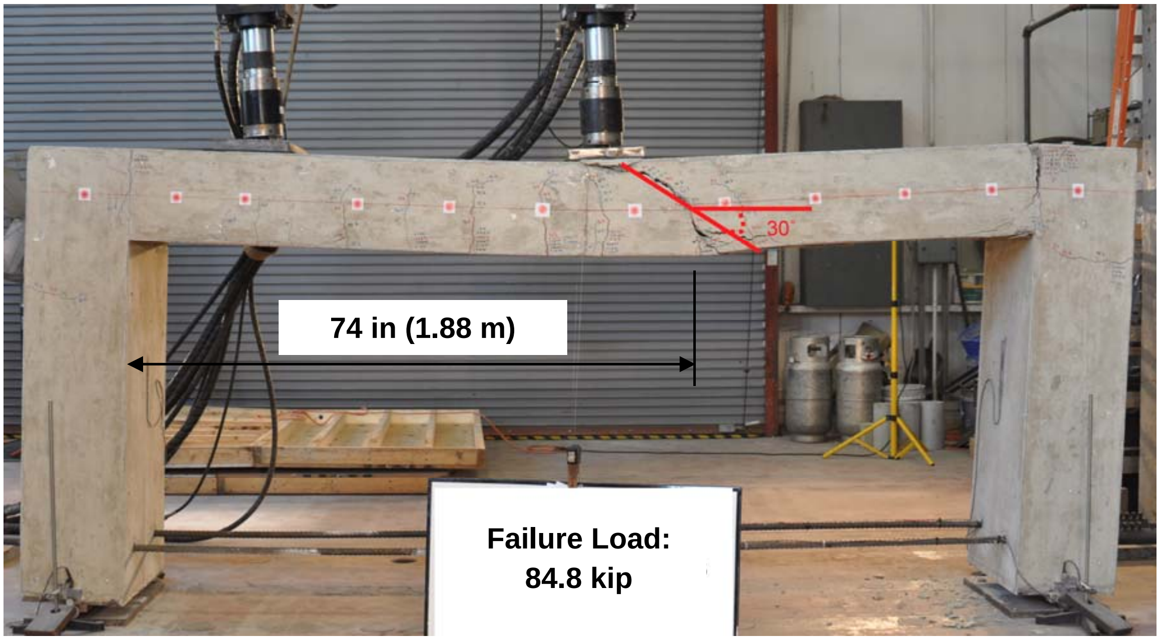

Figure 32. Specimen 3 after failure.

4.3 Specimen 4

Specimen 4 was constructed using wood forms, similar to the first three specimens. The formwork was built using 2 x 4s (51 x 102 mm), 4 x 4s (102 x 102 mm), and ½ in. (13 mm) plywood. The specimen was cast-in-place and in two pours due to its large size. The legs were poured first and after the legs were poured, moist burlap and a thick plastic tarp were placed on the open side of the form until the heat of hydration period of the specimen was completed. The cast specimen remained in the forms until the average concrete compressive strength of the 6 in x 12 in (152 mm x 305 mm) cylinders reached a minimum of 1500 psi (10.3 MPa). The top surfaces of the legs were left unfinished to create the best bond possible with the slab. Once the forms were stripped from the legs, form work was built to cast the slab. A cold joint, similar to what would occur in the field was created between the legs and the bottom of the slab. Prior to each pour, the dimensions were verified. Before casting, all bars were strain gauged for a total of 36 strain gauges. As shown in Section 3.2, Specimen 4 had the same cross section as Specimen 1 through Specimen 3 but the width was significantly larger. Instead of being only 24 in (610 mm) wide, Specimen 4 was 11 ft 4 in (3.45 m) wide. Photos of the construction of Specimen 4 are shown in **Figure 33**. Once again, the reason for doing this was to learn how the specimen distributes the loading transversally.

Figure 33. Specimen 4 during casting. Left: Casting of legs, Right: View of slab before casting.

Specimen 4 was initially loaded with an AASHTO single tire patch (20 in x 10 in (508 mm x 254 mm)) load plate centered at mid-span of the 10 ft (3.05 m) clear span (= Sequence 1). The rebar was arranged such that the load plate was placed in same location as the 24 in (610 mm) specimen (Specimen 1) for comparison. The specimen was loaded at 10 kip (44.5 kN) increments due to the high expected failure load. **Figure 34** shows the plan view location of the load plate.

During the loading increments, the maximum applied load for one actuator was reached at 148 kip (658 kN). At this load, little cracking or deformation was observed. At this point, the loading scenario was changed from a single load plate to two load plates spaced 4 ft (1.22 m) away, in a tandem axle formation, about the centerline (= Sequence 2). The loading continued until a maximum total applied load of 240 kip (1068 kN) was reached (i.e., 120 kip (534 kN) in each actuator). At this loading, there was still little cracking or deformation observed. The loading scenario was changed back to a single load plate. This time two actuators were applied side by side to one plate (= Sequence 3). The loading continued on from 148 kip (658 kN) until the specimen failed at a total applied of 2 x 115 kip = 230 kip (2 x 512 kN = 1023 kN).

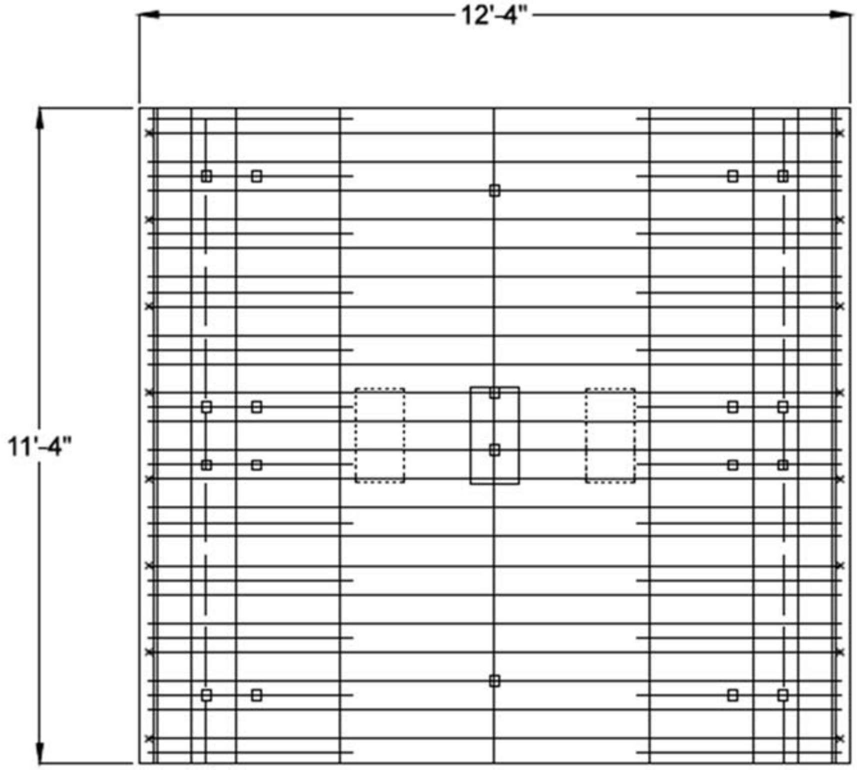

Figure 34. Specimen 4 plan view showing AASHTO single-axle patch loading (Loading Sequence 1 and 3 – full line) and AASHTO tandem-axle patch loading (Loading Sequence 2 – dashed line).

4.3.1 Behavior

The first crack for Specimen 4, with a single load plate (= Sequence 1), was a flexural crack that occurred at an applied load of 80 kip (356 kN). The crack developed on the underside of the specimen directly below the load plate. New flexural cracks began to develop throughout the loading scenario. Prior to switching the loading scenario to the tandem axle set-up (= Sequence 2), there were 10 flexural cracks that developed on the underside of the slab. During the tandem axle loading, the first new flexural crack developed at 190 kip (845 kN). All cracks continued to propagate up until Sequence 2 was stopped. During this time, 8 new cracks developed – four of them were typical flexural cracks and the other four cracks started propagating towards the corners. The set-up was the switched back to a single load plate, this time using two actuators (= Sequence 3). The specimen was loaded to 150 kip (667 kN) and then loaded to failure in 10 kip (44.5 kN) increments, as was previously mentioned. Between 150 kip (667 kN) and failure, no new cracks developed on the underside of the specimen. The flexural cracks that were already open continued to propagate. **Figure 35** shows the underside crack mapping.

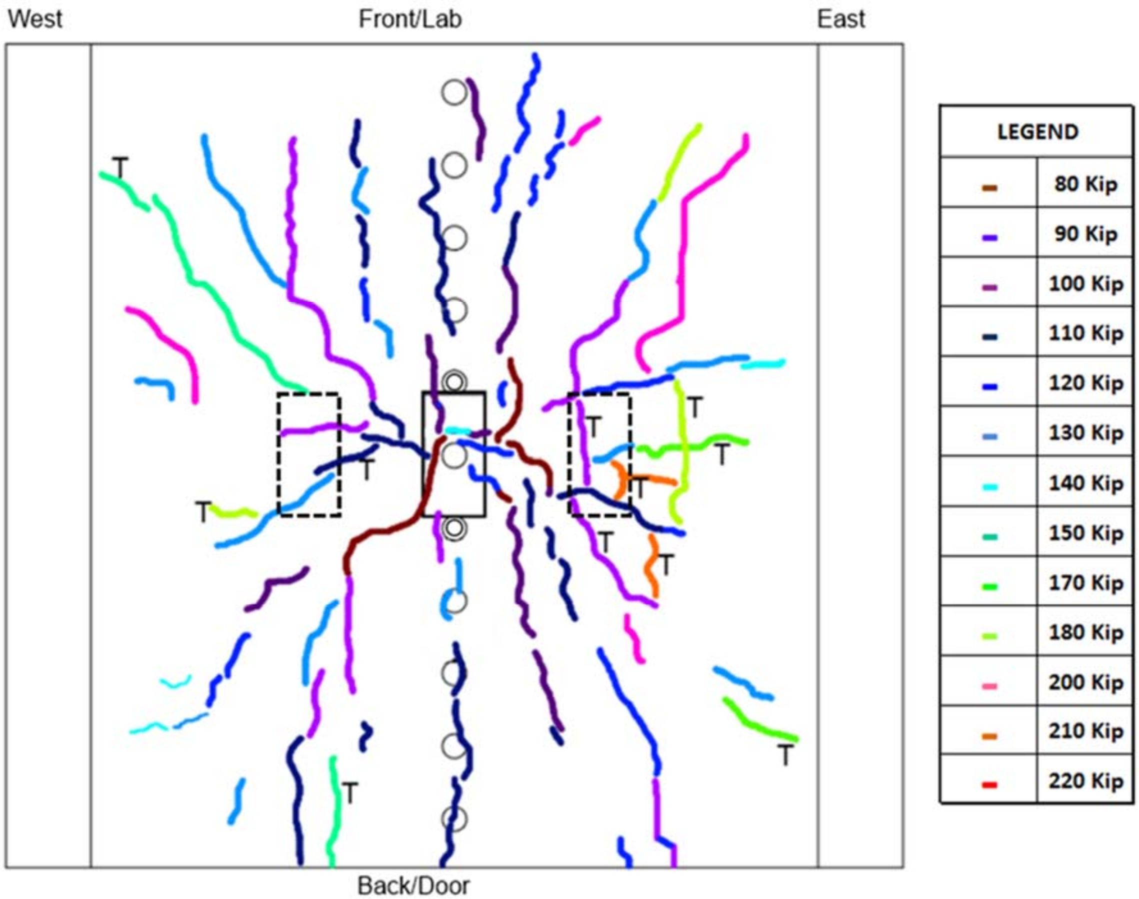

Figure 35. Specimen 4 crack map – Plan view (T denotes cracks that appeared during tandem-axle loading (= Loading Sequence 2) and the grey circles are the locations where vertical displacement was measured; double circles mark the locations that were the same as for Specimens 1 and 2).

Due to the width of Specimen 4, cracking was not immediately visible on the side of the specimen, like for Specimens 1 through 3. The first flexural crack developed at mid-span at 90 kip (400 kN) under the single load plate (= Sequence 1). Between 100 kip (445 kN) and 130 kip (578 kN) four more flexural cracks developed. At a 110 kip (489 kN), a flexural crack developed in the top left corner. At 140 kip (623 kN), the top right corner cracked. No new cracks developed during the tandem axle loading (= Sequence 2). The cracks continued to propagate and widen. **Figure 36** shows the cracking on the side of Specimen 4.

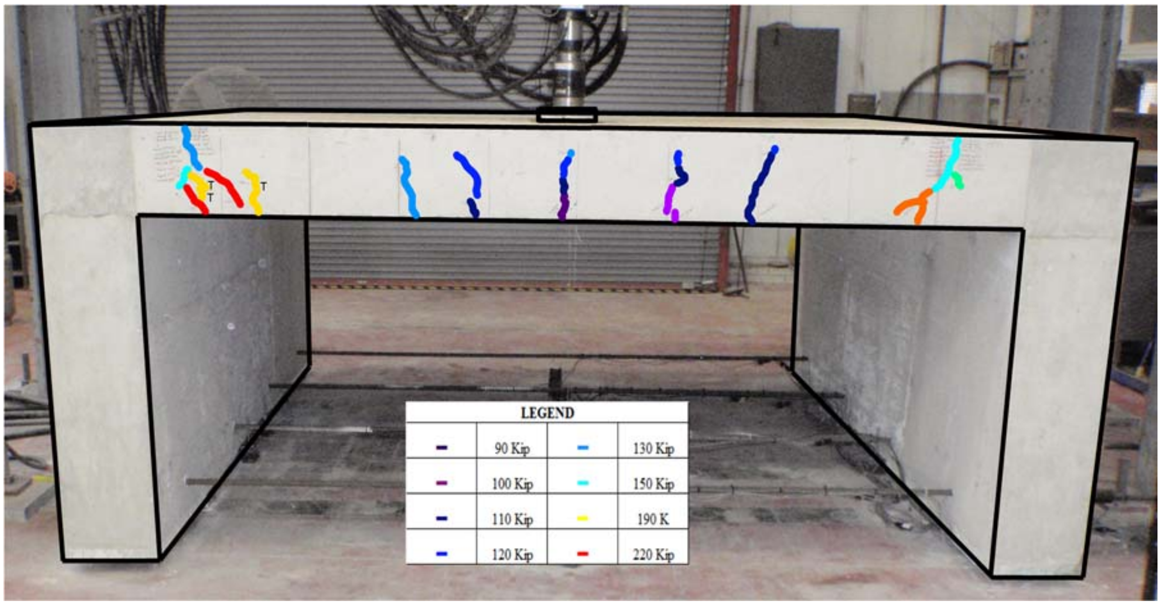

Figure 36. Specimen 4 crack map – Elevation view front/lab (T denotes cracks that appeared during tandem-axle loading (= Loading Sequence 2)).

The cracking on top of the slab of Specimen 4 was typical to that of the 24 in (610 mm) wide specimens – one crack developed in the negative moment region. The initial crack started at mid-span at a load of 110 kip (489 kN). The crack continued to propagate along the leg slab interface. As the cracks propagated towards the sides, the cracks began to move slightly towards the center of the slab. The cracks on the front side and the back right side moved towards the center up to 12 in (305 mm) from the interface. The back left crack moved approximately 36 in (914 mm) from the leg slab interface.

The cracking was noticeable when looking at the load vs. strain graphs (**Figure 37** and **Figure 38**). During Sequence 2, since failure was not reached, there was not any notable strain. At 240 kip (1068 kN), the strain gauges located the hook bar on the leg and 30 ° from the bottom of the slab, had a maximum strain of 1300 με. Many of the strain gauges had strain significantly less than this. The two locations that had the most strain in Specimen 2 exhibited more strain than the other locations. The strain gauge placed at the top corners, Location C, had strain that was a maximum of 2700 με, which is above the theoretical yield. The strain gauges placed at mid-span recorded a maximum strain of 1300 με.

Similar to the tandem axle loading and Specimen 1 through Specimen 3, the strain gauges located on the bottom leg of the hook bar experienced minimal strain, with a maximum of 500 με. The strain gauges located on the hook bar leg in line with the bottom of the slab experience a wide range of strain. The outside bars recorded a maximum strain of 1300 με. The inside bars recorded a maximum strain of 2100 με, which is approximately the theoretical yield of the hook bars. The strain gauges on the hook bar that are located 30 ° from bottom of the slab (Location D) experienced strain ranging from 1500 με to 2100 με besides the back left bar. The hook bar had a recorded a very large strain of 9500 με, which coincides with the cracking that was noticed on top.

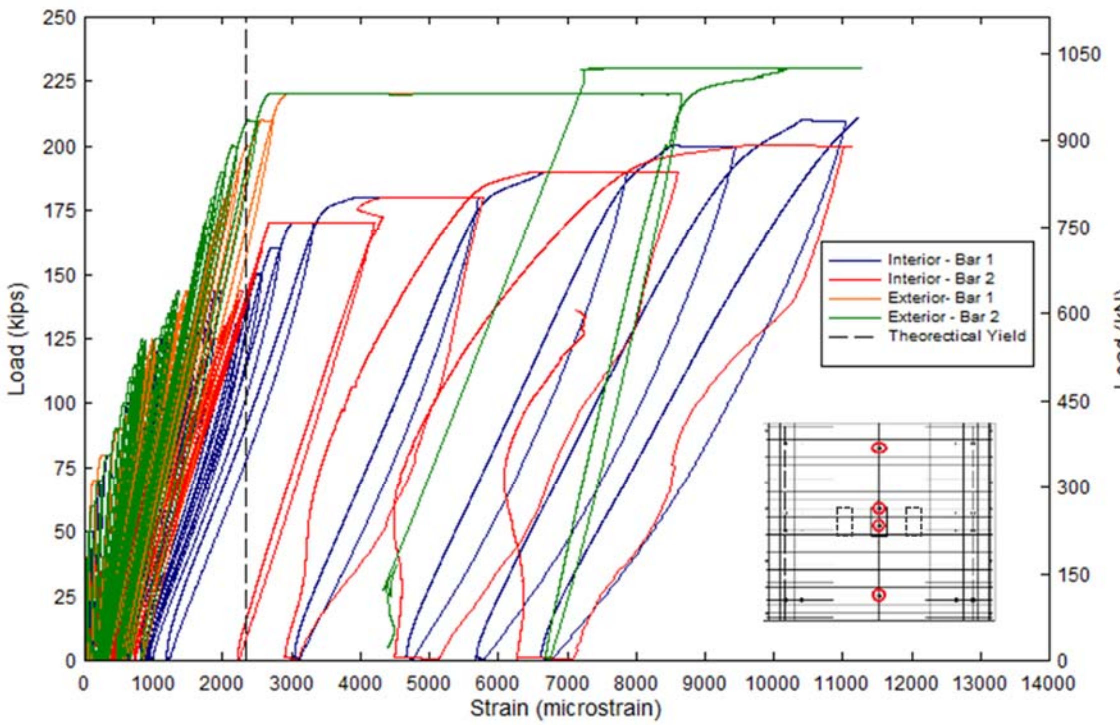

Figure 37. Specimen 4 rebar strain mid-span (Location straight bar – Loading Sequence 1 and 3). The dashed vertical line corresponds to theoretical yield of the rebar.

Unlike the previous three test specimens, the strain readings do not directly match up with the cracking propagation that was observed during the testing. The first crack was observed at 80 kip (356 kN) and five more cracks developed prior to the load vs. strain gauge showed any sign increased residual displacement. The first sign of cracking occurred at 125 kip (556 kN). Specimen 4 was loaded to a 150 kip (667 kN) before the interior mid-span gauges recorded a strain over theorectical yield. The interior mid-span gauges began to have large residuals starting with the 175 kip (778 kN) loading. The exterior mid-span gauges did not reach theorectical yield until the 220 kip (979 kN) loading. At this loading, the strain increased from roughly 2200 με up to 7000 με.

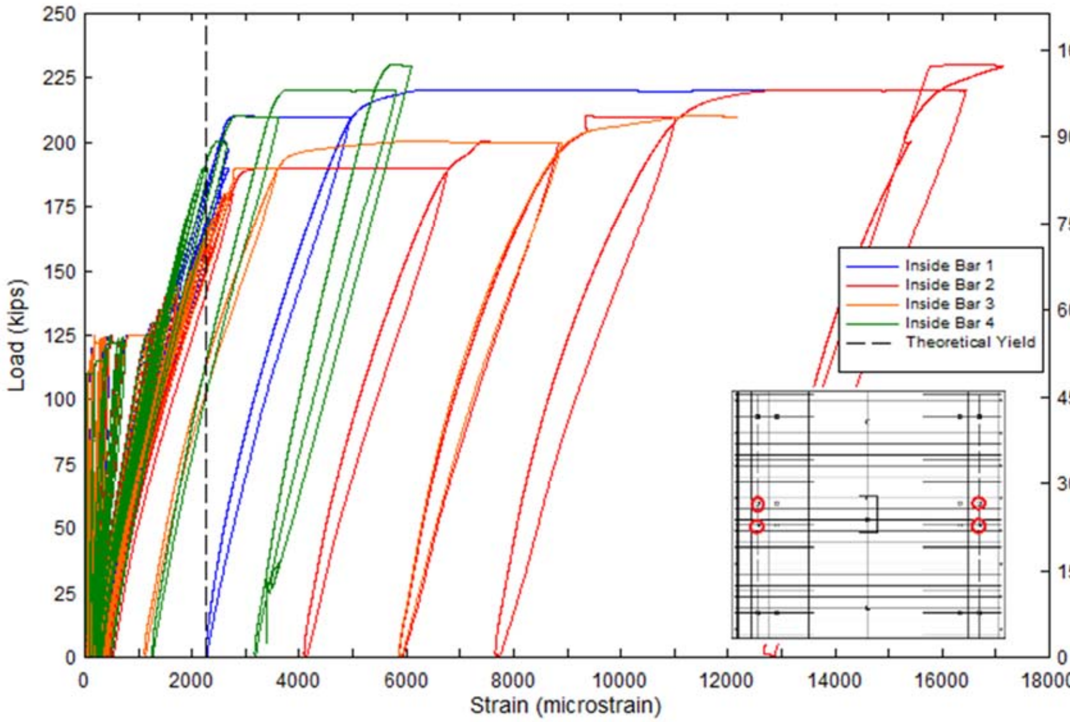

Figure 38. Specimen 4 rebar strain diagonal bars (Location C – Loading Sequence 1 and 3). The dashed vertical line corresponds to theoretical yield of the rebar.

The corner strain gauges (Location C) did not begin to record large strain until the 125 kip (556 kN) loading (**Figure 38**). The load vs. strain graph does not match up with the cracking that was observed. At 125 kip (556 kN), there was significant residual displacement, which typically means that a crack has occurred. However, a crack in this region was observed at the 110 kip (489 kN) loading in the left corner and 130 kip (378 kN) loading in the right corner. Inside Bar 2 and Inside Bar 3 did not reach theoretical yield until the 170 kip (756 kN) loading. Inside Bar 1 and Bar 4 did not reach theoretical yield until 200 kip (890 kN) loading. Once the bars reached theoretical yield, the residual strain developed after every loading. The outside hook bars just reached yielding reaching a maximum of 2110 με. Load vs. strain graphs for locations A, B, and D are shown in Appendix C.

Specimen 4 did not show much deflection during the early loadings. For the single load plate, no measurable deflection occurred until 90 kip (400 kN) as is shown in **Figure 39**. This loading corresponds with first flexural cracks of Specimen 4. The average measured deflection in the middle 24 in (610 mm) was 0.1 in (2.5 mm). Between 90 kip (400 kN) and 140 kip (623 kN) the deflection increased to 0.2 in (5 mm). The deflection continued to slowly increase until 210 kip (934 kN). At this loading the average measured deflection in the middle 24 in (610 mm) was 0.6 in (15.2 mm). During the 220 kip (979 kN) loading, the deflection increased to 0.9 in (22.9 mm). After this loading, the majority of the string potentiometers were removed. The only remaining string potentiometers were located 12 in (305 mm) on each side of mid-span. Prior to failure, the average deflection for Sequence 3 was 1.17 in (29.7 mm). The tandem axle loading (= Sequence 2) reached a maximum of 0.3 in (7.6 mm) during the testing. **Figure 40** shows a comparison of dispalcements of a single point load (= Sequence 3) to the tandem axle loading (= Sequence 2).

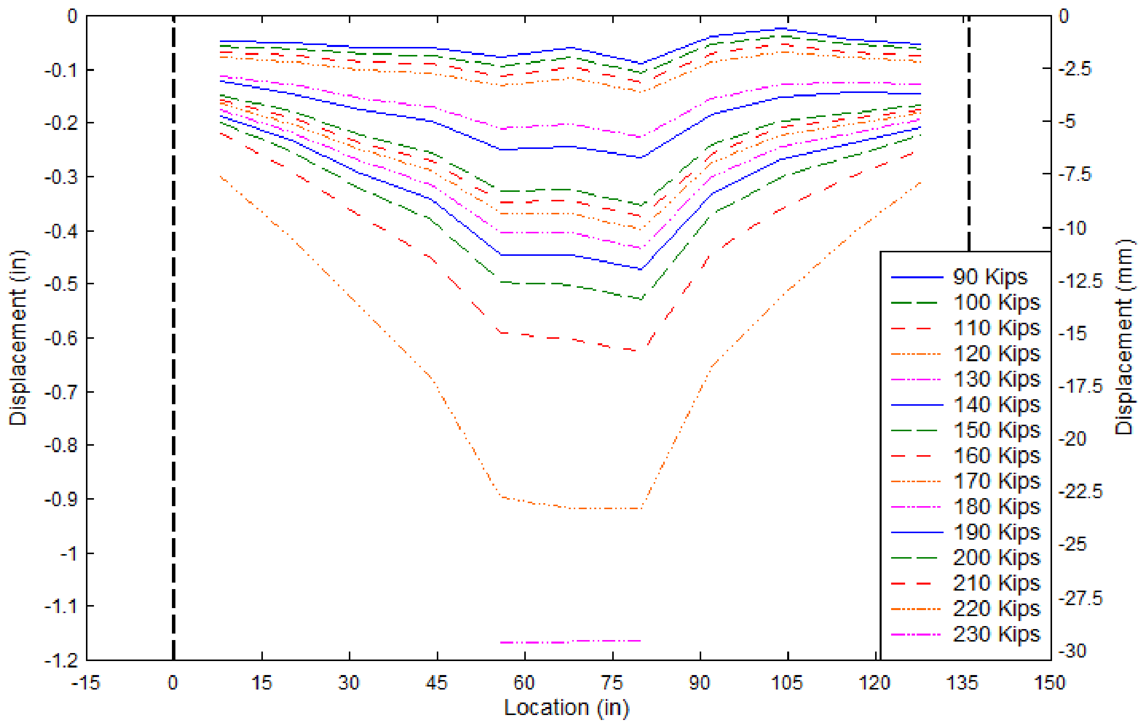

Figure 39. Specimen 4 mid-span displacement for AASHTO single-axle loading (= Loading Sequence 3) (The dashed vertical lines denote the specimen width).

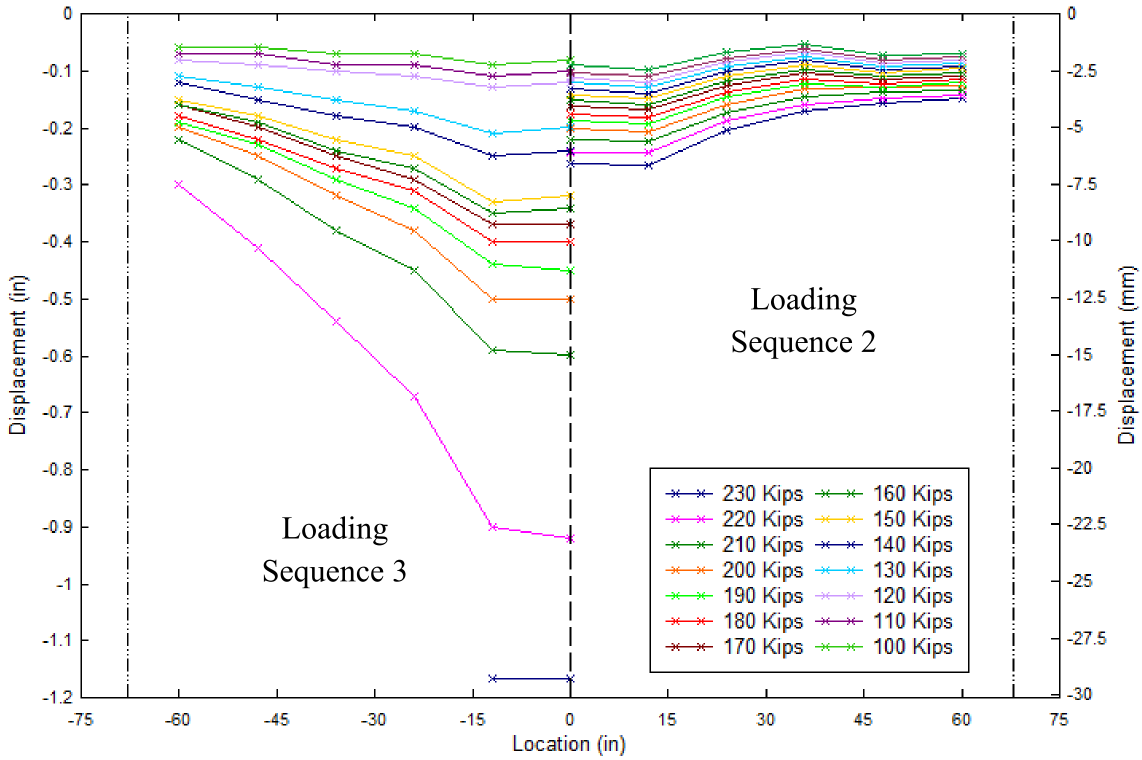

Figure 40. Comparison Loading Sequence 3 (= AASTHO single-axle loading – Left graph) vs. Sequence 2 (= AASHTO tandem-axle loading – Right graph) (The dashed vertical lines denote the edges of the specimen).

4.3.2 Failure

The failure load for Specimen 4 was 230 kip (1023 kN), which was reached during Sequence 3. During this loading increment, the load was held for a moment prior to a sudden two-way (or punching) shear failure (**Figure 41**). The failure cone had an angle of approximately 30 °, as was observed for Specimens 1 to 3. As discussed in Section 4.3.1, the interior mid-span bars and corner bars yielded well before failure. Once the mid-span bars began to show large strain residuals, the deflection began to increase. Two-way shear failure could possibly be seen in an actual culvert given the realistic condition represented by Specimen 4. Prior to testing, it was speculated that the flexural-shear-type failures seen in Specimens 1 to 3 may not occur in Specimen 4 due to the increased width and resulting capability of the slab to carry load in the transverse direction. This was confirmed by this test.

Figure 41. Specimen 4 failure. Top: Two-actuator setup (= Loading Sequence 3) with punched slab. Bottom: Failure cone extracted from slab.

4.4 Comparison between Specimens 1, 2, and 4

A comparison between Specimens 1 and 4 and Specimens 2 and 4 was possible since some of the strain gauge and displacement locations were the same with respect to the applied load. **Figure 42** and **Figure 43** show the graph of the strain of Specimen 1 vs. Specimen 4 (= Loading Sequence 1 and 3) at mid-span and the graph of strain of Specimen 2 vs. Specimen 4 (= Loading Sequence 2) at Location C, respectively. From looking at the graph, it is clear that Specimen 4 (= Loading Sequence 1 and 3) is stiffer prior to yield than Specimen 1 was. Similarly, Specimen 4 (= Loading Sequence 2) is stiffer than Specimen 2. Actual yield for Specimens 1 and 2 occurred at 50 kip (222 kN) compared to 225 kip (1001 kN) for Specimen 4 (all Sequences). Furthermore, **Figure 44** shows a comparison of the stiffnesses based on common mid-span displacement measurements. It can be observed that the increase in stiffness is a function of (1) the loading sequence and (2) the applied load. Overall, Specimen 4 is on average 4.33 and 2.61 times stiffer than Specimen 1 and 2, respectively. This is an observation of a slab's effectiveness to carry loads transversely and will be taking into consideration in Section 5.2.1 to determine the effective strip width for Specimen 4.

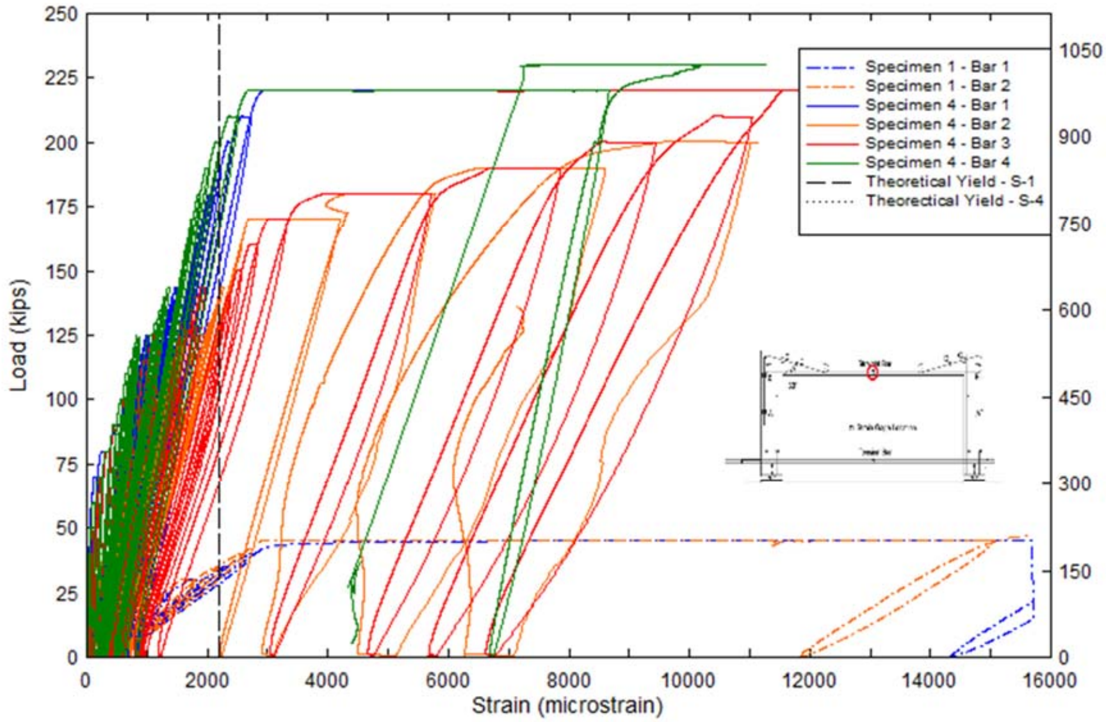

Figure 42. Specimen 1 vs. Specimen 4 (Loading Sequence 1 and 3) rebar strain mid-span (Location straight bar). The dashed vertical line corresponds to theoretical yield of the rebar.

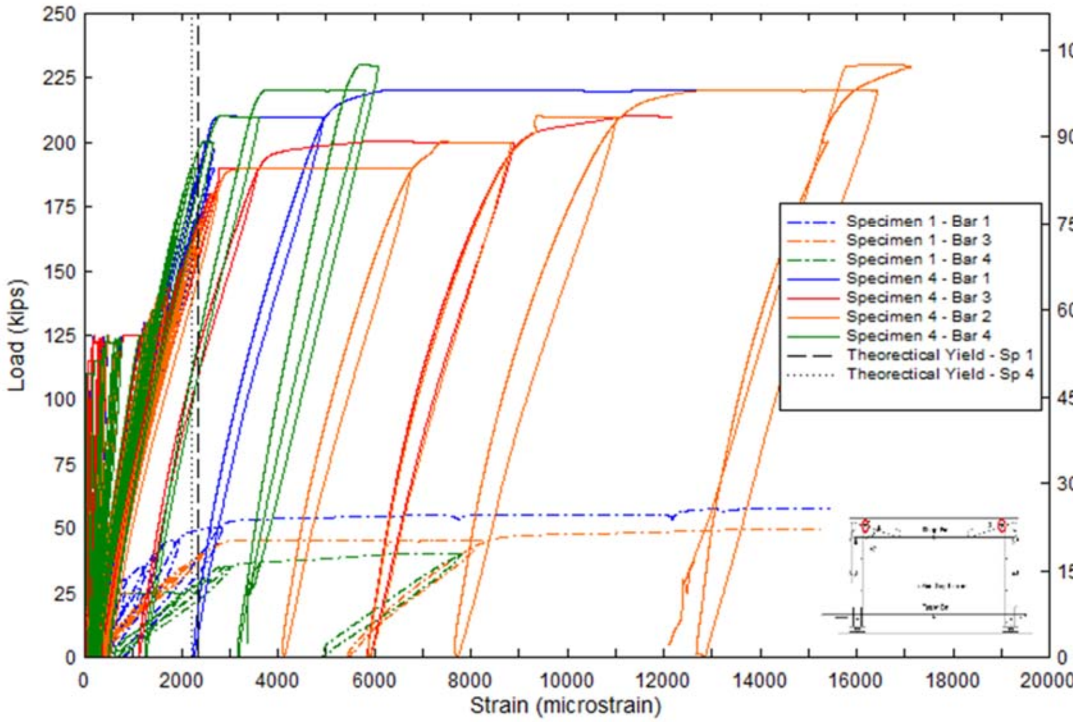

Figure 43. Specimen 2 vs. Specimen 4 (= Loading Sequence 2) strain at Location C. The dashed vertical line corresponds to theoretical yield of the rebar.

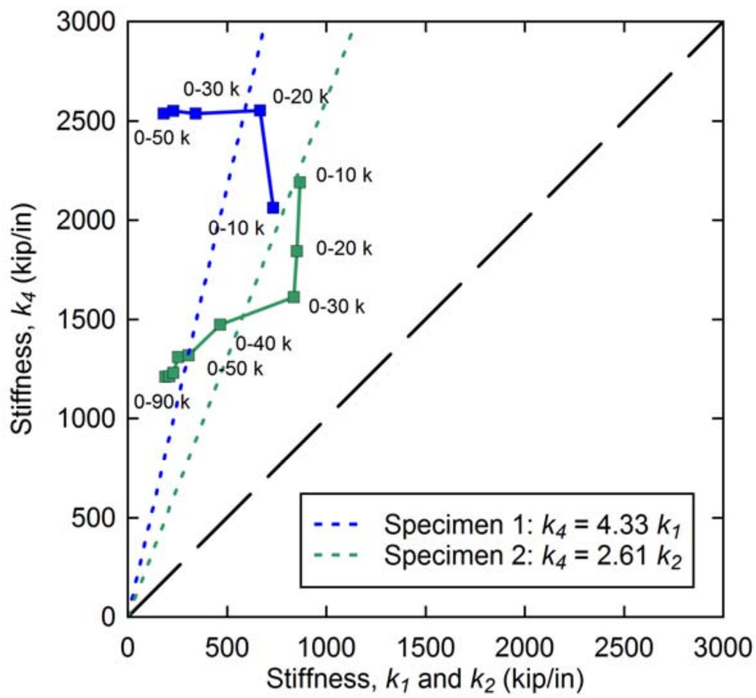

Figure 44. Stiffness of Specimen 1 and 2 compared to Specimen 4.

4.5 Specimen 5

Specimen 5 was constructed using wood forms. The formwork was built using 2 x 4's (51 x 102 mm) and ½ in (13 mm) plywood with the specimen being cast in place, i.e. the open area of the formwork being the top of the specimen. The formwork was measured and dimensions were verified to match the drawings for the specimen. The reinforcement bars were strain gauged prior to casting, similar to Specimens 1 through 4. The specimen was cast in one pour. After the specimen was poured, moist burlap and a thick plastic tarp were placed on the open side of the form until the heat of hydration period of the specimen was completed. The cast specimen remained in the forms until the average of the 6 in x 12 in (152 mm x 305 mm) cylinders reached a minimum compressive strength of 1500 psi (10.3 MPa).

Specimen 5 was loaded with a single AASHTO-type tire patch (20 in x 10 in (508 mm x 254 mm)) load plate centered at mid-span of the 16 ft (4.88 m) clear span. The specimen was loaded at 5 kip (22.2 kN) increments as done with Specimen 1 though Specimen 3. **Figure 45** shows the location of the load plate.

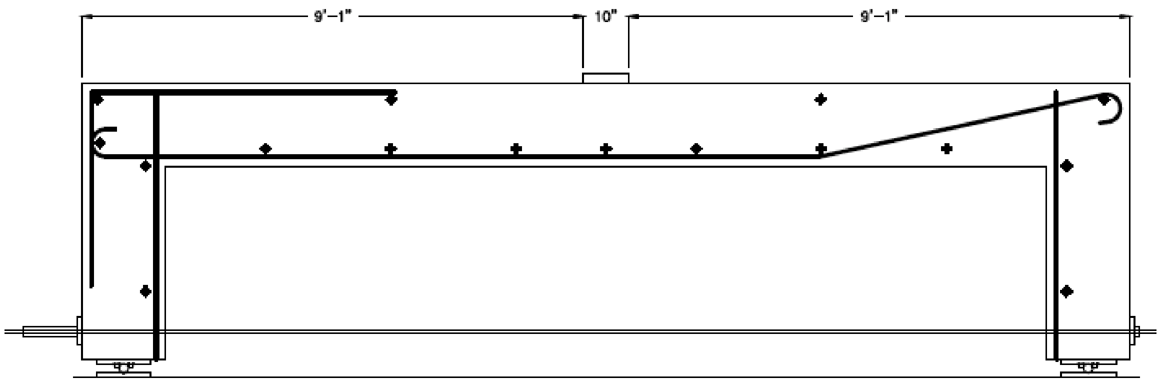

Figure 45. Specimen 5 load plate location (AASHTO single axle patch centered about mid-span).

4.5.1 Behavior

Specimen 5 did not begin to crack until 40 kip (178 kN). Three flexural cracks developed in the positive moment span. One flexural crack developed on the left side of the load plate and two developed directly below the load plate. Another crack developed on the top right of the slab in the negative moment region. At 45 kip (200 kN), the cracks continued to grow at mid-span and a crack developed in the negative moment in the top left of the slab. One flexural crack developed on each leg of the specimen in line with the bottom of the slab. This observation was contrary to the previous four specimens. The increased reinforcement in the negative moment region of the slab caused the negative moment region on the legs to crack significantly earlier. Between 50 kip (222 kN) and 60 kip (267 kN), four more flexural cracks developed in the positive moment region. At 65 kip (289 kN), a shear crack developed on the outside left leg approximately 24 in (610 mm) below the bottom of the slab and a second flexural crack developed in the top left corner. At 70 kip (311 kN), a second flexural crack developed in the top right corner. **Figure 46** shows a crack map showing the development of the cracks during testing.

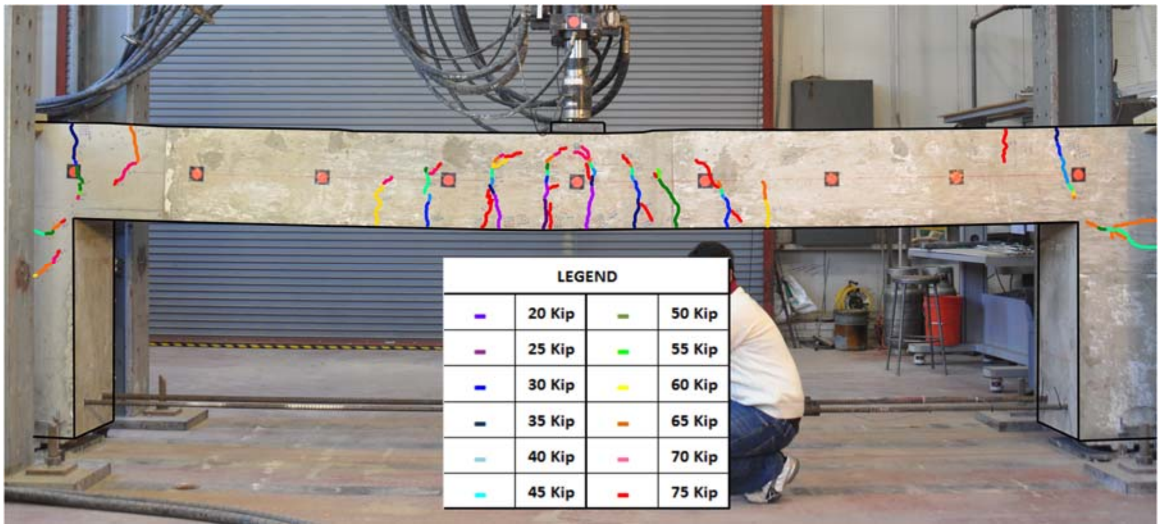

Figure 46. Specimen 5 crack map.

Similar to the previous four experiments, along with crack mapping at each load increment, crack width measurements were taken at crack locations. **Figure 47** shows a graph of the crack widths vs. the normalized load and within the graph is a drawing of which cracks were measured. The largest crack width was located in the top right leg in line with bottom slab, crack M. Between 45 kip (200 kN) to and 65 kip (289 kN), the M crack width increased linearly from 0.01 in (0.3 mm) to 0.05 in (1.3 mm). The largest width increase occurred between 65 kip (289 kN) and 75 kip (334 kN). Between these two applied loads, the crack width increased from 0.05 in (1.3 mm) to 0.20 in (5.1 mm). Crack F and G, located below the load plate reached a maximum width of 0.12 in (3.0 mm) prior to failure. Crack B, located on the left leg in line with the bottom edge of the slab, reached a maximum width of 0.08 in (2.0 mm). The other cracks, including the failure crack A, reached a maximum of 0.04 in (1.0 mm) prior to failure.

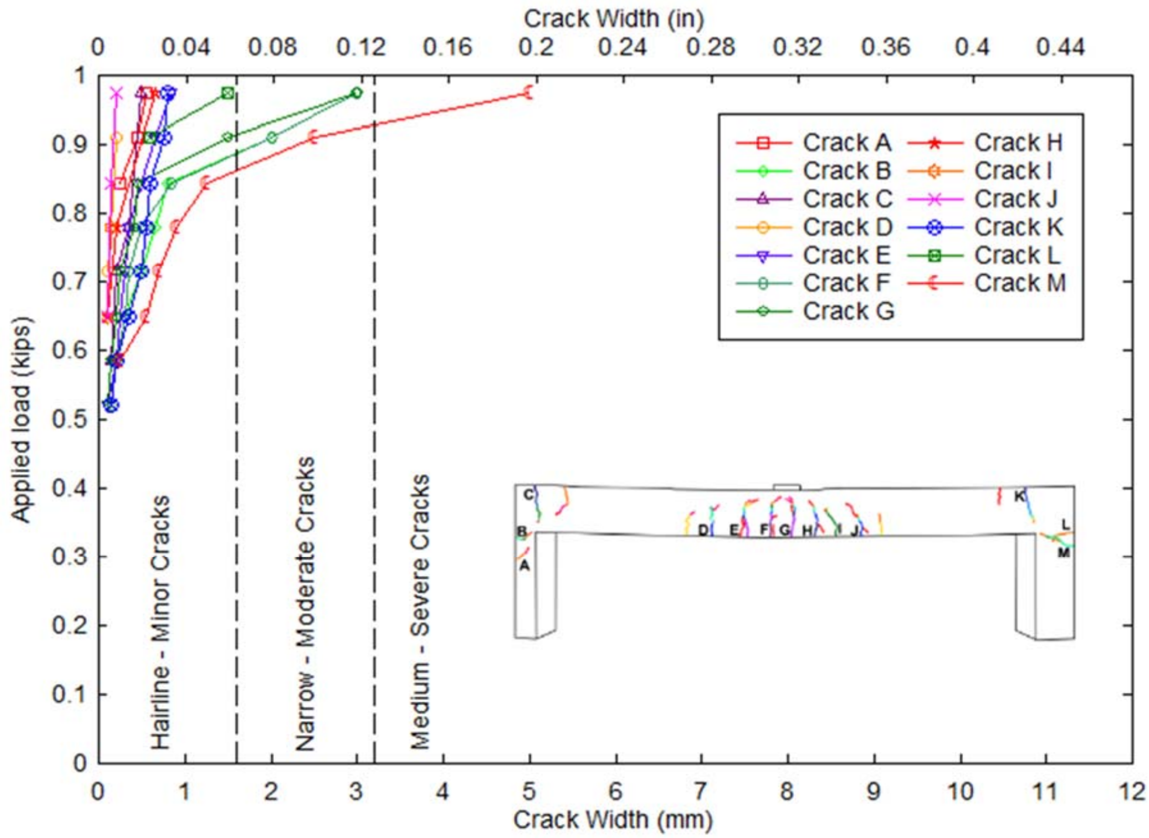

Figure 47. Specimen 5 crack widths. The vertical dashed lines represent crack width limits according to the AASHTO Guide Manual for Element Inspection (AASHTO 2011).

The strain gauge placed on the lower right leg of the 90 ° bar (Location G) experienced little to no strain. The strain at these gauges reached a maximum of 750 με. The gauge placed on the lower right leg experienced strain late in the loading scenario just before failure. The strain exceeded theoretical yield just prior the failure load. The strain gauge placed on the end of the 90 ° bar at a 30 ° angle from the bottom of the slab (Location D) experienced minimal strain. The strain at this location never exceeded 40 με. The strain gauge on the hook bar that is 30 ° angle from the bottom of the slab (Location B) experienced little strain. The strain at this location ranged from 100 με to 450 με.

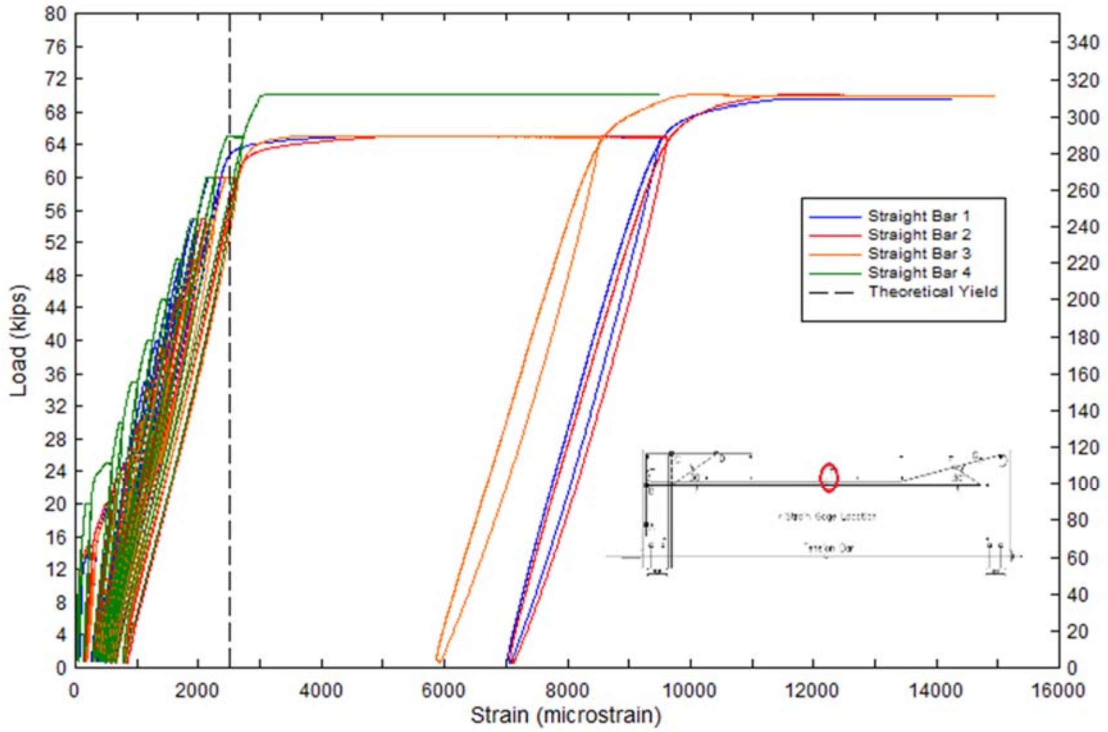

Figure 48. Specimen 5 rebar strain mid-span (Location straight bar). The dashed vertical line corresponds to theoretical yield of the rebar.

The strain gauges placed at the corners (Location B and E) and the strain gauges located at mid-span experienced the most strain. The cracking that was observed matches up with the results recorded from the strain gauges in the corner and the mid-span on the rebar. The first cracking in the center of the clear span, as seen in the load vs. strain, occurred at 40 kip (178 kN), which corresponds with the three flexural cracks that developed at mid-span close to the loading plate. At every new crack or propagation of an already visible crack, in the center of the span, there was a noticeable increase in strain. The graph of the strain gauge in the top corners of the specimen mirrors the cracking that was observed. The first noticeable change in strain occurred on the right corner strain gauge at an applied load of 40 kip (178 kN), which is when the first crack appeared. The top left corner first cracked at an applied load of 45 kip (200 kN) as well as the first significant change in strain. The strain in the top corners was significantly less than in the previous experiments. This is attributed to the increased rebar area and spacing of the rebar. The load vs strain graphs for strain gauges at mid-span and at the top corner (Location A) are shown in **Figure 48** and **Figure 49**, respectively.

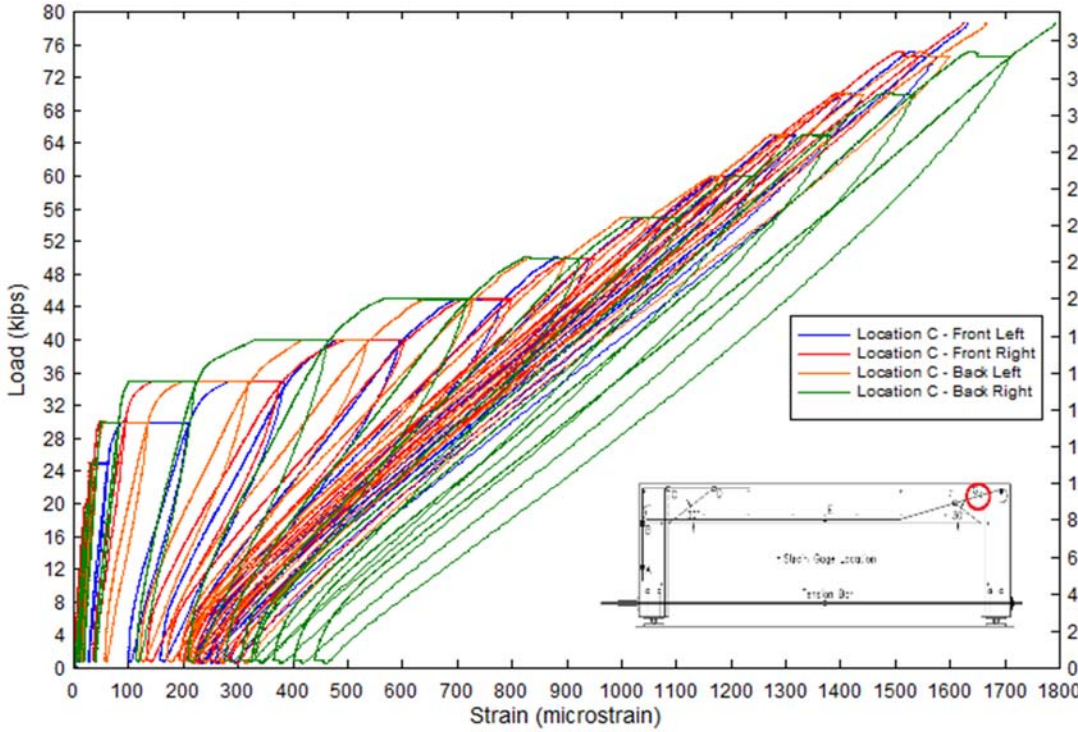

Figure 49. Specimen 5 rebar strain diagonal bars (Location C).

The largest strain values recorded were the gauges on the 90 ° bars in line with the bottom of the slab (Location F). This corresponds with the crack widths, shown in **Figure 47**. After the 60 kip (267 kN) loading, the four strain gauges had exceeded theoretical yield. The recorded strain on the left leg had higher strains in the beginning loading increments than the right leg did. The left leg had the roller support while the right leg was a fixed support. The strain on the left leg had the largest increase after to the 65 kip (289 kN) loading. The strain in the right leg had the largest increase in strain during the 75 kip (334 kN) loading increment. The load vs. strain graph for Location F is shown in **Figure 50**.

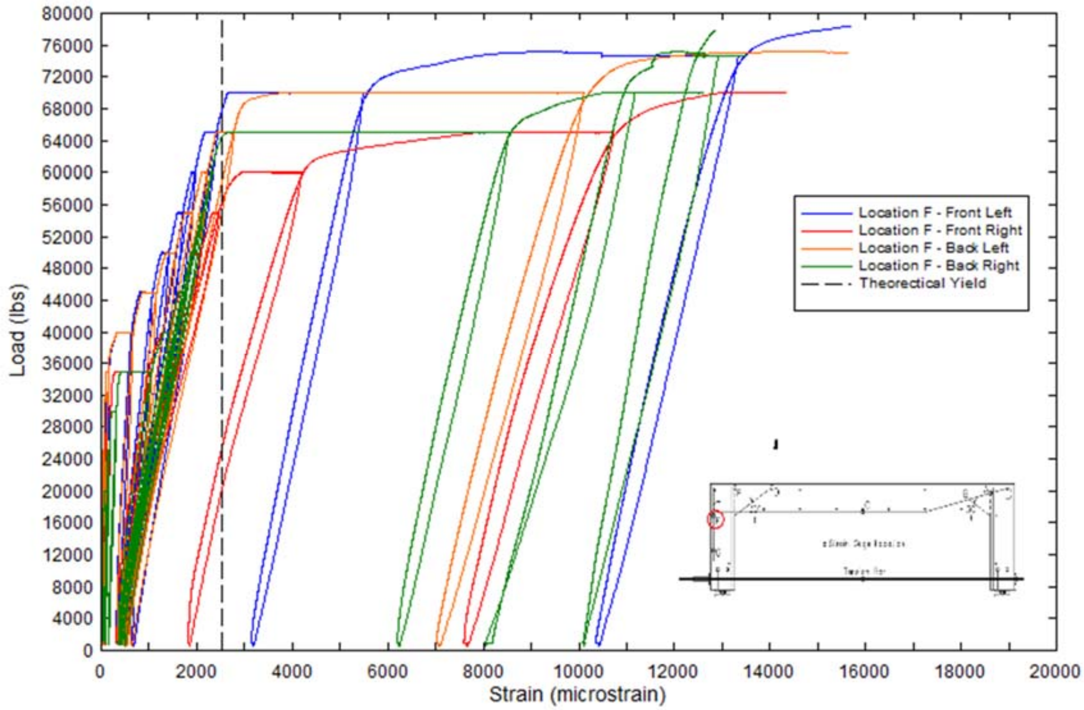

Figure 50. Specimen 5 rebar strain diagonal bars (Location F). The dashed vertical line corresponds to theoretical yield of the rebar.

The displacement results were graphed, load vs. displacement, as was done in with the previous four specimens. The results (shown in **Figure 51**) matched up with the results from the mid-span cracks and crack widths gauge. The first noticeable change in displacement occurred at a loading of 40 kip (178 kN), which corresponds to the first crack developing at mid-span. When the applied 40 kip (178 kN) was held, the displacement began to slowly increase, or creep, until the system stabilized. Between the loading increment of 25 kip (111 kN) and 55 kip (245 kN), the maximum displacement on average increased 0.05 in. (1.3 mm). The largest residual displacement occurred during the 65 kip (289 kN) load increment. The displacement increased from 0.45 in. (11.4 mm) to 0.65 in. (16.5 mm) when the specimen was unloaded. During the 70 kip (311 kN) loading, the string potentiometers were removed to protect them after the specimen failed. The measured displacement was not as much as Specimen 1 through Specimen 3, due to the type of failure the specimen exhibited. Load vs. strain graphs for locations A, B, and D are shown in Appendix C.

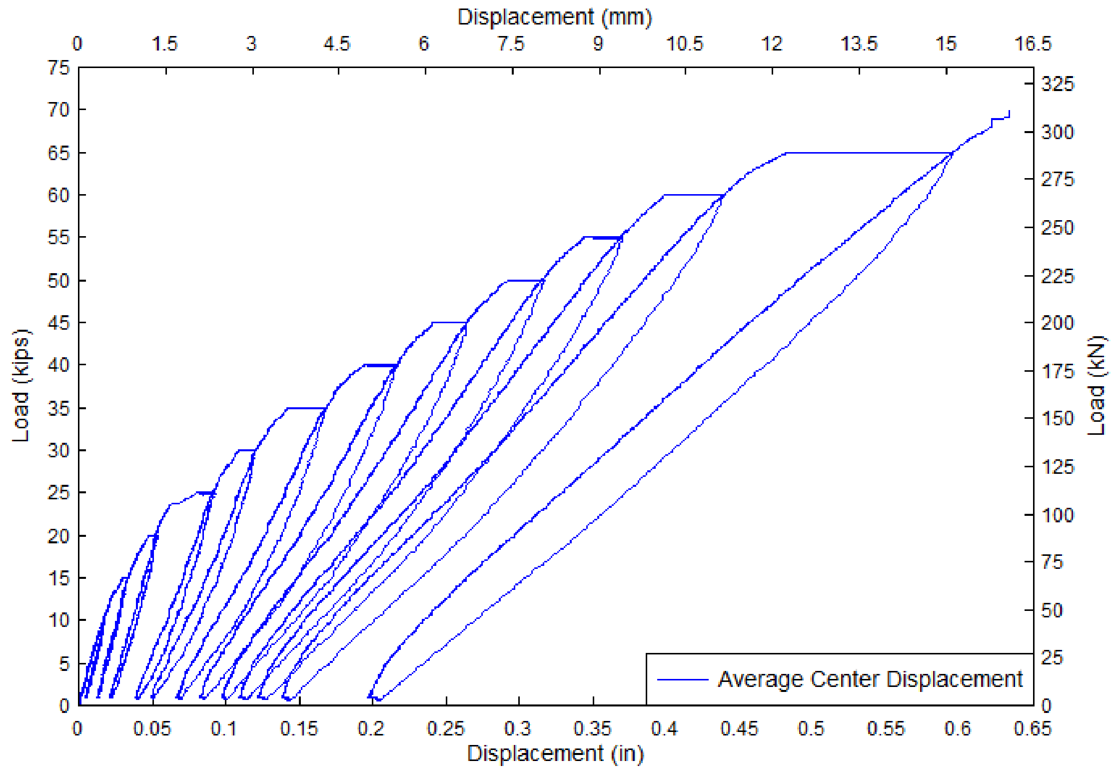

Figure 51. Specimen 5 mid-span displacement.

4.5.2 Failure

The initial failure load for Specimen 5 was 78.6 kip (350 kN). The failure mode was a shear-bearing failure on the left leg (**Figure 52**). A shear crack developed below the 90 ° bar during the load increments, as mentioned above. Prior to the specimen's failure, the mid-span rebar and the side corner rebar yielded. After the rebar yielded, the specimen at mid-span was able to have a larger increase in deflection. It should be noted that this failure would not be typical for an in-service structure since the width of the structure would be significantly larger than the 24 in (610 mm) width of Specimen 5, i.e. the larger width would have significantly higher bearing and shear capacity at the support.

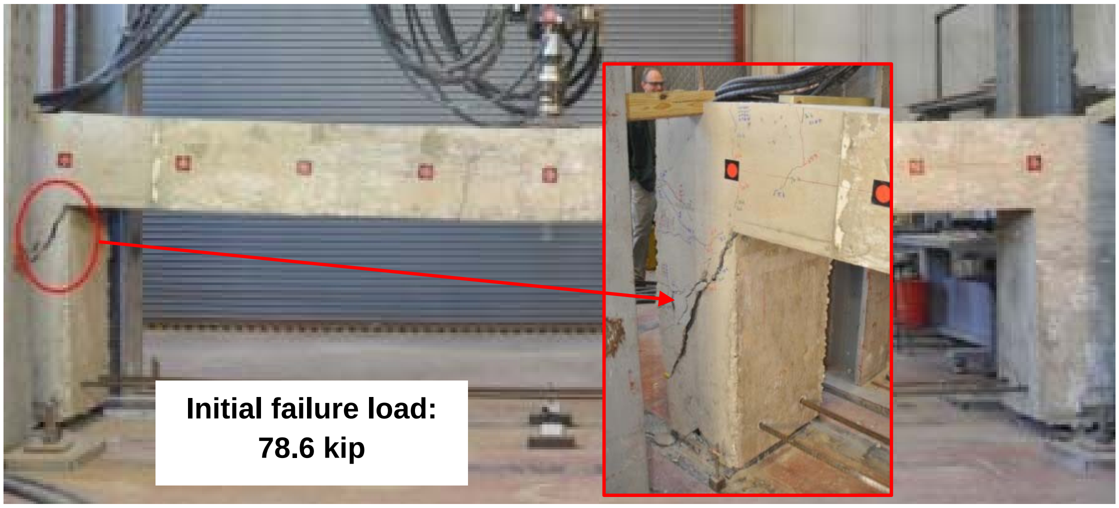

Figure 52. Specimen 5 initial failure crack.

After initial failure had occurred, lateral support was installed around the legs of Specimen 5 and loading continued. The typical 5 kip (22.2 kN) increment loading was not used. The specimen was loaded using displacement controlled loading until the ultimate failure was reached. This failure was a flexural-shear failure similar to Specimens 1 to 3. The crack started at the left edge of the load plate. The inclined crack once again was within mid-span, between the hooked bars. The failure crack formed a 30 ° angle (shown in **Figure 53**) instead of the assumed 45 ° angle the ACI 318-14 assumes for shear, similar to all other specimens tested. The specimen failed at an ultimate load of 76.8 kip (342 kN).

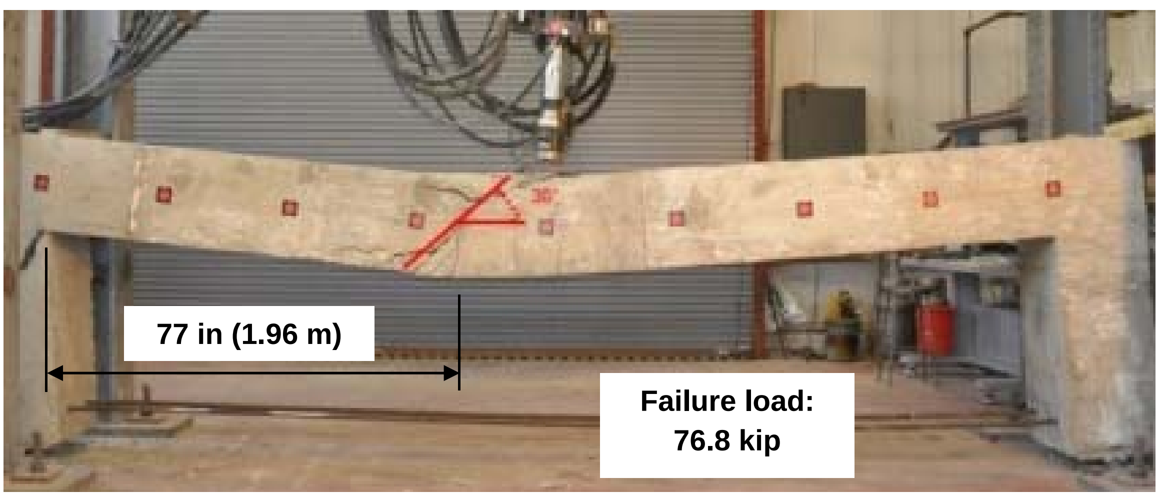

Figure 53. Specimen 5 after failure.

4.6 Summary

Table 3 shows a summary of the key experimental observations. Specimens 1, 2, 3, and 5 all exhibited flexural-shear failure. Specimen 5's flexural-shear failure developed after the initial bearing failure was braced. As shown in previous sections, the rebars of unique corner detail and at mid-span yielded prior to failure for all five specimens. The interior unique corner rebars and straight rebar were the only rebar that yielded for Specimen 4.

Table 3. Summary table with experimental test results.

Specimen	*1*	*2*	*3*	*4*	*5*[5]
Loading configuration (1 or 2 loads)[1]	1-CL	2-CL	2-*d*	1-CL & 2-CL	1-CL
Max. total applied load, kip (kN)	57.8 (257)	97.0 (431)	84.8 (377)	230 (1023)[3]	76.8 (342)
Failure mode[2]	F, S-C	F, S-C	F, S-C	T-S	F, S-C
Failure location x, inch (m)[4]	75 (1.91)	27 (0.686)	74 (1.88)	60 (1.52)	77 (1.96)
Failure crack angle (°)	~ 30	~ 30	~ 30	~ 30	~ 30

[1] CL = centered about mid-span, d = 10.5 in (267 mm) = distance between face of support and edge of loading plate

[2] F = flexural, S-C = shear-compression, T-S = two-way shear

[3] Specimen failed at this applied load in 1-CL loading configuration

[4] Distance between face of the left support and mid-crack location

[5] Initial failure, which was shear failure in the left leg, not reported here (see Section 4.5.2)

5 Analysis

After the testing of the five specimens, analysis was completed. MATLAB code was created to determine an analytical prediction based on ACI 318-14 flexural and shear strength equations (ACI 2014), Eurocode 2 shear strength equations (CEN 2004), and AASHTO MCFT shear equations (AASHTO 2012). For Specimens 1 to 4, flexural and shear strength predictions were computed; for Specimen 4, two-way shear was also computed based on ACI 318-14 and Eurocode 2. Using the created MATLAB code and the actual material properties of each specimen, a maximum corresponding applied force based on the predicted strengths for the different codes were determined.

5.1 Specimen 1, 2, 3, and 5 (2 ft Strip Specimens)

5.1.1 Model Assumptions

A few assumptions were needed to estimate the allowed loading. First, the applied load was assumed to be a distributed load, *w*, that acted at the height of the flexural reinforcement at a 30 ° angle from the top of the load plate, i.e. with no overlay, as shown in **Figure 54**.

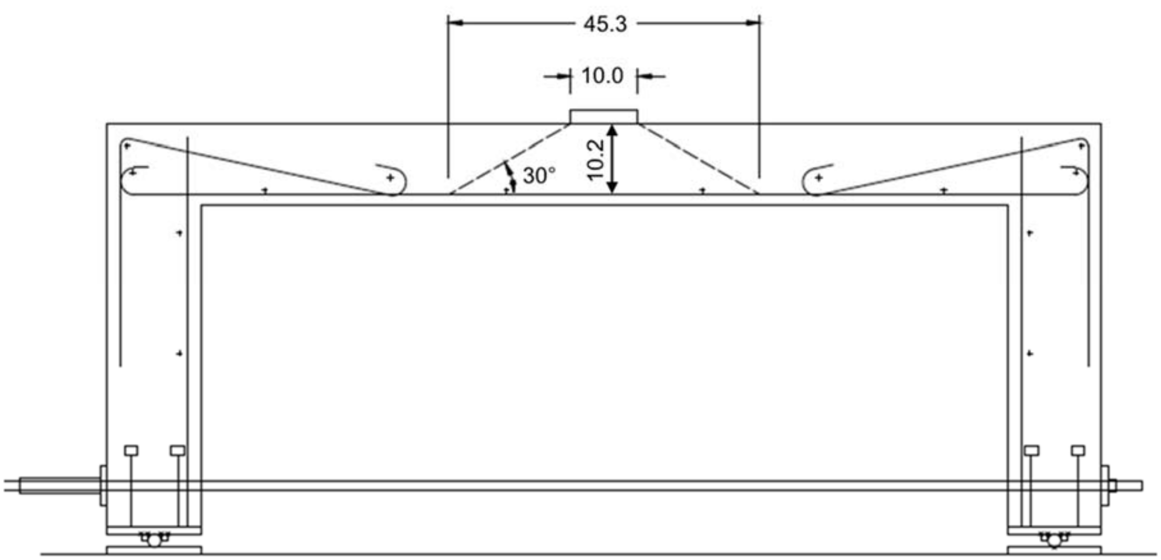

Figure 54. Assumed load distribution. Example: Specimen 1.

The actual span was determined from the point of rotation in the left leg to the point of rotation in the right leg. **Figure 55** shows an example of Specimen 1 and the location of where the span was measured. Given the negligible difference found, it was assumed that the clear span was the span length used to calculate the flexural and shear strengths.

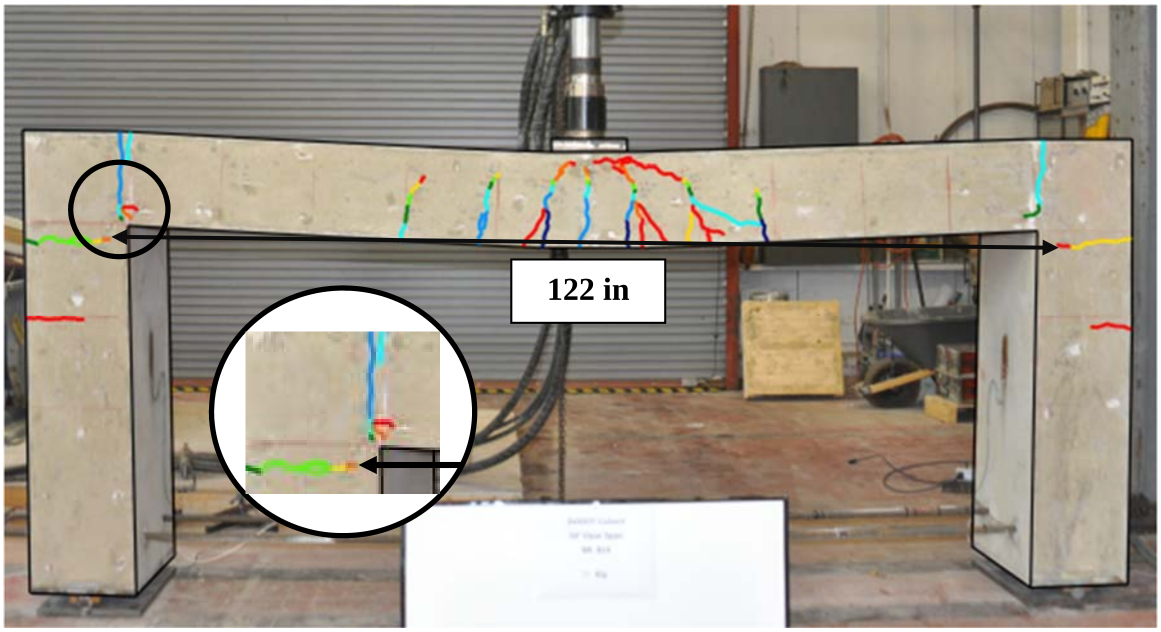

Figure 55. Measured actual span length. Example: Specimen 1.

The final assumption that was used was that as the applied load increases, plastic hinges develop in the negative moment regions at the interface of the clear span and the legs. After those hinges develop, a plastic hinge develops near mid-span, leading to a mechanism which means overall system capacity is reached. This assumption was supported by observations made during the experiments. **Figure 56** shows the developed plastic hinges in Specimen 1. Plastic hinges for the other specimens are shown in Appendix D. Shear forces and bending moments were also computed based on an elastic analysis and are presented in Appendix E.

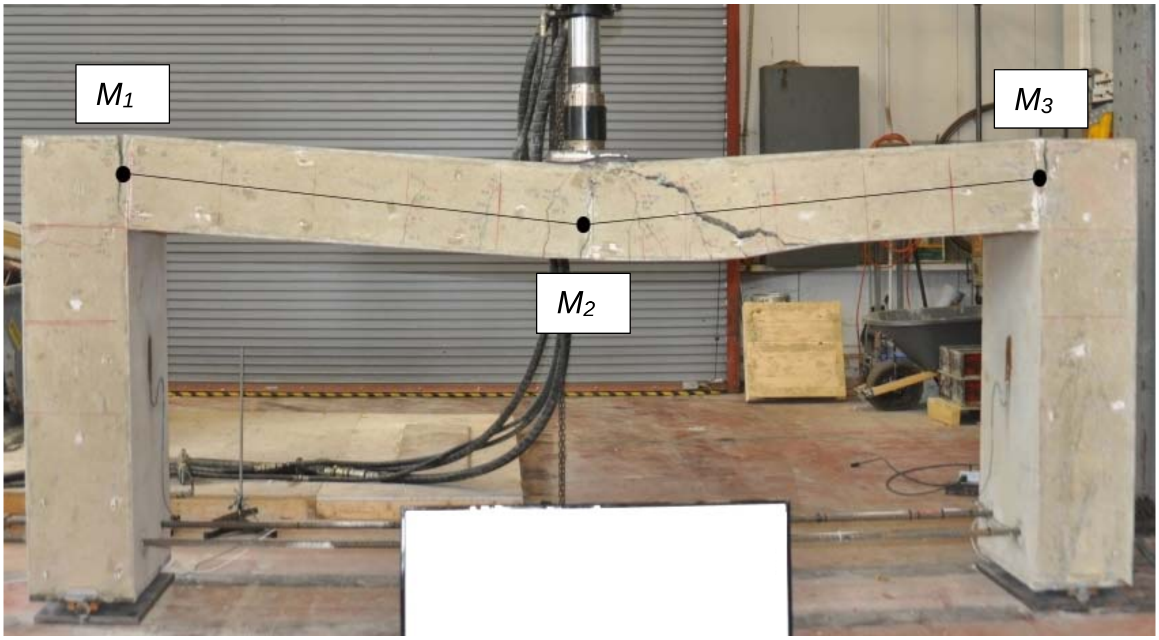

Figure 56. Plastic hinge locations. Example: Specimen 1.

5.1.2 Flexural Strength Predictions

Specimens 1, 2, 3, and 5 were all analyzed using the same MATLAB code, with their respective material properties (see Chapter 2) being used. A constant width of 24 in (610 mm) was used, corresponding to the physical width of the specimens, for both the negative and positive moments. The specimen's flexural strength was calculated based on its actual material properties (**Table 2** and Appendix B) using sectional dimensions shown in **Figure 57**. To determine the overall system capacity of each specimen, the sectional flexural strength was determined at the support and at mid-span corresponding to negative and positive moment regions, respectively. The support cross section was analyzed as a doubly-reinforced cross section with the #5 (16 mm) rebar acting as compression steel, while the mid-span cross section was analyzed as a singly-reinforced cross section. The flexural strengths were determined for a strain range measured at the face where compression strain occurs from 0.00 to 0.014, beyond the ACI 318-14 limit of 0.003. **Figure 58** shows a flow chart with equations and the analysis used to compute the moment for each compressive strain value and location. **Figure 59** shows the computed negative and positive yield and maximum (or probable) flexural strengths for Specimen 1 using a moment-curvature analysis. The first vertical line corresponds to the ACI 318-14 failure strain limit of -0.003 and the second line to the observed maximum moment which was approximately -0.008. For Specimen 5, the section properties for the legs were used to calculate the negative flexural strength due to the observed failure.

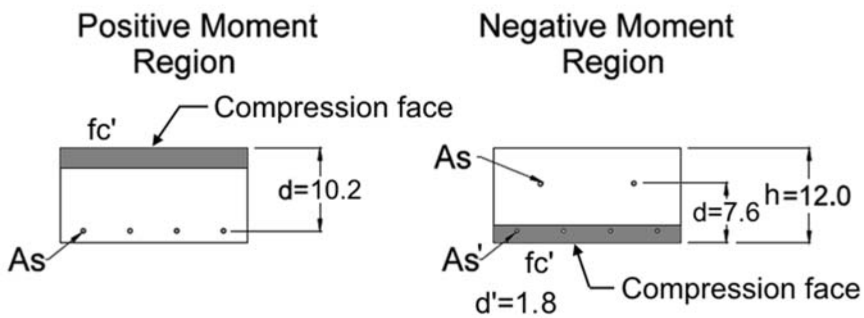

Figure 57. Cross section with parameters used to calculate flexural strength of Specimens 1 to 4. All dimensions in (in).

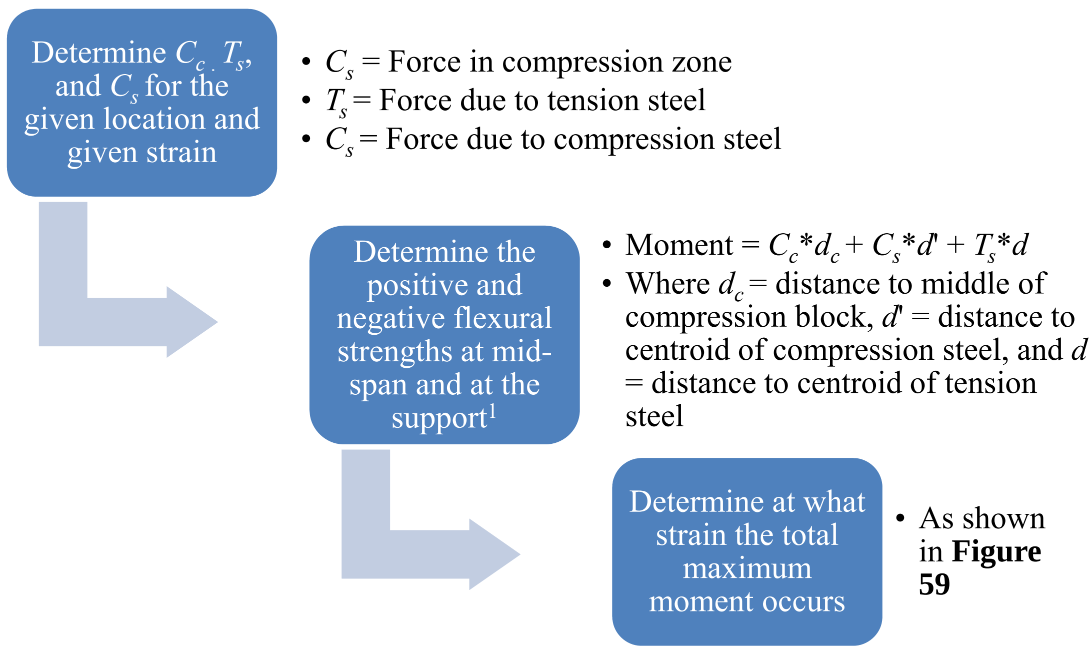

Figure 58. Analysis procedure to determine maximum probable moment.
[1] The smaller of the flexural strength in the slab or the wall is used.

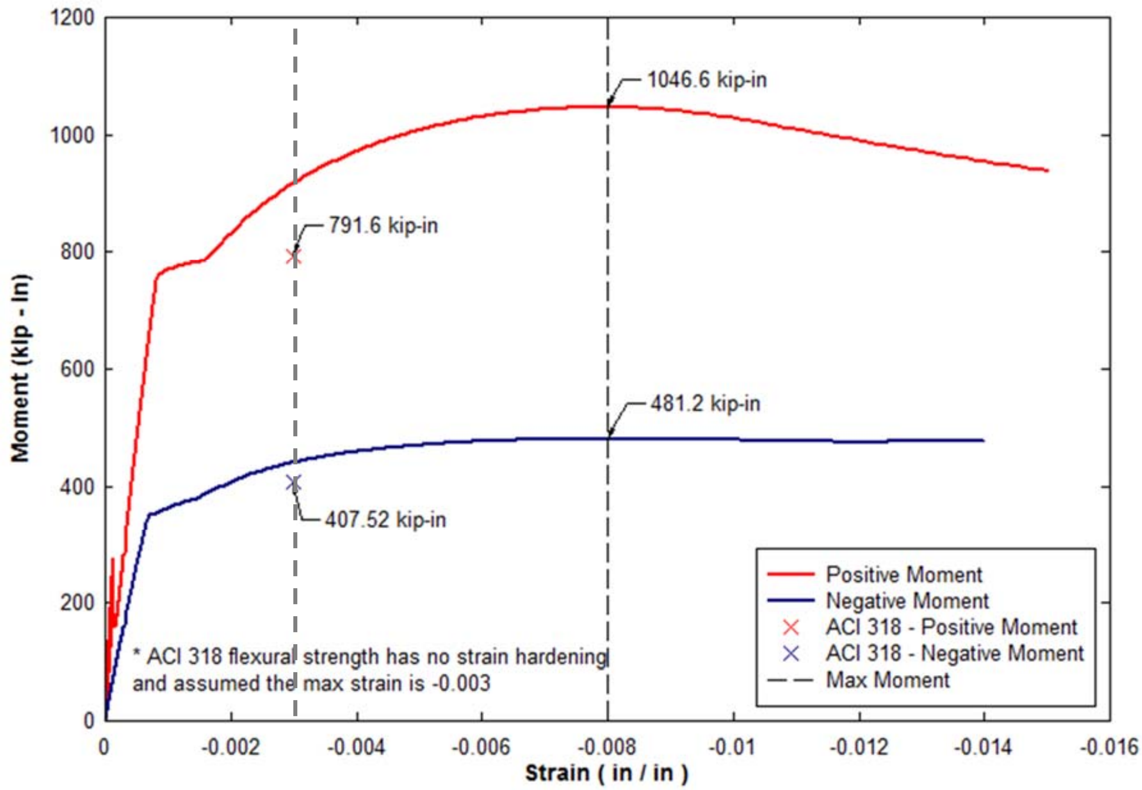

Figure 59. Example flexural strengths based on actual material properties. Example: Specimen 1.

After determining the flexural strengths based on actual material properties, the maximum theoretical plastic moment capacity based on a fixed-fixed boundary condition was determined, assuming that full redistribution of moments is possible. Once three plastic hinges have formed, the system becomes a mechanism, corresponding to the strength based on the upper bound theorem (Nielsen and Hoang 2011). A fixed-fixed boundary condition was used because of the assumption that plastic hinges developed in the corners, which corresponds to a fixed-fixed boundary condition. **Figure 60** shows a plastic mechanism for the case with dead load (w_D) and one tire patch load (w_L) d (this d is different from flexural depth!) away from the left support and distributed over b. M_1 to M_3 are the nominal flexural strengths. For this study, both yield and maximum (or probable) moment, which is based on maximum rebar stress at a concrete compressive strain of -0.008, were computed and evaluated.

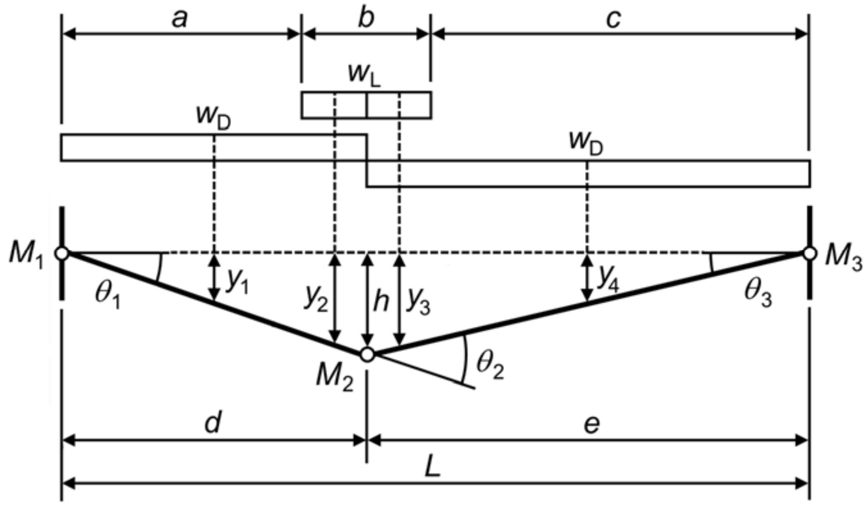

Figure 60. Mechanism with plastic hinges assuming fixed-fixed boundary conditions.

In order to estimate the maximum system capacity based on a mechanism, external and internal work are calculated and set equal (Nielsen and Hoang 2011). Typically, a virtual displacement at the mid-hinge location is assumed as h = 1 in (25.4 mm). External work consists of the applied loads moving through the displacement field of the deformed structure as shown in **Figure 60**. For this example, the external work, E_{ext} is calculated as follows:

$$E_{ext} = w_D\left(d \cdot y_1 + e \cdot y_4\right) + w_L \cdot \frac{b}{2}\left(y_2 + y_3\right),\ \text{where}\ w_L = \frac{P_L}{b} \qquad \textbf{Equation 2}$$

Additional loads, i.e. tire patches, can be readily included by adding their corresponding contribution.

The internal work, E_{int} is represented by the internal moments undergoing a rotation due to the virtual displacement, h, and is calculated as follows:

$$E_{\text{int}} = M_1 \cdot \theta_1 + M_2 \cdot \theta_2 + M_3 \cdot \theta_3 \qquad \textbf{Equation 3}$$

The displacements, y_1 to $y3$ as well as the angles of rotation, θ_1 to θ_3 are calculated based on similar triangles using h = 1 in (25.4 mm).The location of the hinges, d was based on what was observed when the specimens failed. Setting $E_{ext} = E_{int}$, the only unknown is $P_L(w_L)$, which can be solved for readily. Flexural strengths at the hinge points, M_1 to M_3 are calculated based on the procedures explained above. Detailed calculations can be found in Appendix F.

5.1.3 Shear Strength Predictions

After the maximum applied load based on flexural strength was calculated, the maximum applied load for shear strength based on code shear equations was calculated at the location of ailure. **Figure 61** shows the location of the failure crack for Specimen 1 and **Figure 62** shows a free body diagram of the isolated right element. Once the shear strength, in this case V_c, has been calculated, the applied force P_{LL} can be readily calculated by enforcing vertical force equilibrium. The compression force in the slab, *C*, which is balanced by the normal force in the tension bar, *T*, is relatively small and was thus neglected. Detailed shear calculations are shown in Appendix F.

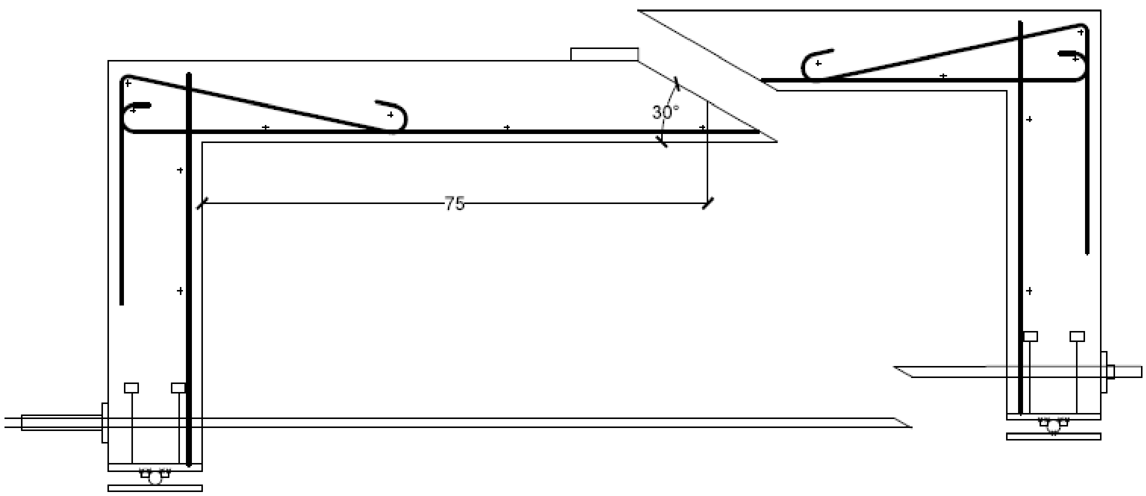

Figure 61. Failure crack location. Example: Specimen 1.

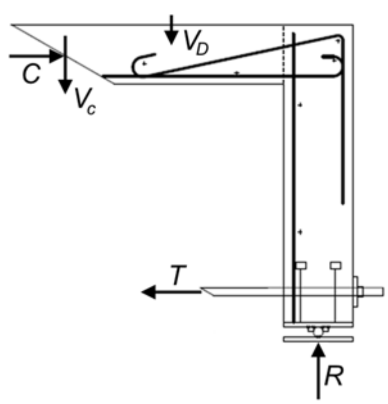

Figure 62. Free body diagram for isolated element. Example: Specimen 1.

First, equation ACI 318-14, 22.5.5.1 (corresponding to AASTHO LRFD, 5.8.3.4.1) was used to determine the simple shear strength of the specimen:

$$V_c = \beta\sqrt{f_c^{'}}b_w d \text{ , where } \beta = 2 \qquad \textbf{Equation 4}$$

where f'_c is concrete strength in psi, b_w is the width of the specimen, and d is the flexural depth of the specimen.

Next, equation ACI 318-14, Table 22.5.5.1 was used to calculate detailed shear strength accounting for the presence of longitudinal flexural reinforcement:

$$V_c = \left[1.9\sqrt{f'c} + 2500\ \rho_w \frac{V_u\ d}{M_u}\right] b_w\ d, \text{ where } f_c\text{' is in (psi)} \qquad \textbf{Equation 5}$$

where ρ_w is the reinforcement ratio, and V_u and M_u are the actual shear force and bending moments acting at the failure location.

After the ACI shear calculations were determined, the Eurocode 2, 6.2.2 shear equation for reinforced concrete members without shear reinforcement was calculated as follows:

$$V_{Rd,c} = \left[\left(\frac{0.18}{\gamma_c}\right) k\ (100\ \rho\ f_{ck})^{\frac{1}{3}} + 0.15\ \sigma_{cp}\right] b_w\ d \qquad \textbf{Equation 6}$$

where $k = 1 + \sqrt{\frac{200}{d}} \leq 2$ is the depth factor with d in (mm), ρ is the shear reinforcement ratio (≤ 0.02), f_{ck} is the characteristic cylinder compressive strength of concrete in (MPa), and σ_{cp} is an applied normal stress in (MPa), here neglected since found to be less than 80 psi (0.552 MPa) for all specimens. γ_c is the partial strength reduction factor for concrete and usually taken as 1.5. Since we are interested in the nominal strength, this factor is here set to $\gamma_c = 1.0$.

Finally, AASHTO's MCFT shear equations were implemented in a MATLAB code to compute sectional strength based on shear-moment interaction. The closed-form solution was used following the equations in AASHTO LRFD, 5.8.3.3:

$$V_n = V_c + V_s + V_p \text{ (not larger than } V_n = 0.25 f_c^{'} b_v d_v + V_p) \qquad \textbf{Equation 7}$$

where $V_s = 0$ and $V_p = 0$ for the culverts discussed in this research. Furthermore,

$$V_c = 0.0316\beta\sqrt{f_c^{'}}b_v d_v \text{, where } f_c\text{' is in (ksi)} \qquad \textbf{Equation 8}$$

Eq. (6) is valid for sections having less than the minimum shear reinforcement, which is the case for the culverts investigated in this research:

$$\beta = \frac{4.8}{(1+750\varepsilon_s)}\frac{51}{(39+s_{xe})} \qquad \textbf{Equation 9}$$

where ε_s is the strain in the longitudinal reinforcement and s_{xe} the distance between longitudinal crack control reinforcement (does not apply here). For β = 2, **Equation 8** essentially corresponds to the simple ACI equation presented in **Equation 4**. Detailed calculations as they pertain to shear strength can be found in Appendix E and G.

5.1.4 Results

The results of the analysis for Specimens 1, 2, 3, and 5 are shown in **Table 4** and the comparison between observed ultimate applied loads and predicted applied loads using the code equations presented in Sections 5.1.3 and 5.1.4 are shown in

Table 5.

Table 4. Predicted sectional strengths corresponding to the ultimate applied load.

	Specimen 1	*Specimen 2*	*Specimen 3*	*Specimen 5*
M_n^+, ACI, kip-ft (kNm)	66.0 (89.5)	66.1 (89.6)	65.6 (88.9)	102 (138)
M_n^+, max., kip-ft (kNm)	86.1 (117)	87.3 (118)	85.6 (116)	155 (210)
M_n^-, ACI, kip-ft (kNm)	31.9 (43.3)	31.9 (43.3)	31.0 (42.0)	52.0 (70.5)*
M_n^-, max., kip-ft (kNm)	36.8 (49.9)	36.8 (49.9)	36.4 (49.4)	77.0 (104)*
$V_n = V_c$, ACI 11.2.1.1, kip (kN)	30.2 (134)	30.1 (134)	28.3 (126)	45.1 (201)
$V_n = V_c$, ACI 11.2.2.1, kip (kN)	30.3 (135)	31.7 (141)	28.4 (126)	44.4 (198)
$V_n = V_c$, Eurocode 2, kip (kN)	28.4 (126)	28.4 (126)	27.2 (121)	33.6 (149)
$V_n = V_c$, AASHTO, kip (kN)	25.2 (112)	23.5 (104)	28.4 (126)	29.2 (130)

* The flexural strength in the legs controlled.

Table 5. Ultimate and predicted total applied loads. Most accurate predictions are highlighted in green.

	Specimen 1	*Specimen 2*	*Specimen 3*	*Specimen 5*
Applied ultimate load, kip (kN)	57.8 (257)	97.0 (431)	84.8 (377)	76.8 (342)
Flexure, ACI, kip (kN)	46.4 (206)	75.0 (334)	70.1 (312)	42.2 (188)
Flexure, max., kip (kN)	58.7 (261)	95.7 (426)	89.3 (397)	65.7 (292)
Shear, ACI 11.2.1.1, kip (kN)	59.5 (265)	58.6 (261)	55.9 (249)	92.9 (413)
Shear, ACI 11.2.2.1, kip (kN)	59.9 (266)	61.8 (275)	56.1 (250)	91.5 (407)
Shear, Eurocode 2, kip (kN)	56.1 (250)	55.2 (245)	53.7 (239)	64.5 (287)
Shear, AASHTO, kip (kN)	49.7 (221)	45.4 (202)	56.1 (250)	58.7 (261)

Specimen 1 has predicted loads close to matching the experimental results. The predicted ultimate load due to maximum flexural strength for Specimen 1 is 58.7 kip (261 kN), which is 0.9 kip (4.00 kN) higher than the actual observed experimental loading of 57.8 kip (257 kN), which is non-conservative by 1.6%. The ACI as well as Eurocode 2 shear strength predictions are also very close. Flexural strength and AASHTO-based shear are conservative. For Specimen 2, the prediction based on maximum flexural strength was closest, being slightly conservative by 1.3%. All other predictions were over-conservative. Specimen 3 had a predicted maximum flexural strength of 89.3 kip (397 kN), which is unconservative by 5.3%. All other predictions were over-conservative. The ACI shear predictions for Specimen 5 were non-conservative. All other predictions were over-conservative. The reason for the high predictions was how Specimen 5 failed. As mentioned before, Specimen 5 had a shear-bearing failure at the left support. After the bearing failure the specimen was loaded again and failed shortly after.

In addition to the strength predictions, the shear strength factor, β, was calculated at the support location when the ultimate load was reached. For comparison, the ACI 318-14 simple shear equation assumes $\beta = 2$, which is the most commonly used value. **Figure 63** shows that this is over-conservative for the case where a concentrated load is close to the support. In this research, observed minimum values of β for Specimens 1, 2, and 3 were found to be 1.99, 2.97, and 3.36, respectively, and are shown as well for comparison. It should be noted that the diagonal likely adds shear strength. However, β values significantly larger than 2 have been found for unreinforced beams decades ago (Kani 1967) and have been confirmed in this research as well.

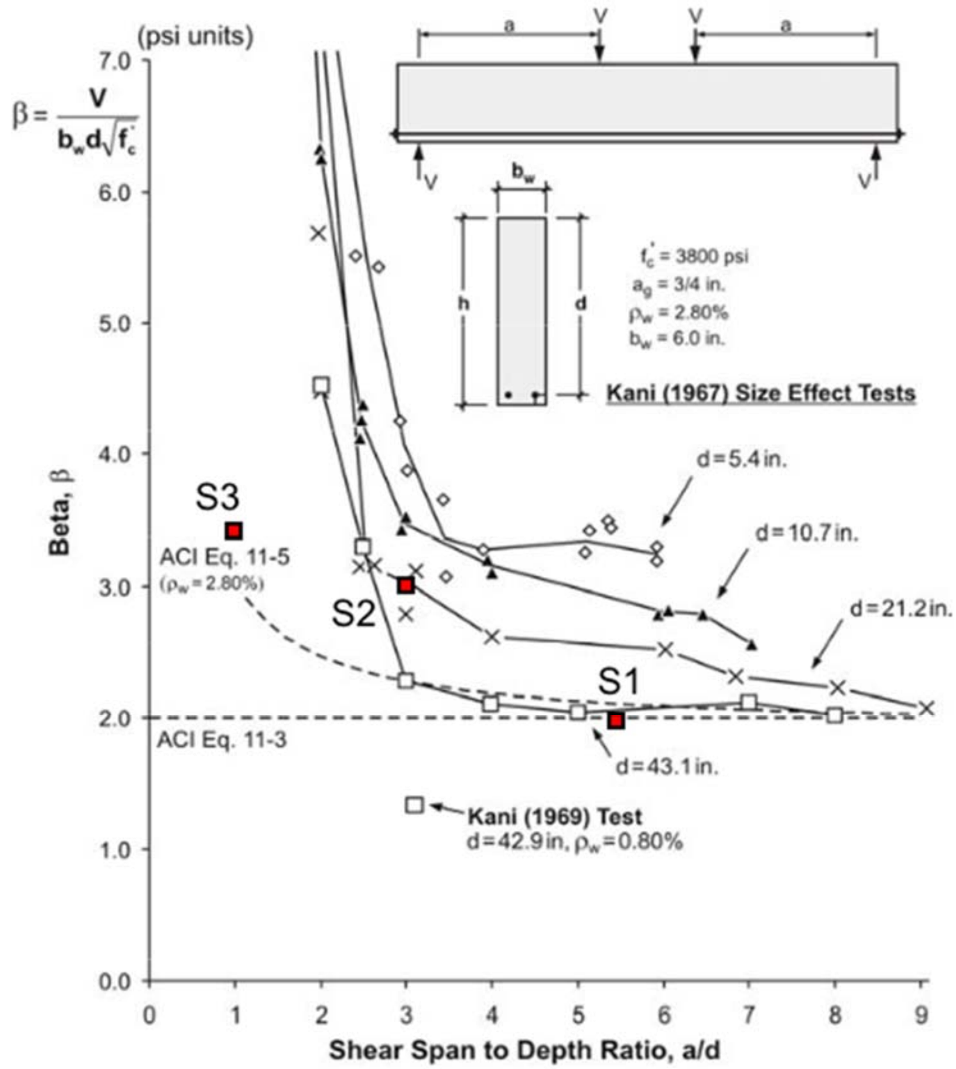

Figure 63. Shear Strength Factor, β vs. Shear Span to Depth Ratio, *a*/*d*. The data points shown in red were added to the figure from (Sherwood 2008) (Original figure from (Kani 1967)) and were computed from Specimens 1 (S1), 2 (S2), and 3 (S3). These represent *minimum* actual observed values.

5.2 Specimen 4 (Wide Specimen)

5.2.1 Model Assumptions

Specimen 4 was 11 ft – 4 in (3.45 m) wide to simulate and investigate the load distribution in an actual culvert slab. For the analysis it was assumed that it is a one-way slab, i.e. load is only carried from support to support over a specific effective width which was to be determined. Therefore the same approach for calculating the maximum predicted load based on flexural strength as Specimen 1, 2, 3, and 5 was used with the only difference of the effective width. Furthermore, the effective width was assumed to be different at mid-span (= positive moment region) compared to over the support (= negative moment region).

Specimen 1, 2, 3, and 5 had a constant section width of 2 ft (610 mm) corresponding to the physical width of the specimens. For Specimen 4, the positive moment effective width was determined using the mid-span deflections recorded during testing. The area under the displacement curve for an applied load of 220 kip (979 kN) was calculated and a representative square determined from it with the maximum displacements kept the same. An effective width of 7.0 ft (2.13 m) was calculated. **Figure 64** shows the representative square. This assumes that the entire width would yield prior to failure. This effective width is similar to the one determined by Jones and Shenton (2012). The effective width using their formula and removing the multiple presence factor is 7.17 ft (2.19 m). Hence, for our predictions we used an effective width for the positive bending region of 7.0 ft (2.13 m) represented by the blue line in **Figure 65**. This strip width also compares well with **Figure 44** as it would produce a factor of 3.5.

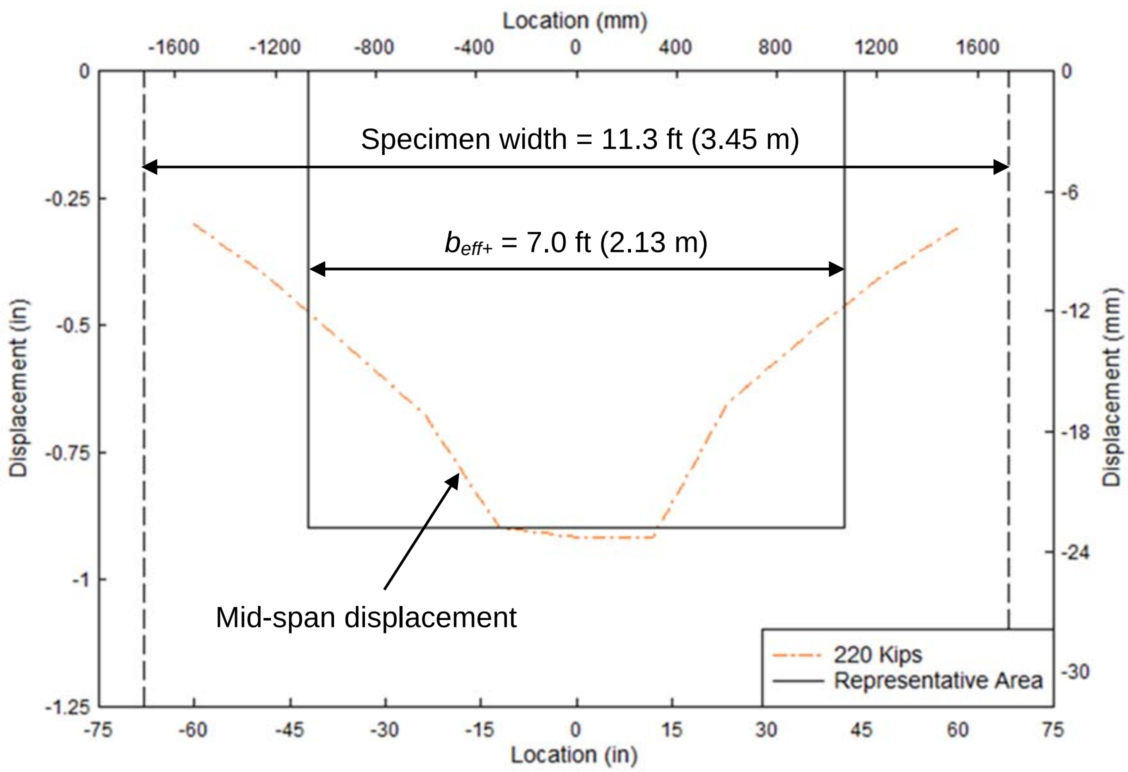

Figure 64. Positive moment effective width for Specimen 4.

From our experimental results, assuming a strip with a constant width using AASHTO's 5.26 ft (1.60 m) and Jones and Shenton's 7.17 ft (2.19 m) resulted in an over-conservative estimate. Assuming a 45 ° load spread angle from the AASHTO loading patch toward the supports as shown in **Figure 65** (dashed line) produced an effective slab width of b_{eff-} = 10.8 ft (3.30 m) at the supports represented by the red line.

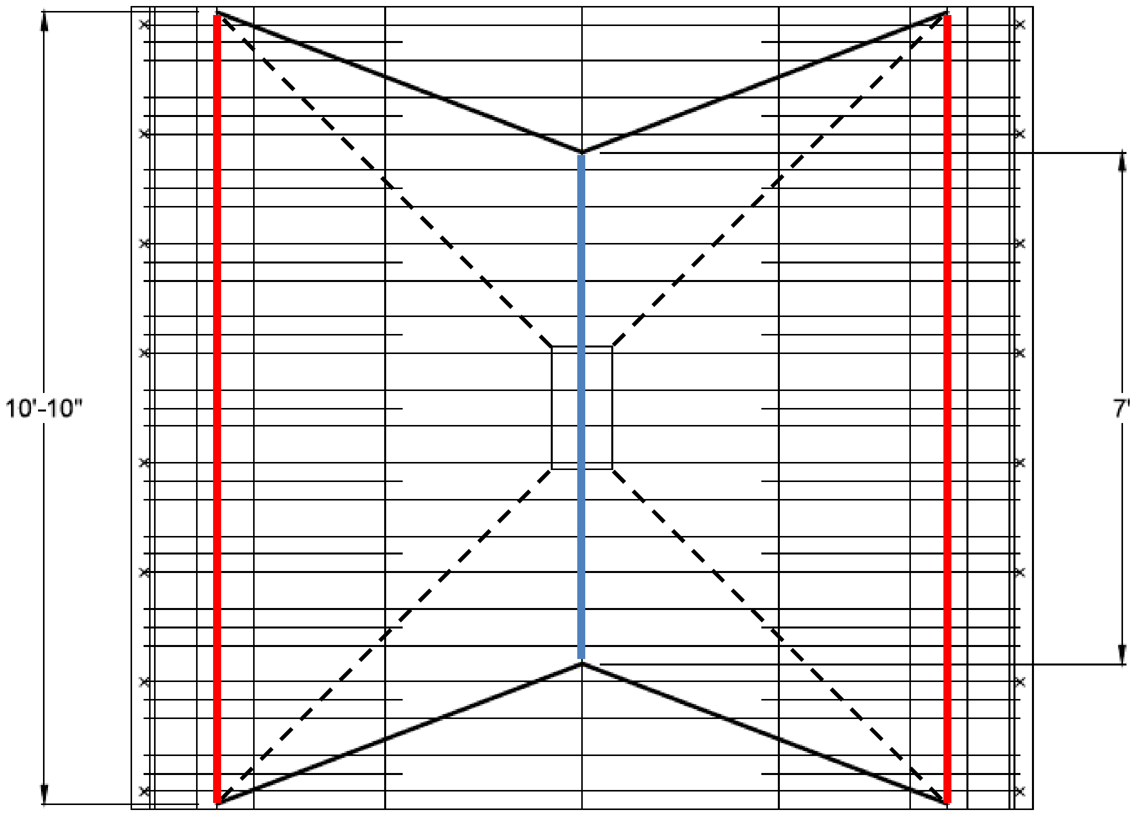

Figure 65. Assumed effective widths for Specimen 4. The blue line represents b_{eff+} and the red line b_{eff-}.

5.2.2 Flexural Strength Predictions

The predictions for flexural strength follow the procedure presented in Section 5.1.2. In order to account for the transverse load distribution, the effective widths are considered by multiplying the calculated unit flexural strengths with those effective widths.

5.2.3 Two-Way Shear Strength Predictions

Since Specimen 4 was assumed to be a one-way slab, the shear calculations used for Specimen 1, 2, 3, and 5 do not apply under load because Specimen 4 is a slab and shear stress occurs on all sides of the load and not just to the left and right of the load, i.e. two-way (or punching) shear has to be considered. The formula used was ACI 318-14, 22.6.5 (= AASHTO LRFD, 5.13.3.6.3) and is as follows:

$$V_c = \left(2 + \frac{4}{\beta}\right)\sqrt{f'c}\, b_o\, d \geq 4\sqrt{f_c'}\, b_0 d \qquad \textbf{Equation 10}$$

where β here is the length-to-width ratio of the loading patch and b_0 is the perimeter of the failure cone. The ACI 318-14 critical section at $d/2$ was used to calculate b_0.

The Eurocode 2 two-way shear equation for reinforced concrete members without shear reinforcement was also calculated. The equation is as follows:

$$V_{Rd,c} = \left[\left(\frac{0.18}{\gamma_c}\right) k \, (100\, \rho\, f_{ck})^{\frac{1}{3}} + 0.1\, \sigma_{cp}\right] u_1\, d \qquad \textbf{Equation 11}$$

where $k = 1 + \sqrt{\frac{200}{d}}$ is the depth factor with d in (mm), ρ is the shear reinforcement ratio and calculated as $\sqrt{\rho_l \rho_t}$ (≤ 0.02), f_{ck} is the characteristic concrete compressive strength in (MPa), and σ_{cp} is an applied normal stress in (MPa), here neglected. γ_c is the partial strength reduction factor for concrete and usually taken as 1.5. Since we are interested in the nominal strength, this factor is here set to γ_c = 1.0. u_1 is the basic control perimeter (equivalent to b_0 in the ACI 318-14 code) and assumed 2d away from the loaded area. Detailed two-way shear calculations can be found in Appendix H.

5.2.4 Results

Table 6 presents the predicted flexural and two-way shear strengths for Specimen 4.

Table 7 shows the predicted vs. the experimental results, indicating which predictions are conservative or unconservative. The Specimen 4 maximum moment prediction was the most accurate, followed by ACI two-way shear. Detailed calculations for two-way shear strength can be found in Appendix H.

Table 6. Predicted strengths.

	Specimen 4
M_n^+, ACI, kip-ft (kNm)	218 (296)
M_n^+, max., kip-ft (kNm)	293 (397)
M_n^-, ACI, kip-ft (kNm)	152 (206)
M_n^-, max., kip-ft (kNm)	182 (247)
$V_{n,two\text{-}way} = V_{c,two\text{-}way}$, ACI 11.11.3.2, kip (kN)	242 (1076)
$V_{n,two\text{-}way} = V_{c,two\text{-}way}$, Eurocode 2, kip (kN)	216 (960)

Table 7. Maximum ultimate and predicted total applied loads. Most accurate predictions are highlighted in green.

	Specimen 4
Applied ultimate load, kip (kN)	230 (1023)
Flexure, ACI, kip (kN)	181 (803)
Flexure, max., kip (kN)	232 (1034)
Two-way Shear, ACI 11.11.3.2, kip (kN)	241 (1072)
Two-way Shear, Eurocode 2, kip (kN)	215 (956)

5.3 Comparison All Specimens

Figure 66 shows a comparison of all observed and predicted strengths in graphical form. As can be seen, the most consistent and accurate prediction is based on a plastic mechanism, assuming maximum values for flexural strength. For the realistic specimen, Specimen 4, two-way (or punching) shear failure was observed and the ACI 318-14 prediction is also close. The shear predictions are mostly conservative with the exception for Specimen 5.

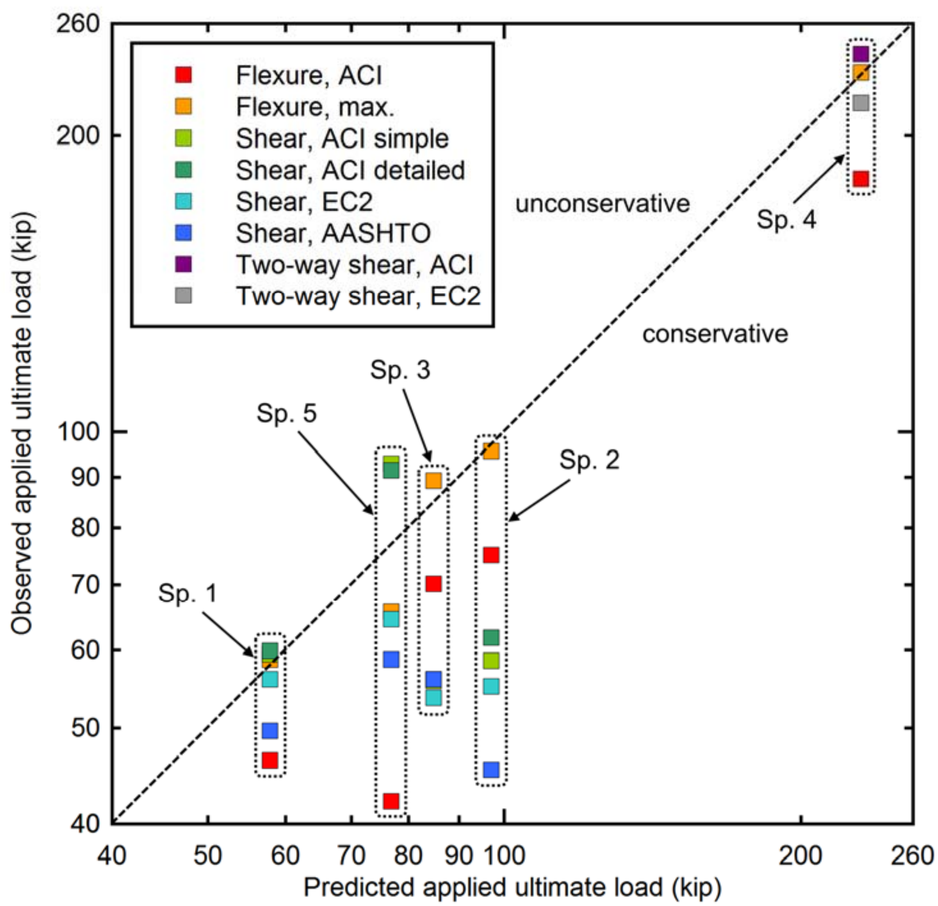

Figure 66. Predicted vs. experimental results Specimen 4.

6 Conclusions and Recommendations for Load Rating

The following can be concluded for Specimens 1, 2, 3, and 5 (24 in (610 mm) width):

- For the unique negative flexural reinforcement (corner) detail in Specimen 1 through 3, one large vertical crack formed, followed by distributed flexural cracking in the positive bending moment region around mid-span.
- Specimen 5 developed, due to the additional horizontal reinforcement, distributed cracking in the negative flexural (corner) region as well.
- Both unique negative flexural reinforcement (corner) details did not lead to failure in shear-mode for any of the strip specimens.
- The unique negative flexural reinforcement detail was able to develop the full plastic moment, i.e. the tension reinforcement yielded, for all strip specimens.
- The 24 in (610 mm) strip specimens were all able to develop a plastic mechanism, i.e. a plastic-plastic analysis can be taken advantage of in order to estimate the ultimate system capacity.
- Ultimate failure occurred in shear-mode due to extensive deflections after the plastic mechanism had formed, i.e. post-peak total applied load.
- The final failure crack was approximately 30 ° for all specimens.
- To calculate the effective load length, a 30 ° load distribution angle can be assumed, as shown in **Figure 54**.
- Ultimate system capacity can be estimated most accurately by assuming a mechanism based on maximum flexural strengths at the plastic hinge locations corresponding to a concrete compressive strain of approximately 0.008.

The following can be concluded for Specimen 4 (11 ft – 4 in (3.45 m) width):

- The load distribution in the slab is much more effective than predicted by any of the currently used strip width methods. For our laboratory specimen, effective widths at mid-span (under the applied load) and at the supports (face of support) were 7.0 ft (2.13 m) and 10.8 ft (3.30 m), respectively.
- The failure mode was punching shear, which was reached prior to flexural capacity.
- Although the observed failure crack was less than 45 °, the capacity was predicted fairly accurately using the ACI 318-14 code provisions for two-way shear.

Based on these observations, the following recommendations can be made for load rating purposes of actual reinforced concrete moment frame culverts with no overlay:

- Ultimate system capacity can be estimated by taking the lower of (a) two-way shear or (b) plastic moment mechanism. In addition, it is recommended that one-way shear also be evaluated at the support.
- The effective strip width below the applied load (= maximum positive bending moment) can be estimated by using a 30 ° load distribution angle.
- The equivalent strip width at the support (= maximum negative bending moment) can be estimated by assuming a 45 ° load spread angle (**Figure 65**) extending from the loading patch.
- Conservatively, a constant effective strip width, b_{eff} assuming a load distribution angle α = 30 ° can be assumed for to evaluation of both flexural and shear strengths. The width of this strip can be calculated as follows:

$$b_{eff} = 20\ \text{in} + \min\left[z,\ \frac{d_s^+}{\tan(\alpha)}\right] + \min\left[26\ \text{in},\ \frac{d_s^+}{\tan(\alpha)}\right]\ (\text{in}) \qquad \textbf{Equation 12}$$

  where d_s^+ is the flexural depth of the slab in (inch), i.e. distance from the top of the slab to the centroid of the flexural tension reinforcement, and z is the distance of the tire to the edge of the slab in (inch). 20 and 26 in correspond to the width of the AASHTO tire patch and half the distance between the two tire patches, respectively.
- One-way shear strength close to the support can be estimated using β = 3.0 rather than 2.0 as recommended in the ACI 318-14 code. The Eurocode 2 can be consulted for guidance on how to decrease that value to 2.0 for locations located > 2*d* away from the support.

  A load rating spreadsheet based on the findings and recommendations of this research is provided as a separate electronic file.

7 References

AASHTO (2011). Guide Manual for Element Inspection. Washington, D.C., American Association of State Highway and Transportation Officials.

AASHTO (2012). LRFD Bridge Design Specifications. Washington, D.C., American Association of State Highway and Transportation Officials.

Abolmaali, A. and A. Garg (2008). "Effect of Wheel Live Load on Shear Behavior of Precast Reinforced Concrete Box Culverts." ASCE Journal of Bridge Engineering **13**(1): 93-99.

ACI (2014). ACI 318-14: Building Code Requirements for Structural Concrete. Farmington Hills, MI, American Concrete Institute.

ASTM (2005). ASTM C39-05: Standard Test Method for Compressive Strength of Cylindrical Concrete Specimens. West Conshohocken, PA, ASTM International.

ASTM (2011). ASTM E8-11: Standard Test Methods for Tension Testing of Metallic Materials. West Conshohocken, PA, ASTM International.

Awwad, E., M. Mabsout, et al. (2008). "Parametric Study of Load Distribution in Four-Sided Concrete Box Culverts." Bridge Structures **4**(2): 99-107.

CEN (2004). Eurocode 2: Design of concrete structures - Part 1-1: General rules and rules for buildings. Brussels, Belgium, European Committee for Standardization.

Frederick, G. R. and K. M. Tarhini (2000). Structural Evaluation of Three-Sided Concrete Culverts. Concrete Piper for the New Millenium. Concrete Pipe for the New Millenium. I. I. Kaspar and J. I. Enyart. Seattle, WA, ASTM. **STP 1368:** 36-44.

Garg, A. and A. Abolmaali (2009). "Finite-Element Modeling and Analysis of Reinforced Concrete Culverts." ASCE Journal of Transportation Engineering **135**(3): 121-128.

Garg, A., A. Abolmaali, et al. (2007). "Experimental Investigation of Shear Capacity of Precast Reinforced Concrete Box Culverts." ASCE Journal of Bridge Engineering **12**(4): 511-517.

Jones, B. P. and H. W. I. Shenton (2012). Effective Width of Concrete Slab Bridges in Delaware. Dover, DE, Delaware Department of Transportation.

Kani, G. N. J. (1967). "How Safe Are Our Large Reinforced Concrete Beams?" ACI Journal **64**(4): 128-141.

Nielsen, M. P. and L. C. Hoang (2011). Limit Analysis and Concrete Plasticity. Boca Raton, FL, CRC Press.

Sherwood, E. G. (2008). One-Way Shear Behaviour of Large, Lightly-Reinforced Concrete Beams and Slabs. PhD PhD Dissertation, University of Toronto.

APPENDIX A: CONCRETE CYLINDER COMPRESSIVE STRENGTH

A.1 Specimen 1

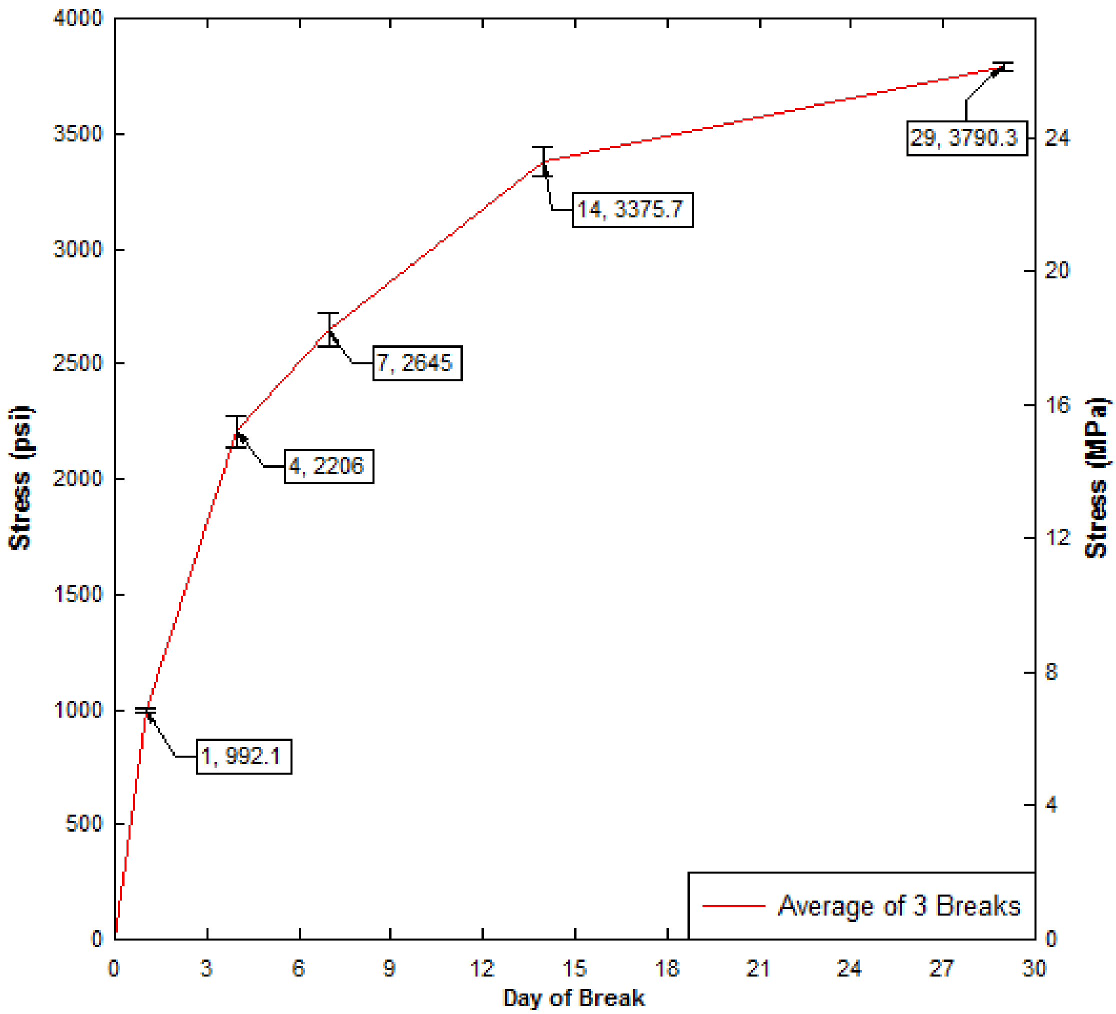

A.2 Specimen 2

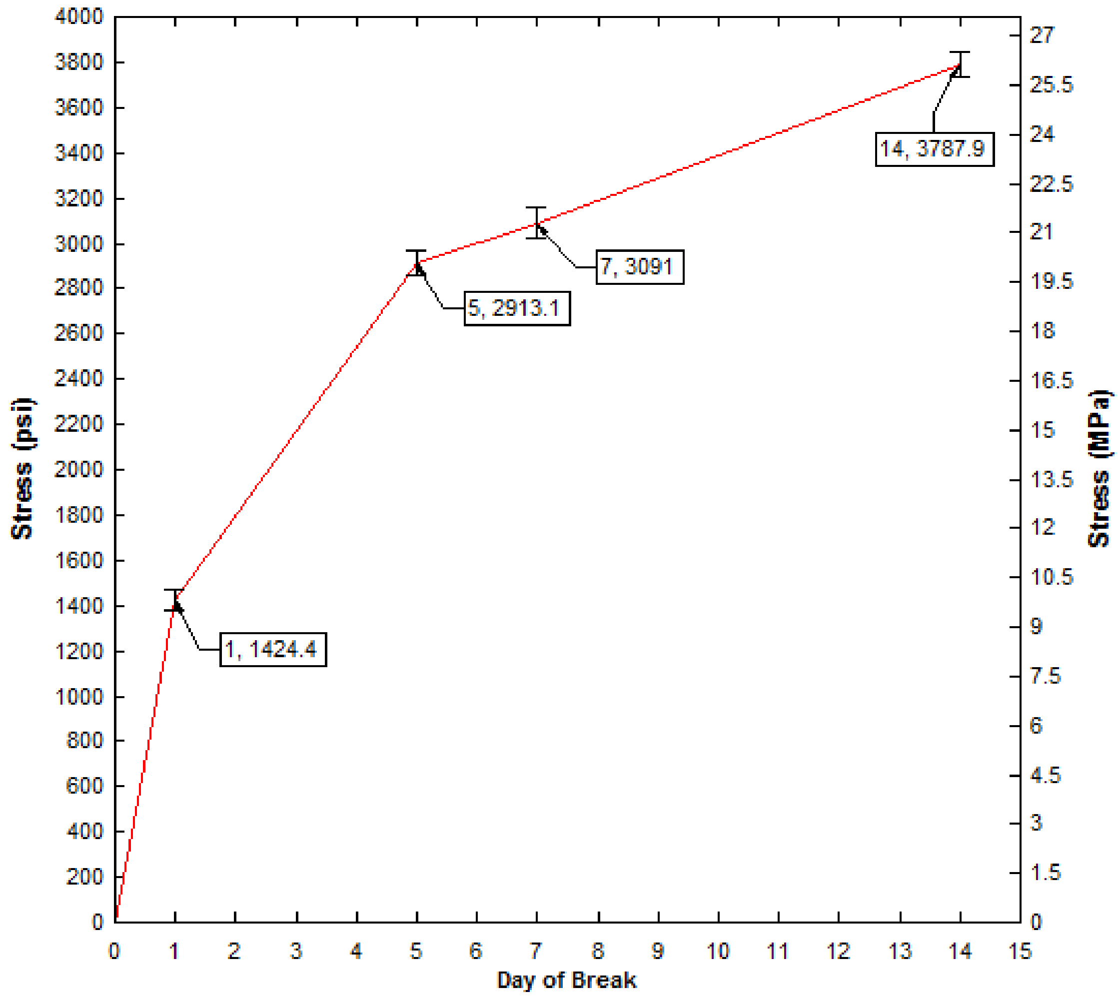

A.3 Specimen 3

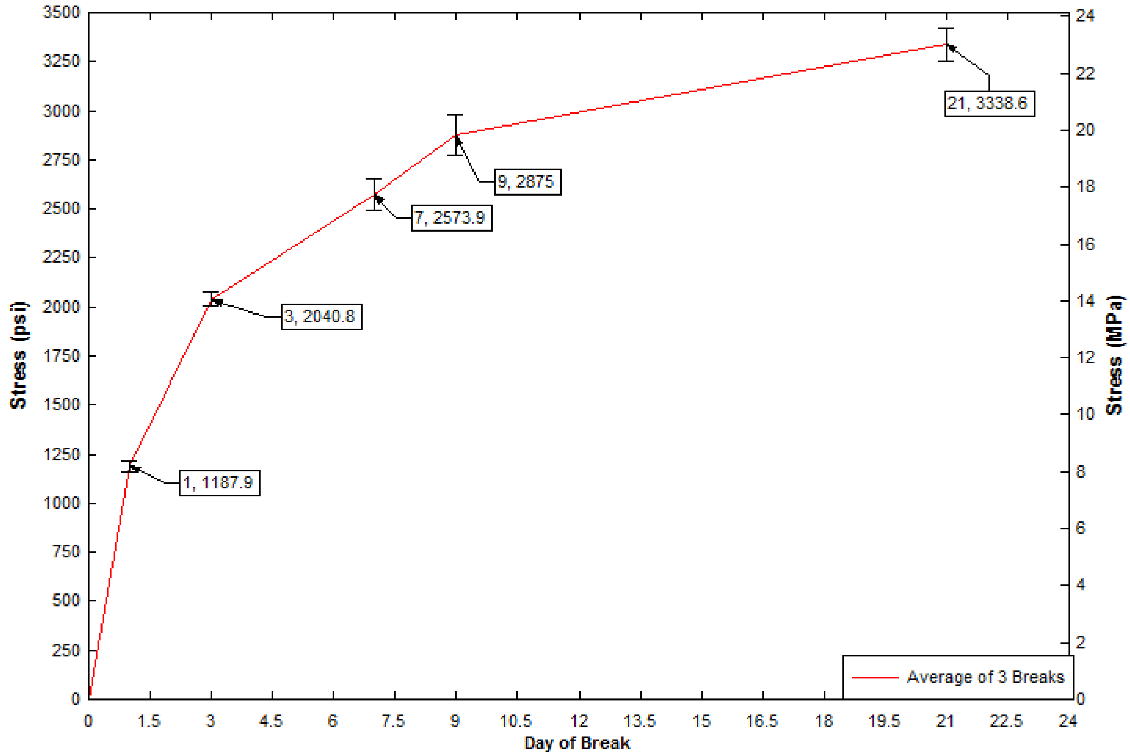

A.4 Specimen 4

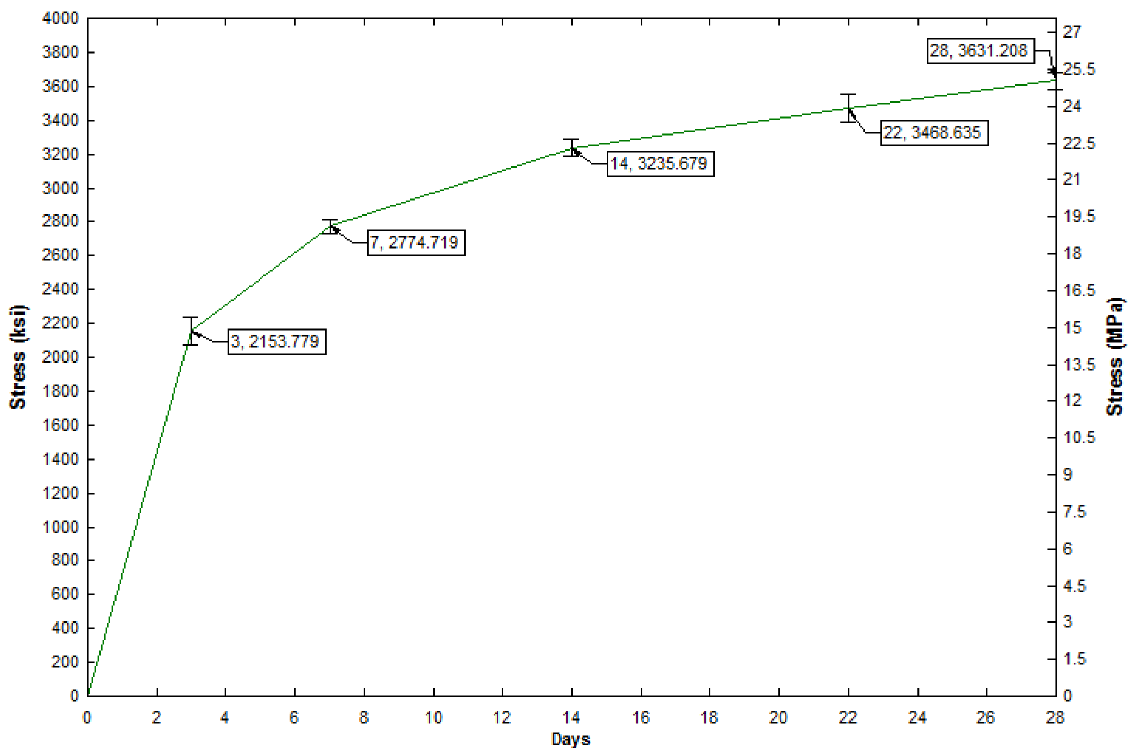

A.5 Specimen 5

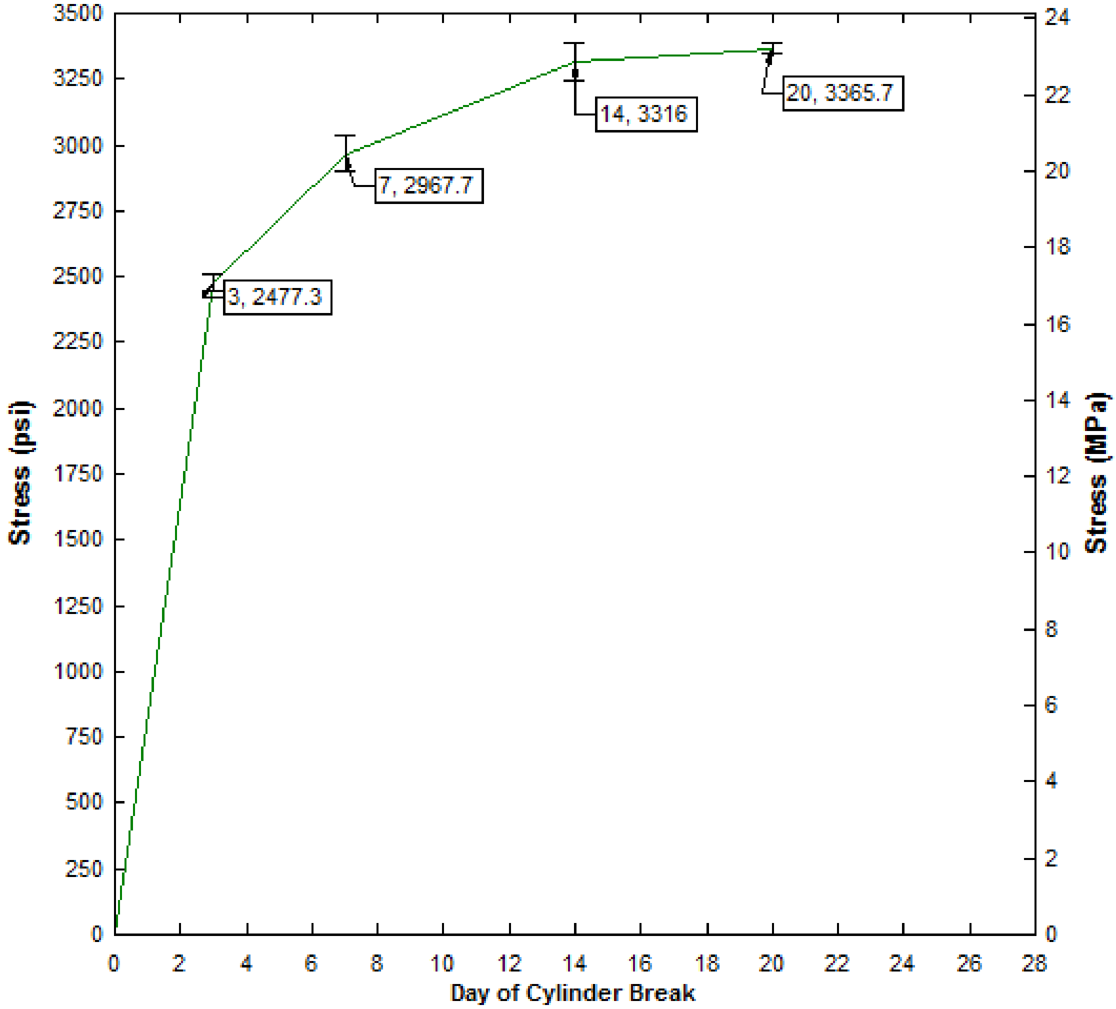

APPENDIX B: STEEL REBAR TENSION TESTS

B.1 Specimen 1

#5 Hooked Bar

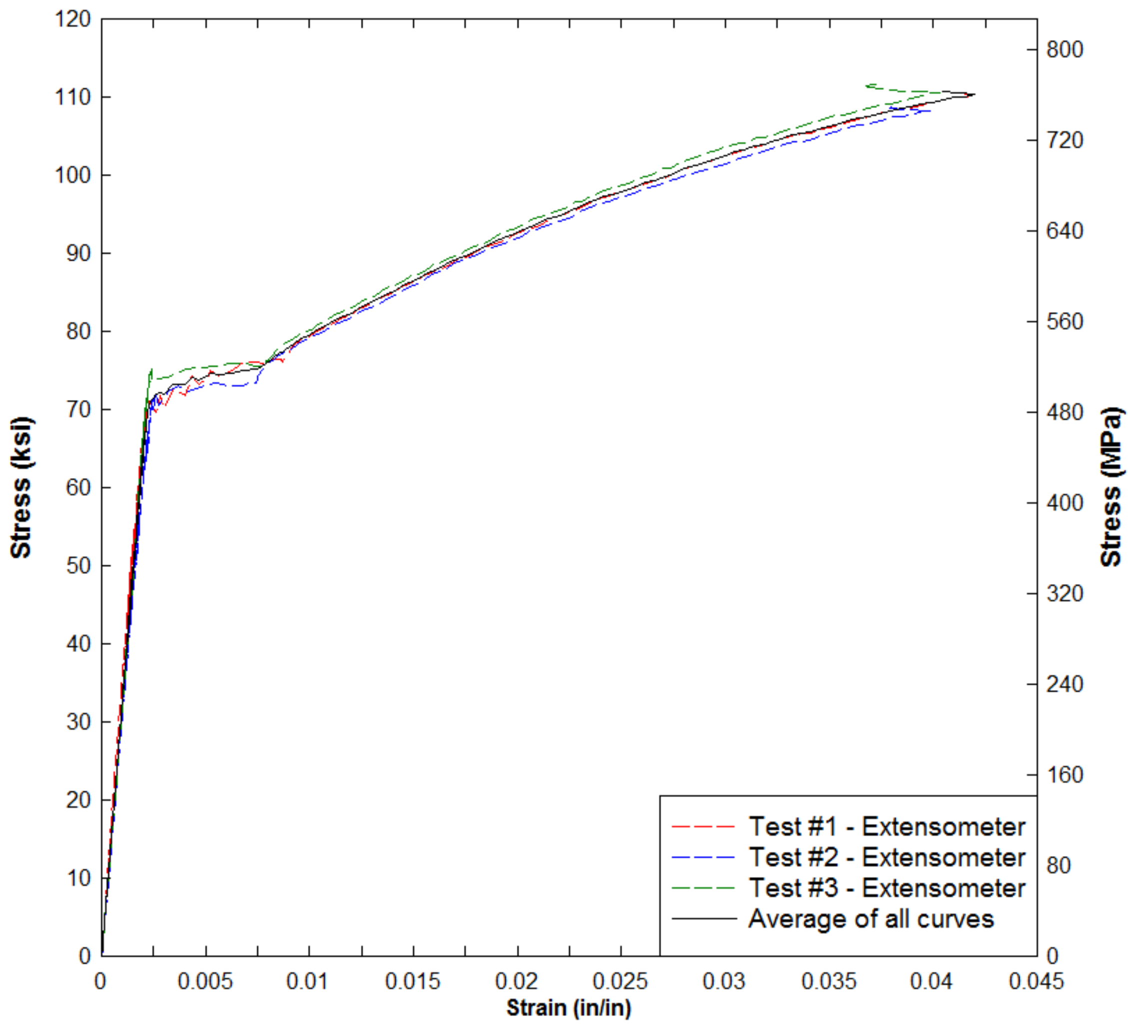

#5 Straight Bar

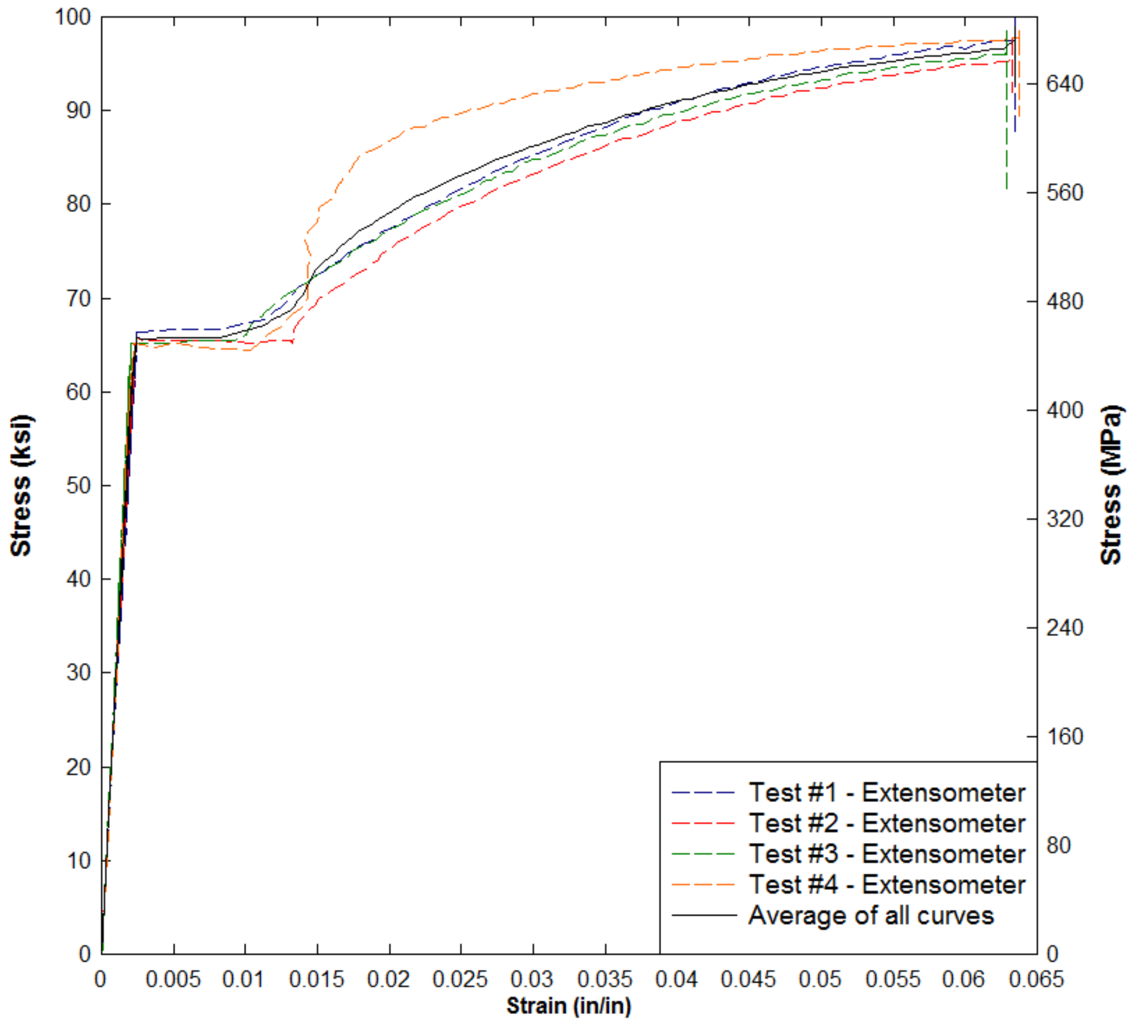

#3 Vertical Bar

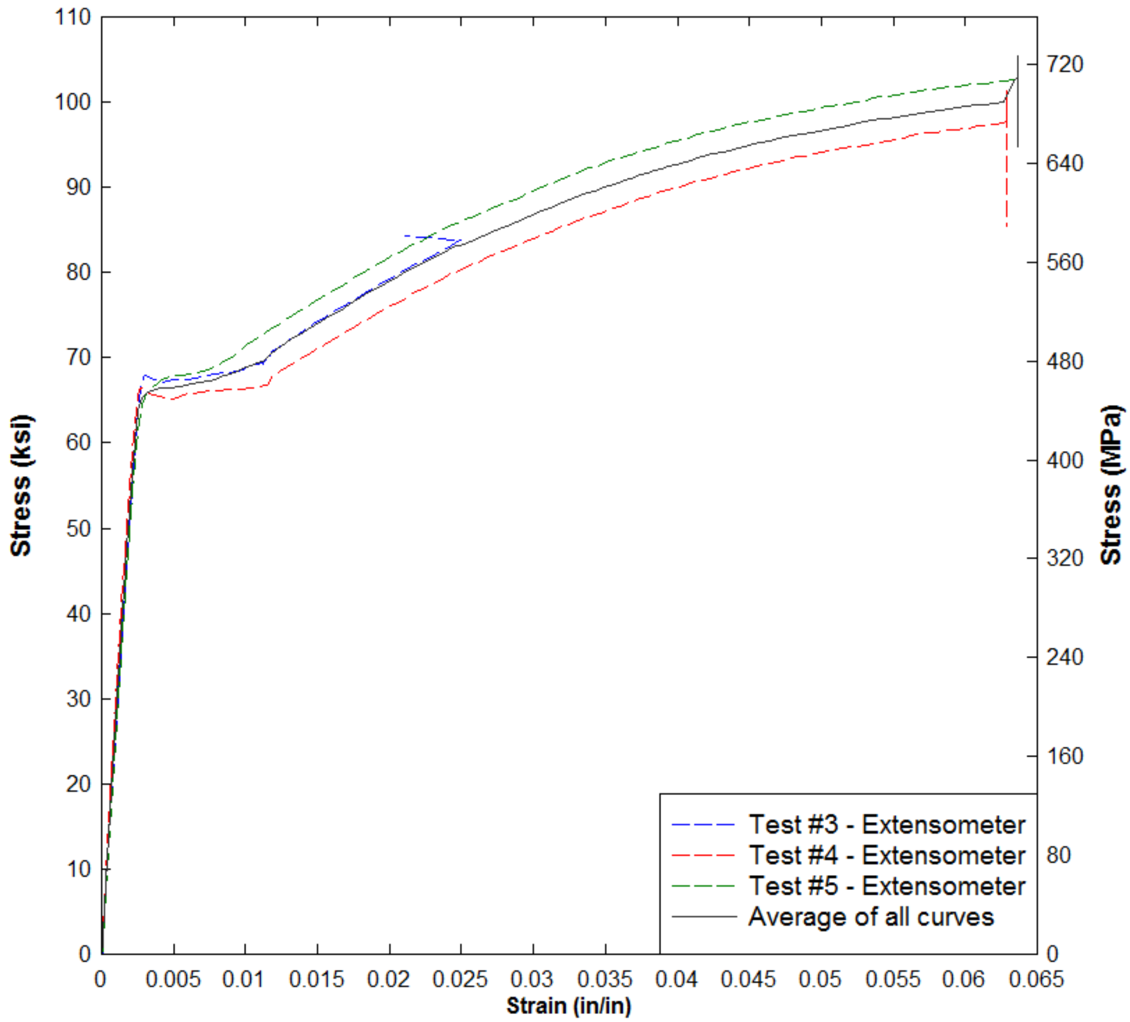

B.2 Specimen 2 and Specimen 3

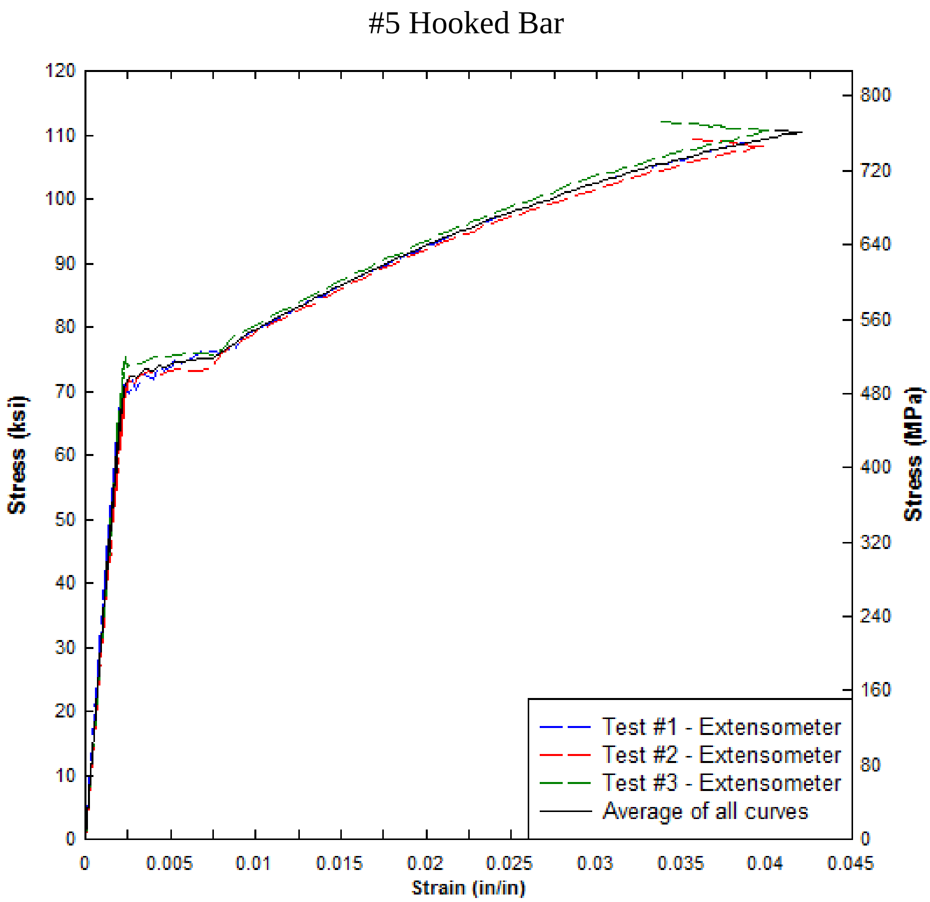

#5 Straight Bar

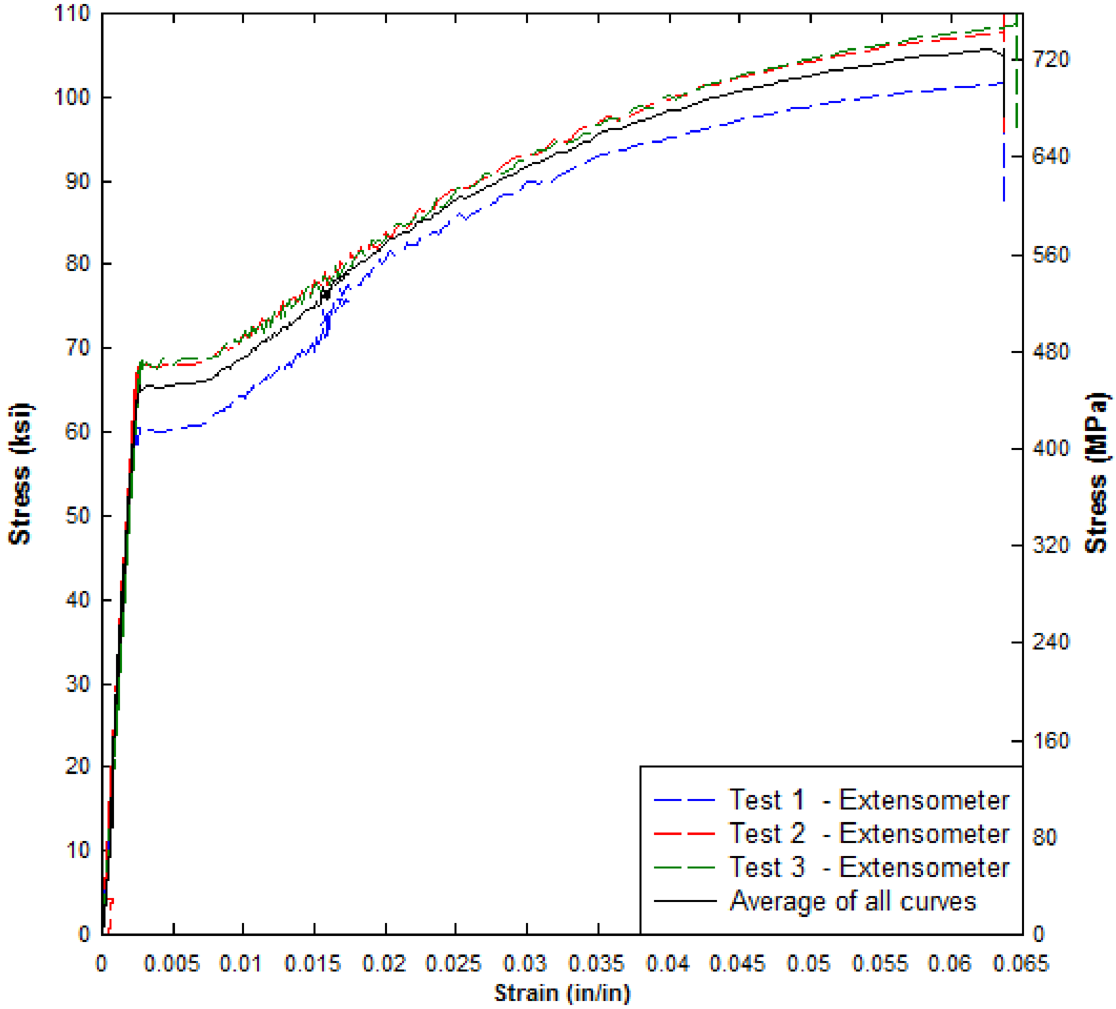

B.3 Specimen 4

#5 Hooked Bar

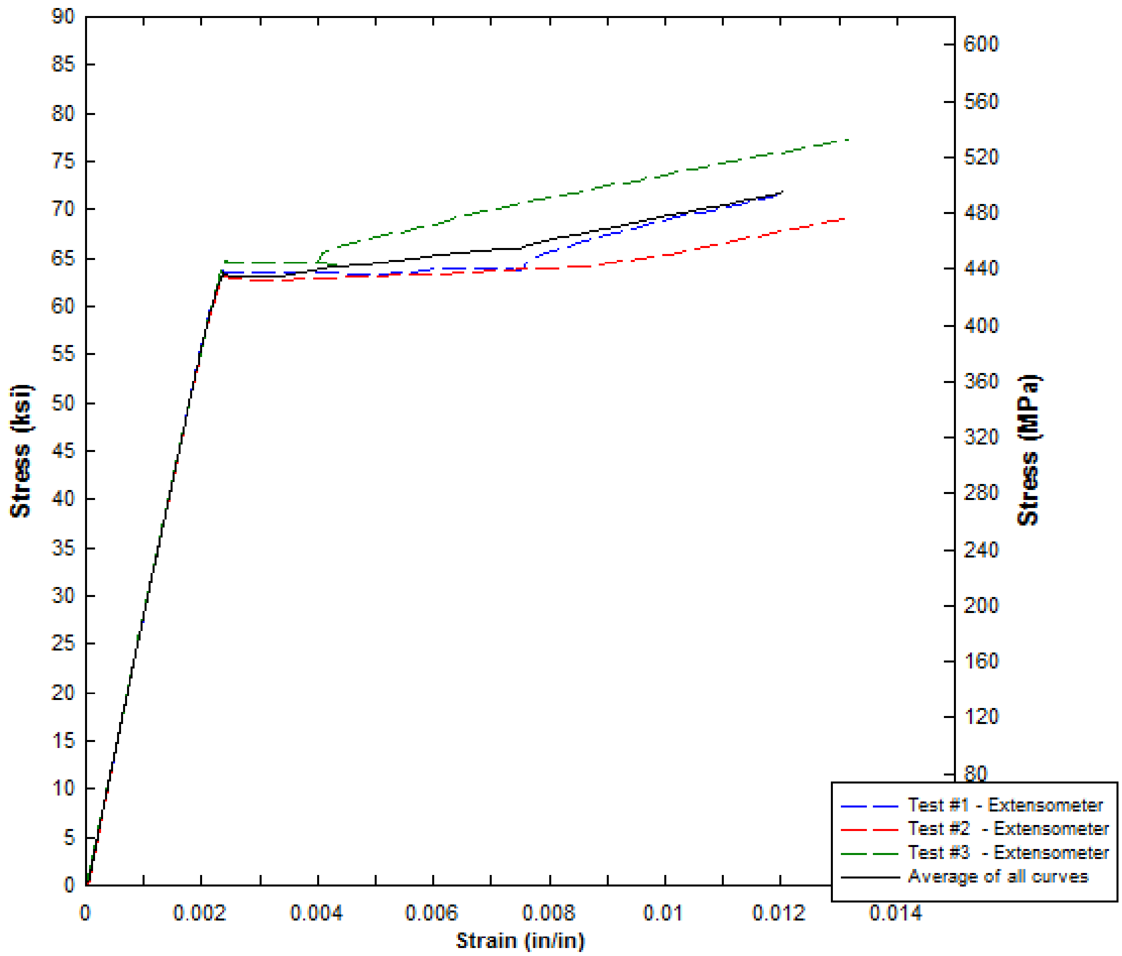

#5 Straight Bar

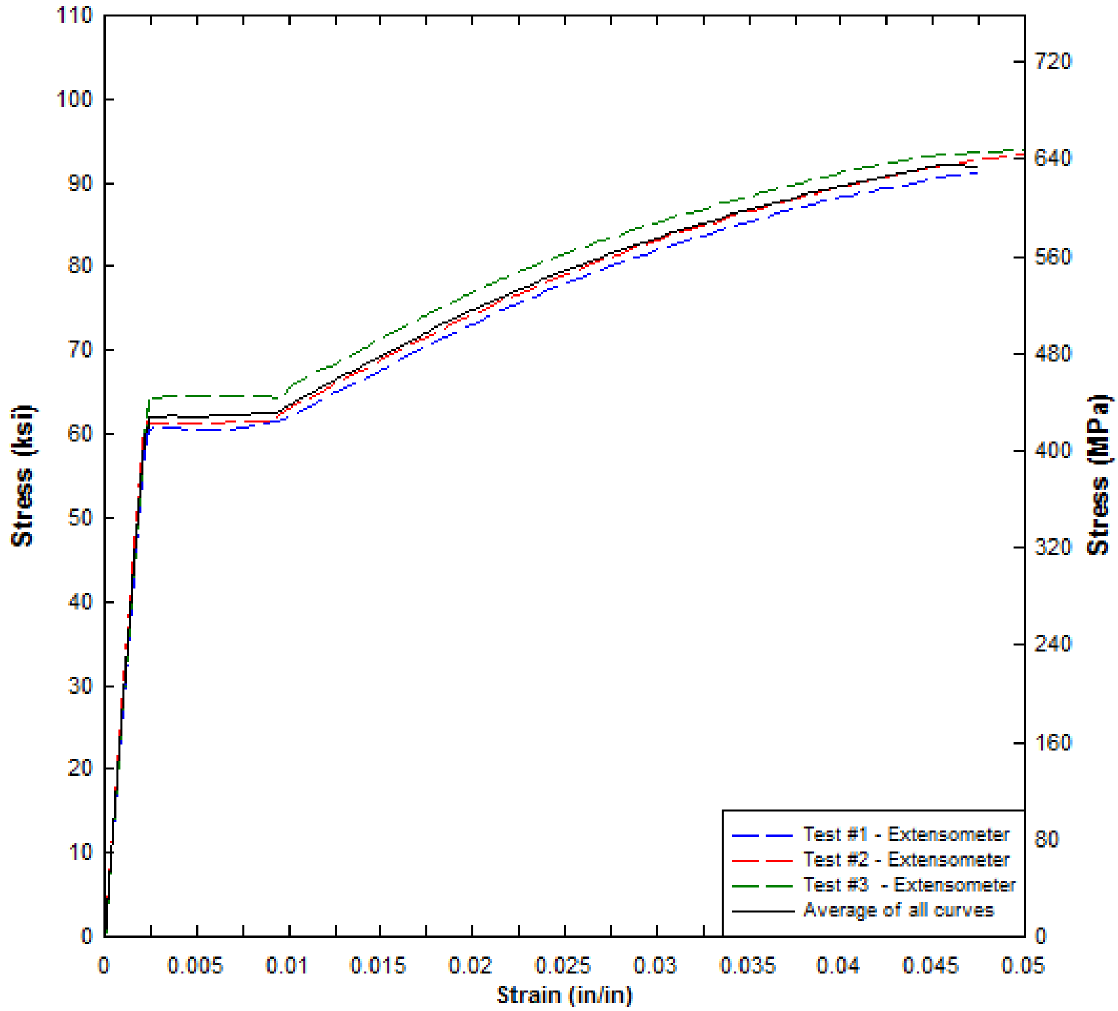

#3 Vertical Bar

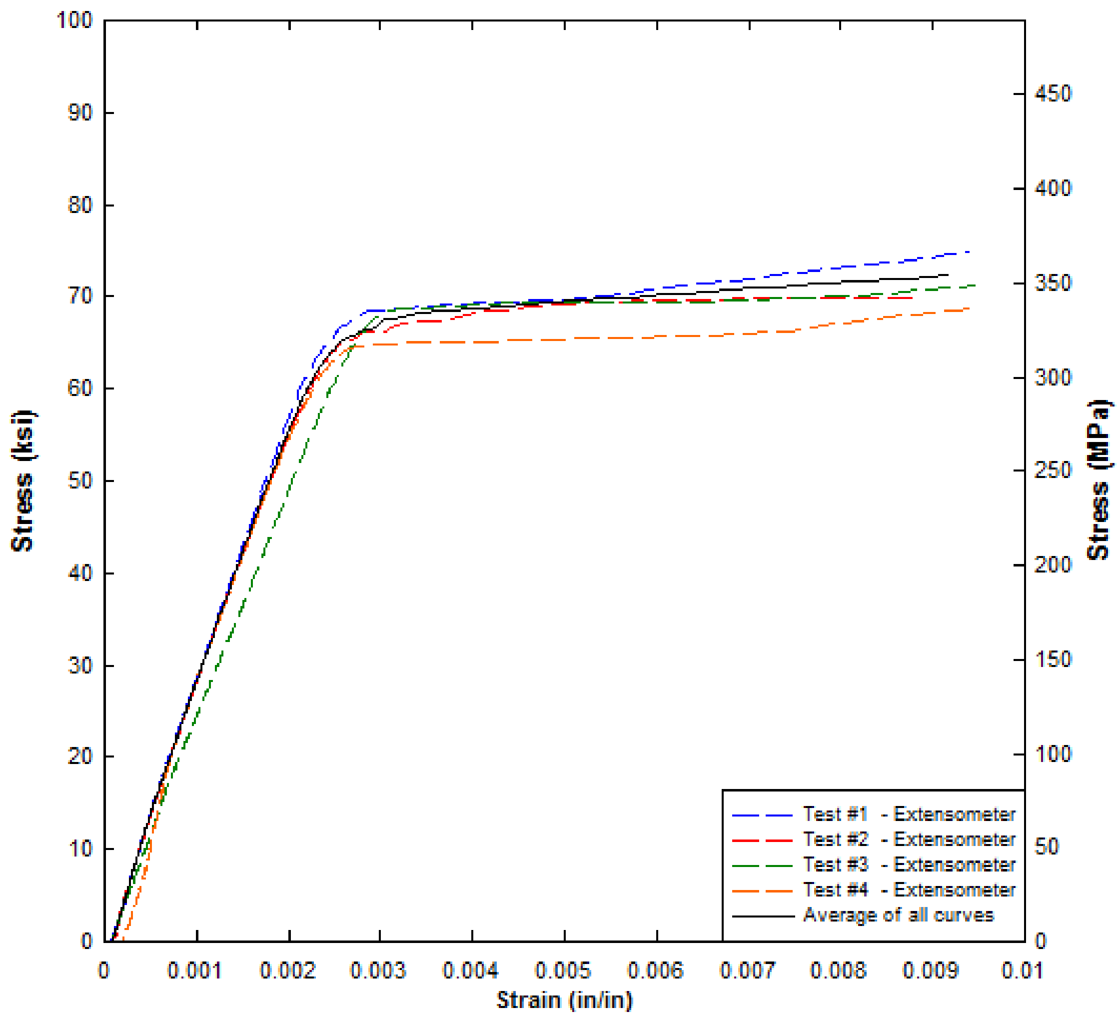

B.4 Specimen 5

90° Bar

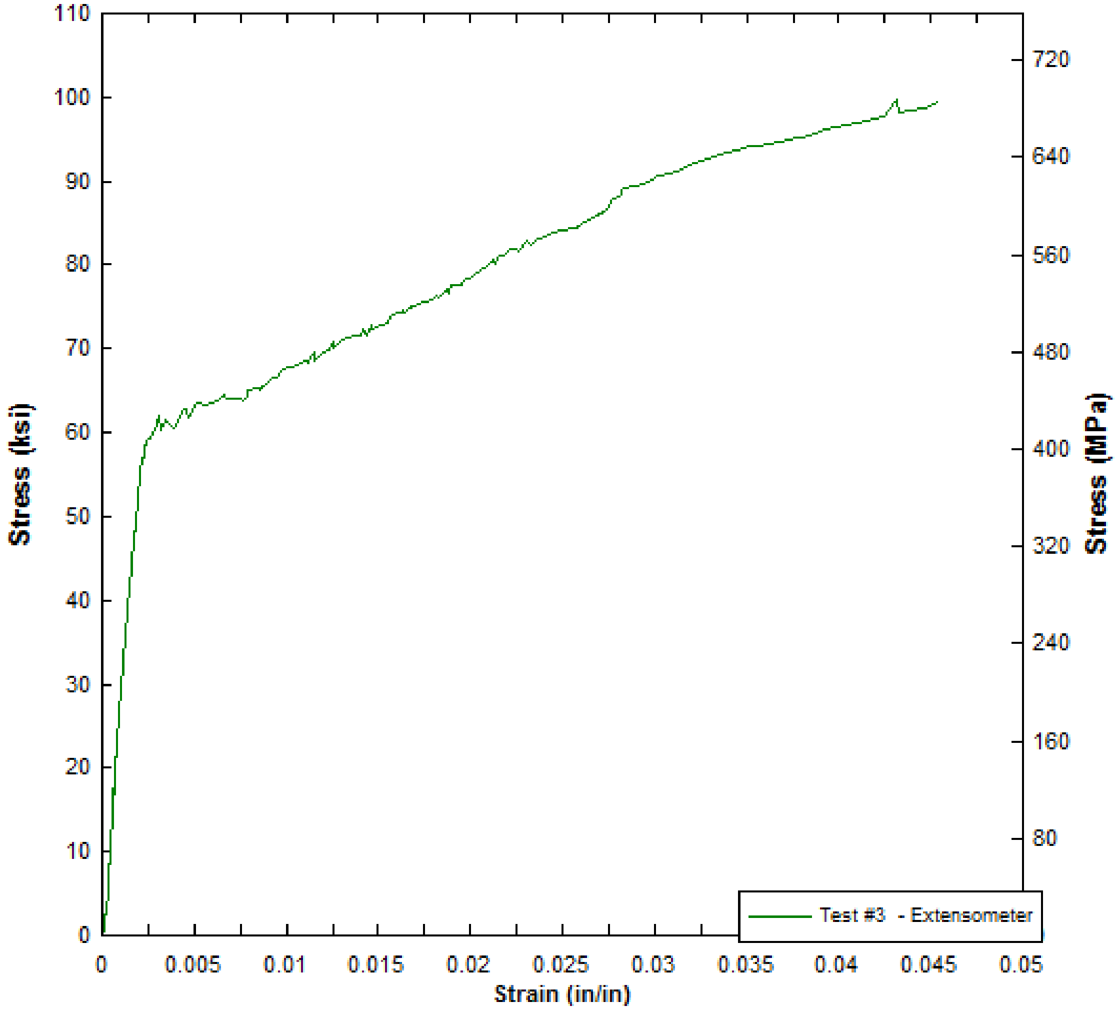

Long/Hooked Bar

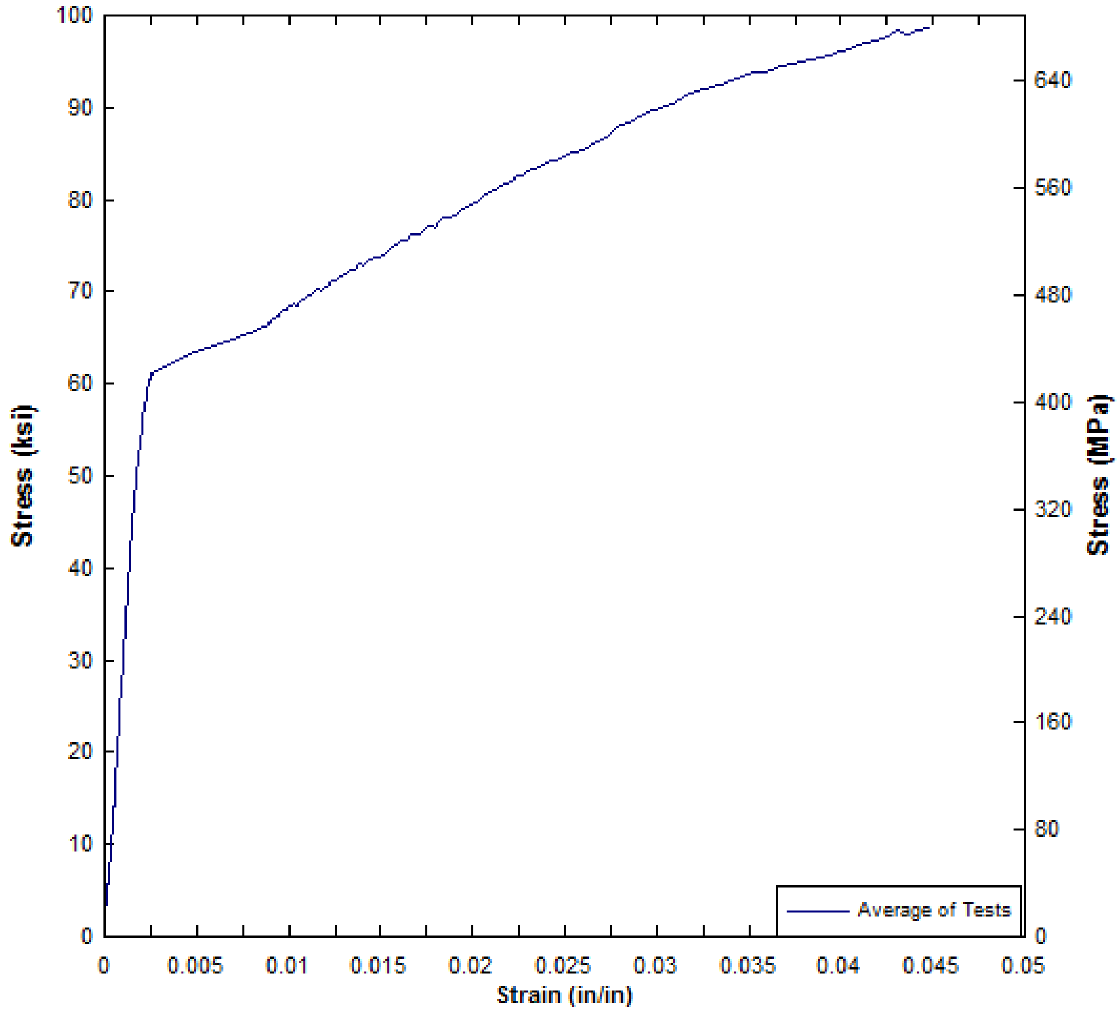

Longitudinal Bar

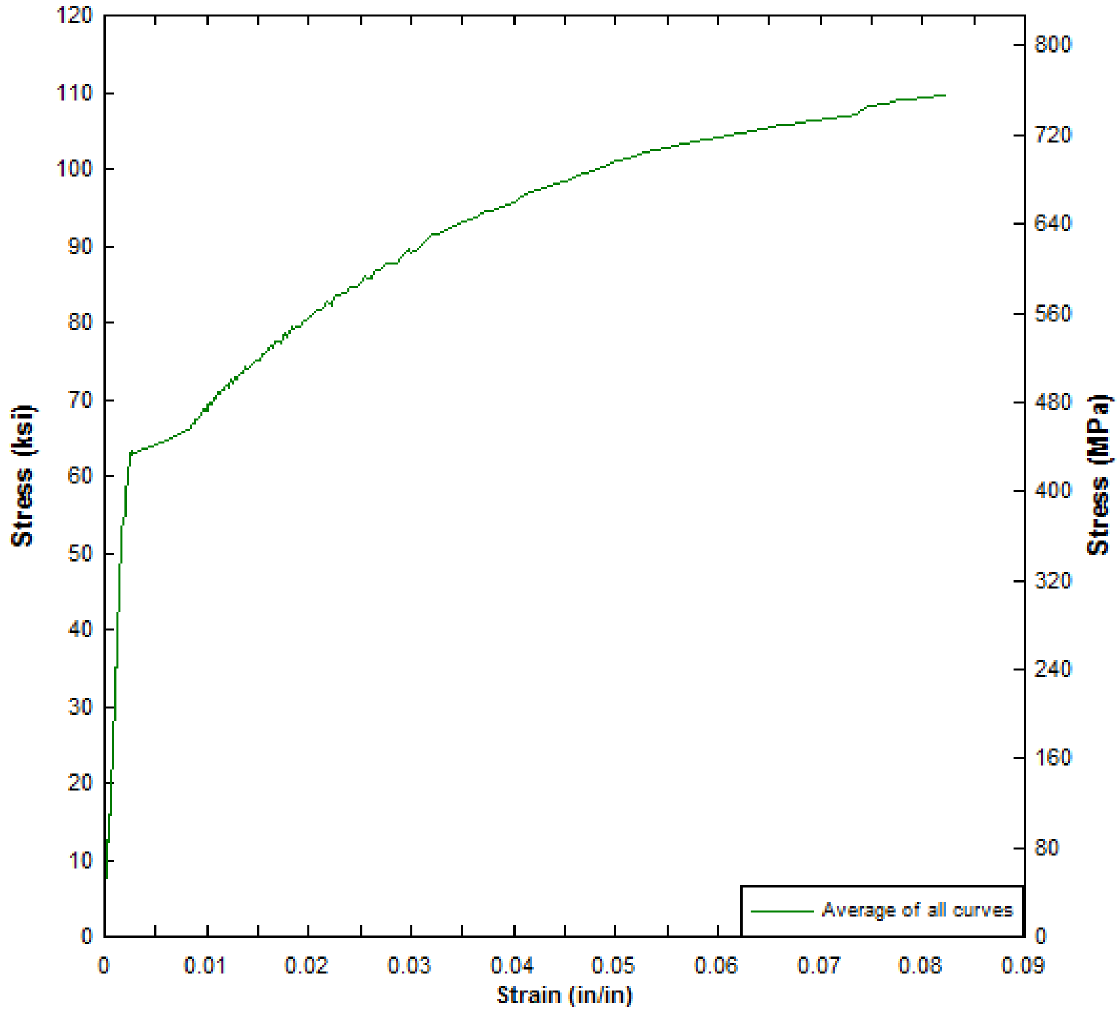

APPENDIX C: LOAD VS. STRAIN GRAPHS

C.1 Specimen 1

Location A

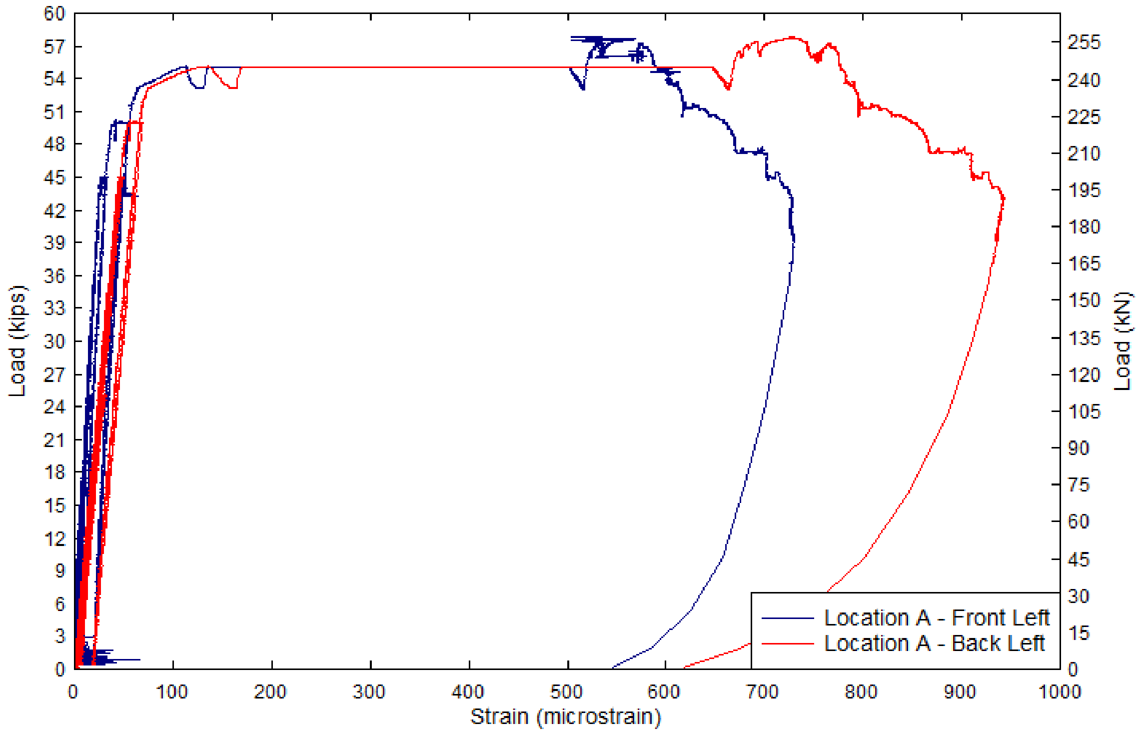

Location B

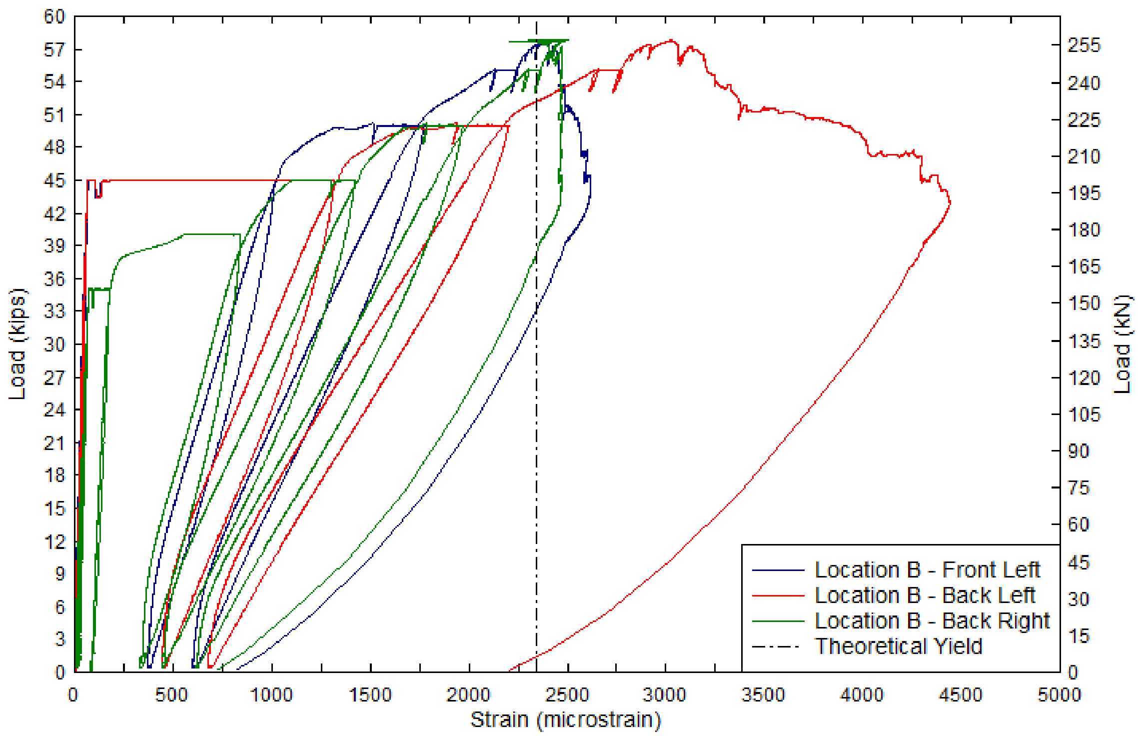

Location D

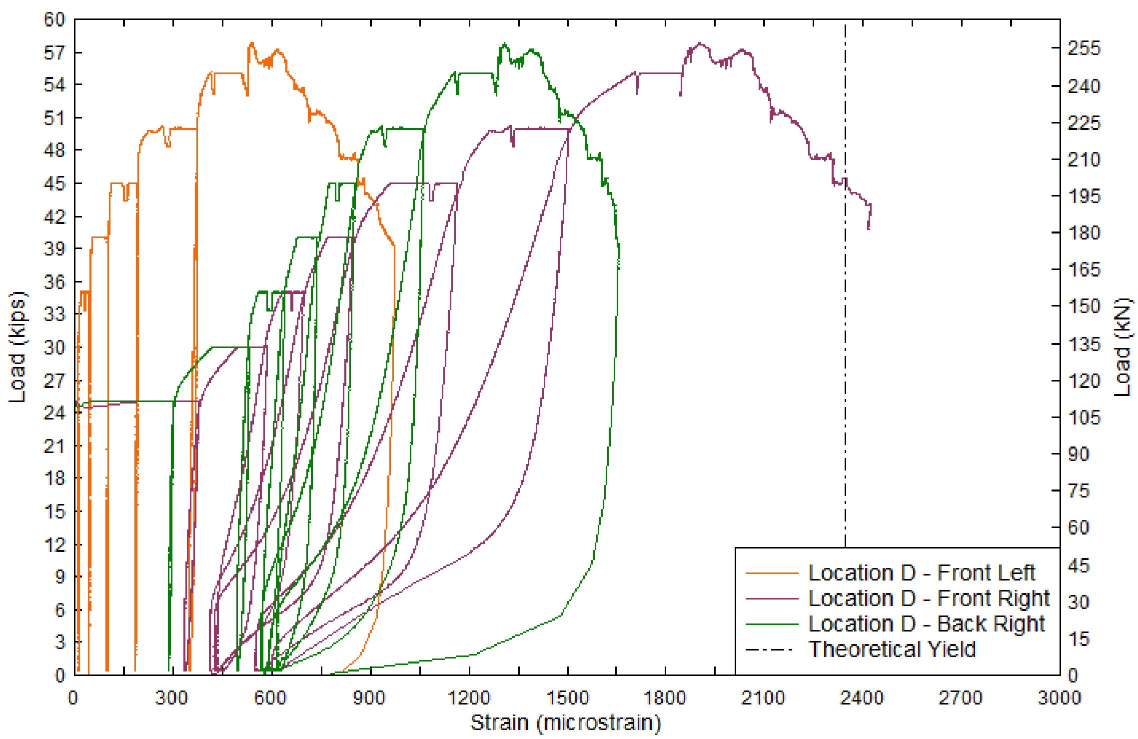

Concrete Gage

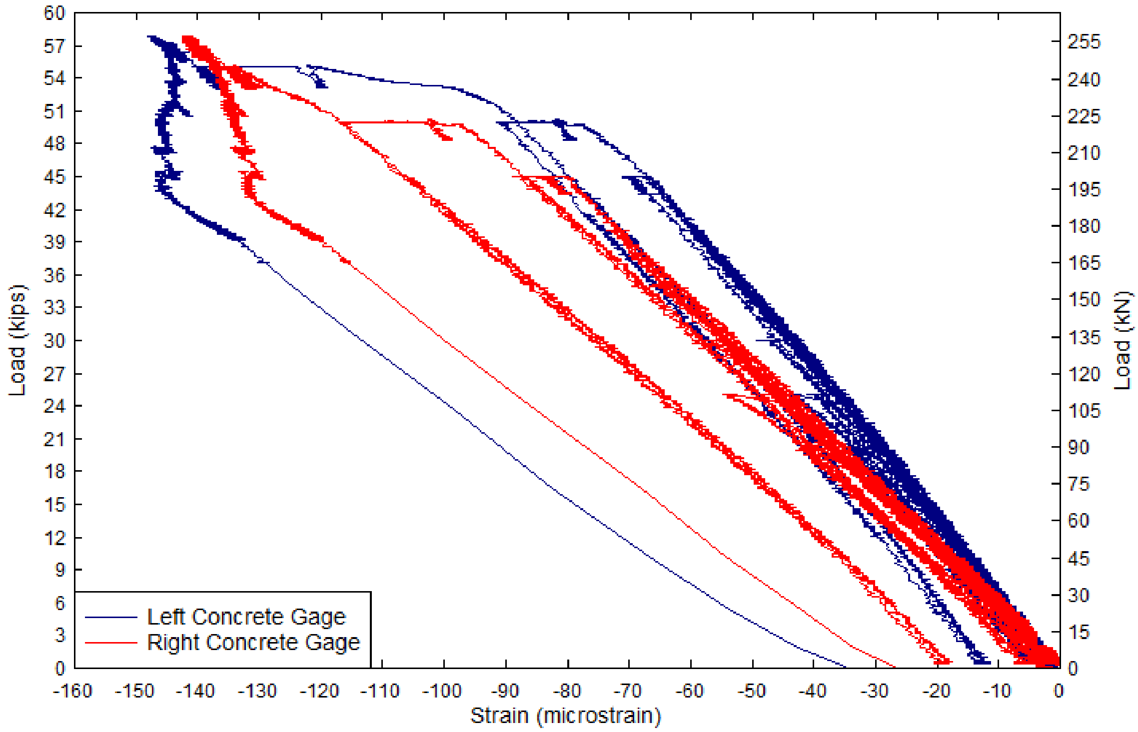

Tension Bar

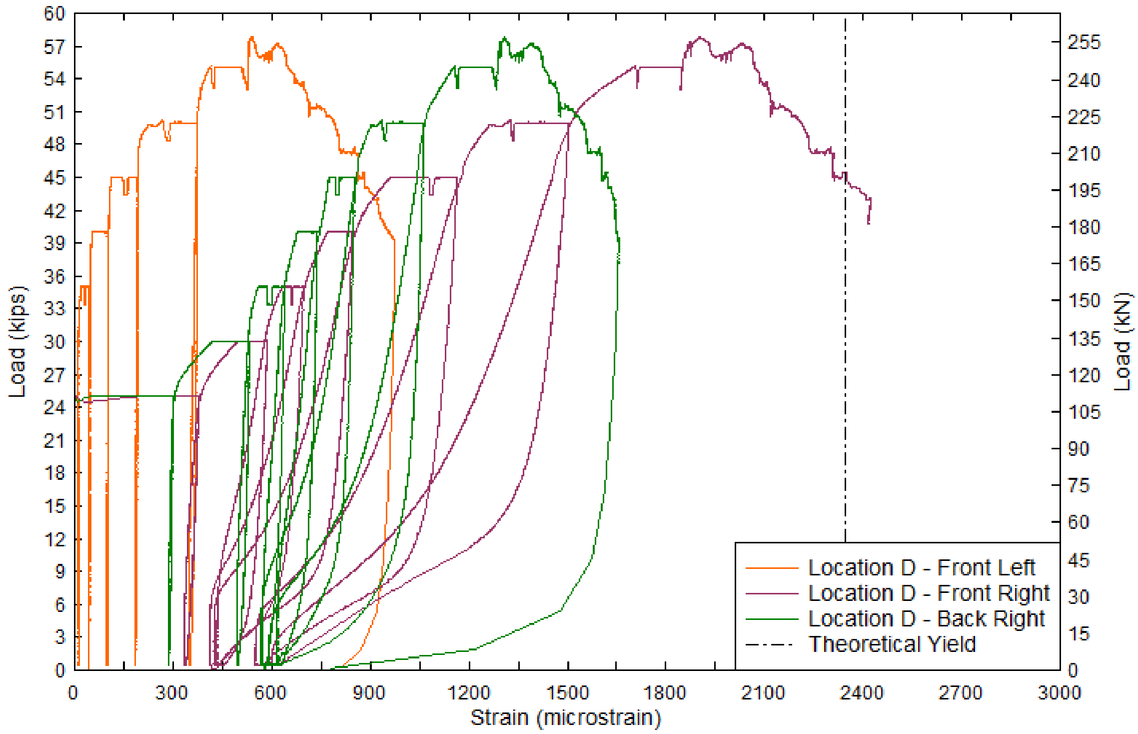

C.2 Specimen 2

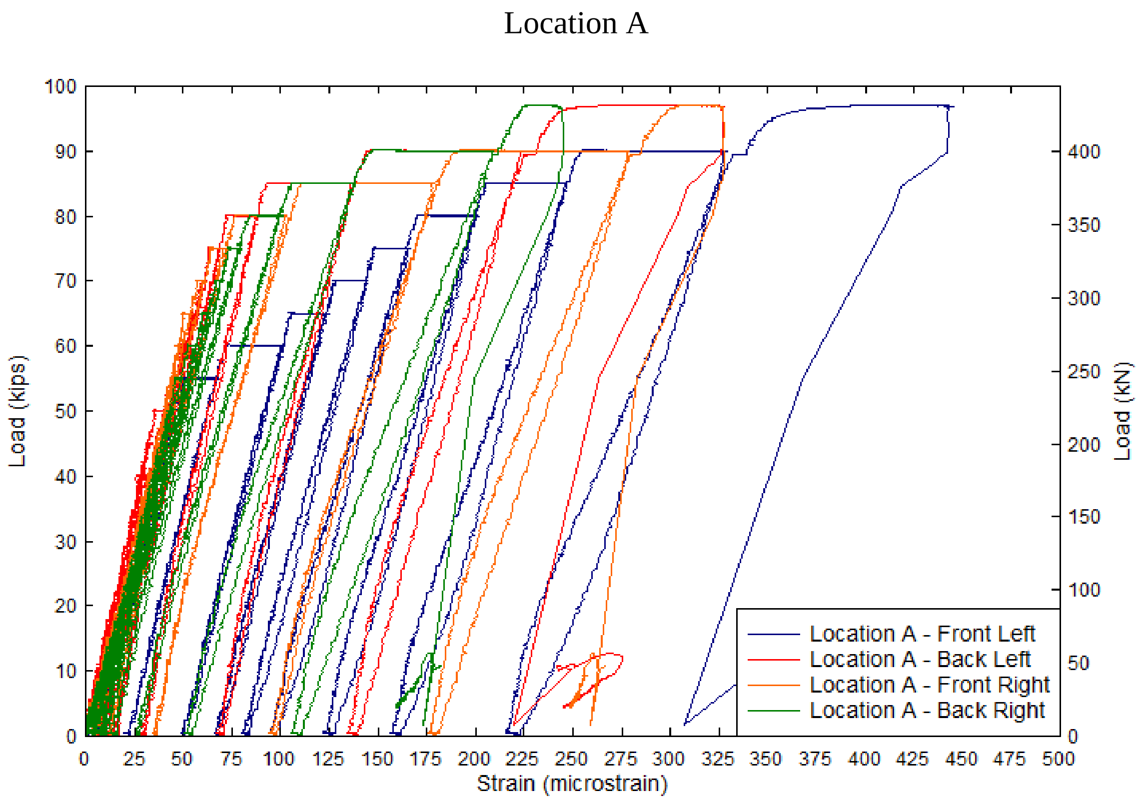

Location B

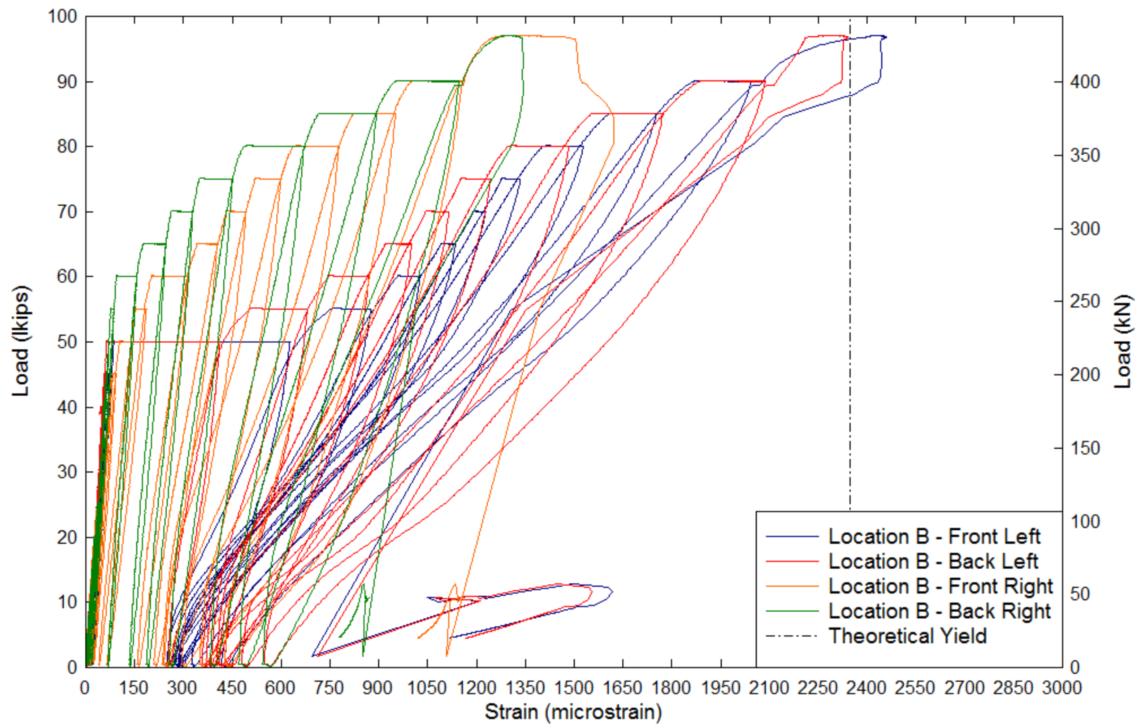

Location D

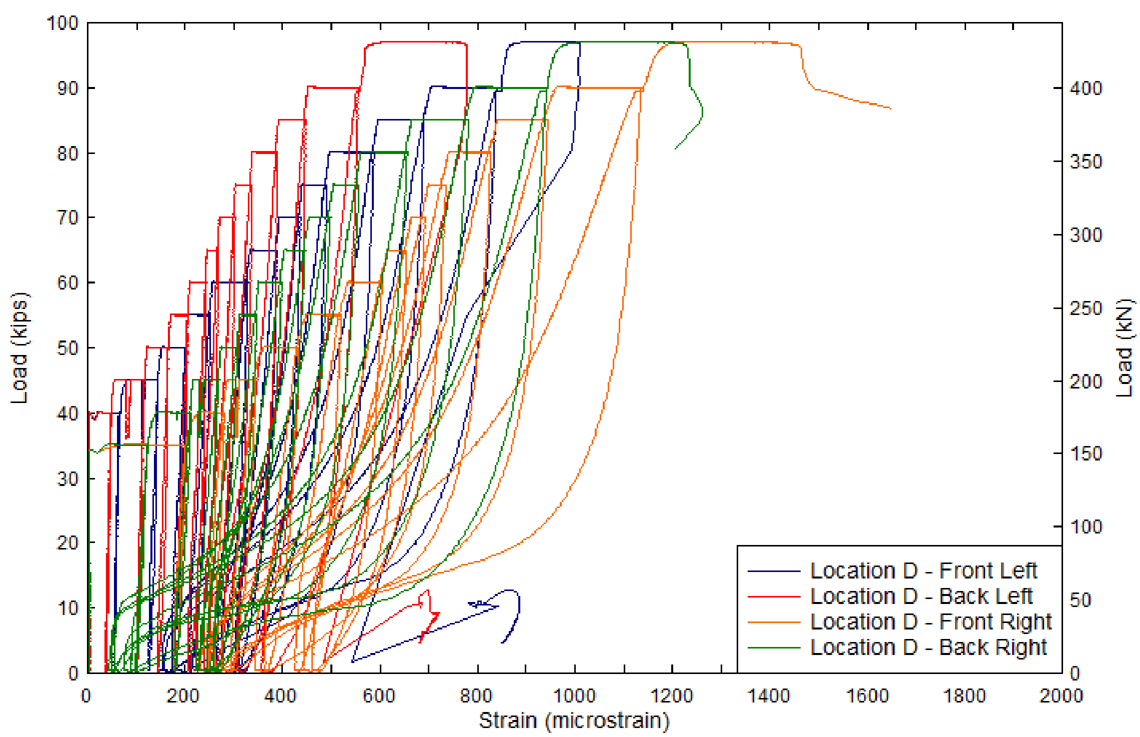

Concrete Gages

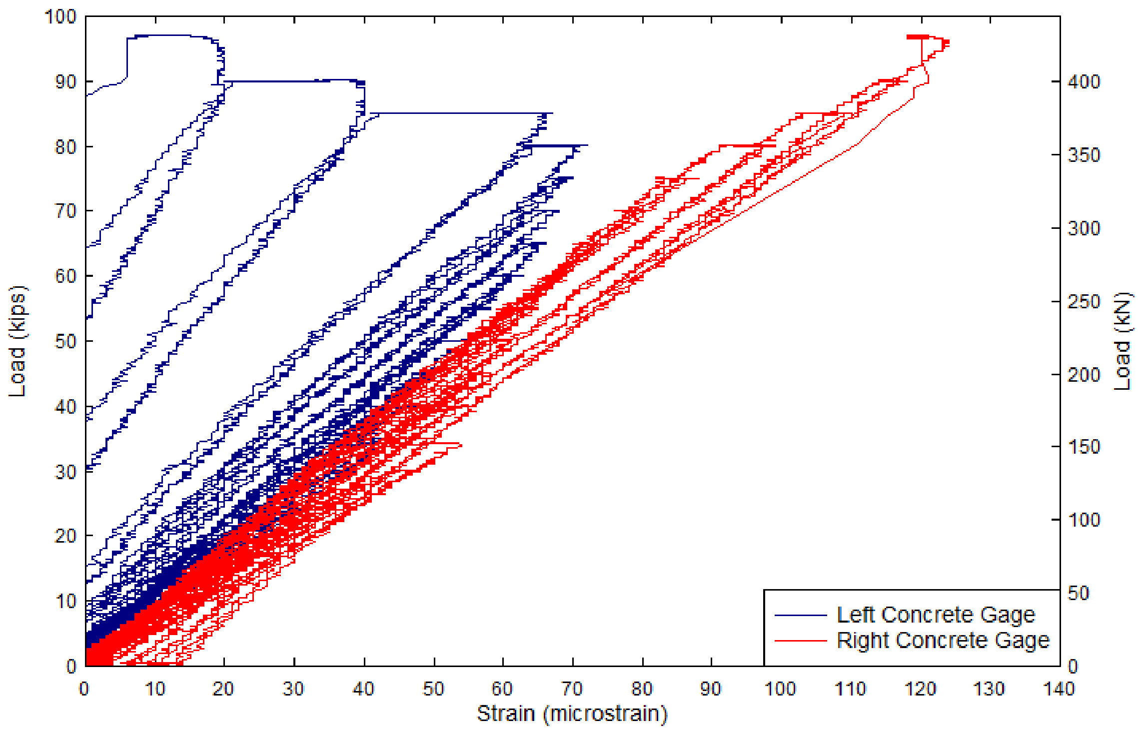

Tension Gages

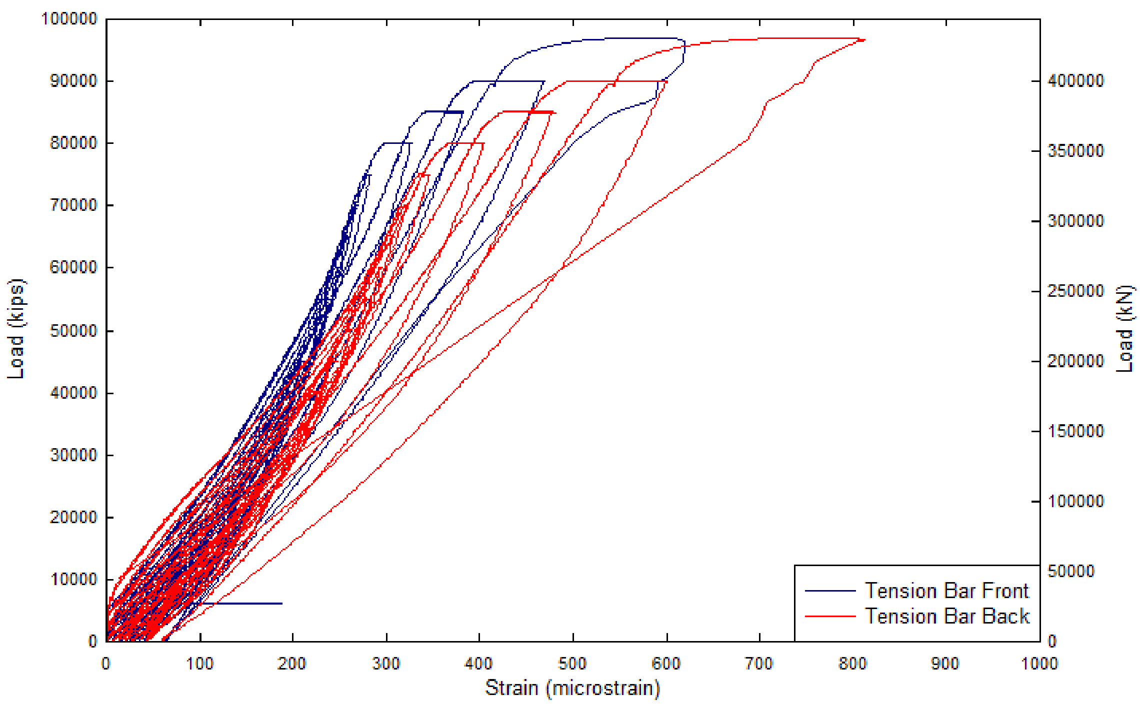

C.3 Specimen 3

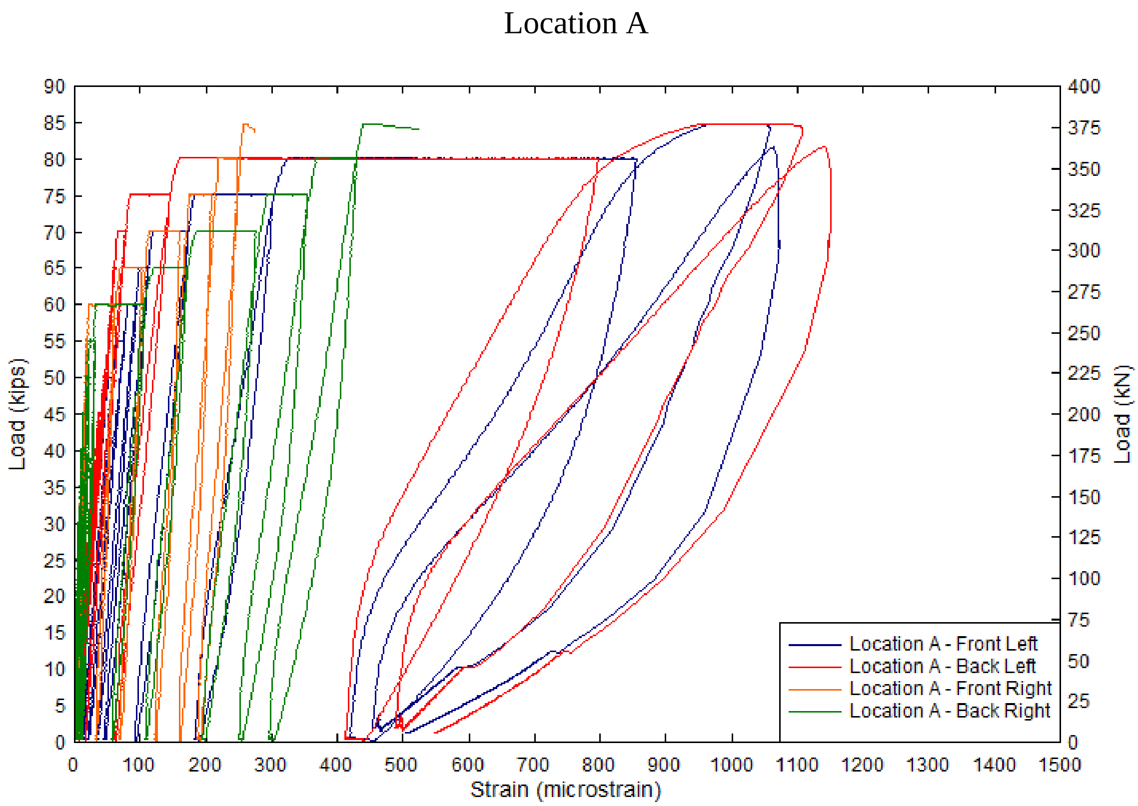

Location B

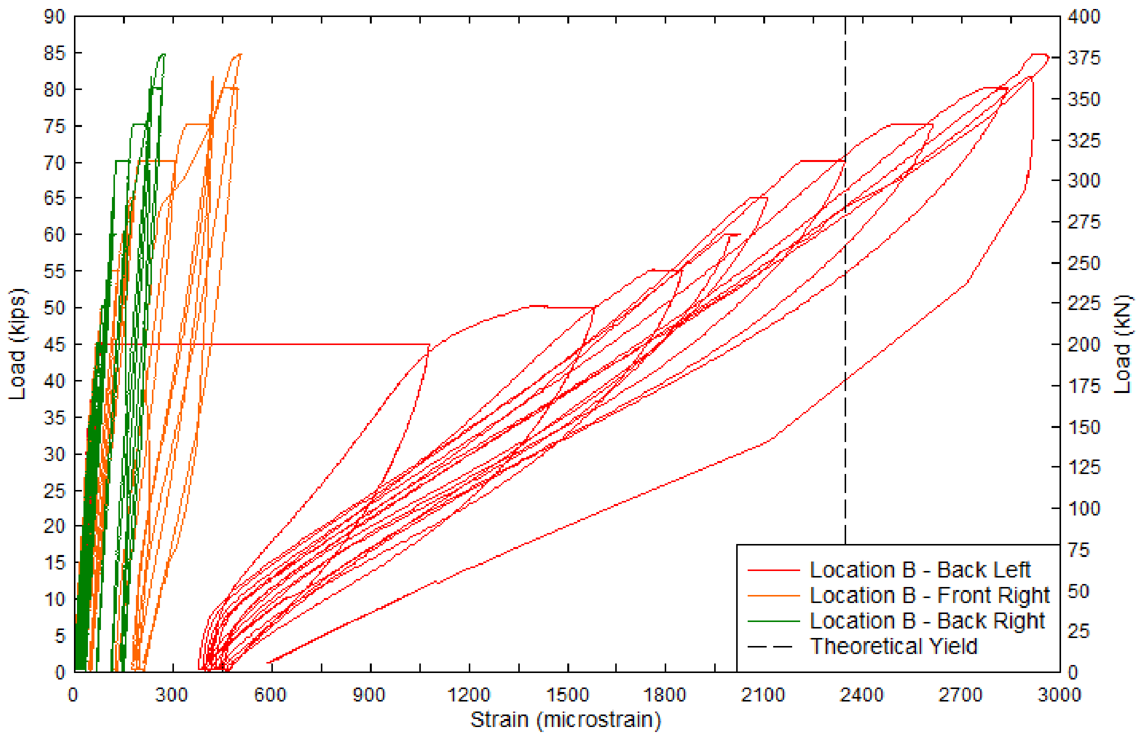

Location D

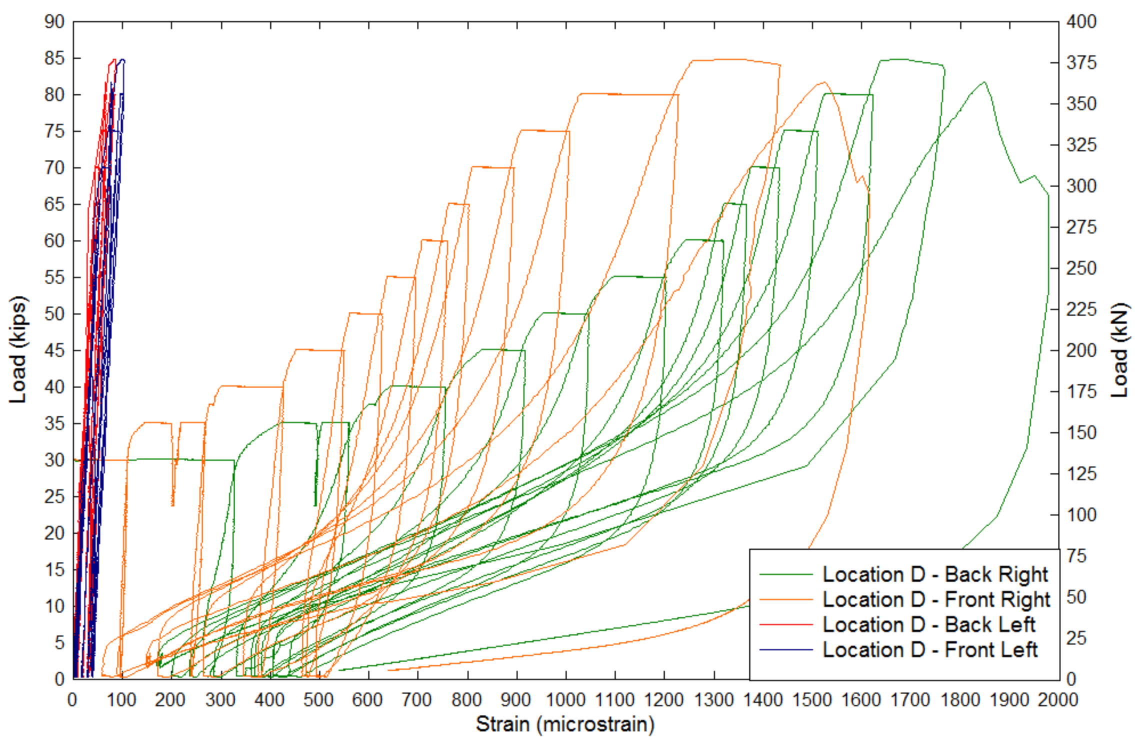

Concrete Gages

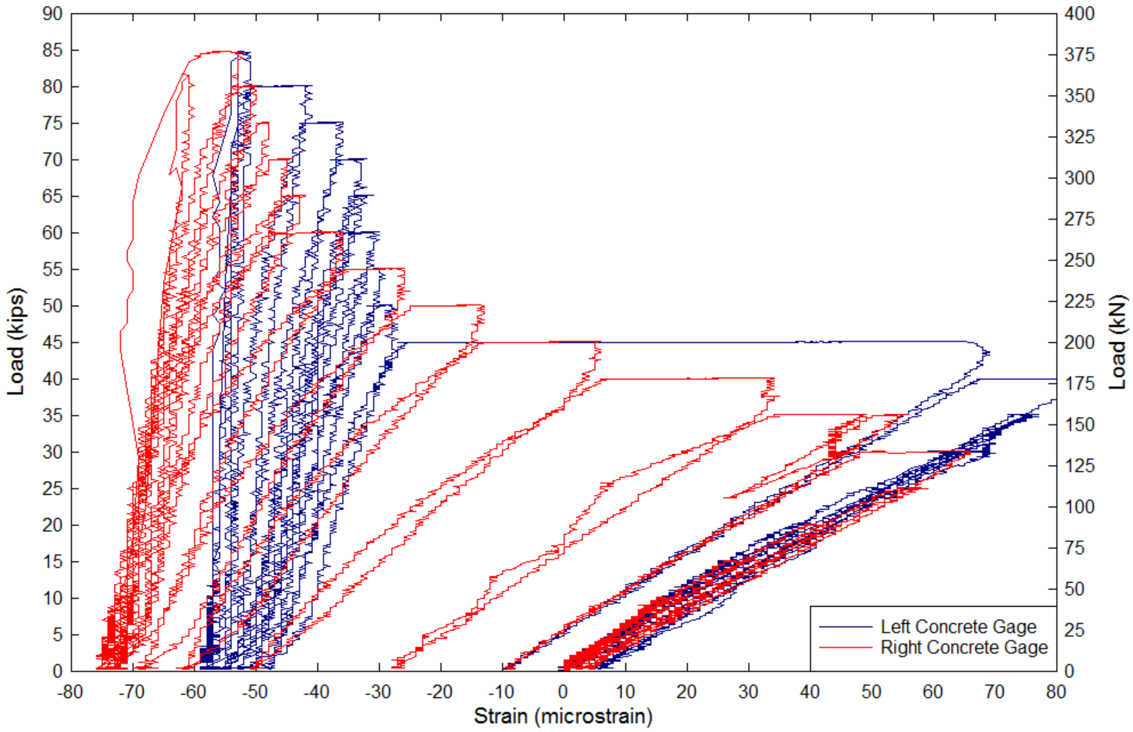

Tension Gages

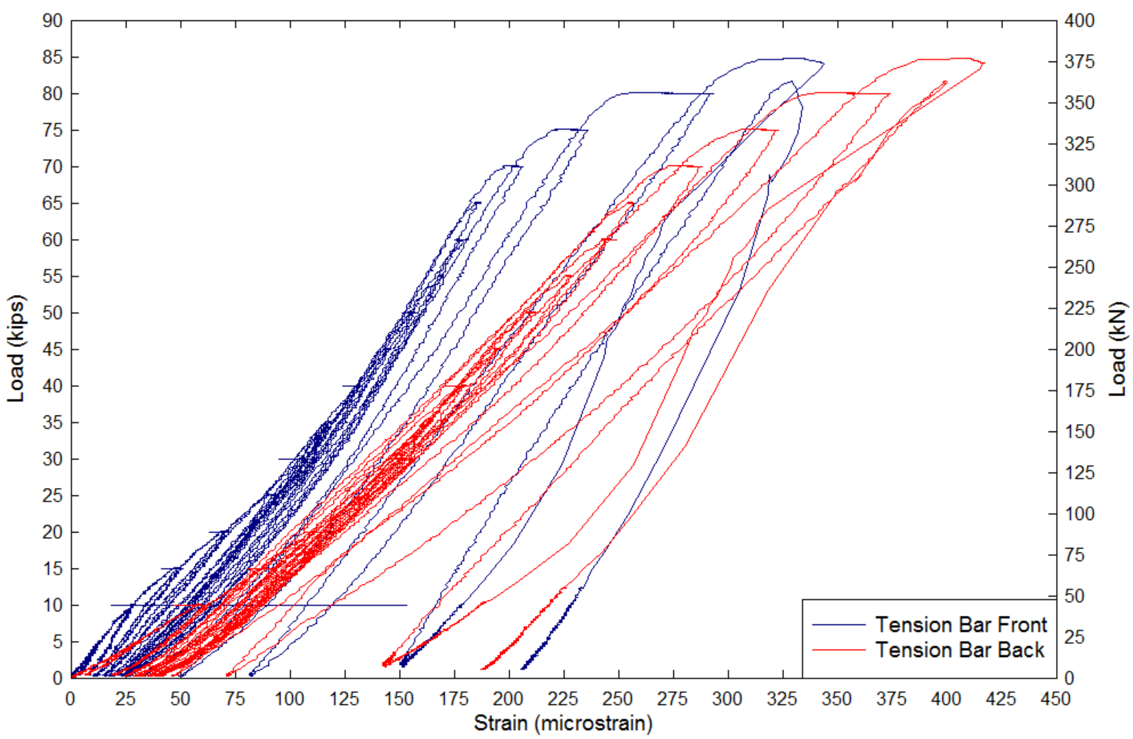

C.4 Specimen 4

Inside Location A

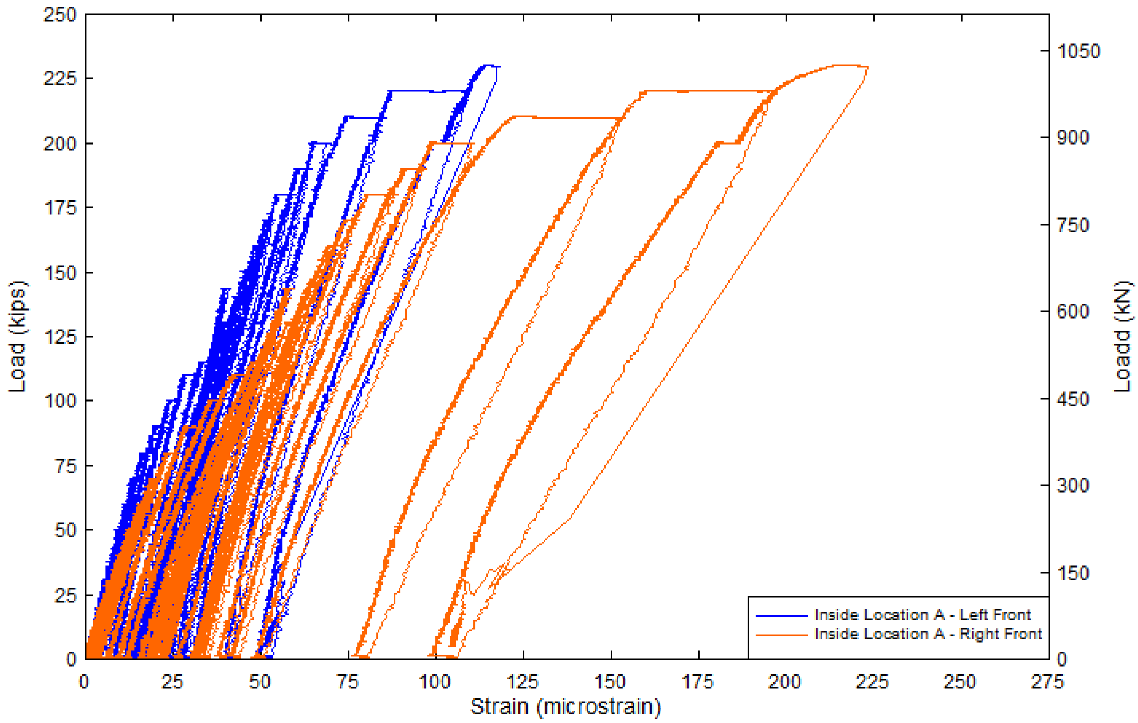

Inside Location B

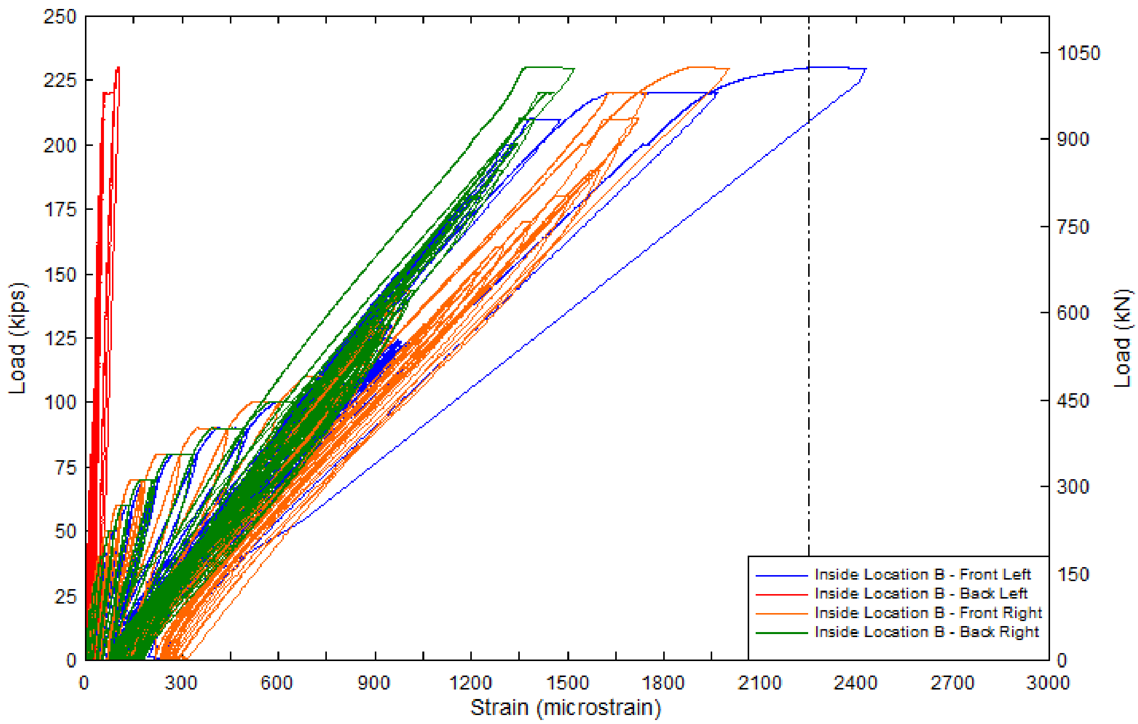

Inside Location D

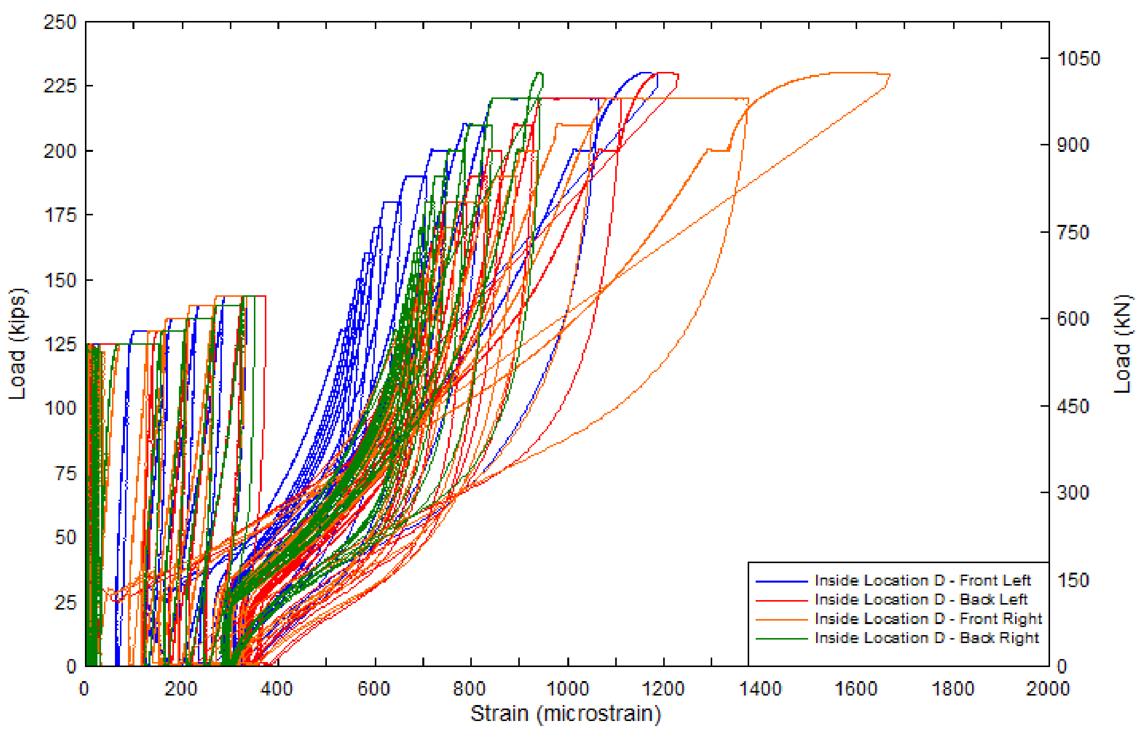

Outside Location A

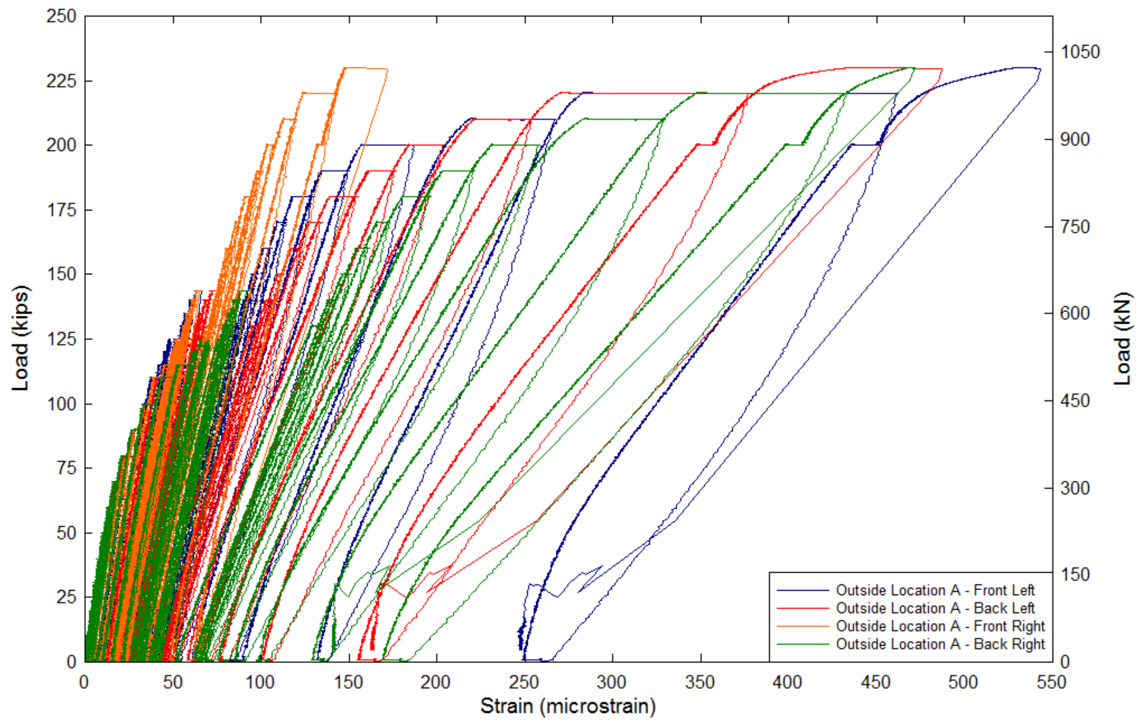

Outside Location B

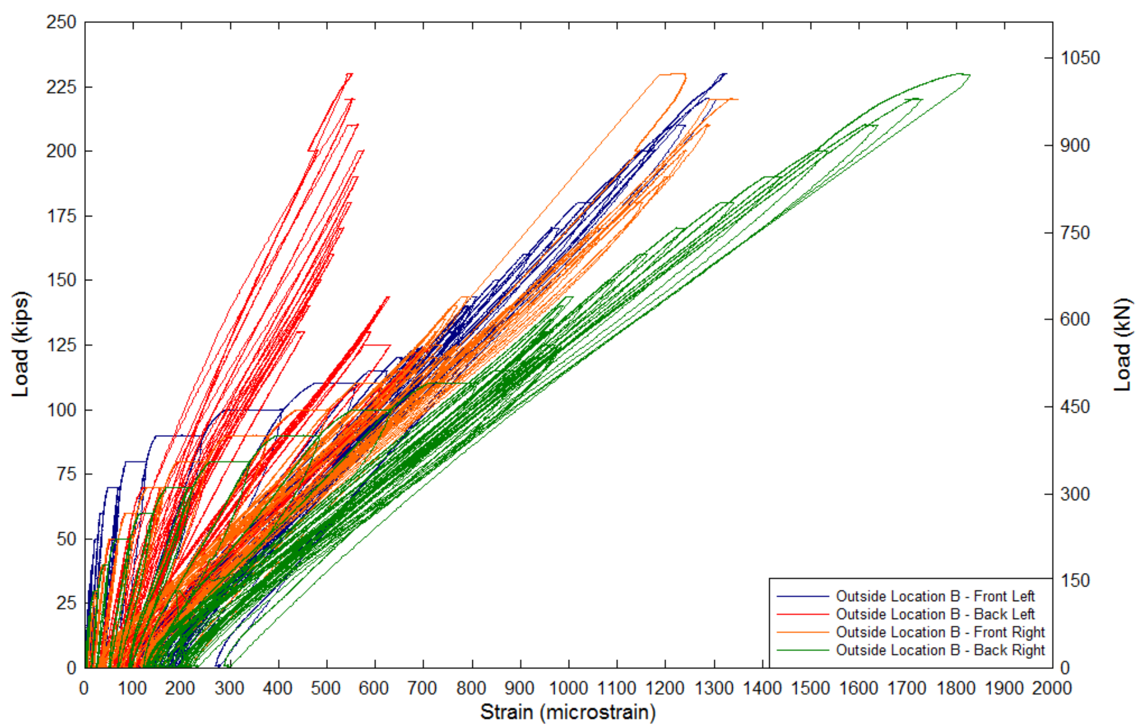

Outside Location C

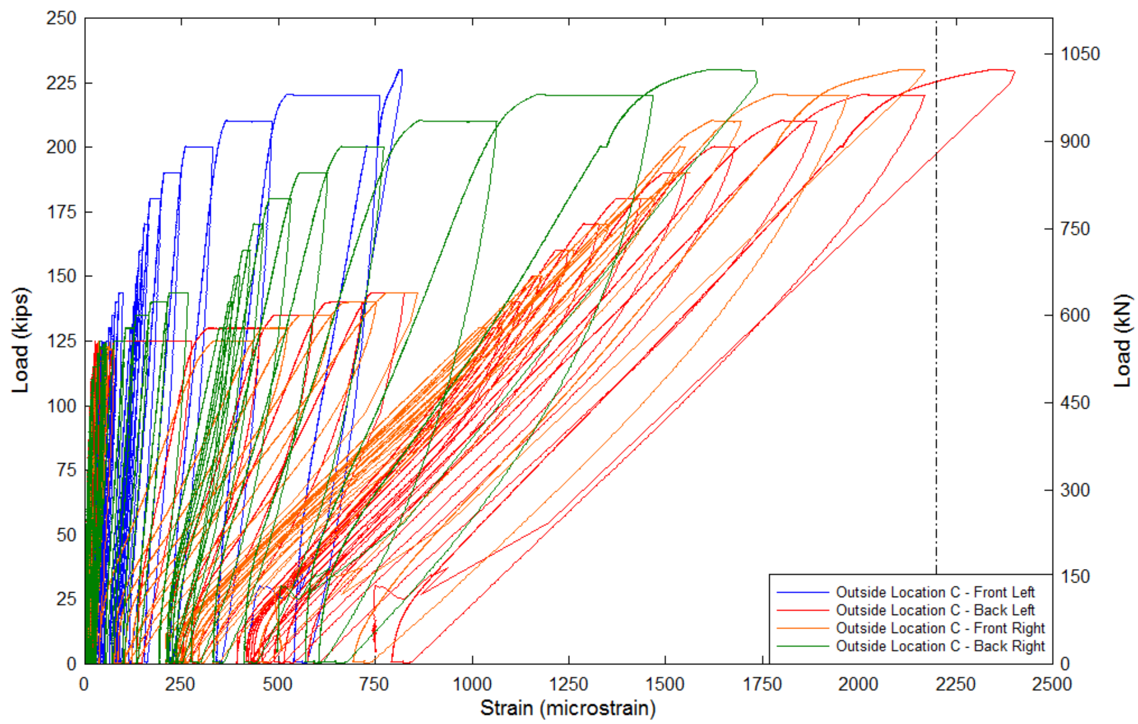

Outside Location C

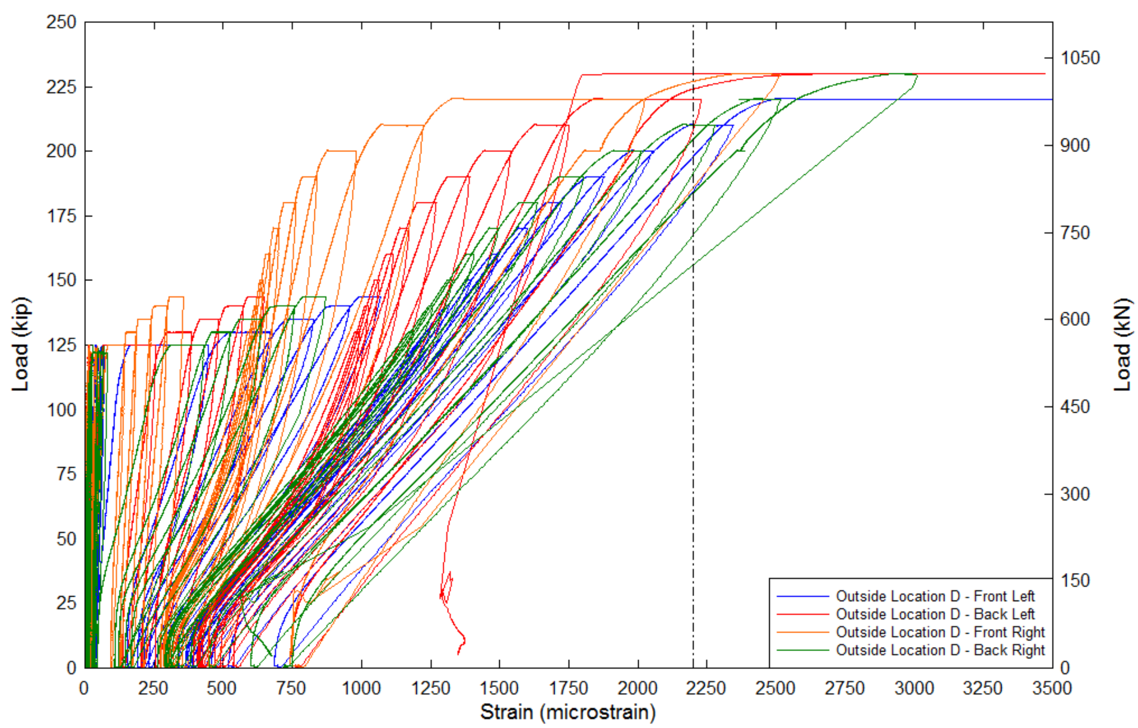

Concrete Gages

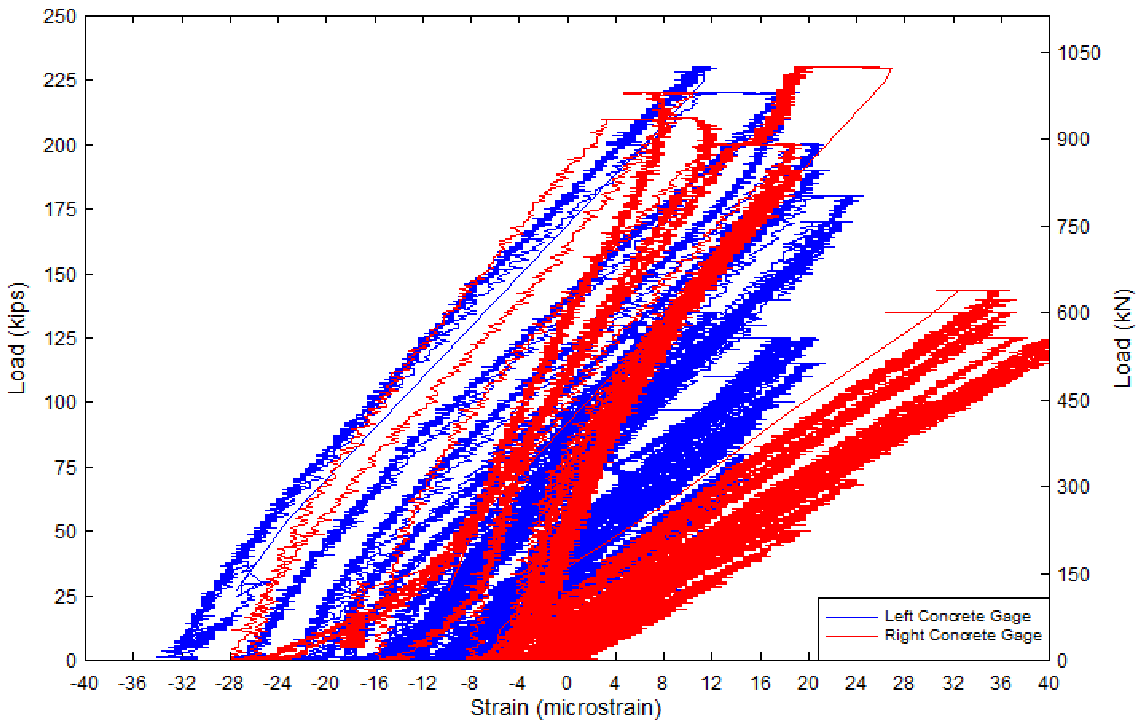

Tension Gages

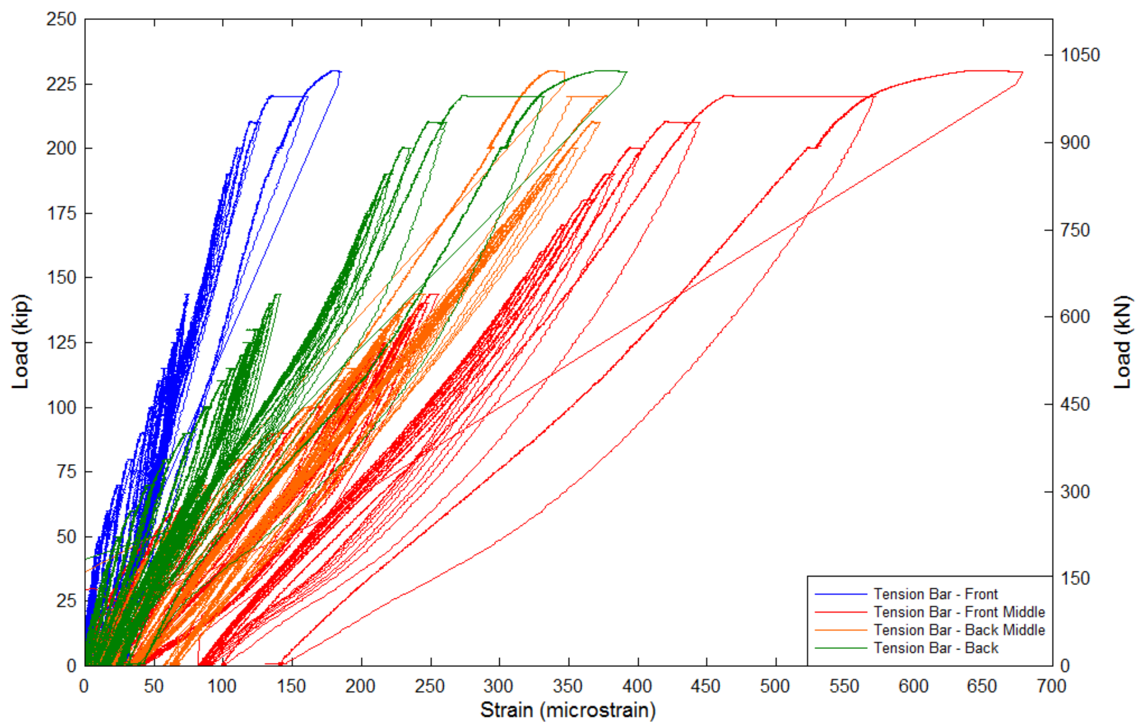

C.5 Specimen 5

Location A

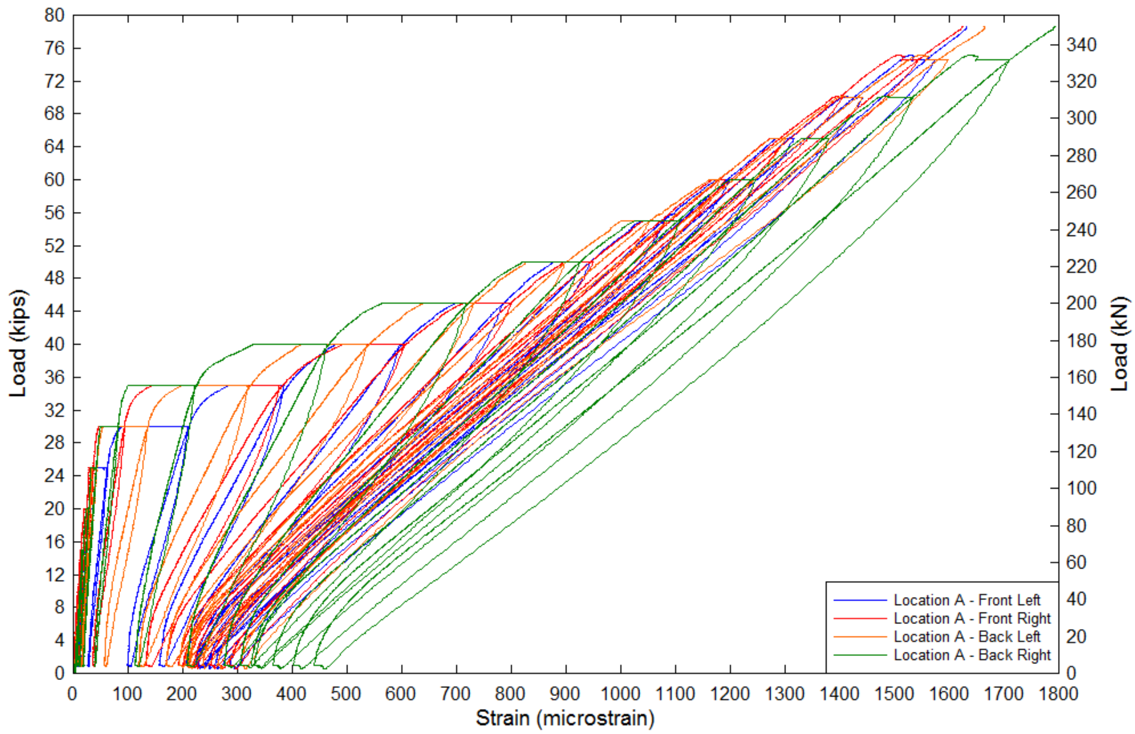

Location B

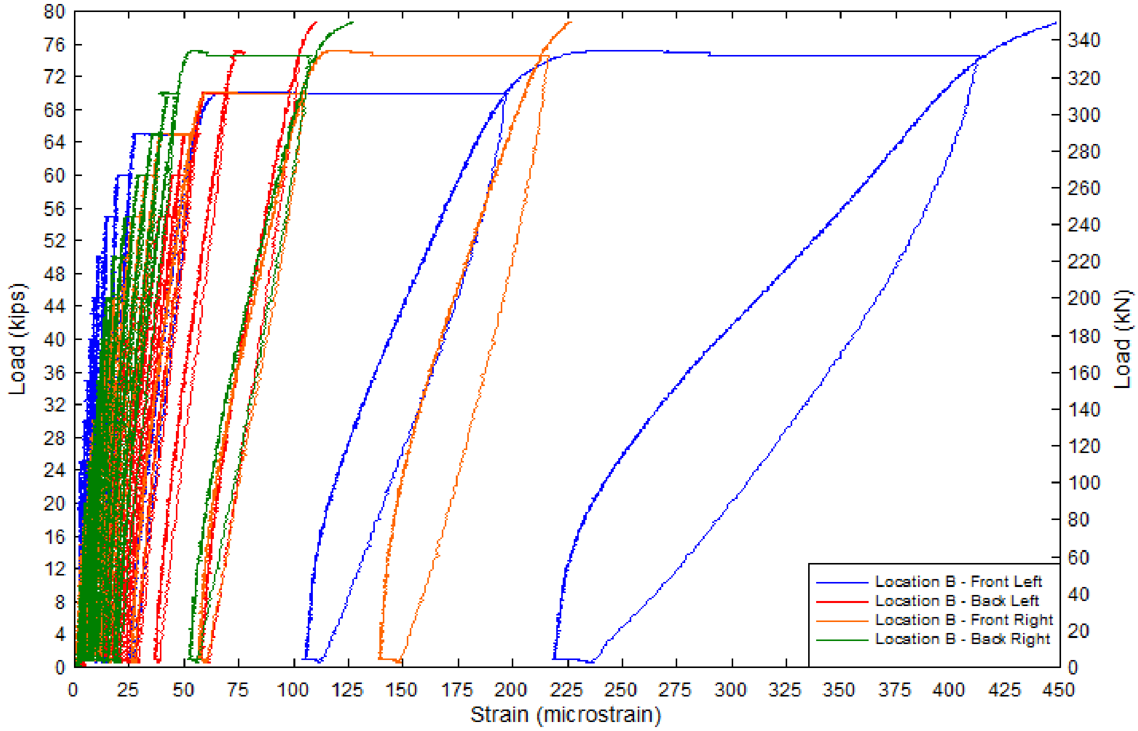

Location D

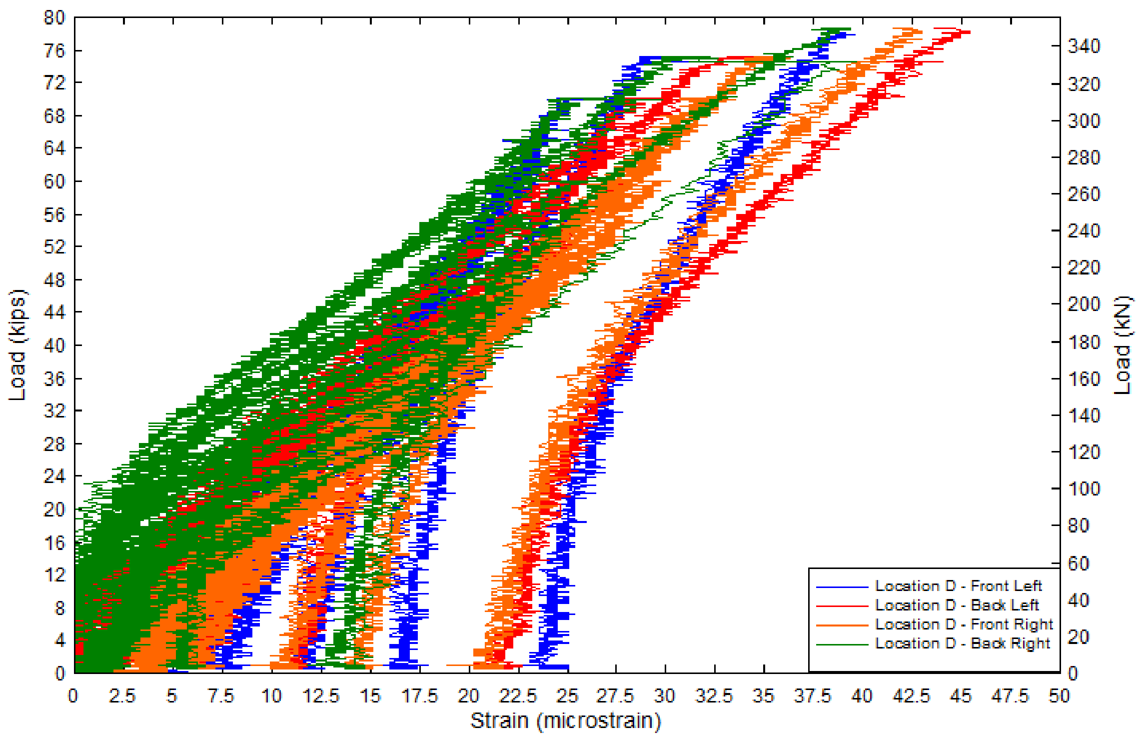

Location E

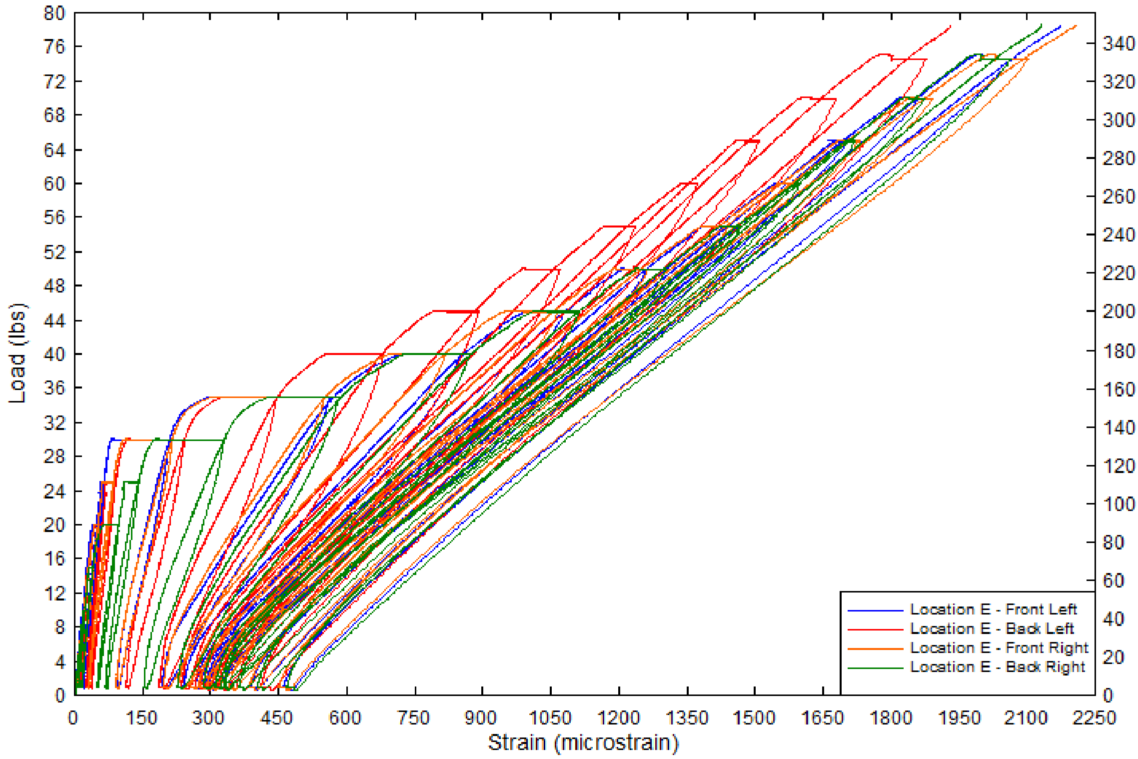

Concrete Gages

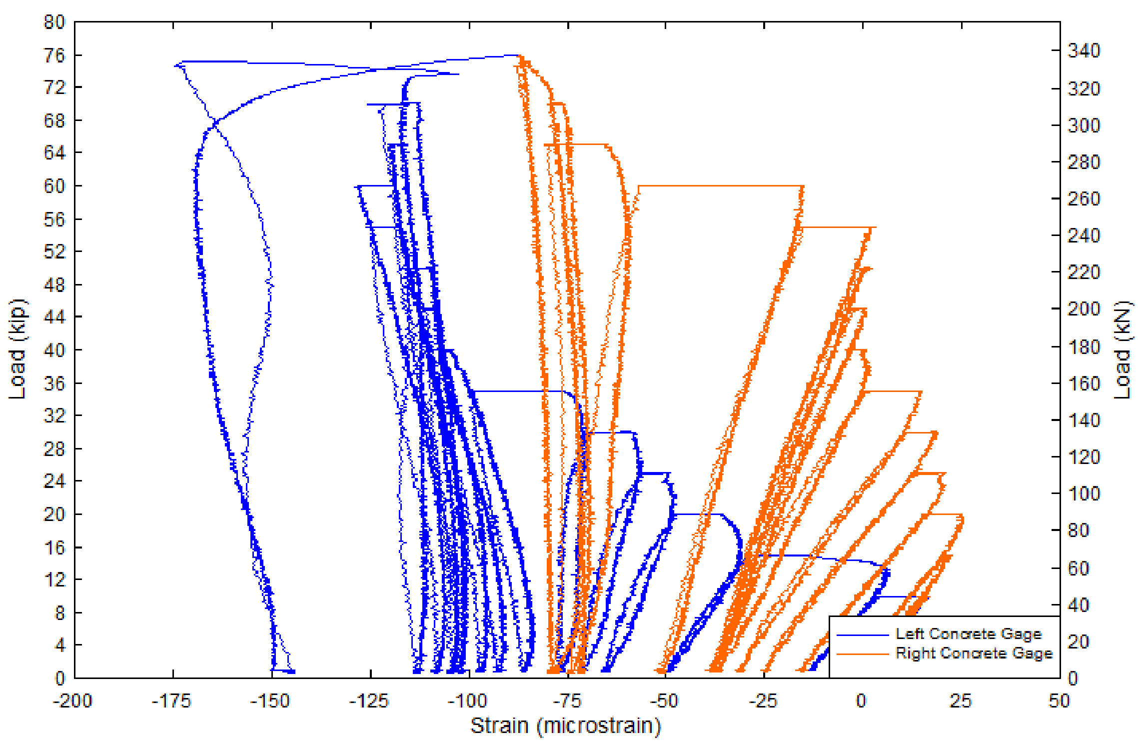

Tension Gages

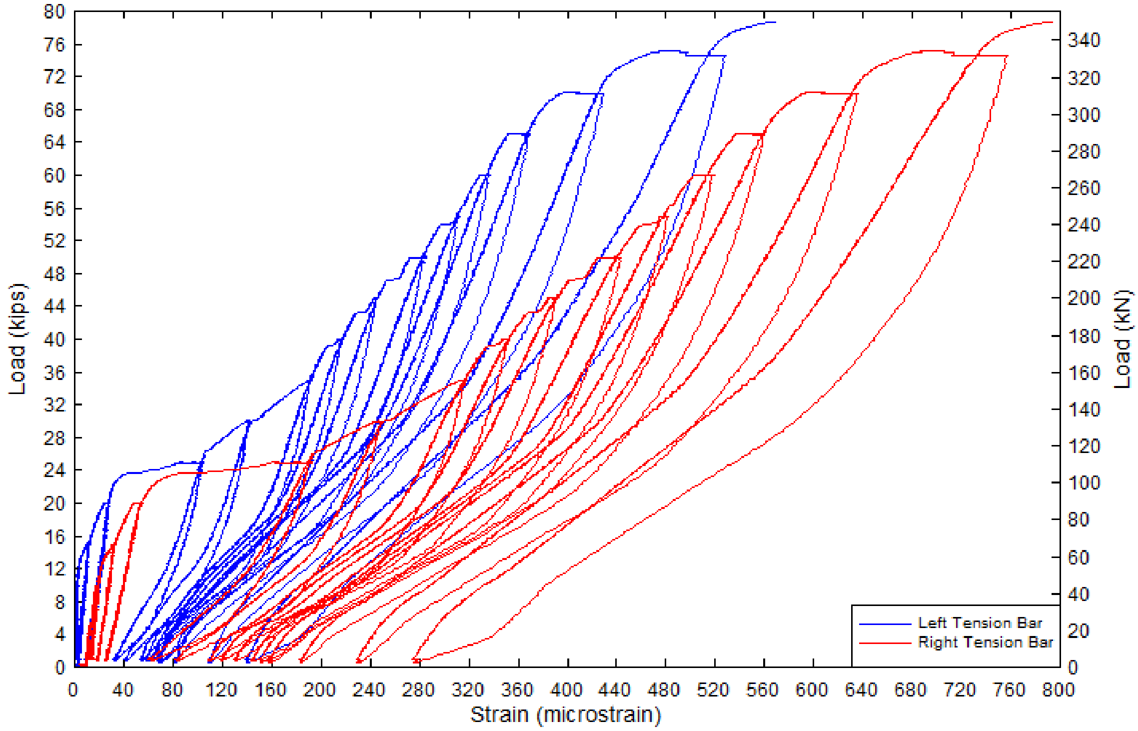

APPENDIX D: PLASTIC HINGE LOCATIONS

D.1 Specimen 2

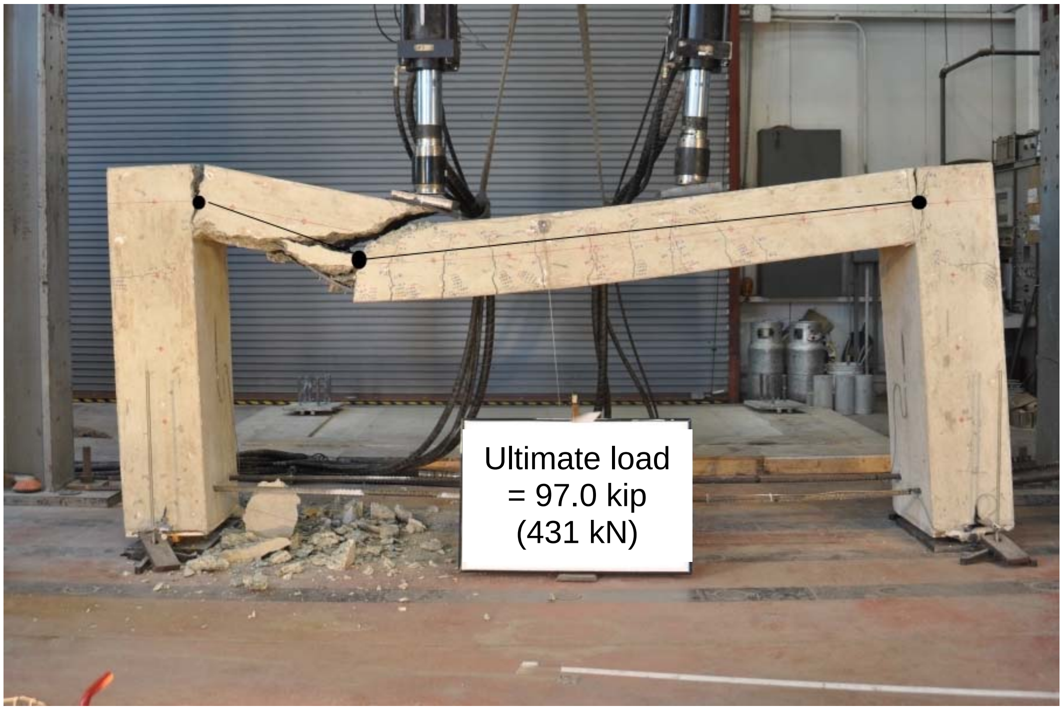

D.2 Specimen 3

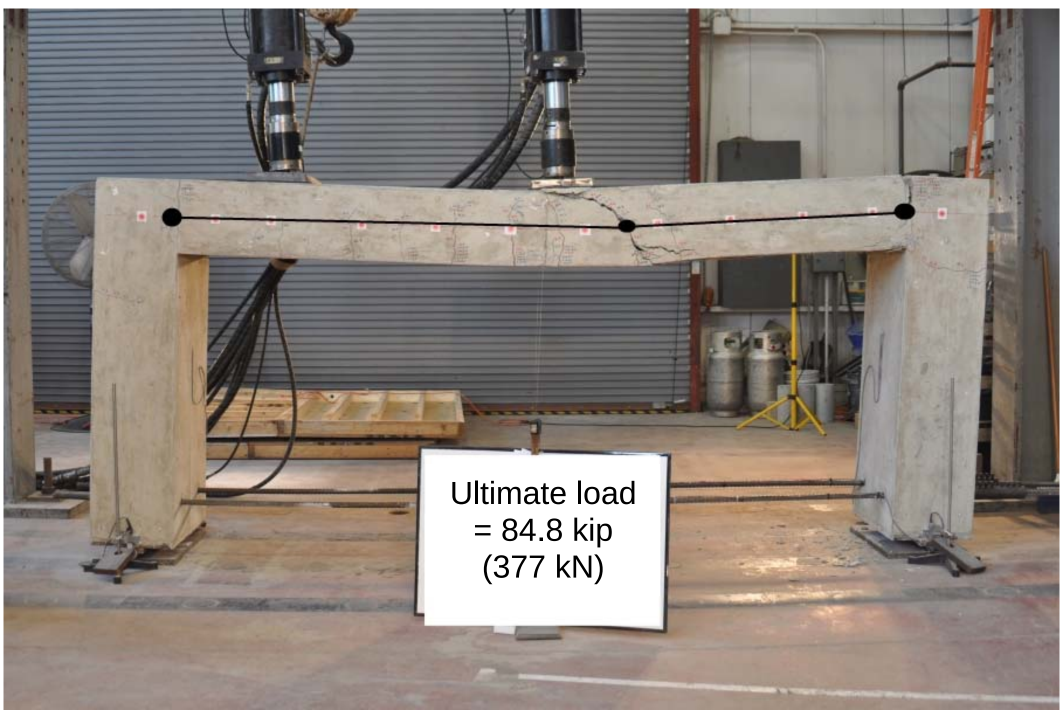

D.3 Specimen 5

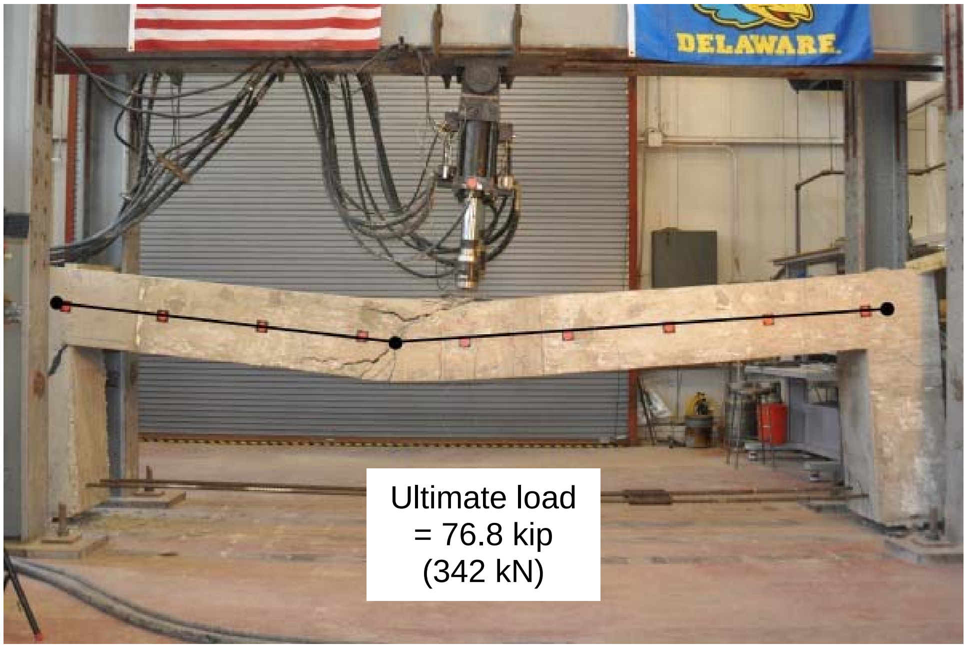

APPENDIX E: INTERNAL FORCES (ELASTIC ANALYSIS)

E1. Specimen 1

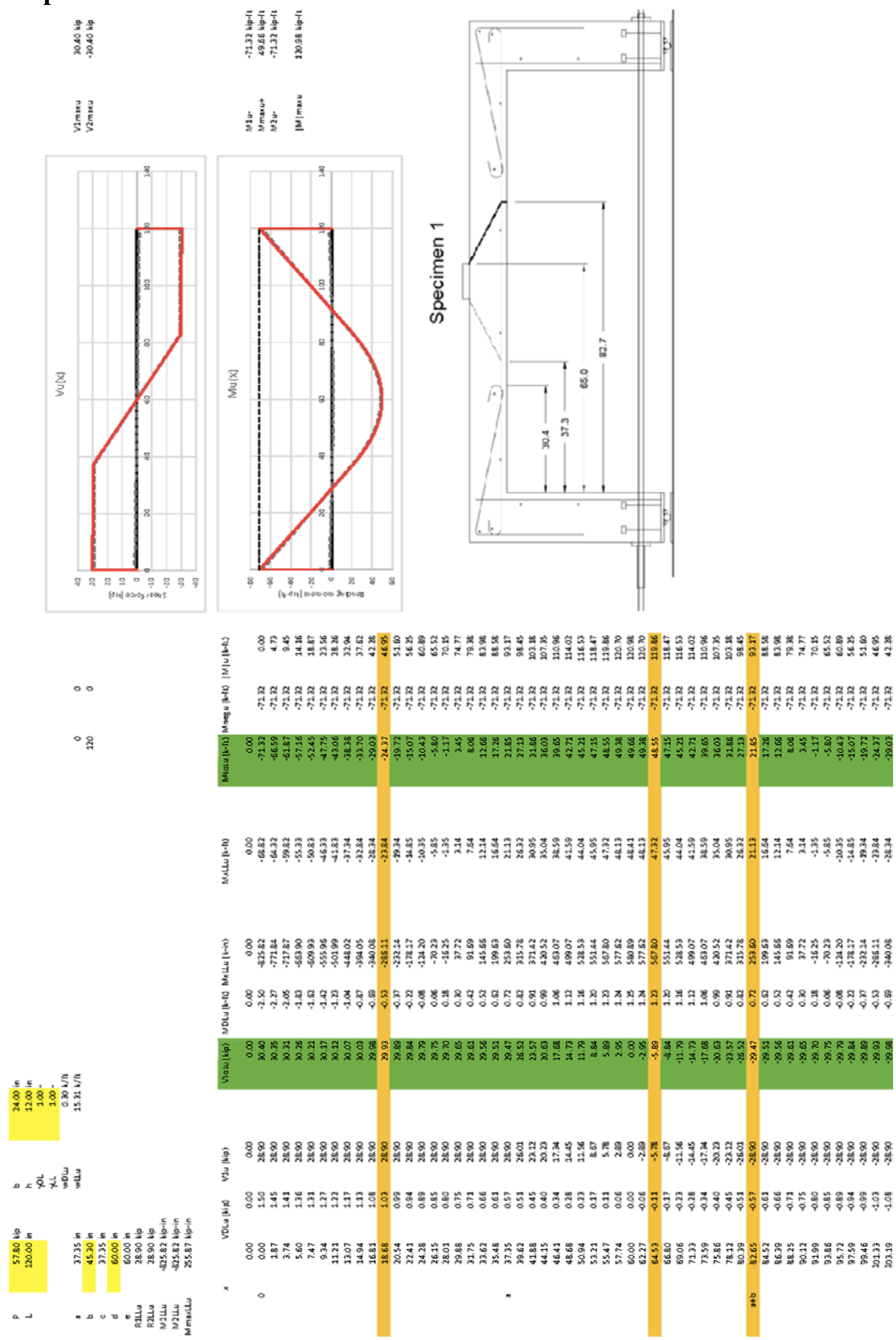

E2. Specimen 2

P	48.50	kip	b	24.00	in
L	120.00	in	h	12.00	in
s	48.00	in	γDL	1.00	-
			γLL	1.00	-

wDLu	0.30	k/ft
wLLu	12.85	k/ft

a1	13.35	in	a2	61.35	in
b1	45.30	in	b2	45.30	in
c1	61.35	in	c2	13.35	in
d1	36.00	in	d2	84.00	in
e1	84.00	in	e2	36.00	in
R11	37.33	kip	R12	11.17	kip
R12	11.17	kip	R22	37.33	kip
M11	-779.51	kip-in	M12	-373.57	kip-in
M21	-373.57	kip-in	M22	-779.51	kip-in
Mmax1	-276.60	kip-in	Mmax2	311.94	kip-in

0	0
120	0

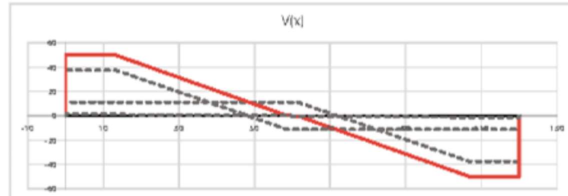

V1max	50.00	kip
V2max	-50.00	kip

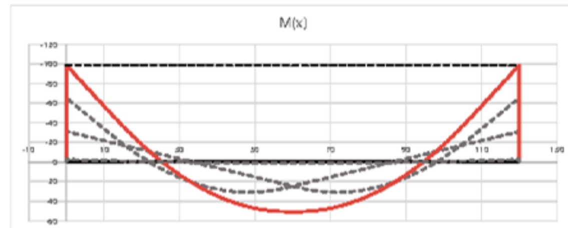

M1-	-98.59	kip-ft
Mmax+	50.66	kip-ft
M2-	-98.59	kip-ft
|M| max	149.25	kip-ft

	x	VDL (kip)	V1 (kip)	V2 (kip)	Vtot (kip)	MDL (k-ft)	Mx1 (k-in)	Mx2 (k-in)	Mx1 (k-ft)	Mx2 (k-ft)	Mtot (k-ft)	Mneg (k-ft)	|M| (k-ft)
	0.00	0.00	0.00	0.00	0.00	0.00	0.00	0.00	0.00	0.00	0.00		
0	0.00	1.50	37.33	11.17	50.00	-2.50	-779.51	-373.57	-64.96	-31.13	-98.59	-98.59	0.00
	0.67	1.48	37.33	11.17	49.98	-2.42	-754.59	-366.12	-62.88	-30.51	-95.81	-98.59	2.78
	1.34	1.47	37.33	11.17	49.97	-2.33	-729.67	-358.66	-60.81	-29.89	-93.03	-98.59	5.56
	2.00	1.45	37.33	11.17	49.95	-2.25	-704.75	-351.21	-58.73	-29.27	-90.25	-98.59	8.34
	2.67	1.43	37.33	11.17	49.93	-2.17	-679.83	-343.76	-56.65	-28.65	-87.47	-98.59	11.12
	3.34	1.42	37.33	11.17	49.92	-2.09	-654.91	-336.30	-54.58	-28.03	-84.70	-98.59	13.89
	4.01	1.40	37.33	11.17	49.90	-2.02	-629.99	-328.85	-52.50	-27.40	-81.92	-98.59	16.67
	4.67	1.38	37.33	11.17	49.88	-1.94	-605.08	-321.39	-50.42	-26.78	-79.14	-98.59	19.45
	5.34	1.37	37.33	11.17	49.87	-1.86	-580.16	-313.94	-48.35	-26.16	-76.37	-98.59	22.22
	6.01	1.35	37.33	11.17	49.85	-1.79	-555.24	-306.48	-46.27	-25.54	-73.60	-98.59	24.99
	6.68	1.33	37.33	11.17	49.83	-1.71	-530.32	-299.03	-44.19	-24.92	-70.82	-98.59	27.77
	7.34	1.32	37.33	11.17	49.82	-1.64	-505.40	-291.58	-42.12	-24.30	-68.05	-98.59	30.54
	8.01	1.30	37.33	11.17	49.80	-1.57	-480.48	-284.12	-40.04	-23.68	-65.28	-98.59	33.31
	8.68	1.28	37.33	11.17	49.78	-1.49	-455.56	-276.67	-37.96	-23.06	-62.51	-98.59	36.08
	9.35	1.27	37.33	11.17	49.77	-1.42	-430.64	-269.21	-35.89	-22.43	-59.74	-98.59	38.85
	10.01	1.25	37.33	11.17	49.75	-1.35	-405.72	-261.76	-33.81	-21.81	-56.98	-98.59	41.61
	10.68	1.23	37.33	11.17	49.73	-1.28	-380.80	-254.31	-31.73	-21.19	-54.21	-98.59	44.38
	11.35	1.22	37.33	11.17	49.72	-1.22	-355.88	-246.85	-29.66	-20.57	-51.44	-98.59	47.15
	12.02	1.20	37.33	11.17	49.70	-1.15	-330.96	-239.40	-27.58	-19.95	-48.68	-98.59	49.91
	12.68	1.18	37.33	11.17	49.68	-1.08	-306.04	-231.94	-25.50	-19.33	-45.91	-98.59	52.68
a1	13.35	1.17	37.33	11.17	49.67	-1.02	-281.12	-224.49	-23.43	-18.71	-43.15	-98.59	55.44
	15.62	1.11	34.91	11.17	47.18	-0.80	-199.31	-199.20	-16.61	-16.60	-34.01	-98.59	64.58
	17.88	1.05	32.48	11.17	44.70	-0.60	-122.99	-173.90	-10.25	-14.49	-25.34	-98.59	73.25
	20.15	1.00	30.06	11.17	42.22	-0.40	-52.16	-148.61	-4.35	-12.38	-17.14	-98.59	81.46
	22.41	0.94	27.63	11.17	39.74	-0.22	13.18	-123.32	1.10	-10.28	-9.40	-98.59	89.19
	24.68	0.88	25.21	11.17	37.26	-0.05	73.02	-98.02	6.08	-8.17	-2.13	-98.59	96.46
	26.94	0.83	22.78	11.17	34.78	0.11	127.37	-72.73	10.61	-6.06	4.66	-98.59	103.26
	29.21	0.77	20.36	11.17	32.29	0.26	176.22	-47.43	14.69	-3.95	10.99	-98.59	109.58
	31.47	0.71	17.93	11.17	29.81	0.40	219.59	-22.14	18.30	-1.85	16.86	-98.59	115.45
	33.74	0.66	15.51	11.17	27.33	0.53	257.46	3.15	21.45	0.26	22.25	-98.59	120.84
	36.00	0.60	13.08	11.17	24.85	0.65	289.84	28.45	24.15	2.37	27.17	-98.59	125.76
	38.27	0.54	10.66	11.17	22.37	0.76	316.72	53.74	26.39	4.48	31.63	-98.59	130.22
	40.53	0.49	8.23	11.17	19.89	0.86	338.12	79.03	28.18	6.59	35.62	-98.59	134.21
	42.80	0.43	5.81	11.17	17.41	0.94	354.02	104.33	29.50	8.69	39.14	-98.59	137.73
	45.06	0.37	3.38	11.17	14.92	1.02	364.43	129.62	30.37	10.80	42.19	-98.59	140.78
	47.33	0.32	0.96	11.17	12.44	1.08	369.34	154.91	30.78	12.91	44.77	-98.59	143.36
	49.59	0.26	-1.47	11.17	9.96	1.14	368.77	180.21	30.73	15.02	46.88	-98.59	145.48
	51.86	0.20	-3.89	11.17	7.48	1.18	362.70	205.50	30.22	17.13	48.53	-98.59	147.12
	54.12	0.15	-6.32	11.17	5.00	1.21	351.14	230.79	29.26	19.23	49.71	-98.59	148.30
	56.39	0.09	-8.74	11.17	2.52	1.24	334.08	256.09	27.84	21.34	50.42	-98.59	149.01
a1+b1	58.65	0.03	-11.17	11.17	0.03	1.25	311.53	281.38	25.96	23.45	50.66	-98.59	149.25
	58.79	0.03	-11.17	11.17	0.03	1.25	310.03	282.89	25.84	23.57	50.66	-98.59	149.25
	58.92	0.03	-11.17	11.17	0.03	1.25	308.52	284.40	25.71	23.70	50.66	-98.59	149.25
	59.06	0.02	-11.17	11.17	0.02	1.25	307.01	285.90	25.58	23.83	50.66	-98.59	149.25
	59.19	0.02	-11.17	11.17	0.02	1.25	305.50	287.41	25.46	23.95	50.66	-98.59	149.25
	59.33	0.02	-11.17	11.17	0.02	1.25	304.00	288.92	25.33	24.08	50.66	-98.59	149.25
	59.46	0.01	-11.17	11.17	0.01	1.25	302.49	290.43	25.21	24.20	50.66	-98.59	149.25
	59.60	0.01	-11.17	11.17	0.01	1.25	300.98	291.94	25.08	24.33	50.66	-98.59	149.25
	59.73	0.01	-11.17	11.17	0.01	1.25	299.47	293.44	24.96	24.45	50.66	-98.59	149.25
	59.87	0.00	-11.17	11.17	0.00	1.25	297.97	294.95	24.83	24.58	50.66	-98.59	149.25
	60.00	0.00	-11.17	11.17	0.00	1.25	296.46	296.46	24.70	24.70	50.66	-98.59	149.25
	60.14	0.00	-11.17	11.17	0.00	1.25	294.95	297.97	24.58	24.83	50.66	-98.59	149.25

Specimen 2

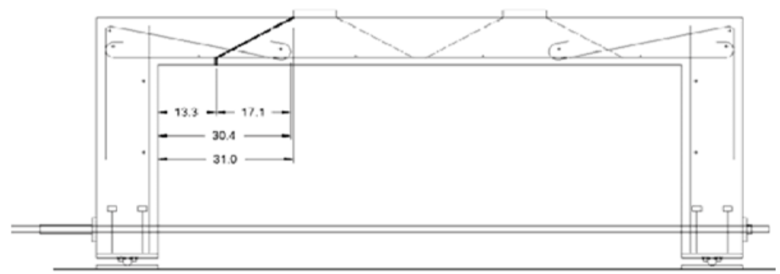

E3. Specimen 3

P	42.40	kip	b	24.00	in			
L	120.00	in	h	12.00	in			
a	48.00	in	γDL	1.00	-	wDLu	0.30	k/ft
			γLL	1.00	-	wLLu	11.23	k/ft

a1	0.00	in	a2	53.50	in	0	0
b1	38.15	in	b2	45.30	in	120	0
c1	81.85	in	c2	21.20	in		
d1	19.08	in	d2	76.15	in		
e1	100.93	in	e2	43.85	in		
R11	32.67	kip	R12	13.25	kip		
R12	3.04	kip	R22	29.15	kip		
M11	-426.82	kip-in	M12	-425.32	kip-in		
M21	-109.94	kip-in	M22	-694.10	kip-in		
Mmax1	-422.86	kip-in	Mmax2	284.41	kip-in		

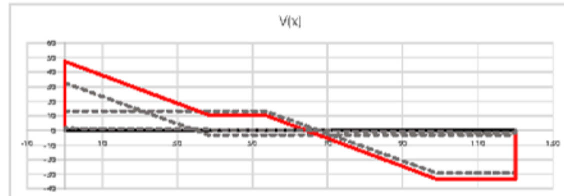

V1max	47.43	kip
V2max	-33.68	kip

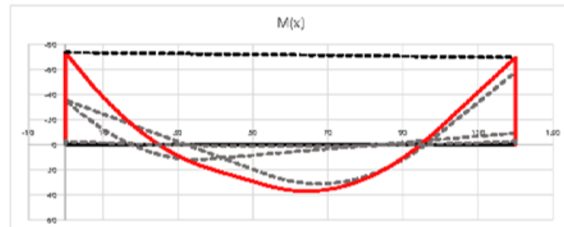

M1-	-73.51	kip-ft
Mmax+	37.17	kip-ft
M2-	-69.50	kip-ft
|M|max	108.52	kip-ft

Specimen 3

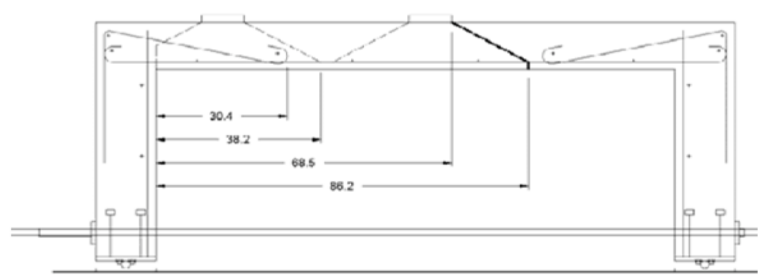

	x	VDL (kip)	V1 (kip)	V2 (kip)	Vtot (kip)	MDL (k-ft)	Mx1 (k-in)	Mx2 (k-in)	Mx1 (k-ft)	Mx2 (k-ft)	Mtot (k-ft)	Mneg (k-ft)	|M| (k-ft)
	0.00	0.00	0.00	0.00	0.00	0.00	0.00	0.00	0.00	0.00	0.00		
0	0.00	1.50	32.67	13.25	47.43	-2.50	-426.82	-425.32	-35.57	-35.44	-73.51	-73.51	0.00
	0.00	1.50	32.67	13.25	47.43	-2.50	-426.82	-425.32	-35.57	-35.44	-73.51	-73.51	0.00
	0.00	1.50	32.67	13.25	47.43	-2.50	-426.82	-425.32	-35.57	-35.44	-73.51	-73.51	0.00
	0.00	1.50	32.67	13.25	47.43	-2.50	-426.82	-425.32	-35.57	-35.44	-73.51	-73.51	0.00
	0.00	1.50	32.67	13.25	47.43	-2.50	-426.82	-425.32	-35.57	-35.44	-73.51	-73.51	0.00
	0.00	1.50	32.67	13.25	47.43	-2.50	-426.82	-425.32	-35.57	-35.44	-73.51	-73.51	0.00
	0.00	1.50	32.67	13.25	47.43	-2.50	-426.82	-425.32	-35.57	-35.44	-73.51	-73.51	0.00
	0.00	1.50	32.67	13.25	47.43	-2.50	-426.82	-425.32	-35.57	-35.44	-73.51	-73.51	0.00
	0.00	1.50	32.67	13.25	47.43	-2.50	-426.82	-425.32	-35.57	-35.44	-73.51	-73.51	0.00
	0.00	1.50	32.67	13.25	47.43	-2.50	-426.82	-425.32	-35.57	-35.44	-73.51	-73.51	0.00
	0.00	1.50	32.67	13.25	47.43	-2.50	-426.82	-425.32	-35.57	-35.44	-73.51	-73.51	0.00
	0.00	1.50	32.67	13.25	47.43	-2.50	-426.82	-425.32	-35.57	-35.44	-73.51	-73.51	0.00
	0.00	1.50	32.67	13.25	47.43	-2.50	-426.82	-425.32	-35.57	-35.44	-73.51	-73.51	0.00
	0.00	1.50	32.67	13.25	47.43	-2.50	-426.82	-425.32	-35.57	-35.44	-73.51	-73.51	0.00
	0.00	1.50	32.67	13.25	47.43	-2.50	-426.82	-425.32	-35.57	-35.44	-73.51	-73.51	0.00
	0.00	1.50	32.67	13.25	47.43	-2.50	-426.82	-425.32	-35.57	-35.44	-73.51	-73.51	0.00
	0.00	1.50	32.67	13.25	47.43	-2.50	-426.82	-425.32	-35.57	-35.44	-73.51	-73.51	0.00
	0.00	1.50	32.67	13.25	47.43	-2.50	-426.82	-425.32	-35.57	-35.44	-73.51	-73.51	0.00
	0.00	1.50	32.67	13.25	47.43	-2.50	-426.82	-425.32	-35.57	-35.44	-73.51	-73.51	0.00
	0.00	1.50	32.67	13.25	47.43	-2.50	-426.82	-425.32	-35.57	-35.44	-73.51	-73.51	0.00
a1	0.00	1.50	32.67	13.25	47.43	-2.50	-426.82	-425.32	-35.57	-35.44	-73.51	-73.51	0.00
	1.91	1.45	30.89	13.25	45.59	-2.27	-366.20	-400.04	-30.52	-33.34	-66.12	-73.45	7.33
	3.82	1.40	29.10	13.25	43.76	-2.04	-308.99	-374.76	-25.75	-31.23	-59.02	-73.38	14.37
	5.72	1.36	27.32	13.25	41.93	-1.82	-255.18	-349.47	-21.27	-29.12	-52.21	-73.32	21.11
	7.63	1.31	25.53	13.25	40.09	-1.61	-204.78	-324.19	-17.06	-27.02	-45.69	-73.26	27.57
	9.54	1.26	23.75	13.25	38.26	-1.40	-157.78	-298.91	-13.15	-24.91	-39.46	-73.19	33.73
	11.45	1.21	21.96	13.25	36.43	-1.21	-114.19	-273.63	-9.52	-22.80	-33.52	-73.13	39.61
	13.35	1.17	20.17	13.25	34.59	-1.02	-74.00	-248.35	-6.17	-20.70	-27.88	-73.07	45.19
	15.26	1.12	18.39	13.25	32.76	-0.84	-37.22	-223.07	-3.10	-18.59	-22.53	-73.00	50.48
	17.17	1.07	16.60	13.25	30.93	-0.66	-3.85	-197.78	-0.32	-16.48	-17.46	-72.94	55.47
	19.08	1.02	14.82	13.25	29.10	-0.49	26.12	-172.50	2.18	-14.38	-12.69	-72.87	60.18
	20.98	0.98	13.03	13.25	27.26	-0.34	52.68	-147.22	4.39	-12.27	-8.21	-72.81	64.60
	22.89	0.93	11.25	13.25	25.43	-0.18	75.84	-121.94	6.32	-10.16	-4.03	-72.75	68.72
	24.80	0.88	9.46	13.25	23.60	-0.04	95.59	-96.66	7.97	-8.05	-0.13	-72.68	72.55
	26.71	0.83	7.68	13.25	21.76	0.10	111.94	-71.38	9.33	-5.95	3.48	-72.62	76.10
	28.61	0.78	5.89	13.25	19.93	0.22	124.88	-46.09	10.41	-3.84	6.79	-72.56	79.35
	30.52	0.74	4.11	13.25	18.10	0.34	134.42	-20.81	11.20	-1.73	9.81	-72.49	82.30
	32.43	0.69	2.32	13.25	16.26	0.46	140.55	4.47	11.71	0.37	12.54	-72.43	84.97
	34.34	0.64	0.54	13.25	14.43	0.56	143.27	29.75	11.94	2.48	14.98	-72.36	87.35
	36.24	0.59	-1.25	13.25	12.60	0.66	142.59	55.03	11.88	4.59	17.13	-72.30	89.43
a1+b1	38.15	0.55	-3.04	13.25	10.76	0.75	138.50	80.31	11.54	6.69	18.99	-72.24	91.22
	38.92	0.53	-3.04	13.25	10.75	0.79	136.17	90.49	11.35	7.54	19.68	-72.21	91.89
	39.69	0.51	-3.04	13.25	10.73	0.82	133.84	100.66	11.15	8.39	20.36	-72.19	92.55
	40.45	0.49	-3.04	13.25	10.71	0.85	131.51	110.83	10.96	9.24	21.05	-72.16	93.21
	41.22	0.47	-3.04	13.25	10.69	0.88	129.18	121.00	10.77	10.08	21.73	-72.14	93.87
	41.99	0.45	-3.04	13.25	10.67	0.91	126.85	131.18	10.57	10.93	22.41	-72.11	94.52
	42.76	0.43	-3.04	13.25	10.65	0.94	124.52	141.35	10.38	11.78	23.10	-72.08	95.18
	43.52	0.41	-3.04	13.25	10.63	0.97	122.20	151.52	10.18	12.63	23.78	-72.06	95.83
	44.29	0.39	-3.04	13.25	10.61	0.99	119.87	161.69	9.99	13.47	24.46	-72.03	96.49
	45.06	0.37	-3.04	13.25	10.59	1.02	117.54	171.86	9.79	14.32	25.13	-72.01	97.14
	45.83	0.35	-3.04	13.25	10.57	1.04	115.21	182.04	9.60	15.17	25.81	-71.98	97.79
	46.59	0.34	-3.04	13.25	10.55	1.06	112.88	192.21	9.41	16.02	26.49	-71.96	98.44

E4. Specimen 4 (SA)

P	230.00	kip	b	107.00	in
L	120.00	in	h	12.00	in
			γDL	1.00	-
			γLL	1.00	-
			wDLu	1.34	k/ft
a	37.35	in	wLLu	60.93	k/ft
b	45.30	in			
c	37.35	in			
d	60.00	in			
e	60.00	in			
R1LLu	115.00	kip			
R2LLu	115.00	kip			
M1LLu	-3286.12	kip-in			
M2LLu	-3286.12	kip-in			
MmaxLLu	1018.18	kip-in			

0	0
120	0

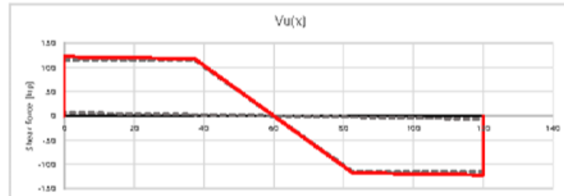

V1maxu	121.69	kip
V2maxu	-121.69	kip

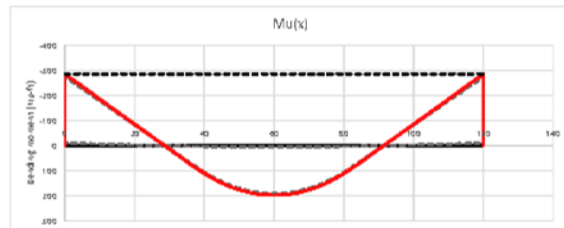

M1u-	-284.99	kip-ft
Mmaxu+	198.20	kip-ft
M2u-	-284.99	kip-ft
|M|maxu	483.19	kip-ft

Specimen 4

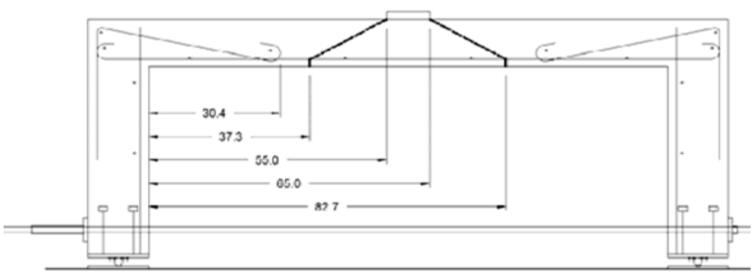

	x	VDLu (kip)	V1u (kip)	Vtotu (kip)	MDLu (k-ft)	MxLLu (k-in)	MxLLu (k-ft)	Mtotu (k-ft)	Mnegu (k-ft)	|M|u (k-ft)
	0.00	0.00	0.00	0.00	0.00	0.00	0.00	0.00		
0	0.00	6.69	115.00	121.69	-11.15	-3286.12	-273.84	-284.99	-284.99	0.00
	1.87	6.48	115.00	121.48	-10.12	-3071.36	-255.95	-266.07	-284.99	18.92
	3.74	6.27	115.00	121.27	-9.13	-2856.59	-238.05	-247.18	-284.99	37.81
	5.60	6.06	115.00	121.06	-8.17	-2641.83	-220.15	-228.32	-284.99	56.67
	7.47	5.85	115.00	120.85	-7.24	-2427.07	-202.26	-209.50	-284.99	75.49
	9.34	5.65	115.00	120.65	-6.35	-2212.31	-184.36	-190.71	-284.99	94.28
	11.21	5.44	115.00	120.44	-5.48	-1997.54	-166.46	-171.95	-284.99	113.04
	13.07	5.23	115.00	120.23	-4.65	-1782.78	-148.57	-153.22	-284.99	131.77
	14.94	5.02	115.00	120.02	-3.86	-1568.02	-130.67	-134.52	-284.99	150.46
	16.81	4.81	115.00	119.81	-3.09	-1353.26	-112.77	-115.86	-284.99	169.13
	18.68	4.61	115.00	119.61	-2.36	-1138.49	-94.87	-97.23	-284.99	187.76
	20.54	4.40	115.00	119.40	-1.66	-923.73	-76.98	-78.63	-284.99	206.35
	22.41	4.19	115.00	119.19	-0.99	-708.97	-59.08	-60.07	-284.99	224.92
	24.28	3.98	115.00	118.98	-0.35	-494.21	-41.18	-41.54	-284.99	243.45
	26.15	3.77	115.00	118.77	0.25	-279.44	-23.29	-23.04	-284.99	261.95
	28.01	3.57	115.00	118.57	0.82	-64.68	-5.39	-4.57	-284.99	280.42
	29.88	3.36	115.00	118.36	1.36	150.08	12.51	13.87	-284.99	298.86
	31.75	3.15	115.00	118.15	1.87	364.84	30.40	32.27	-284.99	317.26
	33.62	2.94	115.00	117.94	2.34	579.61	48.30	50.64	-284.99	335.63
	35.48	2.73	115.00	117.73	2.78	794.37	66.20	68.98	-284.99	353.97
a	37.35	2.52	115.00	117.52	3.19	1009.13	84.09	87.28	-284.99	372.27
	39.62	2.27	103.50	105.77	3.64	1256.58	104.72	108.36	-284.99	393.35
	41.88	2.02	92.00	94.02	4.05	1477.99	123.17	127.21	-284.99	412.20
	44.15	1.77	80.50	82.27	4.41	1673.34	139.45	143.85	-284.99	428.84
	46.41	1.51	69.00	70.51	4.72	1842.65	153.55	158.27	-284.99	443.26
	48.68	1.26	57.50	58.76	4.98	1985.91	165.49	170.47	-284.99	455.46
	50.94	1.01	46.00	47.01	5.19	2103.13	175.26	180.45	-284.99	465.44
	53.21	0.76	34.50	35.26	5.36	2194.29	182.86	188.22	-284.99	473.21
	55.47	0.50	23.00	23.50	5.48	2259.41	188.28	193.76	-284.99	478.75
	57.74	0.25	11.50	11.75	5.55	2298.48	191.54	197.09	-284.99	482.08
	60.00	0.00	0.00	0.00	5.57	2311.51	192.63	198.20	-284.99	483.19
	62.27	-0.25	-11.50	-11.75	5.55	2298.48	191.54	197.09	-284.99	482.08
	64.53	-0.50	-23.00	-23.50	5.48	2259.41	188.28	193.76	-284.99	478.75
	66.80	-0.76	-34.50	-35.26	5.36	2194.29	182.86	188.22	-284.99	473.21
	69.06	-1.01	-46.00	-47.01	5.19	2103.13	175.26	180.45	-284.99	465.44
	71.33	-1.26	-57.50	-58.76	4.98	1985.91	165.49	170.47	-284.99	455.46
	73.59	-1.51	-69.00	-70.51	4.72	1842.65	153.55	158.27	-284.99	443.26
	75.86	-1.77	-80.50	-82.27	4.41	1673.34	139.45	143.85	-284.99	428.84
	78.12	-2.02	-92.00	-94.02	4.05	1477.99	123.17	127.21	-284.99	412.20
	80.39	-2.27	-103.50	-105.77	3.64	1256.58	104.72	108.36	-284.99	393.35
a+b	82.65	-2.52	-115.00	-117.52	3.19	1009.13	84.09	87.28	-284.99	372.27
	84.52	-2.73	-115.00	-117.73	2.78	794.37	66.20	68.98	-284.99	353.97
	86.39	-2.94	-115.00	-117.94	2.34	579.61	48.30	50.64	-284.99	335.63
	88.25	-3.15	-115.00	-118.15	1.87	364.84	30.40	32.27	-284.99	317.26
	90.12	-3.36	-115.00	-118.36	1.36	150.08	12.51	13.87	-284.99	298.86
	91.99	-3.57	-115.00	-118.57	0.82	-64.68	-5.39	-4.57	-284.99	280.42
	93.86	-3.77	-115.00	-118.77	0.25	-279.44	-23.29	-23.04	-284.99	261.95
	95.72	-3.98	-115.00	-118.98	-0.35	-494.21	-41.18	-41.54	-284.99	243.45
	97.59	-4.19	-115.00	-119.19	-0.99	-708.97	-59.08	-60.07	-284.99	224.92
	99.46	-4.40	-115.00	-119.40	-1.66	-923.73	-76.98	-78.63	-284.99	206.35
	101.33	-4.61	-115.00	-119.61	-2.36	-1138.49	-94.87	-97.23	-284.99	187.76
	103.19	-4.81	-115.00	-119.81	-3.09	-1353.26	-112.77	-115.86	-284.99	169.13

E5. Specimen 4 (TA)

P	115.00	kip	b	107.00	in
L	120.00	in	h	12.00	in
s	48.00	in	γDL	1.00	-
			γLL	1.00	-

wDLu	1.34	k/ft
wLLu	30.46	k/ft

a1	13.35	in	a2	61.35	in
b1	45.30	in	b2	45.30	in
c1	61.35	in	c2	13.35	in
d1	36.00	in	d2	84.00	in
e1	84.00	in	e2	36.00	in
R11	88.52	kip	R12	26.48	kip
R12	26.48	kip	R22	88.52	kip
M11	-1848.33	kip-in	M12	-885.79	kip-in
M21	-885.79	kip-in	M22	-1848.33	kip-in
Mmax1	-655.85	kip-in	Mmax2	739.65	kip-in

0	0
120	0

	x	VDL (kip)	V1 (kip)	V2 (kip)	Vtot (kip)	MDL (k-ft)	Mx1 (k-in)	Mx2 (k-in)	Mx1 (k-ft)	Mx2 (k-ft)	Mtot (k-ft)	Mneg (k-ft)	|M| (k-ft)
	0.00	0.00	0.00	0.00	0.00	0.00	0.00	0.00	0.00	0.00	0.00		
0	0.00	6.69	88.52	26.48	121.69	-11.15	-1848.33	-885.79	-154.03	-73.82	-238.99	-238.99	0.00
	0.67	6.61	88.52	26.48	121.61	-10.78	-1789.24	-868.11	-149.10	-72.34	-232.22	-238.99	6.77
	1.34	6.54	88.52	26.48	121.54	-10.41	-1730.15	-850.44	-144.18	-70.87	-225.46	-238.99	13.53
	2.00	6.46	88.52	26.48	121.46	-10.05	-1671.07	-832.76	-139.26	-69.40	-218.70	-238.99	20.29
	2.67	6.39	88.52	26.48	121.39	-9.69	-1611.98	-815.09	-134.33	-67.92	-211.95	-238.99	27.04
	3.34	6.32	88.52	26.48	121.32	-9.34	-1552.89	-797.42	-129.41	-66.45	-205.20	-238.99	33.79
	4.01	6.24	88.52	26.48	121.24	-8.99	-1493.80	-779.74	-124.48	-64.98	-198.45	-238.99	40.54
	4.67	6.17	88.52	26.48	121.17	-8.64	-1434.71	-762.07	-119.56	-63.51	-191.71	-238.99	47.28
	5.34	6.09	88.52	26.48	121.09	-8.30	-1375.63	-744.39	-114.64	-62.03	-184.97	-238.99	54.02
	6.01	6.02	88.52	26.48	121.02	-7.97	-1316.54	-726.72	-109.71	-60.56	-178.24	-238.99	60.75
	6.68	5.94	88.52	26.48	120.94	-7.63	-1257.45	-709.04	-104.79	-59.09	-171.51	-238.99	67.48
	7.34	5.87	88.52	26.48	120.87	-7.30	-1198.36	-691.37	-99.86	-57.61	-164.78	-238.99	74.21
	8.01	5.79	88.52	26.48	120.79	-6.98	-1139.27	-673.69	-94.94	-56.14	-158.06	-238.99	80.93
	8.68	5.72	88.52	26.48	120.72	-6.66	-1080.19	-656.02	-90.02	-54.67	-151.34	-238.99	87.65
	9.35	5.65	88.52	26.48	120.65	-6.34	-1021.10	-638.34	-85.09	-53.20	-144.63	-238.99	94.36
	10.01	5.57	88.52	26.48	120.57	-6.03	-962.01	-620.67	-80.17	-51.72	-137.92	-238.99	101.07
	10.68	5.50	88.52	26.48	120.50	-5.72	-902.92	-602.99	-75.24	-50.25	-131.22	-238.99	107.77
	11.35	5.42	88.52	26.48	120.42	-5.42	-843.84	-585.32	-70.32	-48.78	-124.52	-238.99	114.47
	12.02	5.35	88.52	26.48	120.35	-5.12	-784.75	-567.65	-65.40	-47.30	-117.82	-238.99	121.17
	12.68	5.27	88.52	26.48	120.27	-4.82	-725.66	-549.97	-60.47	-45.83	-111.13	-238.99	127.86
s1	13.35	5.20	88.52	26.48	120.20	-4.53	-666.57	-532.30	-55.55	-44.36	-104.44	-238.99	134.55
	15.62	4.95	82.77	26.48	114.20	-3.58	-472.58	-472.32	-39.38	-39.36	-82.32	-238.99	156.67
	17.88	4.69	77.02	26.48	108.19	-2.67	-291.62	-412.35	-24.30	-34.36	-61.33	-238.99	177.66
	20.15	4.44	71.27	26.48	102.19	-1.80	-123.68	-352.37	-10.31	-29.36	-41.47	-238.99	197.51
	22.41	4.19	65.52	26.48	96.19	-0.99	31.24	-292.40	2.60	-24.37	-22.75	-238.99	216.24
	24.68	3.94	59.77	26.48	90.19	-0.22	173.13	-232.42	14.43	-19.37	-5.16	-238.99	233.83
	26.94	3.68	54.02	26.48	84.18	0.50	302.00	-172.45	25.17	-14.37	11.29	-238.99	250.28
	29.21	3.43	48.27	26.48	78.18	1.17	417.85	-112.47	34.82	-9.37	26.62	-238.99	265.61
	31.47	3.18	42.52	26.48	72.18	1.79	520.67	-52.50	43.39	-4.37	40.81	-238.99	279.80
	33.74	2.93	36.77	26.48	66.18	2.37	610.47	7.47	50.87	0.62	53.86	-238.99	292.85
	36.00	2.68	31.02	26.48	60.18	2.90	687.25	67.45	57.27	5.62	65.79	-238.99	304.78
	38.27	2.42	25.27	26.48	54.17	3.38	751.00	127.42	62.58	10.62	76.58	-238.99	315.57
	40.53	2.17	19.52	26.48	48.17	3.81	801.72	187.40	66.81	15.62	86.24	-238.99	325.23
	42.80	1.92	13.77	26.48	42.17	4.20	839.43	247.37	69.95	20.61	94.76	-238.99	333.75
	45.06	1.67	8.02	26.48	36.17	4.54	864.11	307.35	72.01	25.61	102.16	-238.99	341.15
	47.33	1.41	2.27	26.48	30.16	4.83	875.76	367.32	72.98	30.61	108.42	-238.99	347.41
	49.59	1.16	-3.48	26.48	24.16	5.07	874.40	427.30	72.87	35.61	113.54	-238.99	352.53
	51.86	0.91	-9.23	26.48	18.16	5.26	860.00	487.27	71.67	40.61	117.54	-238.99	356.53
	54.12	0.66	-14.98	26.48	12.16	5.41	832.59	547.25	69.38	45.60	120.40	-238.99	359.39
	56.39	0.40	-20.73	26.48	6.15	5.51	792.15	607.22	66.01	50.60	122.13	-238.99	361.12
s1+b1	58.65	0.15	-26.48	26.48	0.15	5.56	738.69	667.19	61.56	55.60	122.72	-238.99	361.71
	58.79	0.14	-26.48	26.48	0.14	5.57	735.11	670.77	61.26	55.90	122.72	-238.99	361.71
	58.92	0.12	-26.48	26.48	0.12	5.57	731.54	674.34	60.96	56.20	122.72	-238.99	361.71
	59.06	0.11	-26.48	26.48	0.11	5.57	727.96	677.92	60.66	56.49	122.73	-238.99	361.71
	59.19	0.09	-26.48	26.48	0.09	5.57	724.39	681.49	60.37	56.79	122.73	-238.99	361.72
	59.33	0.08	-26.48	26.48	0.08	5.57	720.81	685.07	60.07	57.09	122.73	-238.99	361.72
	59.46	0.06	-26.48	26.48	0.06	5.57	717.24	688.64	59.77	57.39	122.73	-238.99	361.72
	59.60	0.05	-26.48	26.48	0.05	5.57	713.67	692.22	59.47	57.68	122.73	-238.99	361.72
	59.73	0.03	-26.48	26.48	0.03	5.57	710.09	695.79	59.17	57.98	122.73	-238.99	361.72
	59.87	0.02	-26.48	26.48	0.02	5.57	706.52	699.37	58.88	58.28	122.73	-238.99	361.72
	60.00	0.00	-26.48	26.48	0.00	5.57	702.94	702.94	58.58	58.58	122.73	-238.99	361.72
	60.14	-0.02	-26.48	26.48	-0.02	5.57	699.37	706.52	58.28	58.88	122.73	-238.99	361.72

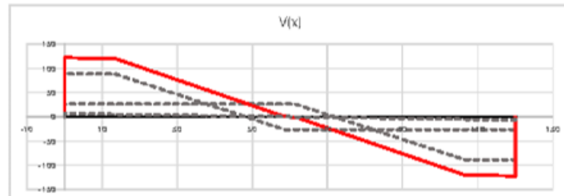

V1max	121.69	kip
V2max	-121.69	kip

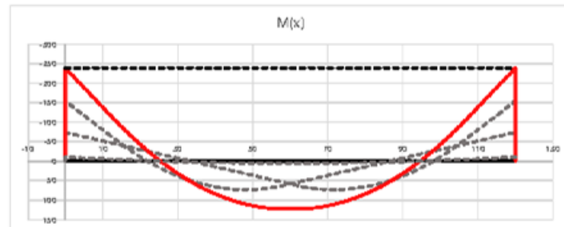

M1-	-238.99	kip-ft
Mmax+	122.73	kip-ft
M2-	-238.99	kip-ft
|M| max	361.72	kip-ft

Specimen 4

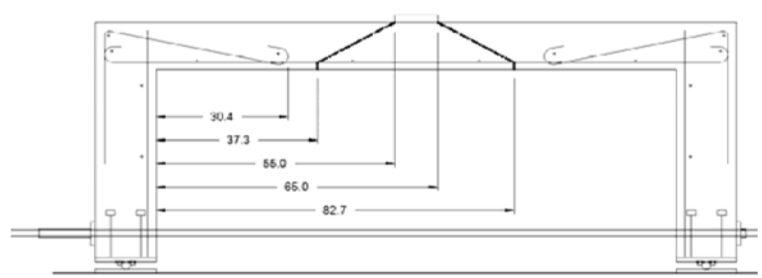

E6. Specimen 5

P	76.80	kip	b	24.00	in
L	192.00	in	h	18.00	in
			γDL	1.00	-
			γLL	1.00	-
			wDLu	0.45	k/ft
a	62.96	in	wLLu	13.95	k/ft
b	66.08	in			
c	62.96	in			
d	96.00	in			
e	96.00	in			
R1LLu	38.40	kip			
R2LLu	38.40	kip			
M1LLu	-1770.42	kip-in			
M2LLu	-1770.42	kip-in			
MmaxLLu	651.65	kip-in			

0	0
192	0

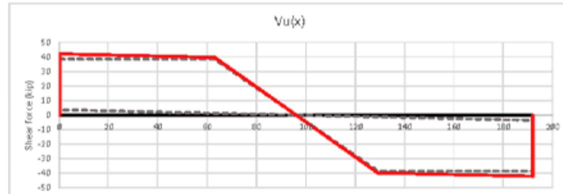

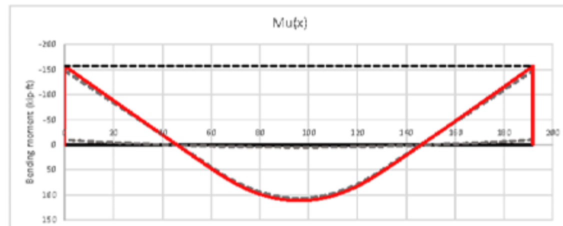

V1maxu	42.00	kip
V2maxu	-42.00	kip
M1u-	-157.14	kip-ft
Mmaxu+	111.60	kip-ft
M2u-	-157.14	kip-ft
|M|maxu	268.74	kip-ft

	x	VDLu (kip)	V1u (kip)	Vtotu (kip)	MDLu (k-ft)	MxLLu (k-in)	MxLLu (k-ft)	Mtotu (k-ft)	Mnegu (k-ft)	|M|u (k-ft)
	0.00	0.00	0.00	0.00	0.00	0.00	0.00	0.00		
0	0.00	3.60	38.40	42.00	-9.60	-1770.42	-147.54	-157.14	-157.14	0.00
	3.15	3.48	38.40	41.88	-8.67	-1649.54	-137.46	-146.13	-157.14	11.00
	6.30	3.36	38.40	41.76	-7.77	-1528.66	-127.39	-135.16	-157.14	21.97
	9.44	3.25	38.40	41.65	-6.91	-1407.77	-117.31	-124.22	-157.14	32.91
	12.59	3.13	38.40	41.53	-6.07	-1286.89	-107.24	-113.31	-157.14	43.82
	15.74	3.01	38.40	41.41	-5.27	-1166.01	-97.17	-102.43	-157.14	54.70
	18.89	2.89	38.40	41.29	-4.49	-1045.12	-87.09	-91.58	-157.14	65.55
	22.04	2.77	38.40	41.17	-3.75	-924.24	-77.02	-80.77	-157.14	76.37
	25.18	2.66	38.40	41.06	-3.04	-803.36	-66.95	-69.98	-157.14	87.15
	28.33	2.54	38.40	40.94	-2.35	-682.48	-56.87	-59.23	-157.14	97.91
	31.48	2.42	38.40	40.82	-1.70	-561.59	-46.80	-48.50	-157.14	108.63
	34.63	2.30	38.40	40.70	-1.09	-440.71	-36.73	-37.81	-157.14	119.32
	37.78	2.18	38.40	40.58	-0.50	-319.83	-26.65	-27.15	-157.14	129.99
	40.92	2.07	38.40	40.47	0.06	-198.94	-16.58	-16.52	-157.14	140.62
	44.07	1.95	38.40	40.35	0.59	-78.06	-6.50	-5.92	-157.14	151.22
	47.22	1.83	38.40	40.23	1.08	42.82	3.57	4.65	-157.14	161.79
	50.37	1.71	38.40	40.11	1.55	163.71	13.64	15.19	-157.14	172.32
	53.52	1.59	38.40	39.99	1.98	284.59	23.72	25.70	-157.14	182.83
	56.66	1.48	38.40	39.88	2.38	405.47	33.79	36.17	-157.14	193.31
	59.81	1.36	38.40	39.76	2.75	526.36	43.86	46.62	-157.14	203.75
a	62.96	1.24	38.40	39.64	3.09	647.24	53.94	57.03	-157.14	214.17
	66.26	1.12	34.56	35.68	3.42	767.77	63.98	67.40	-157.14	224.53
	69.57	0.99	30.72	31.71	3.71	875.61	72.97	76.68	-157.14	233.81
	72.87	0.87	26.88	27.75	3.96	970.77	80.90	84.86	-157.14	242.00
	76.18	0.74	23.04	23.78	4.19	1053.24	87.77	91.96	-157.14	249.09
	79.48	0.62	19.20	19.82	4.37	1123.02	93.58	97.96	-157.14	255.09
	82.78	0.50	15.36	15.86	4.53	1180.11	98.34	102.87	-157.14	260.00
	86.09	0.37	11.52	11.89	4.65	1224.51	102.04	106.69	-157.14	263.82
	89.39	0.25	7.68	7.93	4.73	1256.23	104.69	109.42	-157.14	266.55
	92.70	0.12	3.84	3.96	4.78	1275.26	106.27	111.05	-157.14	268.19
	96.00	0.00	0.00	0.00	4.80	1281.61	106.80	111.60	-157.14	268.74
	99.30	-0.12	-3.84	-3.96	4.78	1275.26	106.27	111.05	-157.14	268.19
	102.61	-0.25	-7.68	-7.93	4.73	1256.23	104.69	109.42	-157.14	266.55
	105.91	-0.37	-11.52	-11.89	4.65	1224.51	102.04	106.69	-157.14	263.82
	109.22	-0.50	-15.36	-15.86	4.53	1180.11	98.34	102.87	-157.14	260.00
	112.52	-0.62	-19.20	-19.82	4.37	1123.02	93.58	97.96	-157.14	255.09
	115.82	-0.74	-23.04	-23.78	4.19	1053.24	87.77	91.96	-157.14	249.09
	119.13	-0.87	-26.88	-27.75	3.96	970.77	80.90	84.86	-157.14	242.00
	122.43	-0.99	-30.72	-31.71	3.71	875.61	72.97	76.68	-157.14	233.81
	125.74	-1.12	-34.56	-35.68	3.42	767.77	63.98	67.40	-157.14	224.53
a+b	129.04	-1.24	-38.40	-39.64	3.09	647.24	53.94	57.03	-157.14	214.17
	132.19	-1.36	-38.40	-39.76	2.75	526.36	43.86	46.62	-157.14	203.75
	135.34	-1.48	-38.40	-39.88	2.38	405.47	33.79	36.17	-157.14	193.31
	138.48	-1.59	-38.40	-39.99	1.98	284.59	23.72	25.70	-157.14	182.83
	141.63	-1.71	-38.40	-40.11	1.55	163.71	13.64	15.19	-157.14	172.32
	144.78	-1.83	-38.40	-40.23	1.08	42.82	3.57	4.65	-157.14	161.79
	147.93	-1.95	-38.40	-40.35	0.59	-78.06	-6.50	-5.92	-157.14	151.22
	151.08	-2.07	-38.40	-40.47	0.06	-198.94	-16.58	-16.52	-157.14	140.62
	154.22	-2.18	-38.40	-40.58	-0.50	-319.83	-26.65	-27.15	-157.14	129.99
	157.37	-2.30	-38.40	-40.70	-1.09	-440.71	-36.73	-37.81	-157.14	119.32
	160.52	-2.42	-38.40	-40.82	-1.70	-561.59	-46.80	-48.50	-157.14	108.63
	163.67	-2.54	-38.40	-40.94	-2.35	-682.48	-56.87	-59.23	-157.14	97.91

Specimen 1 - Flexural strength (mechanism)

$L_c := 10ft = 3.05\,m$

$\alpha := \frac{\pi}{6} = 30 \cdot deg$ Failure angle per experiment

$w_c := 150\frac{lbf}{ft^3} = 23.6 \cdot \frac{kN}{m^3}$

$E_s := 29000ksi$

$A_s := 4 \cdot 0.31in^2 = 1.24 \cdot in^2$

$f_{y\_pos} := 65.8ksi$ $f_{y\_neg} := 73.6ksi$

$a_g := 0.75in$

$f_{c\_prime} := 3790psi$

$b_w := 24in = 610 \cdot mm$

$h_s := 12in = 305 \cdot mm$

$d_{s\_pos} := h_s - 1.5in - \frac{5}{16}in = 10.2 \cdot in$

$P_{LL} := 57.8kip = 257 \cdot kN$ Applied load at failure

$M_{nys\_pos} := 66.0kip \cdot ft = 792 \cdot kip \cdot in$ Yield vs. probable moment

$M_{nps\_pos} := 86.1kip \cdot ft = 1033.2 \cdot kip \cdot in$ Yield vs. probable moment

$M_{nys\_neg} := 31.9kip \cdot ft = 382.8 \cdot kip \cdot in$

$M_{nps\_neg} := 36.8kip \cdot ft = 441.6 \cdot kip \cdot in$

Precalcs

$b := 10in + 2\frac{d_{s\_pos}}{\tan(\alpha)} = 45.3 \cdot in$ $\frac{d_{s\_pos}}{\tan(\alpha)} = 17.6\,in$ Length of load using α

$\rho_w := \frac{A_s}{b_w \cdot d_{s\_pos}} = 0.00507$ Long. reinforcement ratio

$w_{DL} := b_w \cdot h_s \cdot w_c = 0.3 \cdot \frac{kip}{ft}$ Dead load

$w_{LL} := \frac{P_{LL}}{b} = 15.3 \cdot \frac{kip}{ft}$ Live load across length b

Mechanism (one hinge at x = Lc/2)

$x := \frac{L_c}{2} = 60\,\text{in}$

$\theta_1 := \frac{1\text{in}}{x} = 0.017 \qquad \theta_3 := \theta_1 = 0.017 \qquad \theta_2 := \theta_1 + \theta_3 = 0.033$

$E_{ext} := A + w_{LL} \cdot B$

$A := w_{DL} \cdot \left(\frac{x \cdot \theta_1}{2} \cdot x + \frac{x \cdot \theta_3}{2} \cdot x \right) = 1.5 \cdot \text{kip} \cdot \text{in} \qquad B := \frac{b}{2} \cdot \left[\theta_1 \cdot \left(x - \frac{b}{4} \right) + \theta_3 \cdot \left(x - \frac{b}{4} \right) \right] = 36.744 \cdot \text{in}^2$

$E_{int\_y} := M_{nys\_pos} \cdot \theta_2 + M_{nys\_neg} \cdot (\theta_1 + \theta_3) = 39.16 \cdot \text{kip} \cdot \text{in}$

$E_{int\_p} := M_{nps\_pos} \cdot \theta_2 + M_{nps\_neg} \cdot (\theta_1 + \theta_3) = 49.16 \cdot \text{kip} \cdot \text{in}$

$P_{LL\_pred\_y} := \frac{E_{int\_y} - A}{B} \cdot b = 46.42 \cdot \text{kip} \qquad P_{LL\_pred\_y} = 206.486 \cdot \text{kN} \qquad \frac{P_{LL\_pred\_y}}{P_{LL}} = 0.803$

$P_{LL\_pred\_p} := \frac{E_{int\_p} - A}{B} \cdot b = 58.746 \cdot \text{kip} \qquad P_{LL\_pred\_p} = 261.315 \cdot \text{kN} \qquad \frac{P_{LL\_pred\_p}}{P_{LL}} = 1.016$

Specimen 2 - Flexural strength (mechanism)

$L_c := 10ft = 3.05\,m$

$\alpha := \frac{\pi}{6} = 30 \cdot deg$ Failure angle per experiment

$w_c := 150\,\frac{lbf}{ft^3} = 23.6 \cdot \frac{kN}{m^3}$

$E_s := 29000ksi$

$A_s := 4 \cdot 0.31in^2 = 1.24 \cdot in^2$

$f_{y\_pos} := 65.8ksi$ $f_{y\_neg} := 73.6ksi$

$a_g := 0.75in$

$f_{c\_prime} := 3788psi$

$b_w := 2ft = 610 \cdot mm$

$h_s := 12in = 305 \cdot mm$

$d_{s\_pos} := h_s - 1.5in - \frac{5}{16}in = 10.2 \cdot in$

$P_{LL} := 97.0kip = 431 \cdot kN$ Applied load at failure

$M_{nys\_pos} := 66.1kip \cdot ft = 793.2 \cdot kip \cdot in$ Yield vs. probable moment

$M_{nps\_pos} := 87.3kip \cdot ft = 1047.6 \cdot kip \cdot in$ Yield vs. probable moment

$M_{nys\_neg} := 31.9kip \cdot ft = 382.8 \cdot kip \cdot in$

$M_{nps\_neg} := 36.8kip \cdot ft = 441.6 \cdot kip \cdot in$

Precalcs

$b := 10in + 2\,\frac{d_{s\_pos}}{\tan(\alpha)} = 45.3 \cdot in$ $\frac{d_{s\_pos}}{\tan(\alpha)} = 17.6\,in$ Length of load using α

$\rho_w := \frac{A_s}{b_w \cdot d_{s\_pos}} = 0.00507$ Long. reinforcement ratio

$w_{DL} := b_w \cdot h_s \cdot w_c = 0.3 \cdot \frac{kip}{ft}$ Dead load

$w_{LL} := \frac{P_{LL}}{b} = 25.7 \cdot \frac{kip}{ft}$ Live load across length b

Mechanism (one hinge under first load patch at x = 36 in)

$x := 36in$

$\theta_1 := \frac{1in}{x} = 0.028$ $\qquad \theta_3 := \frac{1in}{L_c - x} = 0.012$ $\qquad \theta_2 := \theta_1 + \theta_3 = 0.04$

$E_{ext} := A + w_{LL} \cdot B$

$A := w_{DL} \cdot \left[\frac{x \cdot \theta_1}{2} \cdot x + \frac{(L_c - x) \cdot \theta_3}{2} \cdot (L_c - x) \right] = 1.5 \cdot kip \cdot in$

$B := \frac{b}{2} \cdot \left[\theta_1 \cdot \left(x - \frac{b}{4} \right) + \theta_3 \cdot \left(L_c - x - \frac{b}{4} \right) + \theta_3 \cdot \left(x + \frac{b}{4} \right) + \theta_3 \cdot \left(x - \frac{b}{4} \right) \right] = 54.526 \cdot in^2$

$E_{int\_y} := M_{nys\_pos} \cdot \theta_2 + M_{nys\_neg} \cdot (\theta_1 + \theta_3) = 46.667 \cdot kip \cdot in$

$E_{int\_p} := M_{nps\_pos} \cdot \theta_2 + M_{nps\_neg} \cdot (\theta_1 + \theta_3) = 59.095 \cdot kip \cdot in$

$P_{LL\_pred\_y} := 2 \left(\frac{E_{int\_y} - A}{B} \cdot b \right) = 75.033 \cdot kip$ $\qquad P_{LL\_pred\_y} = 333.763 \cdot kN$ $\qquad \frac{P_{LL\_pred\_y}}{P_{LL}} = 0.774$

$P_{LL\_pred\_p} := 2 \left(\frac{E_{int\_p} - A}{B} \cdot b \right) = 95.68 \cdot kip$ $\qquad P_{LL\_pred\_p} = 425.605 \cdot kN$ $\qquad \frac{P_{LL\_pred\_p}}{P_{LL}} = 0.986$

Specimen 3 - Flexural strength (mechanism)

$L_c := 10ft = 3.05\,m$

$\alpha := \frac{\pi}{6} = 30 \cdot deg$ — Failure angle per experiment

$w_c := 150 \frac{lbf}{ft^3} = 23.6 \cdot \frac{kN}{m^3}$

$E_s := 29000ksi$

$A_s := 4 \cdot 0.31in^2 = 1.24 \cdot in^2$

$f_{y\_pos} := 65.9ksi$ $\quad f_{y\_neg} := 73.6ksi$

$a_g := 0.75in$

$f_{c\_prime} := 3339psi$

$b_w := 24in = 610 \cdot mm$

$h_s := 12in = 305 \cdot mm$

$d_{s\_pos} := h_s - 1.5in - \frac{5}{16}in = 10.2 \cdot in$

$P_{LL} := 84.8kip = 377 \cdot kN$ — Applied load at failure

$M_{nys\_pos} := 65.6kip \cdot ft = 787.2 \cdot kip \cdot in$ — Yield vs. probable moment

$M_{nps\_pos} := 85.6kip \cdot ft = 1027.2 \cdot kip \cdot in$ — Yield vs. probable moment

$M_{nys\_neg} := 31.0kip \cdot ft = 372 \cdot kip \cdot in$

$M_{nps\_neg} := 36.4kip \cdot ft = 436.8 \cdot kip \cdot in$

Precalcs

$b := 10in + 2 \frac{d_{s\_pos}}{\tan(\alpha)} = 45.3 \cdot in$ $\quad \frac{d_{s\_pos}}{\tan(\alpha)} = 17.6 \cdot in$ — Length of load using α

$\rho_w := \frac{A_s}{b_w \cdot d_{s\_pos}} = 0.00507$ — Long. reinforcement ratio

$w_{DL} := b_w \cdot h_s \cdot w_c = 0.3 \cdot \frac{kip}{ft}$ — Dead load

$w_{LL} := \frac{P_{LL}}{b} = 22.5 \cdot \frac{kip}{ft}$ — Live load across length b

Mechanism (one hinge under first load patch at x = 63.5 in)

$x := 15.5\text{in} + 48\text{in} = 63.5\,\text{in}$

$\theta_1 := \dfrac{1\text{in}}{x} = 0.016 \qquad \theta_3 := \dfrac{1\text{in}}{L_c - x} = 0.018 \qquad \theta_2 := \theta_1 + \theta_3 = 0.033$

$E_{ext} := A + w_{LL} \cdot B$

$A := w_{DL} \cdot \left[\dfrac{x \cdot \theta_1}{2} \cdot x + \dfrac{(L_c - x) \cdot \theta_3}{2} \cdot (L_c - x) \right] = 1.5 \cdot \text{kip} \cdot \text{in}$

$B := \dfrac{b}{2} \cdot \left[\theta_1 \cdot \left(\dfrac{15.5\text{in}}{2} \right) \cdot \dfrac{15.5\text{in}}{\frac{b}{2}} + \theta_1 \cdot \left(15.5\text{in} + \dfrac{b}{4} \right) + \theta_1 \cdot \left(x - \dfrac{b}{4} \right) + \theta_3 \cdot \left(L_c - x - \dfrac{b}{4} \right) \right] = 48.172 \cdot \text{in}^2$

$E_{int\_y} := M_{nys\_pos} \cdot \theta_2 + M_{nys\_neg} \cdot (\theta_1 + \theta_3) = 38.772 \cdot \text{kip} \cdot \text{in}$

$E_{int\_p} := M_{nps\_pos} \cdot \theta_2 + M_{nps\_neg} \cdot (\theta_1 + \theta_3) = 48.967 \cdot \text{kip} \cdot \text{in}$

$P_{LL\_pred\_y} := 2 \left(\dfrac{E_{int\_y} - A}{B} \cdot b \right) = 70.085 \cdot \text{kip} \qquad P_{LL\_pred\_y} = 311.755 \cdot \text{kN} \qquad \dfrac{P_{LL\_pred\_y}}{P_{LL}} = 0.826$

$P_{LL\_pred\_p} := 2 \left(\dfrac{E_{int\_p} - A}{B} \cdot b \right) = 89.255 \cdot \text{kip} \qquad P_{LL\_pred\_p} = 397.027 \cdot \text{kN} \qquad \dfrac{P_{LL\_pred\_p}}{P_{LL}} = 1.053$

Specimen 4 (SA) - Flexural strength (mechanism)

$L_c := 10ft = 3.05\,m$

$\alpha := \frac{\pi}{6} = 30\cdot deg$ Failure angle per experiment

$w_c := 150\frac{lbf}{ft^3} = 23.6\cdot\frac{kN}{m^3}$

$E_s := 29000ksi$

$A_s := 4\cdot 0.31in^2 = 1.24\cdot in^2$

$f_{y\_pos} := 62.2ksi$ $f_{y\_neg} := 100ksi$

$a_g := 0.75in$

$f_{c\_prime} := 3469psi$

$b_w := 24in = 610\cdot mm$

$h_s := 12in = 305\cdot mm$

$d_{s\_pos} := h_s - 1.5in - \frac{5}{16}in = 10.2\cdot in$

$P_{LL} := 230kip = 1023\cdot kN$ Applied load at failure

$M_{nys\_pos} := 218kip\cdot ft = 2616\cdot kip\cdot in$ Yield moment

$M_{nps\_pos} := 293kip\cdot ft = 3516\cdot kip\cdot in$ Probable moment

$M_{nys\_neg} := 152kip\cdot ft = 1824\cdot kip\cdot in$ Yield moment

$M_{nps\_neg} := 182kip\cdot ft = 2184\cdot kip\cdot in$ Probable moment

Precalcs

$b := 10in + 2\frac{d_{s\_pos}}{\tan(\alpha)} = 45.3\cdot in$ $\frac{d_{s\_pos}}{\tan(\alpha)} = 17.6\cdot in$ Length of load using α

$\rho_w := \frac{A_s}{b_w\cdot d_{s\_pos}} = 0.00507$ Long. reinforcement ratio

$w_{DL} := b_w\cdot h_s\cdot w_c = 0.3\cdot\frac{kip}{ft}$ Dead load

$w_{LL} := \frac{P_{LL}}{b} = 60.9\cdot\frac{kip}{ft}$ Live load across length b

Mechanism (one hinge at x = Lc/2)

$x := \frac{L_c}{2} = 60 \cdot in$

$\theta_1 := \frac{1in}{x} = 0.017 \qquad \theta_3 := \theta_1 = 0.017 \qquad \theta_2 := \theta_1 + \theta_3 = 0.033$

$E_{ext} := A + w_{LL} \cdot B$

$A := w_{DL} \cdot \left(\frac{x \cdot \theta_1}{2} \cdot x + \frac{x \cdot \theta_3}{2} \cdot x \right) = 1.5 \cdot kip \cdot in \qquad B := \frac{b}{2} \cdot \left[\theta_1 \cdot \left(x - \frac{b}{4} \right) + \theta_3 \cdot \left(x - \frac{b}{4} \right) \right] = 36.744 \cdot in^2$

$E_{int\_y} := M_{nys\_pos} \cdot \theta_2 + M_{nys\_neg} \cdot (\theta_1 + \theta_3) = 148 \cdot kip \cdot in$

$E_{int\_p} := M_{nps\_pos} \cdot \theta_2 + M_{nps\_neg} \cdot (\theta_1 + \theta_3) = 190 \cdot kip \cdot in$

$P_{LL\_pred\_y} := \frac{E_{int\_y} - A}{B} \cdot b = 180.577 \cdot kip \qquad P_{LL\_pred\_y} = 803.245 \cdot kN \qquad \frac{P_{LL\_pred\_y}}{P_{LL}} = 0.785$

$P_{LL\_pred\_p} := \frac{E_{int\_p} - A}{B} \cdot b = 232.346 \cdot kip \qquad P_{LL\_pred\_p} = 1.034 \times 10^3 \cdot kN \qquad \frac{P_{LL\_pred\_p}}{P_{LL}} = 1.01$

Specimen 5 - Flexural strength (mechanism)

$L_c := 16ft = 4.88\,m$

$\alpha := \frac{\pi}{6} = 30 \cdot deg$ Failure angle per experiment

$w_c := 150 \frac{lbf}{ft^3} = 23.6 \cdot \frac{kN}{m^3}$

$E_s := 29000ksi$

$A_s := 4 \cdot 0.31in^2 = 1.24 \cdot in^2$

$f_{y\_pos} := 65.8ksi$ $f_{y\_neg} := 73.6ksi$

$a_g := 0.75in$

$f_{c\_prime} := 3366psi$

$b_w := 2ft = 610 \cdot mm$

$h_s := 18in = 457 \cdot mm$

$d_{s\_pos} := h_s - 1.5in - \frac{5}{16}in = 16.2 \cdot in$

$P_{LL} := 76.8kip = 342 \cdot kN$ Applied load at failure

$M_{nys\_pos} := 102kip \cdot ft = 1224 \cdot kip \cdot in$ Yield vs. probable moment

$M_{nps\_pos} := 155kip \cdot ft = 1860 \cdot kip \cdot in$ Yield vs. probable moment

$M_{nys\_neg} := 52.0kip \cdot ft = 624 \cdot kip \cdot in$

$M_{nps\_neg} := 77.0kip \cdot ft = 924 \cdot kip \cdot in$

Precalcs

$b := 10in + 2 \frac{d_{s\_pos}}{\tan(\alpha)} = 66.1 \cdot in$ $\frac{d_{s\_pos}}{\tan(\alpha)} = 28 \cdot in$ Length of load using α

$\rho_w := \frac{A_s}{b_w \cdot d_{s\_pos}} = 0.00319$ Long. reinforcement ratio

$w_{DL} := b_w \cdot h_s \cdot w_c = 0.45 \cdot \frac{kip}{ft}$ Dead load

$w_{LL} := \frac{P_{LL}}{b} = 13.9 \cdot \frac{kip}{ft}$ Live load across length b

Mechanism (one hinge at x = Lc/2)

$x := 96in$

$\theta_1 := \frac{1in}{x} = 0.01$ $\qquad \theta_3 := \theta_1 = 0.01$ $\qquad \theta_2 := \theta_1 + \theta_3 = 0.021$

$E_{ext} := A + w_{LL} \cdot B$

$A := w_{DL} \cdot \left(\frac{x \cdot \theta_1}{2} \cdot x + \frac{x \cdot \theta_3}{2} \cdot x \right) = 3.6 \cdot kip \cdot in$ $\qquad B := \frac{b}{2} \cdot \left[\theta_1 \cdot \left(x - \frac{b}{4} \right) + \theta_3 \cdot \left(x - \frac{b}{4} \right) \right] = 54.706 \cdot in^2$

$E_{int\_y} := M_{nys\_pos} \cdot \theta_2 + M_{nys\_neg} \cdot (\theta_1 + \theta_3) = 38.5 \cdot kip \cdot in$

$E_{int\_p} := M_{nps\_pos} \cdot \theta_2 + M_{nps\_neg} \cdot (\theta_1 + \theta_3) = 58 \cdot kip \cdot in$

$P_{LL\_pred\_y} := \frac{E_{int\_y} - A}{B} \cdot b = 42.153 \cdot kip$ $\qquad P_{LL\_pred\_y} = 187.507 \cdot kN$ $\qquad \frac{P_{LL\_pred\_y}}{P_{LL}} = 0.549$

$P_{LL\_pred\_p} := \frac{E_{int\_p} - A}{B} \cdot b = 65.706 \cdot kip$ $\qquad P_{LL\_pred\_p} = 292.275 \cdot kN$ $\qquad \frac{P_{LL\_pred\_p}}{P_{LL}} = 0.856$

Specimen 1 - Shear strength

$L_c := 10ft = 3.05\,m$

$\alpha := \frac{\pi}{6} = 30\cdot deg$ Failure angle per experiment

$w_c := 150\frac{lbf}{ft^3} = 23.6\cdot\frac{kN}{m^3}$

$E_s := 29000ksi$

$A_s := 4\cdot 0.31in^2 = 1.24\cdot in^2$

$f_{y\_pos} := 65.8ksi$ $f_{y\_neg} := 73.6ksi$

$f_{su\_pos} := 73.6ksi$ $f_{su\_neg} := 120ksi$

$a_g := 0.75in$

$f_{c\_prime} := 3790psi$

$b_w := 24in = 610\cdot mm$

$h_s := 12in = 305\cdot mm$

$d_{s\_pos} := h_s - 1.5in - \frac{5}{16}in = 10.2\cdot in$

$P_{LL} := 57.8kip = 257\cdot kN$ Applied load at failure

$M_{nys\_pos} := 66.0kip\cdot ft$ $M_{nps\_pos} := 86.1kip\cdot ft$ Yield vs. probable moment

$M_{nys\_neg} := 31.9kip\cdot ft$ $M_{nps\_neg} := 36.8kip\cdot ft$ Yield vs. probable moment

Precalcs

$b := 10in + 2\frac{d_{s\_pos}}{\tan(\alpha)} = 45.3\cdot in$ Length of load using α

$\rho_w := \frac{A_s}{b_w\cdot d_{s\_pos}} = 0.00507$ Long. reinforcement ratio

$w_{DL} := b_w\cdot h_s\cdot w_c = 0.3\cdot\frac{kip}{ft}$ Dead load

$w_{LL} := \frac{P_{LL}}{b} = 15.3\cdot\frac{kip}{ft}$ Live load across length b

Internal forces

$V_n := 29.5kip$ Shear force @ x = 83 in

$M_n := 48.5kip \cdot ft$ Bending moment @ x = 65 in

Shear strengths

ACI 318-14 simplified

$V_{c\_ACI\_simple} := 2 \cdot \sqrt{f_{c\_prime}} \cdot \sqrt{psi} \cdot b_w \cdot d_{s\_pos} = 30.1 \cdot kip$

$\boxed{V_{n\_ACI\_simple} := V_{c\_ACI\_simple} = 30.1 \cdot kip}$ $V_{n\_ACI\_simple\_SI} := V_{n\_ACI\_simple} = 134 \cdot kN$

ACI 318-14 detailed

$\left|\min\left(M_n, M_{nys\_pos}\right)\right| = 48.5 \cdot kip \cdot ft$

$$V_{c\_ACI\_det\_1} := \left(1.9 \cdot \sqrt{f_{c\_prime}} \cdot \sqrt{psi} + 2500 \cdot \rho_w \cdot \frac{\left|V_n\right| \cdot d_{s\_pos}}{\left|\min\left(M_n, M_{nys\_pos}\right)\right|} \cdot psi\right) \cdot b_w \cdot d_{s\_pos} = 30.2 \cdot kip$$

$$V_{c\_ACI\_det\_2} := \left(1.9 \cdot \sqrt{f_{c\_prime}} \cdot \sqrt{psi} + 2500 \cdot \rho_w \cdot psi\right) \cdot b_w \cdot d_{s\_pos} = 31.7 \cdot kip$$

$$V_{c\_ACI\_det\_3} := 3.5 \cdot \sqrt{f_{c\_prime}} \cdot \sqrt{psi} \cdot b_w \cdot d_{s\_pos} = 52.7 \cdot kip$$

$$V_{c\_ACI\_det} := \min\left(V_{c\_ACI\_det\_1}, V_{c\_ACI\_det\_2}, V_{c\_ACI\_det\_3}\right) = 30.2 \cdot kip$$

$\boxed{V_{n\_ACI\_det} := V_{c\_ACI\_det} = 30.2 \cdot kip}$ $V_{n\_ACI\_det\_SI} := V_{n\_ACI\_det} = 134 \cdot kN$

Eurocode 2 (unreinforced section)

$\gamma_c := 1.0$ Partial safety factor, set to 1.0

$C_{Rd\_c} := \frac{0.18}{\gamma_c}$ Experimental coefficient

$k := 1 + \sqrt{\frac{200}{\frac{d_{s\_pos}}{mm}}} = 1.879$ Max. value = 2

$\rho_l := \rho_w = 0.00507$ Longitudinal reinf. ratio

$f_{ck} := f_{c\_prime} = 3790 \cdot psi$ Concrete cube strength

$$V_{Rd\_c} := C_{Rd\_c} \cdot k \cdot \left(100 \cdot \rho_l \cdot \frac{f_{ck}}{MPa}\right)^{\frac{1}{3}} \cdot \frac{b_w}{mm} \cdot \frac{d_{s\_pos}}{mm} \cdot N = 28.4 \cdot kip$$

$\boxed{V_{n\_EC2} := V_{Rd\_c} = 28.4 \cdot kip}$ $V_{n\_EC2\_SI} := V_{n\_EC2} = 126 \cdot kN$

AASHTO LRFD

$d_v := \dfrac{M_{nys\_pos}}{A_s \cdot f_{y\_pos}} = 9.707 \cdot in$ $\qquad \dfrac{d_v}{d_{s\_pos}} = 0.953$

$\left|\min\left(M_n, M_{nys\_pos}\right)\right| = 48.5 \cdot kip \cdot ft$

$\max\left(\left|\min\left(M_n, M_{nys\_pos}\right)\right|, \left|V_n \cdot d_v\right|\right) = 48.5 \cdot kip \cdot ft$

$$\varepsilon_s := \frac{\dfrac{\max\left(\left|\min\left(M_n, M_{nys\_pos}\right)\right|, \left|V_n \cdot d_v\right|\right)}{d_v} + V_n}{E_s \cdot A_s} = 0.002488$$

less than 0.006

$s_x := d_v \qquad s_{xe} := \max\left(s_x \cdot \dfrac{1.38}{\dfrac{a_g}{in} + 0.63}, 12in\right) = 12 \cdot in$

$\beta := \dfrac{4.8}{1 + 750 \cdot \varepsilon_s} \cdot \dfrac{51}{39 + \dfrac{s_{xe}}{in}} = 1.675 \qquad \theta := 29 + 3500 \cdot \varepsilon_s = 37.707$

$V_{c\_AASHTO} := 0.0316 \cdot \beta \cdot \sqrt{f_{c\_prime}} \cdot \sqrt{1000} \cdot \sqrt{psi} \cdot b_w \cdot d_{s\_pos} = 25.193 \cdot kip$

$\boxed{V_{n\_AASHTO} := V_{c\_AASHTO} = 25.193 \cdot kip} \qquad V_{n\_AASHTO\_SI} := V_{n\_AASHTO} = 112 \cdot kN$

Actual Shear Strength @ Support

$V_{n\_sup} := 29.9kip$ $\qquad$ *b* = 18 in away from the face of the support

$\beta_{min\_actual} := \dfrac{V_{n\_sup}}{\left(\sqrt{f_{c\_prime}} \cdot \sqrt{psi} \cdot b_w \cdot d_{s\_pos}\right)} = 1.986$ $\qquad$ Min. actual shear strength factor

$a\_to\_d\_ratio := \dfrac{55.0in}{d_{s\_pos}} = 5.399$ $\qquad$ Shear span to depth ratio

Comment: It is safe to assume that this represents the actual min. shear strength, given that the observed shear failure was following flexural failure. Also, failure at the observed location near the load application points would be governed by two-way shear, which is much higher than one-way shear.

Specimen 2 - Shear strength

$L_c := 12ft = 3.66\,m$

$\alpha := \frac{\pi}{6} = 30\cdot deg$ — Failure angle per experiment

$w_c := 150\frac{lbf}{ft^3} = 23.6\cdot\frac{kN}{m^3}$

$E_s := 29000ksi$

$A_s := 4\cdot 0.31in^2 = 1.24\cdot in^2$

$f_{y\_pos} := 65.9ksi$ $\quad f_{y\_neg} := 73.6ksi$

$f_{su\_pos} := 108ksi$ $\quad f_{su\_neg} := 120ksi$

$a_g := 0.75in$

$f_{c\_prime} := 3788psi$

$b_w := 2ft = 610\cdot mm$

$h_s := 12in = 305\cdot mm$

$d_{s\_pos} := h_s - 1.5in - \frac{5}{16}in = 10.2\cdot in$

$P_{LL} := 97.0kip = 97\cdot kip$ — Applied load at failure

$M_{nys\_pos} := 66.1kip\cdot ft$ $\quad M_{nps\_pos} := 87.3kip\cdot ft$ — Yield vs. probable moment

$M_{nys\_neg} := 31.9kip\cdot ft$ $\quad M_{nps\_neg} := 36.8kip\cdot ft$ — Yield vs. probable moment

Precalcs

$b := 10in + 2\frac{d_{s\_pos}}{\tan(\alpha)} = 45.3\cdot in$ — Length of load using α

$\rho_w := \frac{A_s}{b_w\cdot d_{s\_pos}} = 0.00507$ — Long. reinforcement ratio

$w_{DL} := b_w\cdot h_s\cdot w_c = 0.3\cdot\frac{kip}{ft}$ — Dead load

$w_{LL} := \frac{P_{LL}}{b} = 25.7\cdot\frac{kip}{ft}$ — Live load across length b

Internal forces

$V_n := 49.7\text{kip}$ Shear force @ x = 13 in

$M_n := 16.9\text{kip}\cdot\text{ft}$ Bending moment @ x = 31 in

Shear strengths

ACI 318-14 simplified

$$V_{c\_ACI\_simple} := 2\cdot\sqrt{f_{c\_prime}}\cdot\sqrt{\text{psi}}\cdot b_w\cdot d_{s\_pos} = 30.1\cdot\text{kip}$$

$\boxed{V_{n\_ACI\_simple} := V_{c\_ACI\_simple} = 30.1\cdot\text{kip}}$ $V_{n\_ACI\_simple\_SI} := V_{n\_ACI\_simple} = 134\cdot\text{kN}$

ACI 318-14 detailed

$$\left|\min\left(M_n, M_{nys\_pos}\right)\right| = 16.9\cdot\text{kip}\cdot\text{ft}$$

$$V_{c\_ACI\_det\_1} := \left(1.9\cdot\sqrt{f_{c\_prime}}\cdot\sqrt{\text{psi}} + 2500\cdot\rho_w\cdot\frac{\left|V_n\right|\cdot d_{s\_pos}}{\left|\min\left(M_n, M_{nys\_pos}\right)\right|}\cdot\text{psi}\right)\cdot b_w\cdot d_{s\_pos} = 36.3\cdot\text{kip}$$

$$V_{c\_ACI\_det\_2} := \left(1.9\cdot\sqrt{f_{c\_prime}}\cdot\sqrt{\text{psi}} + 2500\cdot\rho_w\cdot\text{psi}\right)\cdot b_w\cdot d_{s\_pos} = 31.7\cdot\text{kip}$$

$$V_{c\_ACI\_det\_3} := 3.5\cdot\sqrt{f_{c\_prime}}\cdot\sqrt{\text{psi}}\cdot b_w\cdot d_{s\_pos} = 52.7\cdot\text{kip}$$

$$V_{c\_ACI\_det} := \min\left(V_{c\_ACI\_det\_1}, V_{c\_ACI\_det\_2}, V_{c\_ACI\_det\_3}\right) = 31.7\cdot\text{kip}$$

$\boxed{V_{n\_ACI\_det} := V_{c\_ACI\_det} = 31.7\cdot\text{kip}}$ $V_{n\_ACI\_det\_SI} := V_{n\_ACI\_det} = 141\cdot\text{kN}$

Eurocode 2 (unreinforced section)

$\gamma_c := 1.0$ Partial safety factor, set to 1.0

$C_{Rd\_c} := \dfrac{0.18}{\gamma_c}$ Experimental coefficient

$k := 1 + \sqrt{\dfrac{200}{\dfrac{d_{s\_pos}}{\text{mm}}}} = 1.879$ Max. value = 2

$\rho_l := \rho_w = 0.00507$ Longitudinal reinf. ratio

$f_{ck} := f_{c\_prime} = 3788\cdot\text{psi}$ Concrete cube strength

$$V_{Rd\_c} := C_{Rd\_c}\cdot k\cdot\left(100\cdot\rho_l\cdot\frac{f_{ck}}{\text{MPa}}\right)^{\frac{1}{3}}\cdot\frac{b_w}{\text{mm}}\cdot\frac{d_{s\_pos}}{\text{mm}}\cdot\text{N} = 28.4\cdot\text{kip}$$

$\boxed{V_{n\_EC2} := V_{Rd\_c} = 28.4\cdot\text{kip}}$ $V_{n\_EC2\_SI} := V_{n\_EC2} = 126\cdot\text{kN}$

AASHTO LRFD

$$d_v := \frac{M_{nys\_pos}}{A_s \cdot f_{y\_pos}} = 9.707 \cdot in \qquad \frac{d_v}{d_{s\_pos}} = 0.953$$

$$\left|\min\left(M_n, M_{nys\_pos}\right)\right| = 16.9 \cdot kip \cdot ft$$

$$\max\left(\left|\min\left(M_n, M_{nys\_pos}\right)\right|, \left|V_n \cdot d_v\right|\right) = 40.202 \cdot kip \cdot ft$$

$$\varepsilon_s := \frac{\dfrac{\max\left(\left|\min\left(M_n, M_{nys\_pos}\right)\right|, \left|V_n \cdot d_v\right|\right)}{d_v} + V_n}{E_s \cdot A_s} = 0.002764$$

$$s_x := d_v \qquad s_{xe} := \max\left(s_x \cdot \frac{1.38}{\dfrac{a_g}{in} + 0.63}, 12in\right) = 12 \cdot in$$

$$\beta := \frac{4.8}{1 + 750 \cdot \varepsilon_s} \cdot \frac{51}{39 + \dfrac{s_{xe}}{in}} = 1.562$$

$$V_{c\_AASHTO} := 0.0316 \cdot \beta \cdot \sqrt{f_{c\_prime}} \cdot \sqrt{1000} \cdot \sqrt{psi} \cdot b_w \cdot d_{s\_pos} = 23.487 \cdot kip$$

$$\boxed{V_{n\_AASHTO} := V_{c\_AASHTO} = 23.487 \cdot kip} \qquad V_{n\_AASHTO\_SI} := V_{n\_AASHTO} = 104 \cdot kN$$

Actual Shear Strength @ Support

$V_{n\_sup} := 44.7kip$ $\qquad$ *b* = 18 in away from the face of the support

$$\beta_{min\_actual} := \frac{V_{n\_sup}}{\left(\sqrt{f_{c\_prime}} \cdot \sqrt{psi} \cdot b_w \cdot d_{s\_pos}\right)} = 2.97$$

Min. actual shear strength factor

$$a\_to\_d\_ratio := \frac{31.0in}{d_{s\_pos}} = 3.043$$

Shear span to depth ratio

Comment: It is safe to assume that this represents the actual min. shear strength, given that the observed shear failure was following flexural failure. Also, failure at the observed location near the load application points would be governed by two-way shear, which is much higher than one-way shear.

Specimen 3 - Shear strength

$L_c := 12ft = 3.66\,m$

$\alpha := \frac{\pi}{6} = 30 \cdot deg$ — Failure angle per experiment

$w_c := 150\frac{lbf}{ft^3} = 23.6 \cdot \frac{kN}{m^3}$

$E_s := 29000ksi$

$A_s := 4 \cdot 0.31in^2 = 1.24 \cdot in^2$

$f_{y\_pos} := 65.9ksi$ $\quad f_{y\_neg} := 73.6ksi$

$f_{su\_pos} := 108ksi$ $\quad f_{su\_neg} := 120ksi$

$a_g := 0.75in$

$f_{c\_prime} := 3339psi$

$b_w := 2ft = 610 \cdot mm$

$h_s := 12in = 305 \cdot mm$

$d_{s\_pos} := h_s - 1.5in - \frac{5}{16}in = 10.2 \cdot in$

$P_{LL} := 84.4kip = 84.4 \cdot kip$ — Applied load at failure

$M_{nys\_pos} := 65.6kip \cdot ft$ $\quad M_{nps\_pos} := 85.6kip \cdot ft$ — Yield vs. probable moment

$M_{nys\_neg} := 31.0kip \cdot ft$ $\quad M_{nps\_neg} := 36.4kip \cdot ft$ — Yield vs. probable moment

Precalcs

$b := 10in + 2\frac{d_{s\_pos}}{\tan(\alpha)} = 45.3 \cdot in$ — Length of load using α

$\rho_w := \frac{A_s}{b_w \cdot d_{s\_pos}} = 0.00507$ — Long. reinforcement ratio

$w_{DL} := b_w \cdot h_s \cdot w_c = 0.3 \cdot \frac{kip}{ft}$ — Dead load

$w_{LL} := \frac{P_{LL}}{b} = 22.4 \cdot \frac{kip}{ft}$ — Live load across length b

Internal forces

$V_n := 21.0\text{kip}$ Shear force @ x = 86 in

$M_n := 36.5\text{kip}\cdot\text{ft}$ Bending moment @ x = 69 in

Shear strengths

ACI 318-14 simplified

$$V_{c\_ACI\_simple} := 2\cdot\sqrt{f_{c\_prime}}\cdot\sqrt{\text{psi}}\cdot b_w\cdot d_{s\_pos} = 28.3\cdot\text{kip}$$

$$\boxed{V_{n\_ACI\_simple} := V_{c\_ACI\_simple} = 28.3\cdot\text{kip}} \qquad V_{n\_ACI\_simple\_SI} := V_{n\_ACI\_simple} = 126\cdot\text{kN}$$

ACI 318-14 detailed

$$\left|\min\left(M_n, M_{nys\_pos}\right)\right| = 36.5\cdot\text{kip}\cdot\text{ft}$$

$$V_{c\_ACI\_det\_1} := \left(1.9\cdot\sqrt{f_{c\_prime}}\cdot\sqrt{\text{psi}} + 2500\cdot\rho_w\cdot\frac{\left|V_n\right|\cdot d_{s\_pos}}{\left|\min\left(M_n, M_{nys\_pos}\right)\right|}\cdot\text{psi}\right)\cdot b_w\cdot d_{s\_pos} = 28.4\cdot\text{kip}$$

$$V_{c\_ACI\_det\_2} := \left(1.9\cdot\sqrt{f_{c\_prime}}\cdot\sqrt{\text{psi}} + 2500\cdot\rho_w\cdot\text{psi}\right)\cdot b_w\cdot d_{s\_pos} = 29.9\cdot\text{kip}$$

$$V_{c\_ACI\_det\_3} := 3.5\cdot\sqrt{f_{c\_prime}}\cdot\sqrt{\text{psi}}\cdot b_w\cdot d_{s\_pos} = 49.4\cdot\text{kip}$$

$$V_{c\_ACI\_det} := \min\left(V_{c\_ACI\_det\_1}, V_{c\_ACI\_det\_2}, V_{c\_ACI\_det\_3}\right) = 28.4\cdot\text{kip}$$

$$\boxed{V_{n\_ACI\_det} := V_{c\_ACI\_det} = 28.4\cdot\text{kip}} \qquad V_{n\_ACI\_det\_SI} := V_{n\_ACI\_det} = 126\cdot\text{kN}$$

Eurocode 2 (unreinforced section)

$\gamma_c := 1.0$ Partial safety factor, set to 1.0

$C_{Rd\_c} := \frac{0.18}{\gamma_c}$ Experimental coefficient

$k := 1 + \sqrt{\frac{200}{\frac{d_{s\_pos}}{\text{mm}}}} = 1.879$ Max. value = 2

$\rho_l := \rho_w = 0.00507$ Longitudinal reinf. ratio

$f_{ck} := f_{c\_prime} = 3339\cdot\text{psi}$ Concrete cube strength

$$V_{Rd\_c} := C_{Rd\_c}\cdot k\cdot\left(100\cdot\rho_l\cdot\frac{f_{ck}}{\text{MPa}}\right)^{\frac{1}{3}}\cdot\frac{b_w}{\text{mm}}\cdot\frac{d_{s\_pos}}{\text{mm}}\cdot\text{N} = 27.2\cdot\text{kip}$$

$$\boxed{V_{n\_EC2} := V_{Rd\_c} = 27.2\cdot\text{kip}} \qquad V_{n\_EC2\_SI} := V_{n\_EC2} = 121\cdot\text{kN}$$

AASHTO LRFD

$$d_v := \frac{M_{nys\_pos}}{A_s \cdot f_{y\_pos}} = 9.633 \cdot in \qquad \frac{d_v}{d_{s\_pos}} = 0.946$$

$$\left|\min\left(M_n, M_{nys\_pos}\right)\right| = 36.5 \cdot kip \cdot ft$$

$$\max\left(\left|\min\left(M_n, M_{nys\_pos}\right)\right|, \left|V_n \cdot d_v\right|\right) = 36.5 \cdot kip \cdot ft$$

$$\varepsilon_s := \frac{\dfrac{\max\left(\left|\min\left(M_n, M_{nys\_pos}\right)\right|, \left|V_n \cdot d_v\right|\right)}{d_v} + V_n}{E_s \cdot A_s} = 0.001848$$

$$s_x := d_v \qquad s_{xe} := \max\left(s_x \cdot \frac{1.38}{\dfrac{a_g}{in} + 0.63}, 12in\right) = 12 \cdot in$$

$$\beta := \frac{4.8}{1 + 750 \cdot \varepsilon_s} \cdot \frac{51}{39 + \dfrac{s_{xe}}{in}} = 2.012$$

$$V_{c\_AASHTO} := 0.0316 \cdot \beta \cdot \sqrt{f_{c\_prime}} \cdot \sqrt{1000} \cdot \sqrt{psi} \cdot b_w \cdot d_{s\_pos} = 28.399 \cdot kip$$

$$\boxed{V_{n\_AASHTO} := V_{c\_AASHTO} = 28.399 \cdot kip} \qquad V_{n\_AASHTO\_SI} := V_{n\_AASHTO} = 126 \cdot kN$$

Actual Shear Strength @ Support

$V_{n\_sup} := 47.4kip$ *b* = 0 in away from the face of the support

$$\beta_{min\_actual} := \frac{V_{n\_sup}}{\left(\sqrt{f_{c\_prime}} \cdot \sqrt{psi} \cdot b_w \cdot d_{s\_pos}\right)} = 3.355$$ Min. actual shear strength factor

$$a\_to\_d\_ratio := \frac{10.5in}{d_{s\_pos}} = 1.031$$ Shear span to depth ratio

Comment: It is safe to assume that this represents the actual min. shear strength, given that the observed shear failure was following flexural failure. Also, failure at the observed location near the load application points would be governed by two-way shear, which is much higher than one-way shear.

APPENDIX G: SHEAR STRENGTH CALCULATIONS

Specimen 4 - Shear strength

$l := 120\text{in} = 3.05\,\text{m}$

$\alpha := \frac{\pi}{6} = 30\cdot\text{deg}$ Failure angle per experiment

$w_c := 150\,\frac{\text{lbf}}{\text{ft}^3} = 23.6\cdot\frac{\text{kN}}{\text{m}^3}$

$E_s := 29000\text{ksi}$

$A_s := 4\cdot 0.31\text{in}^2 = 1.24\cdot\text{in}^2$

$f_{y\_pos} := 62.2\text{ksi}$ $f_{y\_neg} := 64.3\text{ksi}$

$f_{su\_pos} := 100\text{ksi}$ $f_{su\_neg} := 102\text{ksi}$

$a_g := 0.75\text{in}$

$f_{c\_prime} := 3469\text{psi}$

$h_s := 12\text{in} = 305\cdot\text{mm}$

$d_{s\_pos} := h_s - 1.5\text{in} - \frac{5}{16}\text{in} = 10.2\cdot\text{in}$

$P_{LL} := 57.8\text{kip} = 257\cdot\text{kN}$ Applied load at failure

$M_{nys\_pos} := 218\text{kip}\cdot\text{ft}$ $M_{nps\_pos} := 293\text{kip}\cdot\text{ft}$ Yield vs. probable moment

$M_{nys\_neg} := 152\text{kip}\cdot\text{ft}$ $M_{nps\_neg} := 182\text{kip}\cdot\text{ft}$ Yield vs. probable moment

Precalcs

$b := 10\text{in} + 2\,\frac{d_{s\_pos}}{\tan(\alpha)} = 45.3\cdot\text{in}$ Length of load using α

Shear Strength @ Support for SA Loading

$V_{n\_sup} := 119.6kip$ *b* = 18 in away from the face of the support

$b_w := 130in = 3302 \cdot mm$

$$\beta_{min\_actual} := \frac{V_{n\_sup}}{\left(\sqrt{f_{c\_prime}} \cdot \sqrt{psi} \cdot b_w \cdot d_{s\_pos}\right)} = 1.533$$ Min. actual shear strength factor

$$a\_to\_d\_ratio := \frac{55.0in}{d_{s\_pos}} = 5.399$$ Shear span to depth ratio

Comment: It is safe to assume that this represents the actual min. shear strength, given that the observed shear failure was following flexural failure. Also, failure at the observed location near the load application points would be governed by two-way shear, which is much higher than one-way shear.

Shear Strength @ Support for TA Loading

$V_{n\_sup} := 108.2kip$ *b* = 18 in away from the face of the support

$b_w := 82in = 2083 \cdot mm$

$$\beta_{min\_actual} := \frac{V_{n\_sup}}{\left(\sqrt{f_{c\_prime}} \cdot \sqrt{psi} \cdot b_w \cdot d_{s\_pos}\right)} = 2.199$$ Min. actual shear strength factor

$$a\_to\_d\_ratio := \frac{31.0in}{d_{s\_pos}} = 3.043$$ Shear span to depth ratio

Comment: It is safe to assume that this represents the actual min. shear strength, given that the observed shear failure was following flexural failure. Also, failure at the observed location near the load application points would be governed by two-way shear, which is much higher than one-way shear.

Specimen 5 - Shear strength

$L_c := 16ft = 4.88m$

$\alpha := \frac{\pi}{6} = 30\cdot deg$ Failure angle per experiment

$w_c := 150\frac{lbf}{ft^3} = 23.6\frac{kN}{m^3}$

$E_s := 29000ksi$

$A_s := 4\cdot 0.31in^2 = 1.24\cdot in^2$

$f_{y\_pos} := 63.2ksi$ $f_{y\_neg} := 63.2ksi$

$f_{su\_pos} := 102ksi$ $f_{su\_neg} := 102ksi$

$a_g := 0.75in$

$f_{c\_prime} := 3366psi$

$b_w := 24in = 610\cdot mm$

$h_s := 18in = 457\cdot mm$

$d_{s\_pos} := h_s - 1.5in - \frac{5}{16}in = 16.2\cdot in$

$P_{LL} := 76.8kip = 342\cdot kN$ Applied load at failure

$M_{nys\_pos} := 102kip\cdot ft$ $M_{nps\_pos} := 155kip\cdot ft$ Yield vs. probable moment

$M_{nys\_neg} := 52.0kip\cdot ft$ $M_{nps\_neg} := 77.0kip\cdot ft$ Yield vs. probable moment

Precalcs

$b := 10in + 2\frac{d_{s\_pos}}{\tan(\alpha)} = 66.1\cdot in$ $\frac{d_{s\_pos}}{\tan(\alpha)} = 28.038\cdot in$ Length of load using α

$\rho_w := \frac{A_s}{b_w\cdot d_{s\_pos}} = 0.00319$ Long. reinforcement ratio

$w_{DL} := b_w\cdot h_s\cdot w_c = 0.45\cdot\frac{kip}{ft}$ Dead load

$w_{LL} := \frac{P_{LL}}{b} = 13.9\cdot\frac{kip}{ft}$ Live load across length b

Internal forces

$V_n := 39.5\text{kip}$ Shear force @ x = 63 in

$M_n := 110\text{kip}\cdot\text{ft}$ Bending moment @ x = 91 in

Shear strengths

ACI 318-14 simplified

$V_{c\_ACI\_simple} := 2\cdot\sqrt{f_{c\_prime}}\cdot\sqrt{psi}\cdot b_w\cdot d_{s\_pos} = 45.1\cdot kip$

$\boxed{V_{n\_ACI\_simple} := V_{c\_ACI\_simple} = 45.1\cdot kip}$ $V_{n\_ACI\_simple\_SI} := V_{n\_ACI\_simple} = 201\cdot kN$

ACI 318-14 detailed

$\left|\min\left(M_n, M_{nys\_pos}\right)\right| = 102\cdot kip\cdot ft$

$$V_{c\_ACI\_det\_1} := \left(1.9\cdot\sqrt{f_{c\_prime}}\cdot\sqrt{psi} + 2500\cdot\rho_w\cdot\frac{\left|V_n\right|\cdot d_{s\_pos}}{\left|\min\left(M_n, M_{nys\_pos}\right)\right|}\cdot psi\right)\cdot b_w\cdot d_{s\_pos} = 44.4\cdot kip$$

$$V_{c\_ACI\_det\_2} := \left(1.9\cdot\sqrt{f_{c\_prime}}\cdot\sqrt{psi} + 2500\cdot\rho_w\cdot psi\right)\cdot b_w\cdot d_{s\_pos} = 45.9\cdot kip$$

$$V_{c\_ACI\_det\_3} := 3.5\cdot\sqrt{f_{c\_prime}}\cdot\sqrt{psi}\cdot b_w\cdot d_{s\_pos} = 78.9\cdot kip$$

$$V_{c\_ACI\_det} := \min\left(V_{c\_ACI\_det\_1}, V_{c\_ACI\_det\_2}, V_{c\_ACI\_det\_3}\right) = 44.4\cdot kip$$

$\boxed{V_{n\_ACI\_det} := V_{c\_ACI\_det} = 44.4\cdot kip}$ $V_{n\_ACI\_det\_SI} := V_{n\_ACI\_det} = 198\cdot kN$

Eurocode 2 (unreinforced section)

$\gamma_c := 1.0$ Partial safety factor, set to 1.0

$C_{Rd\_c} := \frac{0.18}{\gamma_c}$ Experimental coefficient

$k := 1 + \sqrt{\frac{200}{\frac{d_{s\_pos}}{mm}}} = 1.697$ Max. value = 2

$\rho_l := \rho_w = 0.00319$ Longitudinal reinf. ratio

$f_{ck} := 1.25 f_{c\_prime} = 4208\cdot psi$ Concrete cube strength

$$V_{Rd\_c} := C_{Rd\_c}\cdot k\cdot\left(100\cdot\rho_l\cdot\frac{f_{ck}}{MPa}\right)^{\frac{1}{3}}\cdot\frac{b_w}{mm}\cdot\frac{d_{s\_pos}}{mm}\cdot N = 36.2\cdot kip$$

$\boxed{V_{n\_EC2} := V_{Rd\_c} = 36.2\cdot kip}$ $V_{n\_EC2\_SI} := V_{n\_EC2} = 161\cdot kN$

AASHTO LRFD

$$d_v := \frac{M_{nys\_pos}}{A_s \cdot f_{y\_pos}} = 15.619 \cdot in \qquad \frac{d_v}{d_{s\_pos}} = 0.965$$

$$\left|\min\left(M_n, M_{nys\_pos}\right)\right| = 102 \cdot kip \cdot ft$$

$$\max\left(\left|\min\left(M_n, M_{nys\_pos}\right)\right|, \left|V_n \cdot d_v\right|\right) = 102 \cdot kip \cdot ft$$

$$\varepsilon_s := \frac{\dfrac{\max\left(\left|\min\left(M_n, M_{nys\_pos}\right)\right|, \left|V_n \cdot d_v\right|\right)}{d_v} + V_n}{E_s \cdot A_s} = 0.003278$$

$$s_x := d_v \qquad s_{xe} := \max\left(s_x \cdot \frac{1.38}{\frac{a_g}{in} + 0.63}, 12in\right) = 15.619 \cdot in \qquad 25.2kip = 112.095 \cdot kN$$

$$\beta := \frac{4.8}{1 + 750 \cdot \varepsilon_s} \cdot \frac{51}{39 + \frac{s_{xe}}{in}} = 1.296$$

$$V_{c\_AASHTO} := 0.0316 \cdot \beta \cdot \sqrt{f_{c\_prime}} \cdot \sqrt{1000} \cdot \sqrt{psi} \cdot b_w \cdot d_{s\_pos} = 29.19 \cdot kip$$

$$\boxed{V_{n\_AASHTO} := V_{c\_AASHTO} = 29.19 \cdot kip} \qquad V_{n\_AASHTO\_SI} := V_{n\_AASHTO} = 130 \cdot kN$$

Actual Shear Strength @ Support

$V_{n\_sup} := 40.9kip$ $\qquad$ *b* = 28 in away from the face of the support

$$\beta_{min\_actual} := \frac{V_{n\_sup}}{\left(\sqrt{f_{c\_prime}} \cdot \sqrt{psi} \cdot b_w \cdot d_{s\_pos}\right)} = 1.815$$

Min. actual shear strength factor

$$a\_to\_d\_ratio := \frac{91in}{d_{s\_pos}} = 5.622$$

Shear span to depth ratio

Comment: It is safe to assume that this represents the actual min. shear strength, given that the observed shear failure was following flexural failure. Also, failure at the observed location near the load application points would be governed by two-way shear, which is much higher than one-way shear.

Specimen 4 - Two-way Shear Strength

$l := 12\text{ft} = 3.66\,\text{m}$

$\alpha := \frac{\pi}{6} = 30\cdot\text{deg}$ Failure angle per experiment

$w_c := 150\,\frac{\text{lbf}}{\text{ft}^3} = 23.6\cdot\frac{\text{kN}}{\text{m}^3}$

$E_s := 29000\text{ksi}$

$A_s := 4\cdot 0.31\text{in}^2 = 1.24\cdot\text{in}^2$

$f_{c\_prime} := 3469\text{psi}$

$b_w := 2\text{ft} = 610\cdot\text{mm}$

$h_s := 12\text{in} = 305\cdot\text{mm}$

$d_{s\_pos} := h_s - 1.5\text{in} - \frac{5}{16}\text{in} = 258.8\cdot\text{mm}$

$P_{LL} := 230\text{kip} = 1023\cdot\text{kN}$ Applied load at failure

Precalcs

$b := 10\text{in} + 2\,\frac{d_{s\_pos}}{\tan(\alpha)} = 45.3\cdot\text{in}$ Length of load using α

$\rho_w := \frac{A_s}{b_w\cdot d_{s\_pos}} = 0.00507$ Long. reinforcement ratio

$w_{DL} := b_w\cdot h_s\cdot w_c = 0.3\cdot\frac{\text{kip}}{\text{ft}}$ Dead load

$w_{LL} := \frac{P_{LL}}{b} = 60.9\cdot\frac{\text{kip}}{\text{ft}}$ Live load across length b

Two-way Shear Strength (SA)

ACI 318-14

$\beta := \frac{20\text{in}}{10\text{in}} = 2$

$b_0 := 2\cdot\left(10\text{in} + d_{s\_pos}\right) + 2\cdot\left(20\text{in} + d_{s\_pos}\right) = 100.75\cdot\text{in}$ Perimeter

$\boxed{V_{c\_ACI} := \left(2 + \frac{4}{\beta}\right)\cdot\sqrt{f_{c\_prime}}\sqrt{\text{psi}}\cdot b_0\cdot d_{s\_pos} = 242\cdot\text{kip}}$ $V_{c\_ACI} = 1076\cdot\text{kN}$

Eurocode 2 (unreinforced section)

$\gamma_c := 1.0$ — Partial safety factor, set to 1.0

$C_{Rd\_c} := \frac{0.18}{\gamma_c}$ — Experimental coefficient

$k := 1 + \sqrt{\frac{200}{\frac{d_{s\_pos}}{mm}}} = 1.879$ — Max. value = 2

$\rho := \rho_w = 0.00507$ — Longitudinal reinf. ratio

$f_{ck} := f_{c\_prime} = 24 \cdot MPa$ — Concrete cube strength

$u_1 := 2 \cdot 10in + 2 \cdot 20in + 4d_{s\_pos} \cdot \pi = 188.02 \cdot in$ — Perimeter

$$V_{Rd\_c} := C_{Rd\_c} \cdot k \cdot \left(100 \cdot \rho \cdot \frac{f_{ck}}{MPa}\right)^{\frac{1}{3}} \frac{u_1}{mm} \cdot \frac{d_{s\_pos}}{mm} \cdot N = 216 \cdot kip$$

$V_{Rd\_c} = 960 \cdot kN$

Two-way Shear Strength (TA)

ACI 318-14

$\beta := \frac{20in}{10in} = 2$

$b_{0\_1} := 2 \cdot (10in + d_{s\_pos}) + 2 \cdot (20in + d_{s\_pos}) = 100.75 \cdot in$ — Perimeter 1

$b_{0\_2} := 2 \cdot \left(10in + \frac{d_{s\_pos}}{2} + 19in\right) + (20in + d_{s\_pos}) = 98.375 \cdot in$ — Perimeter 2

$$V_{c\_ACI} := \left(2 + \frac{4}{\beta}\right) \cdot \sqrt{f_{c\_prime}} \sqrt{psi} \cdot \min(b_{0\_1}, b_{0\_2}) \cdot d_{s\_pos} = 236 \cdot kip$$

$V_{c\_ACI} = 1050 \cdot kN$

Eurocode 2 (unreinforced section)

$\gamma_c := 1.0$ — Partial safety factor, set to 1.0

$C_{Rd\_c} := \frac{0.18}{\gamma_c}$ — Experimental coefficient

$k := 1 + \sqrt{\frac{200}{\frac{d_{s\_pos}}{mm}}} = 1.879$ — Max. value = 2

$\rho := \rho_w = 0.00507$ Longitudinal reinf. ratio

$f_{ck} := f_{c\_prime} = 24 \cdot MPa$ Concrete cube strength

$u_{1\_1} := 2 \cdot 10in + 2 \cdot 20in + 4d_{s\_pos} \cdot \pi = 188.02 \cdot in$ Perimeter 1

$u_{1\_2} := 2 \cdot 10in + 20in + 2 \cdot 19in + 2 \cdot d_{s\_pos} = 98.375 \cdot in$ Perimeter 2

$$\boxed{V_{Rd\_c} := 2C_{Rd\_c} \cdot k \cdot \left(100 \cdot \rho \cdot \frac{f_{ck}}{MPa}\right)^{\frac{1}{3}} \frac{\min(u_{1\_1}, u_{1\_2})}{mm} \cdot \frac{d_{s\_pos}}{mm} \cdot N = 226 \cdot kip} \qquad V_{Rd\_c} = 1005 \cdot kN$$

Delaware Center for Transportation University of Delaware Newark, Delaware 19716